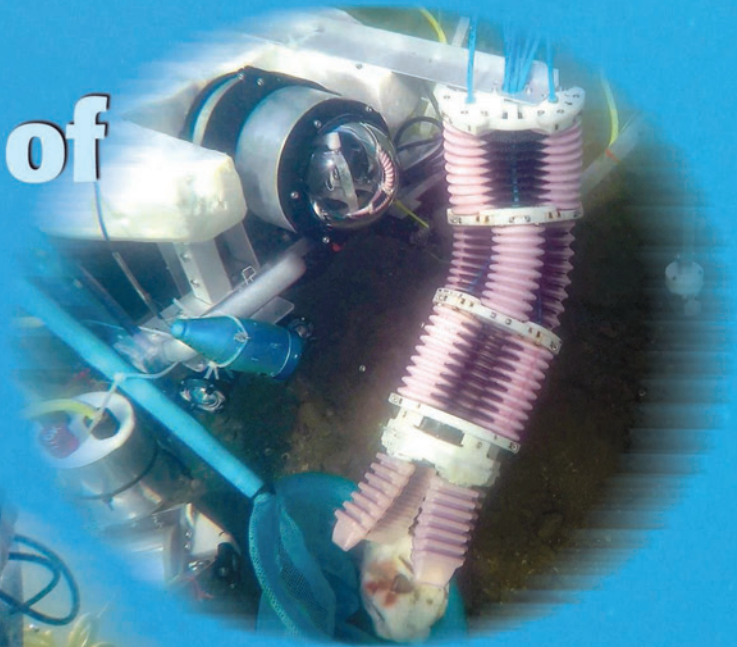


IEEE ROBOTICS & AUTOMATION MAGAZINE

Vol. 27, No. 4 December 2020
ISSN 1070-9932
<http://www.ieee-ras.org/publications/ram>

Design Optimization of Soft Robots



force dimension

Displaying the world in your hands. Inventing new ways to interact.

Force Dimension designs and manufactures the finest **master haptic devices** for leading-edge applications in research, medical, industry, and human exploration.



From space ESA astronaut Luca Parmitano uses the haptic platform to control a robot manipulator ©2019 ESA

In collaboration with the **Human Robot Interaction Lab** at the **European Space Agency**, our most advanced haptic device, the **sigma.7**, was launched to the International Space Station (ISS). The haptic device is part of the ESA METERON experiment which explores new ways to operate robots from space using the sense of touch.

Designed and manufactured in Switzerland, the **sigma.7** is the first 3D haptic device certified for use in space.

Force Dimension
Switzerland

www.forcedimension.com
info@forcedimension.com

FEATURES

- 12 Underwater Mobile Manipulation**
A Soft Arm on a Benthic Legged Robot
By Jiaqi Liu, Saverio Iacononi, Cecilia Laschi, Li Wen, and Marcello Calisti
- 27 Design Optimization of Soft Robots**
A Review of the State of the Art
By Feifei Chen and Michael Yu Wang
- 44 Room Temperature Self-Healing in Soft Pneumatic Robotics**
Autonomous Self-Healing in a Diels-Alder Polymer Network
By Seppe Terryn, Joost Brancart, Ellen Roels, Guy Van Assche, and Bram Vanderborght



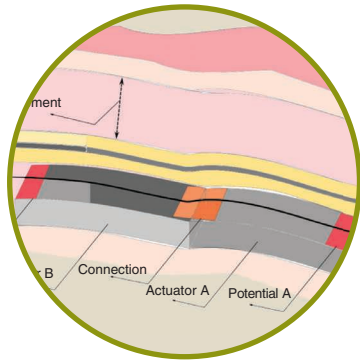
ON THE COVER

This special issue of *IEEE Robotics and Automation Magazine* provides an overview of the state of the art in the design optimization of soft robots and identifies common perspectives and challenges, shared scientific goals, and high-impact applications.

BACKGROUND IMAGE: ©SHUTTERSTOCK/JUSTINESSY

- 56 Design and Optimization of a Dexterous Robotic Finger**
Incorporating a Sliding, Rotating, and Soft-Bending Mechanism While Maximizing Dexterity and Minimizing Dimensions
By Amir Pagoli, Frédéric Chapelle, Juan-Antonio Corrales-Ramon, Youcef Mezouar, and Yuri Lapusta
- 65 Expanding Pouch Motor Patterns for Programmable Soft Bending Actuation**
Enabling Soft Robotic System Adaptations
By Haneol Lee, Namsoo Oh, and Hugo Rodrigue





COLUMNS & DEPARTMENTS

- 4 FROM THE EDITOR'S DESK**
- 6 PRESIDENT'S MESSAGE**
- 9 STUDENT'S CORNER**
- 10 FROM THE GUEST EDITORS**
- 75 TC SPOTLIGHT**
- 78 WOMEN IN ENGINEERING**
- 81 SOCIETY NEWS**
- 88 CALENDAR**

EDITORIAL BOARD

Editor-in-Chief
Bram Vanderborcht
(ram-eic@ieee.org)
Vrije Universiteit Brussel (Belgium)

Editors
Fabio Bonsignorio
Heron Robots (Italy)
Yi Guo
Stevens Institute of Technology (USA)

Associate Editors
Pinhas Ben-Tzvi
Virginia Tech (USA)
Elena De Momi
Politecnico di Milano (Italy)
Alexander Dietrich
German Aerospace Center-DLR (Germany)
Angela Faragasso
University of Tokyo (Japan)

Xiang Li
Tsinghua University (China)
Perla Maiolino
University of Cambridge (UK)
Sören Schwertfeger
ShanghaiTech University, School of
Information Science and
Technology (China)

Yue Wang
Clemson University (USA)

Past Editor-in-Chief
Eugenio Guglielmelli
Università Campus Bio-Medico (Italy)

RAM Column Manager
Amy Reeder (USA)

RAM Editorial Assistant
Antonella Benvenuto
Università Campus Bio-Medico (Italy)

COLUMNS

Competitions: Minoru Asada (Japan)
and Yu Sun (USA)

Education: Jory Denny (USA)

Ethical, Legal, and Societal Issues:
Currently vacant

From the Editor's Desk: Bram
Vanderborcht (Belgium)

Industry News: Tamas Haidegger
(Hungary)

Humanitarian Technology:
Lino Marques (Portugal)

Standards: Craig Schlenoff (USA)

President's Message: Seth Hutchinson (USA)

Regional Spotlight: Megan Emmons (USA)

Student's Corner: Marwa El Dinwiny
(The Netherlands)

TC Spotlight: Yasuhisa Hirata (Japan)

Turning Point: Bram Vanderborcht (Belgium)

Women in Engineering: Lydia Tapia (USA)

**IEEE RAS Vice-President
of Publication Activities**
Aude Billard
EPFL (Switzerland)

RAM home page:
<http://www.ieee-ras.org/publications/ram>

**IEEE Robotics and Automation Society
Executive Office**
Kathy Colabaugh
Society Operations Manager
Amy Reeder
Program Specialist
ras@ieee.org

Advertising Sales
Mark David
Director, Business Development—Media &
Advertising
Tel: +1 732 465 6473
Fax: +1 732 981 1855
m.david@ieee.org

**IEEE Periodicals
Magazines Department**
Mark Gallaher
Managing Editor

Geraldine Krolin-Taylor
Senior Managing Editor

Janet Dudar
Senior Art Director

Gail A. Schnitzer
Associate Art Director

Theresa L. Smith
Production Coordinator

Felicia Spagnoli
Advertising Production Manager

Peter M. Tuohy
Production Director

Kevin Lisankie
Editorial Services Director

Dawn M. Melley
Staff Director,
Publishing Operations

**IEEE-RAS Membership
and Subscription Information:**

+1 800 678 IEEE (4333)

Fax: +1 732 463 3657

http://www.ieee.org/membership_services/membership/societies/ras.html

Digital Object Identifier 10.1109/MRA.2020.3023814

IEEE Robotics and Automation Magazine (ISSN 1070-9932) (IRAMEB) is published quarterly by the Institute of Electrical and Electronics Engineers, Inc. Headquarters: 3 Park Avenue, 17th Floor, New York, NY 10016-5997 USA, Telephone: +1 212 419 7900. Responsibility for the content rests upon the authors and not upon the IEEE, the Society or its members. IEEE Service Center (for orders, subscriptions, address changes): 445 Hoes Lane, P.O. Box 1331, Piscataway, NJ 08855 USA. Telephone: +1 732 981 0060. Individual copies: IEEE Members US\$20.00 (first copy only), non-Members US\$135 per copy. Subscription rates: Annual subscription rates included in IEEE Robotics and Automation Society member dues. Subscription rates available on request. Copyright and reprint permission: Abstracting is permitted with credit to the source. Libraries are permitted to

IEEE prohibits discrimination, harassment, and bullying. For more information, visit <http://www.ieee.org/web/aboutus/whatis/policies/p9-26.html>.

photocopy beyond the limits of U.S. Copyright law for the private use of patrons 1) those post-1977 articles that carry a code at the bottom of the first page, provided the per-copy fee indicated in the code is paid through the Copyright Clearance Center, 222 Rosewood Drive, Danvers, MA 01923 USA; 2) pre-1978 articles without a fee. For other copying, reprint, or republication permission, write Copyrights and Permissions Department, IEEE Service Center, 445 Hoes Lane, Piscataway, NJ 08854. Copyright © 2020 by the Institute of Electrical and Electronics Engineers Inc. All rights reserved. Periodicals postage paid at New York and additional mailing offices. Postmaster: Send address changes to IEEE Robotics and Automation Magazine, IEEE, 445 Hoes Lane, Piscataway, NJ 08854 USA. Canadian GST #125634188

PRINTED IN THE U.S.A.



KUKA



Say Hello_to the next robotic innovator

Research teams from around the globe were asked to submit their concepts on the topic of “Artificial Intelligence” for the KUKA Innovation Award. Five teams made it to the finals and will be presenting their projects in 2021. The award comes with a 20,000-euro prize. **Meet our five finalists for 2021.**



KUKA Innovation Award 2021



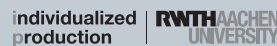
Team BlindGrasp, IISc & MIT, India & USA
“We aim to make use of tactile sensing for manipulation in vision denied environments. We equip the LBR iiwa with a novel gripper which has tactile sensors all over the surface and make use of reinforcement learning to explore, recognize and pick objects.”



Team CHRIS: Collaborative Human-Robot Intelligent System, A*STAR Institute for Infocomm Research, Singapore
“Our project intends to develop a collaborative AI technology that enables a cobot to interact with human co-worker in a natural, purposeful, and safe manner in order to provide workstream support functions to their human counterparts.”



Team Chorrobot, KU Leuven and Flanders Make@KU Leuven, Belgium
“Our project leverages a synergy between learned and modelled information to facilitate the commissioning of bimanual tasks. These include assembly operations involving non-rigid and non-fixed elements, as well as bimanual inspection operations in non-structured environments.”



Team CRC, Chair for Individualized Production RWTH Aachen, Germany
“Our goal is to integrate automation & online collaboration. With Cloud Remote Control, we can increase accessibility to worldwide robotic production. CRC adds layers of Artificial Intelligence to path planning and Internet of Things to device communication.”



Team ARAS – Advanced Robot Assistance Solution, Brandenburg University of Technology Cottbus-Senftenberg, Chair of Automation Technology, Germany
“From manual assembly processes to automated robot manufacturing using gesture recognition. Closing the interaction gap between human and robots using AI to recognize manual operations on the shop floor and translate them into robot task descriptions.”

Looking Back and Looking Forward

By Bram Vanderborght

This will be my last editorial, as my five-year term as editor-in-chief (EIC) of *IEEE Robotics and Automation Magazine* (RAM) ends with this issue. It was a unique experience to cooperate with the different fields of our Society on articles, columns, and special issues; tighten the connection with our flagship conferences; work on aspects like reproducible research; and celebrate 25 years of the magazine. I take this opportunity to thank all members of the current and past RAM editorial boards who have been key to guaranteeing the success and uniqueness of the magazine.

Robotics and automation have the potential to create new markets, businesses, and jobs that never existed before.

Also, special thanks to Eugenio Guglielmelli, previous RAM EIC and later vice president (VP) of Publications, for his wise guidance and support; Aude Billard, current VP of Publications; and Kyu-jin Cho, associate VP. Thanks to the IEEE Robotics and Automation Society (RAS) presidents during my term as EIC: Satoshi Tadokoro, Wolfram Burgard, and Seth Hutchinson. Special thanks to RAS staff at IEEE—Amy Reeder, Kathy Colabaugh, and Alexis

Simoes—for all of the valuable help and to IEEE managing editors—Debby Nowicki and afterward Mark Gallaher—and their team for all of the effort to bring our texts and pictures to a glossy magazine, winning international prizes for its layout. For daily help, I could count on the editorial assistant, Antonella Benvenuto; thanks a lot for the fluent collaboration. Also, thanks to Pradeep Misra for his work on PaperCept.

Our current RAS president, Seth Hutchinson, appointed a new RAM EIC, Yi Guo, who will take on this wonderful job. She started as the associate editor in 2013 and afterward became an editor for the magazine, so she is already well versed. I am sure that I leave the magazine in very good hands to guide its successful track, and I wish her all of the best. One of the most challenging aspects was writing the editorials; on the other hand, it was also a privileged forum to express my opinions on issues such as gender, ethics, societal challenges, the right to fail, making profitable robotic companies, and so on.

My last topic started five years ago, when 93 countries agreed on the United Nations Sustainable Development Goals (SDGs), representing a blueprint to achieve a better and more sustainable future for all. As a successor to the Millennium Development Goals, the SDGs address global challenges, including those related to poverty, inequality, climate, environmental degradation, prosperity, peace, and justice. They aim to



leave no one behind by 2030. Robotics will have a great impact on our society and hence the potential to speed up progress toward these developmental goals, but robotics also brings complex challenges.

For example, the World Food Program is looking into self-driving trucks for transporting food in war zones and drones with sensors for performing artificial intelligence analyses. Since almost 50% of crops are currently lost through waste, overconsumption, and production inefficiencies, these technologies have the potential to increase agricultural productivity. Many medical robots are developed for improving health and preventing injuries, for example, at work. Robots are used to deliver high-quality education, especially in science, technology, engineering, and mathematics and computational thinking. They monitor our climate and life below water as well as on land. Robotics and automation have the potential to create new markets, businesses, and jobs that never existed before.

On the other hand, studies suggest that the burden of job losses due to robotization is likely to be borne primarily by low-wage countries as the traditional advantage of low labor costs is eroded. It will also be much more difficult for these countries to put in place social measures, such as improved education and redistribution models, due to their much smaller economic base.

(continued on page 8)

KELO ROBILE

As simple as toys as powerful as industrial robots

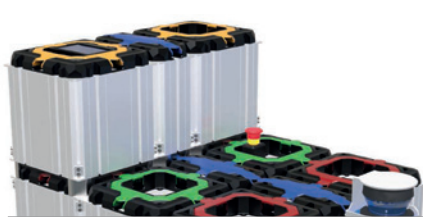


Design and build your own omni-directional industrial mobile robot in one afternoon

KELO ROBILE is a collection of modular industrial robotic components (bricks), which allow you in no time to design a mobile robot platform with the performance of an industrial robot. All bricks have standardized sizes (full brick: 230 mm x 230 mm or half brick: 230 mm x 115 mm) and can be connected in arbitrary configurations only with a set of fasteners and cables. KELO ROBILE supports a wide variety of designs ranging from minimal configurations for educational purposes to rapid prototypes of full-fledged professional mobile service robot applications. Initial configurations can be quickly changed and extended, once more budget becomes available or requirements change. KELO ROBILE is compatible and can be combined with aluminum system profiles (T-slot 8) from other manufacturers.

Key components:

- Active wheel:** 24 VDC / 20A (continuous), EtherCAT controlled drive unit supporting omnidirectional robot motion based on KELO Drive 105; payload per wheel: 125 kg
- Passive wheel:** Industrial Caster wheel (to support minimal configuration and increase payload capacity; payload per wheel 125 kg)
- Onboard CPU:** Powered by Intel NUC, 1 x EtherCAT master port, 4 x Ethernet ports, 2 x USB 3.0 ports, 1 x HDMI, 24 VDC in and out power ports
- Master battery and PMU:** 24V 512 Wh LiFePO4 battery, supports backup battery to increase capacity, EtherCAT slave communication port
- Graphical user interface:** 4.3 inch IPS display, capacitive touch screen, OS support for Android and Linux, Ethernet port, in and out power ports
- Sensor holder:** Universal adapter for different sensor mount (2D lidar, 3D lidar, RGBD)
- Software:** Configurable platform controller with velocity control (open source)



Advanced configuration: Omni-directional mobile robot with four active wheel bricks, a CPU brick with sensor holder, a battery and PMU brick, and a GUI brick. Payload: 500 kg



Minimal configuration: Single active wheel with sensor holder, two passive wheel bricks, a PMU and master battery, and an onboard CPU brick. Payload: 375 kg

KELO Robotics



Active wheel



Passive caster wheel



Onboard CPU



PMU & master battery



Graphical user interface



IEEE and RAS Diversity and Inclusion Initiatives

By Seth Hutchinson

In my September 2020 “President’s Message,” I wrote about personal responsibility for social justice in the context of our professional lives as roboticists, engineers, and scientists, focusing on the issues of diversity and inclusion. In this column, I focus on organization-level initiatives for diversity and inclusion at the IEEE and Society levels.

In 2019, under the direction of then IEEE President José Moura, IEEE created the ad hoc Committee on Diversity, Inclusion, and Professional Ethics (CDIE), whose charge included developing and implementing mechanisms to improve diversity and inclusion across the entirety of IEEE. The CDIE held discussions with

IEEE organizational units about their diversity and inclusion efforts, developed a mechanism for collecting and evaluating diversity data (including a new Diversity Dashboard), solicited recommendations from stakeholders, and proposed an action plan to the IEEE Board of Directors. In addition, the CDIE has formulated an IEEE diversity statement and is preparing a com-

prehensive report that will include new policies and initiatives, best practices, and comprehensive diversity data.

Significantly, it was acknowledged that the work of the CDIE was not that of a single year but requires an ongoing commitment by IEEE to embed these values into the culture of the organization. As a first step in this continual commitment, Toshio Fukuda (2020 IEEE president and roboticist) renewed the CDIE, and it is likely that one forthcoming recommendation will be the creation of a standing, permanent IEEE Committee on Diversity and Inclusion.

The IEEE Technical Activities Board—the part of IEEE that includes most IEEE Robotics and Automation Society (RAS) activities—has created its own standing Committee on Diversity and Inclusion (Table 401), whose charge includes

- developing strategies to increase the engagement of underrepresented groups
- ensuring inclusive recognition of achievements within IEEE
- identifying processes that are barriers to representation and inclusion
- continually suggesting improvements to existing policies and procedures.

Specific procedural changes have already been adopted, including mandatory training to recognize implicit bias for members of various award selection committees, revised guidelines to ensure diversity in award selection committees, and the adoption of a



diversity statement for the IEEE Awards Program. Even in its early stages, progress can be seen; for example, the 2020 Fellow class recorded the highest number of women ever, selected from a pool of nominees that also included the highest number of women ever.

The CDIE and Table 401 have also identified a set of best practices for Societies to promote diversity and inclusion, leveraging experience and insight from a broad collection of technical communities and synthesizing these into a set of actionable principles on matters such as Society governance, membership, awards, and conferences. This includes dozens of specific recommendations, ranging from high-level guidance (e.g., encourage a diverse pool of candidates for governance positions and attempt gender and geographical balance on all technical committees) to specific, pragmatic advice (e.g., offer childcare at conferences, hold unconscious bias trainings and awareness panels, and appoint a diversity and inclusion chair for each conference).

Within the RAS, a subcommittee of our Member Activities Board has spent the last year collecting data to evaluate our own progress toward diversity and inclusion. A preliminary version of its findings will be presented to our governing boards and to the RAS Administrative Committee during our Society Meeting Series held in conjunction with the 2020 IEEE/RSJ International Conference on Intelligent Robots and Systems. The goal is to educate our

Digital Object Identifier 10.1109/MRA.2020.3031777
Date of current version: 9 December 2020



Call for Award Nominations for the 7th Nagamori Awards

2021
NAGAMORI AWARDS
永守賞

Since motors appeared in the early 19th century, they have been used in all types of electrical appliances and are now an indispensable part of our daily lives. Today, a huge number of motors are used in a wide range of applications, and it is claimed motors account for more than 55% of the world's power consumption.

Therefore, motor research is extremely important if we are to maintain our affluent lives while also perpetually conserving the global environment.

We created these Nagamori Awards to bring vitality to technological research of motors and related fields, such as generators and actuators, and also to support the researchers and development engineers who strive each day to fulfill their dreams.

For more information, please visit:
<https://www.nidec.com/en/nagamori-f/>



S. Nagamori

● The 7th Nagamori Awards ●

Areas Covered : Technical fields related to motors, actuators and power generators, and their control methods, application technologies, etc.

Awards : Grand Nagamori Award - 5 Million Yen
Nagamori Award - 2 Million Yen

Application Period : November 01 2020 - January 31 2021

Contact information: Nagamori Foundation
Address: 338 Kuzetonoshiro-cho, Minami-ku, Kyoto 601-8205, JAPAN
Tel: +81-75-935-7731 E-mail: n.awards@nidec.com


To ensure lasting and meaningful change, it is essential to put into place well-founded policies and procedures.

leadership and solicit feedback (and, more importantly, volunteers) for our continuing efforts. My intention is to appoint an RAS ad hoc Committee on Diversity

and Inclusion at the conclusion of these meetings, which will be responsible for implementing existing recommendations and developing new programs and

policies going forward, with the long-term goal of creating either a standing committee or even a new RAS Diversity and Inclusion Board with its own vice president—the specific structure of which will be determined over the next year or so.

Although a great deal of volunteer time and effort has already been invested in improving diversity and inclusion within both IEEE and the RAS, these may seem to be only small steps, particularly when measured along the axis of visible change. I understand that the slow pace of progress can be

frustrating, particularly in times of global social unrest. Nevertheless, I believe that to ensure lasting and meaningful change, it is essential to put into place well-founded policies and procedures and rigorous structures that will withstand the capricious whims of changing public opinion and not depend solely upon the commitment and diligence of well-intentioned individuals. All of this requires considerable front-end work, work done by volunteers who are determined to effect positive social change. I encourage you to join our efforts! 

FROM THE EDITOR'S DESK *(continued from page 4)*

Not only will certain jobs disappear as a result of technology, the content of our jobs will also change. In such a rapidly transforming world, learning does not stop when schooling finishes. To prevent employees from missing the boat in this area, we must continue to encourage and support life-long learning in the workplace. Sadly, there are several cases where robotic systems violate our privacy or harm equality rights.

Robots are often made of rare-earth and/or difficult-to-access materials, which are used in their electronics and sensors (dysprosium and also gold), batteries (cobalt, which is mined by Congolese children), and motors (neodymium). Robots are also developed to mine, for example, the ocean floor, raising concerns among ecologists and biologists about the potential effect on fragile aquatic ecosystems. E-waste resulting from poor recycling (every year almost 50 million tons of technological scrap are produced, including tablets, computers, and smartphones) presents a danger to the environment because such waste contains elements

like cadmium, lead, antimony, nickel, and mercury. What will happen with future household and other service robots at the end of their life? Contrarily, robots are being developed to assist in the recycling process. Improving energy efficiency related to processing (both onboard and in the cloud) and actuators is also a relevant research topic.

In fact, we don't really know what the full impact of robotics will be. Studies take many different directions and are often based on guesswork. Rather than predicting the future, we will have to create it for ourselves. As a Society, we have a joint responsibility to work on these United Nations SDGs. Get informed about those goals, use this knowledge in your education, and persuade your university or company to take action. Our professional work experience and our skills and insights can make a catalytic impact in reaching them. Disseminate how your work impacts the SDGs and inspire others. Politicians, civil society, and trade unions will need to take sci-

entific studies as the basis related to drawing up guidelines that allow robots to be used in a way that creates a sustainable world.

This special issue aims to summarize the state of the art and disseminate current advances concerning the design optimization of soft robots. For example, with self-healing soft robots, damaged parts do not need to be thrown away or replaced, which suggests a goal for more sustainable robots. Or, as on this issue's front cover, a benthic-legged platform and soft continuum manipulator perform real-world underwater mission-like experiments. I would like to thank the guest editors: Surya Nurzaman (Monash University, Malaysia), Liyu Wang (University of California Berkeley), Fumiya Iida (University of Cambridge, United Kingdom), Jeffrey Lipton (University of Washington), Dario Floreano (Swiss Federal Institute of Technology, Lausanne, Switzerland), and Daniela Rus (Massachusetts Institute of Technology). Enjoy the issue!



Thoughts on Modeling

By Marwa ElDiwiny

Were there any directions you thought would work out very well, but empirical results proved otherwise? What is an area or direction of research you think is very promising even though the community seems to disagree or does not currently give much attention to? The answer is “modeling,” but is this statement still true for soft robots? Do we understand how soft robots behave and the most important aspects that should be considered in their design? First of all, there is no certain definition of *soft robots*—they could have a completely soft or a hybrid design. It is crystal clear that the field has limitations; for example, there is a tradeoff between mechanical performance and bandwidth, which leads to other questions: Do we have a deep understanding of how materials behave? What is the missing piece between Mother Nature and bioinspired soft robots?

Let me tell you that modeling is challenging. However, having a physical, descriptive model that captures the physics is essential for figuring out the most significant parameters for designing soft robots. I give the simple example of a smart soft actuator (an ionic electroactive polymer) that simultaneously works as an actuator and a sensor for stimulating a passive material (a catheter); see Figure 1. It turns out that thickness plays a significant role in the force produced and the actuator response time. What are the modeling scales? The scales are micro,

meso, and macro. Then the question becomes: Which modeling scale do we go for, taking into account that we are looking for a design recipe and real-time application? To answer this, the community seems to agree on the macro scale (or continuum scale).

I asked Prof. Carmel Maijdi from Carnegie Mellon University for his thoughts about modeling, “For enhancing the modeling and simulation of soft robotics, you can depend on data-driven models,” he said, emphasizing that there is still a need for deterministic modeling. He thinks there are interesting data-driven techniques and learning methods in a variety of contexts. There are diverse tools—including the Large-scale Atomic/Molecular Massively Parallel Simulator and the finite element method (FEM)—that are effective for modeling on different

scales. There have been many demonstrations of how the predictions generated using such tools agree with experimental measurements.

However, computational tools are quite slow. But Prof. Maijdi thinks that in soft robotics—when we want to use computational techniques and then loop them into controls, path planning, genetic algorithms, and thousands or hundreds of thousands of simulations to come up with a new design—there is a

We have to take a deeper look at designing descriptive models, taking into account the morphology of the dynamic shape.

(continued on page 77)

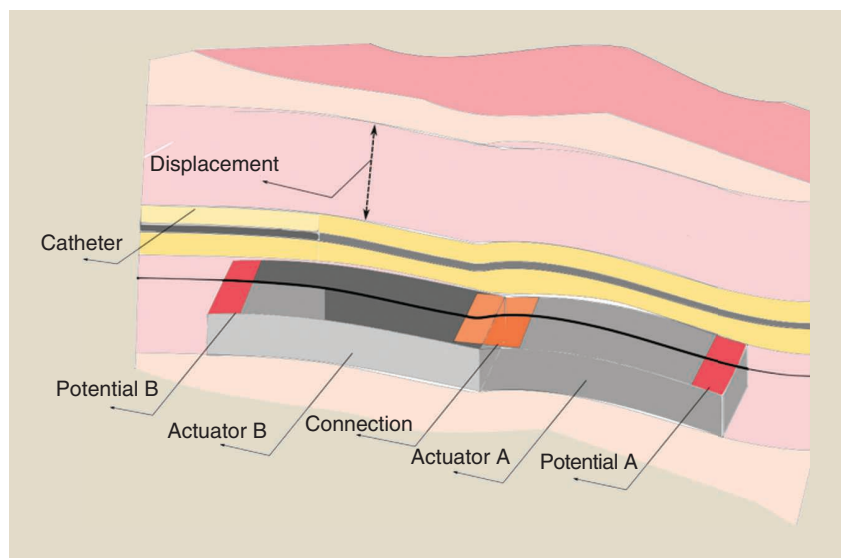


Figure 1. The design of the ionic electroactive polymer-actuating passive catheter.

Design Optimization of Soft Robots

By Surya G. Nurzaman, Liyu Wang, Fumiya Iida, Jeffrey Lipton, Dario Floreano, and Daniela Rus

The past few years have seen a significant increase in research activities that focus on the use of active or passive compliance in robotic systems. The emerging field, generally known as *soft robotics*, promises robotic systems that are safer, more resilient to damage, richly sensorized, and more adaptable than conventional rigid-bodied robots, emphasizing the importance of soft and deformable structures. Several unique aspects can characterize soft robotic systems, such as their elastic and deformable bodies, the large number of degrees of freedom, the viable use of unconventional material, the involvement of intrinsic passive mechanical dynamics, and the display of proprioception and exteroception.

The last few years have also seen the emergence of a modern view of intelligence, known as *embodied intelligence* or *morphological computation*, that leverages the properties of soft robots. Embodied intelligence emphasizes the importance of the codesign, or coevolution, of the brain (controller) and morphology (shape, size, and materials) of a machine to best fit the environment in which it operates. From the perspective of this view of intelligence, optimizing the design of the soft robot is, therefore, of great importance. Such design optimization can be led by machines and/or humans, or it can take inspiration from the coevolutionary processes of biological systems.

The goal of this special issue is to provide an overview of the state of the art in the design optimization of soft robots and identify common perspectives and challenges, shared scientific goals, and high-impact applications. The accepted articles were carefully selected for novelty, thoroughness, and clarity.

In the first article, Liu et al. present an integrated mobile benthic platform and a soft manipulator that can be used for seafloor exploration, marine samples collection, and other underwater tasks. The benthic platform consists of a six-legged, crab-inspired robot, and the manipulator consists of a four-fingered soft gripper that can perform delicate grasping. Both systems are designed and optimized separately to serve as general-purpose underwater robots with locomotion and manipulation capabilities. The benthic platform is designed to have a payload for instruments, sensors, or a robot arm, and the soft arm is designed to be mounted on underwater vehicles. Based on the integrated platform, the authors experimentally employ spatial manipulation with inverse kinematics specifically for collecting tasks in a natural underwater environment. They show that the soft manipulator's workspace can be significantly extended by adding a benthic legged robot as a mobile base. Furthermore, they find that the designed system can approach objects precisely and effectively and perform dexterous grasping tasks, including retrieving objects from deep apertures in overhanging environments.

In the second article, Chen and Wang provide a comprehensive review of the state of the art in the design of soft robots. They refer to "design optimization" as the broad innovations in any design aspect that lead to better performance by soft robots, including algorithms for solving a formulated mathematical problem related to design. The survey considers the design optimization of soft robots as a process to improve material/structure and properties/performance relations. The article not only covers nearly 100 references in modeling, simulation, and computational optimization but, more importantly, also connects them in a much more detailed manner than previous surveys have. For example, the article categorizes geometry, material, and actuation as the three areas where design variables may be identified for modeling soft robots, with the acknowledgment that the boundaries between those variables may change. It also describes simulation methods based on spring-mass models, finite elements, kinematic geometric transformation, and a nonsmooth Newton approach. Finally, the authors provide a high-level comparison of optimization methods, including gradient-based algorithms, evolutionary computation, and bio-inspired design. In the end, the survey identifies three main challenges in the design of soft robots.

- 1) Present models are usually simple, restrictive, and customized for a particular class of tasks, providing only limited insights into design problems.
- 2) An effective, efficient, and robust simulation tool that allows rapid

performance evaluation of a design candidate is lacking.

3) Reliable and robust optimization algorithms are yet to be developed.

It also highlights four areas where future work may be done by modeling material and robot dynamics, simulation, and optimization algorithms.

In the third article, Terryn et al. present a healable soft gripper and soft hand whose flexible membranes are composed of Diels–Alder polymer networks. The authors argue that soft robotic actuators based on their approach are able to recover their performance after severe damage at room temperature without the need for an externally applied stimulus. They also argue that this healing ability can help reduce the over dimensioning of systems and optimize designs based on function instead of on potential damaging conditions. The healing process can take seconds or up to a week, depending on the location and extension of the damage. As an extreme case, after cutting the actuator in two parts, it took seven days to heal without the need for any external heat stimulus, and the actuator performance recovered, too.

Next, Pagoli et al. present the design optimization of a robotic finger with a sliding, rotating, and soft bending mechanism. The novelty of the mechanism is its potential larger workspace compared to prior robots with soft appendages. The finger can rotate 300° about its axis, and the mechanism consists of three actuators: two stepper motors for sliding and rotating motion along the longitudinal axis and an air pump for bending. The design optimization relies on the nondominated sorted genetic algorithm II to find optimal values for seven geometric parameters of the soft joint and thus maximize the bending angle and minimize joint dimensions (i.e., length and diameter) under a given pressure. A prototype fabricated after the optimal design is evaluated for different bending angles and tip forces.

Finally, Lee et al. propose the design of pouch motors with geometric constraints that result in versatile and repeatable patterns of bending deformations with a

controllable force. The pouch motors rely on the inflation of thin hollow pockets instead of material stretching. The authors describe a system of four pouch motors with geometric constraints allowing the actuator to produce a programmable bending deformation. They suggest that the proposed pouch pattern can be adapted to both soft robotic fingers and soft robotic joints. To demonstrate the efficacy of their approach, they assembled a soft robotic arm with three degrees of freedom and show that it can perform pick-and-place operations and change its stiffness for safe operation around humans. They also build a larger soft robotic gripper for grabbing larger objects.

We hope that the articles presented in this special issue provide new or better insights in the field of soft robot design and inspire the design of a new generation of adaptive, compliant, and reliable soft robots.

Surya G. Nurzaman, Monash University, Malaysia. Email: surya.nurzaman@monash.edu.

Liyu Wang, University of California Berkeley. Email: liyu.wang@wadh.oxon.org.

Fumiya Iida, University of Cambridge, United Kingdom. Email: fi224@cam.ac.uk.

Jeffrey Lipton, University of Washington, Seattle. Email: jilipton@uw.edu.

Dario Floreano, Swiss Federal Institute of Technology, Lausanne. Email: dario.floreano@epfl.ch.

Daniela Rus, Massachusetts Institute of Technology, Cambridge. Email: rus@csail.mit.edu.



Butterfly Haptics



Magnetic Levitation Haptic Interfaces



Highest fidelity interaction
for teleoperation and virtual
environments

<http://butterflyhaptics.com>

Underwater Mobile Manipulation

A Soft Arm on a Benthic Legged Robot

By Jiaqi Liu, Saverio Iacoponi, Cecilia Laschi, Li Wen, and Marcello Calisti

Robotic systems that can explore the sea floor, collect marine samples, gather shallow water refuse, and perform other underwater tasks are interesting and important in several fields, from biology and ecology to off-shore industry. In this article, we present a robotic platform that is, to our knowledge, the first to combine benthic legged locomotion and soft continuum manipulation to perform real-world underwater mission-like

experiments. We experimentally exploit inverse kinematics for spatial manipulation in a laboratory environment and then examine the robot's workspace extensibility, force, energy consumption, and grasping ability in different undersea scenarios.

A six-legged benthic robotic platform, the Seabed Interaction Legged Vehicle for Exploration and Research, Version 2 (SILVER2), acted as the soft manipulation system's mobile base. The results show that the soft manipulator's workspace can be significantly extended by adding a benthic legged robot as a mobile base. We show that this system can precisely

Digital Object Identifier 10.1109/MRA.2020.3024001

Date of current version: 7 October 2020



©SHUTTERSTOCK/KATHERINE WALLIS

and effectively approach objects and perform dexterous grasping tasks, including retrieving objects from deep apertures in overhang environments. This robotic system has the potential to scale up to make shallow water collection tasks safer and more efficient.

Deep Sea Challenges

Oceanic exploration is considered a frontier for understanding our planet and its changes, searching for new resources, sustaining populations, and even discovering novel medical therapies. At present, however, less than five percent of our oceans has been thoroughly explored. Oceanic exploration can be costly, dangerous, impractical, and logistically challenging [1]. During recent years, demand for robots capable of underwater exploration and manipulation has grown immensely and is expected to continue to increase during the coming decades. Researchers and marine enterprises require reliable and low-cost underwater robots to unveil the mysteries of the oceans and boost the so-called blue economy [2].

Underwater Mobile Manipulation

The two main categories of underwater robots are remotely operated vehicles (ROVs) and autonomous underwater vehicles (AUVs). ROVs are usually employed for interaction tasks, with manipulators mounted to the main frame to facilitate remote operation. This subcategory of ROVs, known as the *underwater vehicle–manipulator system (UVMS)*, is essentially a mobile robot that performs so-called floating manipulation [3]. This complex task requires a shared controller between the operator and the vehicle: high-level requests from the operator to hold a position or interact with an object are transformed into an actuator command for a vehicle's thrust and manipulation systems. But optimal UVMS performance is challenged by the mathematical complexity of the robotic system, imprecise modeling of thruster dynamics, limited sensing capabilities, and harsh and rapidly changing environmental conditions [4]. Researchers have devoted considerable attention to improving the floating manipulation and control of UVMSs during recent years. In simulations [5], undisturbed swimming pools [6], and pools with a current-like disturbance, researchers have demonstrated control capabilities that have errors on the order of a few centimeters. Despite these promising results, most ROVs still need to rest on the seafloor for stability when manipulation is required [7].

Another class of underwater vehicles, called *benthic crawlers*, facilitates interaction with underwater structures, without increasing control complexity, by maneuvering on the seabed via tracks and wheels. They are routinely used for heavy work duties, shallow water investigations, and long-term monitoring despite the fact that they are limited to substrates where tracks and wheels can be used [8]. A few recent examples of legged benthic robots, developed to withstand high currents [9], [10], move across uneven

terrain [11], operate without disturbing the environment [12], and work in shallow water, promise to integrate the advantages of benthic crawlers with the dexterity of legged robots. With legged systems, researchers envision the possibility of precise and swift seabed interaction without the added complexity of controlling underwater stability. In addition, improved visibility can be achieved by the benthic crawler's legs (compared to propellers) while performing locomotion on sandy substrates. The actions of propellers often raise sand particles, which can reduce visibility; in our case, precise and slow positioning of the legs could prevent this from happening.

Underwater Soft Manipulation

A robot's manipulator system is another essential component to facilitate optimal underwater performance. Traditional underwater hydraulic robotic arms and grippers are designed for missions with heavy payloads and high levels of force [13]. These metal components are poorly suited for grasping fragile and squishable objects. Additionally, a massive metal arm has a large inertia, making underwater mobility challenging for a robot in unsteady conditions. Soft materials and bioinspired structures have immense potential to integrate flexible, lightweight elements into manipulators to reduce the mass and decrease the chance of damaging fragile objects. For example, previous work on an octopus-inspired soft arm achieved tethered motion under water [14], and a dexterous subsea hand [15] has been tested as a gripper. More recently, studies on soft robotic manipulation have begun to focus on underwater applications [16], [17], a silicone–rubber gripper [18], a modular soft robotic wrist [19], a dexterous glove-based soft arm [20], and a jamming gripper [21] have all been tested to grasp delicate underwater organisms at shallow-to-deep-sea depths. Thus, a soft manipulator—a combination of a soft arm and a gripper—may be a practical tool for real-world mobile underwater manipulation.

In this article, we investigate, for the first time, an integrated mobile benthic platform and a soft manipulator (Figure 1). For the benthic platform, we use SILVER2 [22], a six-legged, crab-inspired robot developed for exploration and environmental monitoring. For the manipulator, we use a soft device with a four-fingered soft gripper that can move in a 3D domain and perform delicate grasping. We experimentally employ spatial manipulation with inverse kinematics specifically for collecting tasks in a natural underwater environment. Both systems have been separately designed and

Demand for robots capable of underwater exploration and manipulation has grown immensely and is expected to continue to increase.

optimized to serve as general-purpose underwater robots with locomotion and manipulation capabilities, respectively. SILVER2 was designed to have payload capacity for instruments, sensors, and a robot arm. The soft arm was planned to be mounted on underwater vehicles in a general way, and it fits SILVER2, as well. The possibility of integrating these two robots offers unique opportunities for testing each system and showing the benthic operation of robots. We hypothesize that fusing a benthic platform and a soft manipulator will combine the advantages of both innovative solutions for underwater operations.

Experimental Platform

The SILVER2 platform has several promising features, including efficient aquatic walking ability, underwater self-stabilization, and functional payload capacity for supporting the soft arm. SILVER2 was previously introduced

in [12] and is briefly reviewed here for the necessary context. It consists of a central body with six articulated legs. The body is an open frame structure composed of two vertical plates connected by horizontal beams. Two main canisters (pressurized cylinders) mounted on the frame contain the battery pack (with a 300-Wh lithium polymer battery) and all the electronic components of the system (excluding cameras and actuators), respectively. A third auxiliary canister, with a transparent dome and two cameras, is attached to the front. The cameras are fixed to an actuated gimbal with two degrees of freedom (DoF). Floating foam and weights are attached to the frame to balance the system and obtain a weak negative buoyancy. Extra weights can be added to achieve a desired wet weight, depending on the nature of the mission. In the present study, the wet weight of the robot, including the manipulator, was 4.4 kg.

Each leg is composed of two links and three actuators. The links are square aluminum bars, and each actuator is encapsulated in its own dedicated canister. The first actuator (the coxa motor) controls the yaw [q_1 in Figure 2(a) and (b)] of the leg compared to the main body and is fixed to the main frame. The second actuator (the femur motor) is mounted close to the first and attached to the shaft of the first through an aluminum connector. The second and third actuators (the tibia motor) move the two-leg segments on the vertical plane [with angles q_2 and q_3 , as shown in Figure 2(c)]. The second segment is connected to the third actuator shaft through a torsional elastic joint that is tuned to achieve the behavior predicted by the underwater spring-loaded inverted pendulum (USLIP) model, as in previous multilegged implementations [11]. The elastic joint and the third actuator form the serial elastic actuator (SEA) of the leg [23].

SILVER2 is capable of static and dynamic locomotion. Static gaits are preprogrammed walking cycles for which the operator can choose the direction, speed, and other parameters. Dynamic locomotion is based on a hopping gait according to USLIP dynamics [24]. The operator can select key locomotion parameters on a computer, and self-stabilizing open-loop cycles ensure terrain negotiation. Due to the short distance required for the present analysis, only static walking gaits were employed. Each of the second segments of SILVER2's legs has a foot. A foot consists of an encapsulated piezoelectric disk and a hammer-hinge mechanism that compresses the piezoelectric component on contact with the ground, which sends a signal to the electronics canister. All canisters are connected with flexible underwater wires and penetrators.

A cable connects the platform to a floating buoy equipped with a Wi-Fi antenna to connect the operator and SILVER2. For all the present tests, a mechanical interface component was added to enable the addition of the soft arm. The arm was fixed at the top left of the structural frame. An additional underwater camera was mounted on the top right to provide visual feedback for the arm's operator.

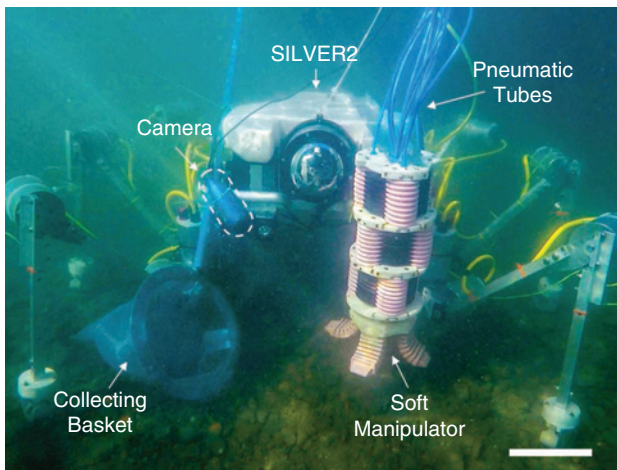


Figure 1. SILVER2 and its soft manipulator collecting a plastic bottle from the seabed. Scale bar: 15 cm.

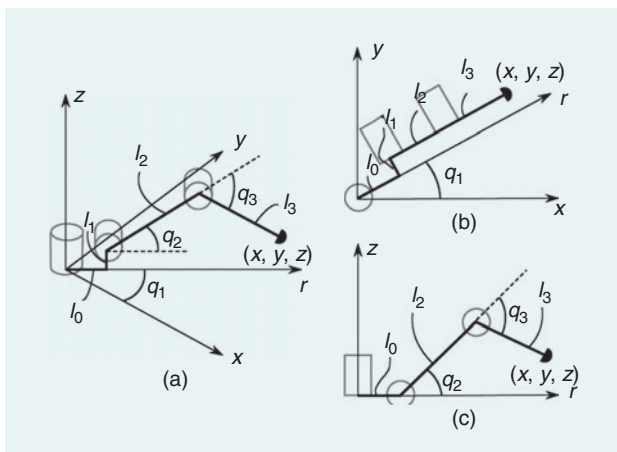


Figure 2. SILVER2's leg kinematics. (a) One leg's geometries, with a reference frame centered on the shaft of the coxa motor. All motors are represented as shadowed cylinders. Auxiliary views are reported in (b) and (c). Plane (r, z) in (c) is also called the *coxa plane*: its orientation around the z -axis is given by q_1 , while the leg's position within the coxa plane is defined by angles q_2 and q_3 .

SILVER2 Kinematics

For convenience, this section briefly summarizes SILVER2's kinematics and control; for further details, consult [12]. Using Figure 2(a)–(c) as a reference, the (x, y, z) position (see Figure 2 for the notation) of a SILVER2 leg is derived from direct kinematics:

$$\begin{cases} x = (l_0 + l_2 \cos q_2 + l_3 \cos(q_2 - q_3)) \cos q_1 - l_1 \cos q_1 \\ y = (l_0 + l_2 \cos q_2 + l_3 \cos(q_2 - q_3)) \sin q_1 - l_1 \sin q_1 \\ z = l_2 \sin q_2 + l_3 \sin(q_2 - q_3). \end{cases} \quad (1a)$$

Angles are retrieved by inverse kinematic equations:

$$\begin{cases} L = \sqrt{x^2 + y^2} \\ \beta = \text{atan2}(y, x) \\ \gamma = \text{atan2}(l_1, \sqrt{L^2 - l_1^2}) \\ r = L \cos(\gamma) - l_0 \\ m = \sqrt{r^2 + z^2} \\ q_1 = \beta - \gamma \\ q_2 = \text{acos}\left(\frac{l_2^2 + m^2 - l_3^2}{2l_2 m}\right) + \text{atan2}(z, r) \\ q_3 = \pi - \text{acos}\left(\frac{l_2^2 - m^2 + l_3^2}{2l_2 l_3}\right), \end{cases} \quad (1b)$$

where l_0 and l_1 are the lengths of an L-shaped connecting element that links the coxa motor to the femur motor and the first segment of the leg, l_2 . Eventually, link l_3 connects the knee of the leg to the foot. The DoF are the angular quantities q_1, q_2, q_3 and L, β, γ, r , and m denotes simple auxiliary geometrical quantities that are easily derived from Figure 2(a)–(c). In Figure 2, r is an auxiliary axis that defines the plane of the second and third segments of a leg. Since this plane is defined by the coxa angle q_1 , we refer to it as the *coxa plane*. The femur and tibia motors move the leg within the coxa plane (r, z) , as shown in Figure 2(b). (The femur and tibia actually belong to a plane parallel to the coxa plane since segment l_1 produces a normal translation.)

By exploiting the relationships in (1a) and (1b), we implement a walking gait as linear trajectories (stance phases) followed by arcs (gliding phases) executed continuously by all the feet [see Figure 2(b)]. Feet trajectories are defined by two parameters: the elevation of the arc z_f and the linear distance on the ground d_f . Additional parameters can be selected to define different gaits, such as the elevation of the body from the ground, the width of the stance, the period required to execute the foot trajectory, the phase difference among leg activations, the duty factor of the walking motion, and the walking direction [12].

Soft Manipulator Kinematics

The soft manipulator is designed and fabricated for underwater grasping; its structure is shown in Figure 3. It primarily consists of three soft actuator modules and one soft gripper as

the end effector and also has 10 pneumatic chambers there are three bending segments, and each has three chambers. The end effector four-fingered soft gripper is actuated by a single air inlet. The soft actuator modules and the soft gripper are modularly assembled by 3D-printed connectors and universal pneumatic joints. The soft manipulator is 435 mm in length (the soft arm is 310 mm, and the gripper is 125 mm) and 48 mm in diameter, with a total mass of 2,050 g in the air (210 g in water).

The inverse kinematics of soft continuum robots have attracted researchers' attention for a long time [25]–[27]. Here, we propose a rapid inverse solution based on the opposing actuation pattern [28]. We positioned the second soft actuator module to be a mirror image of the first segment. This optimized design simplifies the inverse kinematics modeling: by actuating opposite chambers in the first two segments, the segments generate the same curvature but in opposite directions, thus forming a sigmoidal “S” shape [Figure 3(a)]. Because of this structural design, the attitudes of the two bending segments are directly related. As a result, solving the inverse kinematics of a soft manipulator with opposing bending curvature requires computing only geometric functions when modeling the whole manipulator, so less computation time and fewer hardware resources are necessary. This actuation coupling reduces the modeling complexity of the soft manipulator.

When solving the inverse kinematics, we resolve the transformation from the given end effector coordinate $\{x_3, y_3, z_3, \theta_3, \varphi_3\}$ to chamber length $\{l_{ij}\}$, then to chamber pressure $\{p_{ij}\}$, where the transformation is from the task space to the joint space, and, finally, to the actuation space. More specifically, $\{p_{ij}\}$ represents the pressure within the chambers, and $\{l_{ij}\}$ indicates the chamber lengths, where, for p_{ij} and l_{ij} , the indexes $i = 1, 2, 3$ and $j = 1, 2, 3$ refer to the i th segment and the j th chamber. In addition, the initial length of the chambers $\{l_{ij \text{ int}}\}$ and constant parameter d could be measured before initiating actuation.

The constraints of our kinematics modeling were

$$\begin{cases} \theta_1 = \theta_2 \\ \varphi_1 = \varphi_2 + \pi \\ r_1 = r_2 \\ l_{1i} = l_{2i} \quad (i = 1, 2, 3). \end{cases} \quad (1c)$$

As discussed previously, the manipulator has five DoF in coordinate space $\{x_3, y_3, z_3, \theta_3, \varphi_3\}$ and six independent chambers $\{l_{11}(l_{21}), l_{12}(l_{22}), l_{13}(l_{23}) \text{ and } l_{31}, l_{32}, l_{33}\}$. To obtain the chamber lengths (six outputs) from the coordinates (five inputs), we implement another constraint condition for the inverse kinematics: at most, two chambers in the third segment are actuated at the same time, and at least one chamber in the third segment remains at its initial length.

With this constraint, the first step of this approach is determining which chamber of the third segment should not be actuated. Based on the geometric relationship shown in

Figure 3(c) and (d), we developed an equation that represents the initial lengths regarding the arc parameters $\{r_3, \varphi_3, \theta_3\}$:

$$\left\{ \begin{array}{l} l_{31\text{int}} = \theta_3 \cdot r_{31} = \theta_3 \cdot (r_3 - d \sin \varphi_3), \\ \quad \text{if } \frac{\pi}{6} \leq \varphi_3 < \frac{5\pi}{6} \\ l_{32\text{int}} = \theta_3 \cdot r_{32} = \theta_3 \cdot \left[r_3 + d \cos \left(\varphi_3 - \frac{\pi}{6} \right) \right], \\ \quad \text{if } \frac{5\pi}{6} \leq \varphi_3 < \frac{3\pi}{2} \\ l_{33\text{int}} = \theta_3 \cdot r_{33} = \theta_3 \cdot \left[r_3 - d \cos \left(\varphi_3 + \frac{\pi}{6} \right) \right], \\ \quad \text{if } \frac{3\pi}{2} \leq \varphi_3 < 2\pi \text{ or } 0 \leq \varphi_3 < \frac{\pi}{6}. \end{array} \right. \quad (1d)$$

By combining the given end effector coordinate $\{x_3, y_3, z_3, \theta_3, \varphi_3\}$ and (1d), we can obtain the value of r_3 and θ_3 . Then, based on the geometric relationship shown in Figure 3(a), we developed another equation from the given coordinates:

$$\left\{ \begin{array}{l} x_1 = \frac{x_3 - r_3(1 - \cos \theta_3) \cos \varphi_3}{2} = r_1(1 - \cos \theta_1) \cos \varphi_1 \\ y_1 = \frac{y_3 - r_3(1 - \cos \theta_3) \sin \varphi_3}{2} = r_1(1 - \cos \theta_1) \sin \varphi_1 \\ z_1 = \frac{z_3 - r_3 \sin \theta_3}{2} = r_1 \sin \theta_1. \end{array} \right. \quad (1e)$$

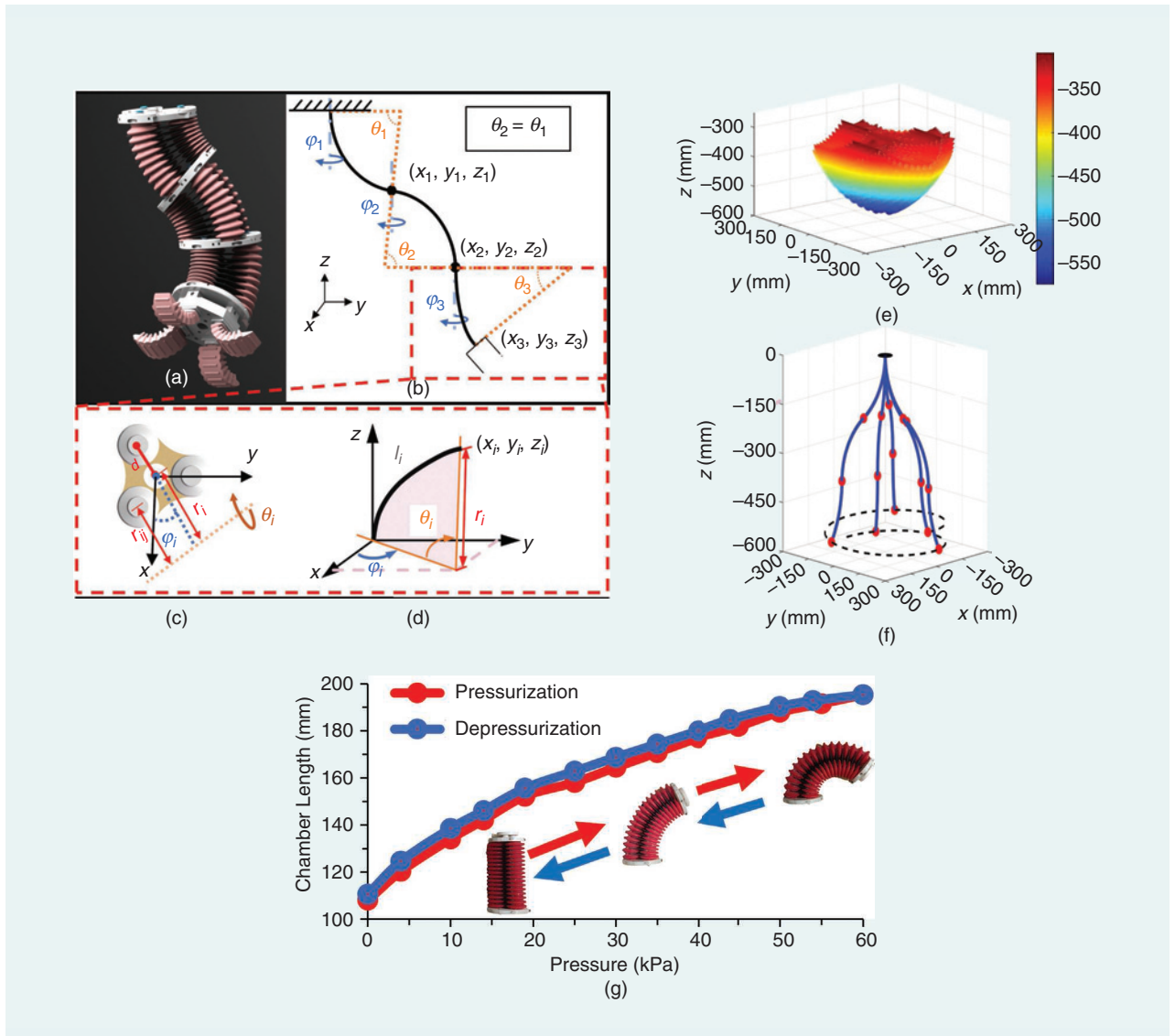


Figure 3. (a) A digital rendering of the soft manipulator. (b) A schema of the soft manipulator. (c) The geometric schematic of the bending segment of the constant-curvature soft manipulator. (d) The geometric functions in a bending segment, where φ_i is the deflection angle around the z -axis, θ_i is the curvature angle around the y -axis, and r_i is the curvature radius. (e) The simulated workspace of the soft manipulator. (f) The programmed trajectory paths based on the inverse kinematics method. Dashed lines indicate the helical-shaped trajectory, red dots denote the connection between chambers, and blue curves represent the time histories of soft arm movements during the tracking process. (g) The chamber lengths of the bending segments as a hysteretic function of the actuation pressure (0–60 kPa) in pressurization (red) and depressurization (blue).

In (1e), only r_1 , φ_1 , and θ_1 are unknown. Combining (1d) and (1e) enables r_1 , φ_1 , and θ_1 to be analytically solved. Next, the calculated arc parameters $\{r_i, \varphi_i, \theta_i\}$ provide all the chamber parameters $\{l_{i1}, l_{i2}, l_{i3}\}$:

$$\begin{cases} l_{i1} = \theta_i \cdot (r_i - d \sin \varphi_i) \\ l_{i2} = \theta_i \cdot \left[r_i + d \cos\left(\varphi_i - \frac{\pi}{6}\right) \right] \\ l_{i3} = \theta_i \cdot \left[r_i - d \cos\left(\varphi_i + \frac{\pi}{6}\right) \right]. \end{cases} \quad (1f)$$

Thus, we obtained a specific inverse transformation from $\{x_3, y_3, z_3, \theta_3, \varphi_3\}$ to $\{l_{11}(l_{21}), l_{12}(l_{22}), l_{13}(l_{23}), l_{31}, l_{32}, l_{33}\}$. Adding a calibrated pressure length relationship [Figure 3(e)] enables us to calculate the driving pressure $\{p_{i1}, p_{i2}, p_{i3}\}$ from the chamber length $\{l_{11}(l_{21}), l_{12}(l_{22}), l_{13}(l_{23}), l_{31}, l_{32}, l_{33}\}$ to complete the model-based control.

Considering the influence of the rigid interface and buoyancy in the underwater environment, laboratory tests were carried out to compensate for the angle loss by adding a pneumatic pressure offset for each chamber to ensure that the opposite-bending S shape is maintained. In the calibration process, we use a parameter a to adjust the air pressure in the bending segments,

$$p_{1j} = a \cdot p_{2j} + b, \quad (1g)$$

where p_{1j} is the pressure of the j th chamber in segment 1 and p_{2j} is the pressure of the j th chamber in segment 2. This equation is fitted with the experimental calibration. The experiment suggests, that when $a = 1.02$ and $b = -0.89$ (linear fitting $R^2 = 0.9996$), (1g) works for the pneumatics actuation. As a result, the first and second segments of the soft manipulator achieve the expected orientation, i.e., the S-shape bend.

The simulated workspace of the manipulator is displayed in Figure 3(f). The result shows that the manipulator can operate within a 3D space with a length of 500 mm, a width of 520 mm, and a height of 304 mm. The soft manipulator is actuated and controlled via the multichannel pneumatic control system presented in Figure 4. This system generates a separate pressure for all 10 pneumatic chambers, according to the inverse kinematic model. This system was offboarded and above water during all tests. Pneumatic tubes connect the system and the soft manipulator.

Experimental Protocols

We experimentally verified our system through a bottom-up approach that ended with mission-like trials. Protocols from A to C tested specific capabilities—the manipulator’s force and precision—that could be compared with state-of-the-art results from traditional underwater robots. We further confirmed the system’s effectiveness through two additional protocols, D and E, which aimed to 1) collect varied and fragile objects from the seabed and 2) manipulate objects in confined spaces, respectively. All experiments were performed in real shallow water mission conditions in the Tyrrhenian Sea,

on the seabed at a specific depth of roughly 1.2 m, and all tests were repeated at least five times.

Force Protocol

The first protocol aimed to measure the maximum pulling forces generated by SILVER2 and the soft arm system [Figure 5(a)]. Similar to conducting a vertical bollard pull, only static vertical pulling forces were measured in this study. For all tests, a hemispherical rubber handle was fixed close to the ground. The handle was attached to a load cell connected vertically to a plate. The plate was firmly anchored to the seafloor by a substantial amount of lead weight. The load cell was then connected to a force gauge (PCE_FM1000). For each test, the robot was manually positioned above the handle to ensure the vertical alignment of the arm and the correct gripper position. The test was interrupted when the maximum force value was reached or when the gripping failed. The highest force value was then recorded.

Since the robotic system can generate pulling force by either actuating the arm or extending the legs, we tested different configurations to highlight different capabilities. In configuration A, we measured the pulling force of the legs alone. The gripper was actuated to hold the handle, and then the legs were quickly extended (~ 200 mm/s) to generate a pulling force. In configuration B, we measured the maximum pulling force of the arm alone (~ 50 mm/s) while SILVER2 maintained a static position. In configuration C, we measured the interaction of the two main systems: the gripper grasped the handle, and the arm and the legs jointly performed a pulling action. In configuration D, we replicated the configuration

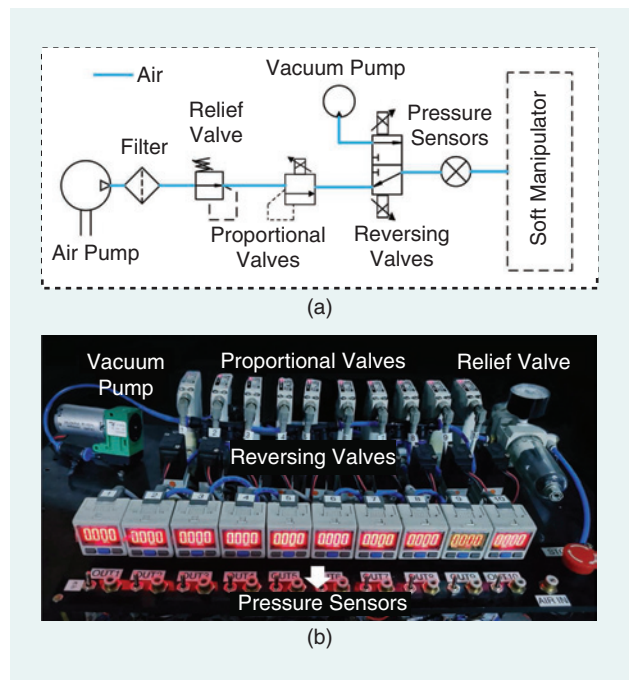


Figure 4. The multichannel pneumatic control system for the soft manipulator. (a) The framework of the system. (b) The hardware of the system, which contains a vacuum pump, 10 proportional valves, and 10 air pressure sensors.

A design but with the legs extending slowly (~50 mm/s). Finally, in configuration E, we connected SILVER2, without the arm, directly to the handle with a not-extensible wire. SILVER2's movements were monitored by an operator, and the arm movement was controlled with a camera mounted on the SILVER2 platform itself.

Workspace Protocol

The workspace protocol focused on measuring the enlargement of the manipulator workspace when it was mounted on SILVER2. In this protocol, SILVER2 and the manipulator grasped an object from a lower platform and released it in a target area at a height of 37 cm [Figure 5(b)]. The test consisted of two steps: first, SILVER2 was placed in front of

the platform, and the soft manipulator grasped the object from the lower platform. Second, SILVER2 extended its legs without walking, and the manipulator executed several movements (~50 mm/s) to release the object at the target location. Specifically, the legs were elongated to gain approximately 20 cm in the vertical direction. Releasing the object on the target could be considered a success. The error was measured as the distance between the center of the object and that of the red, circular target. We also tested the performance of the soft manipulator without SILVER2. We placed the soft manipulator alone in the water tank and performed the same soft manipulator routine: moving an object from the bottom of the target area. Then, we measured the maximum height of the target area to which the soft manipulator could reach and release the object.

Mobile Pick-and-Place Protocol

This protocol [Figure 5(c)] was used to measure the performance of the whole system in a typical mobile manipulation task. It enabled us to estimate the precision and effectiveness of the combined SILVER2-manipulator arm system. The test began with the arm grabbing the target object (a shell) and lifting it from the platform. Then, SILVER2 initiated a lateral walking gait (~150 mm/s) to reach the target zone, which was 2 m from the starting point. Once the target was within the workspace of the arm, the arm was actuated to place and release the object onto the target plate. The system's performance was evaluated by measuring the distance between the center of the object and that of the red circle for each trial. Releasing the object on the target plate could be considered a success.

Collecting Litter and Objects

With this protocol, we aimed to qualitatively assess the system's performance during a typical collection mission, either to perform seabed cleaning or retrieve a fragile biological specimen. The selected test objects were a hard silicone seashell; an eggshell, which simulated a fragile biological specimen; and three pieces of common trash found on the seabed: a plastic shopping bag, a plastic bottle (0.5 L), and a nylon fishing net (400 cm²). Additionally, the net was tested in an entangled condition: a small rock (0.35 kg) was

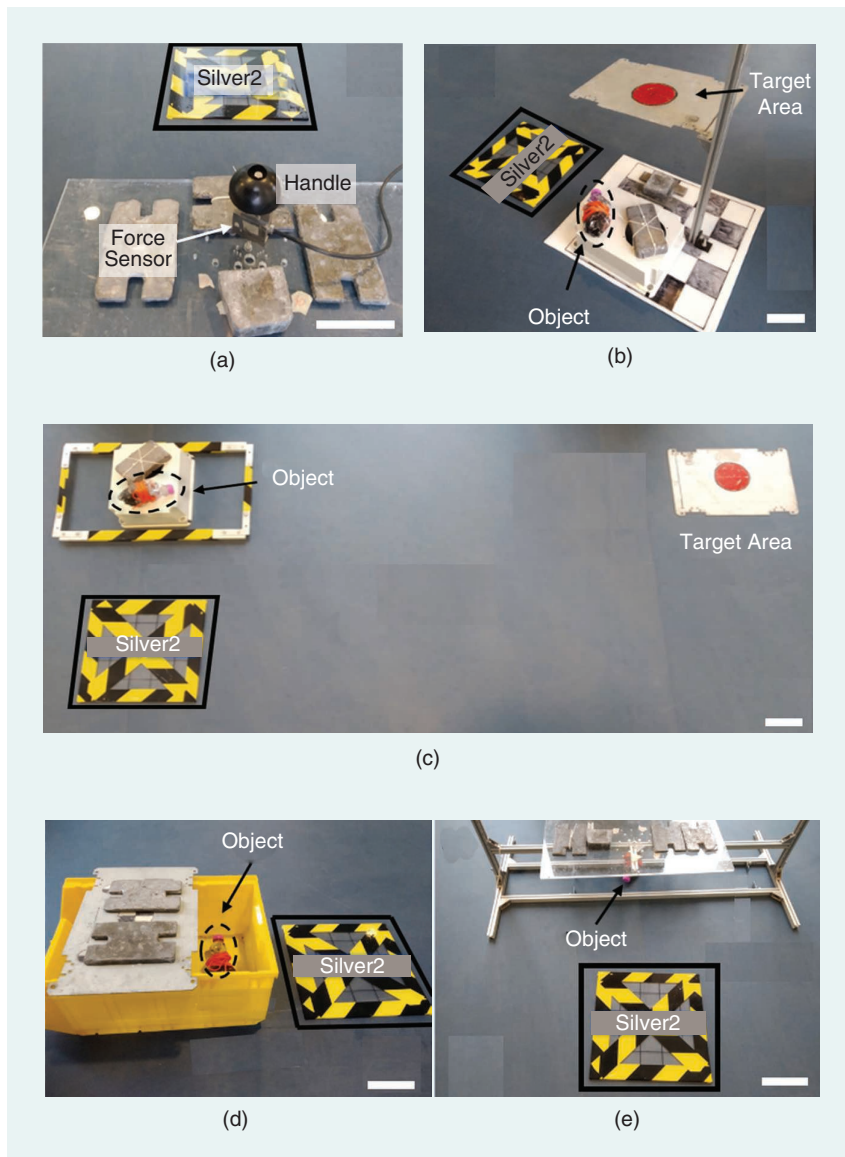


Figure 5. The experimental setup for different protocols conducted on the seafloor (depicted here as a dry environment for demonstration purposes). The (a) force protocol, (b) workspace protocol, (c) mobile pick-and-place protocol, and (d) and (e) confined environment protocol. The robot's initial position is represented by a labeled square. Scale bar: 15 cm.

positioned directly in the middle of the net and placed onto the seabed.

The system's performance was evaluated by verifying whether the equipment was capable of completing the task. As is shown in Figure 6, the following steps were carried out and evaluated.

- 1) *Approaching the object*: The system should move roughly 2 m until the object is within the arm's workspace.
- 2) *Grasping the object*: The arm should retrieve the object from the seabed and firmly hold it against hydrodynamic disturbances.
- 3) *Releasing the object*: The gripper should be able to open its fingers to allow the object to fall freely.
- 4) *Collecting the object*: The target object should be stored in the side-mounted basket.

Collecting Objects in Confined Spaces

In this protocol, we investigated whether our soft manipulator could retrieve objects from confined spaces and whether its light weight and compliance would be beneficial for underwater manipulation. Two tests were carried out to estimate the performance of the manipulator in a confined underwater environment. The first focused on collecting objects from a half-open box [Figure 5(d)]. The object and a real-time underwater camera (transmitting images via cables) were placed on the bottom of the box, and half of the box was then covered by a metal plate. The grasping task was executed in three steps:

- 1) SILVER2 was placed in front of the box, with the manipulator fully contracted, and it extended its legs to ensure that the manipulator was above the box.
- 2) SILVER2 lowered its legs, and the manipulator was able to reach into the box.
- 3) The manipulator grasped the object via the arm inverse kinematics model and took the article out of the box.

The performance during this test was evaluated by measuring the length of the opening area and verifying whether the system successfully grasped and collected the object.

The second test was carried out to collect objects from a simulated overhang environment [Figure 5(e)]. A transparent plate was fixed to a frame to create an overhang barrier, and the object was placed on the seabed. The grasping task consisted of two steps:

- 1) SILVER2 was placed in front of the frame, with the soft manipulator fully contracted.
- 2) The manipulator grasped the object using the soft arm (via the inverse kinematics model) and took the object from beneath the overhang.

The system's performance was evaluated by measuring the height of the plate and verifying whether the manipulator successfully grasped and collected the object.

Results

We conducted all experiments in realistic sea conditions, on both cloudy and sunny days without rain. The average depth

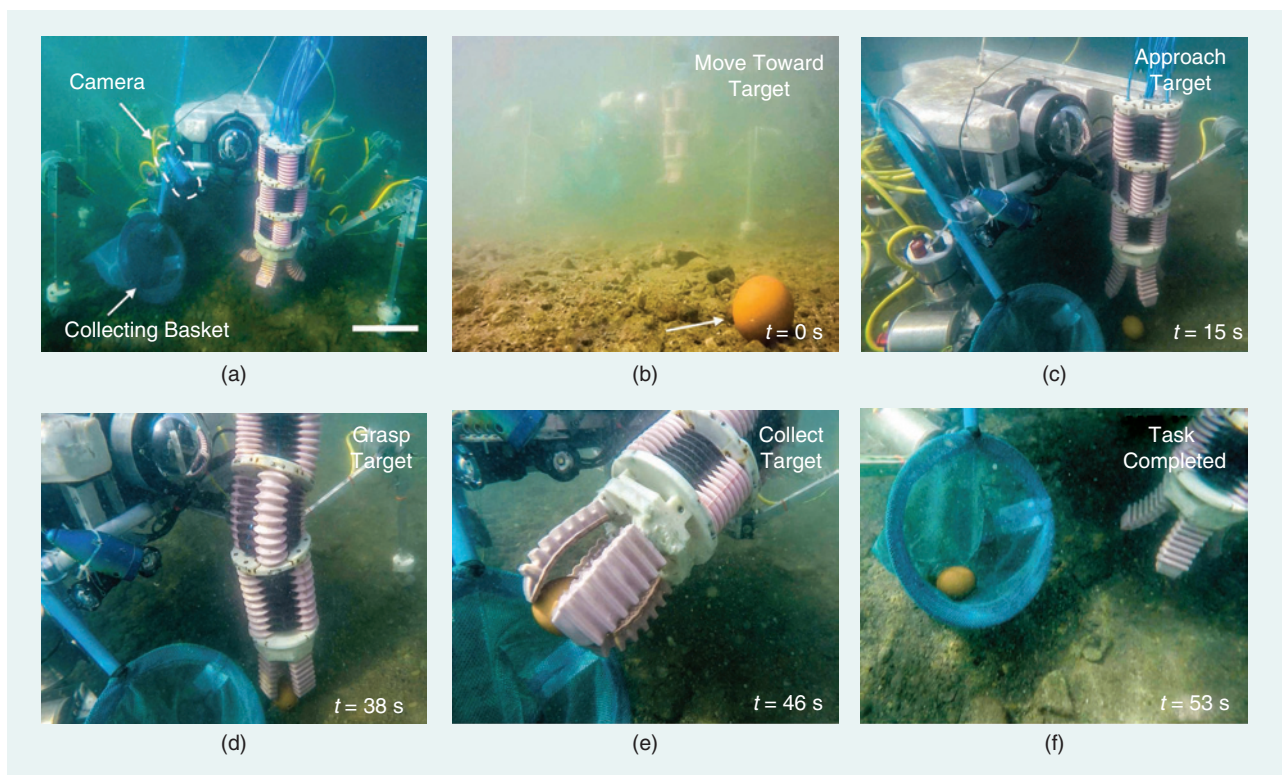


Figure 6. An example of fragile object collection. (a) The robot starts a few meters away from the object and (b) moves close enough so that the object (c) is within the arm's workspace. (d) The soft manipulator grasps the object via the inverse kinematics model and (e) moves it into (f) the onboard collection basket. Scale bar: 15 cm.

of the robot for all tests was approximately 0.8 m; a pressure sensor placed beside one of the canisters recorded the actual depth of the body, which was above the seabed. A movie of the experiments is available in the supplementary video, which can be found on IEEE *Xplore*.

Force Experiments

Figure 7 conveys the results of the force tests. By evaluating different components separately and together, we were able to determine the relationship between the system's energy consumption and exerted force. The arm alone can exert a significant pulling force of roughly 16 N, on average (Figure 7b), using only the manipulator's pneumatic chambers. As a reaction to the pulling force, the legs required additional thrust to the motors to hold a static position, which led to a slightly increased energy consumption (electrical power from ~30 to ~36 W). This result can be directly compared to the power consumption of intervention AUVs (I-AUVs), which, like SILVER2, have onboard batteries.

Experiments from 6-h operations of the Girona 500 show an overall energy consumption (during underwater transects and without actual arm interaction) of 1,026 Wh, with 570 Wh powering the thrusters and the remaining 456 Wh considered to be hotel energy. In the case of SILVER2 with an attached arm, operating (e.g., pulling an object) for 6 h will drain only 180 Wh of energy from the legs' motors, of which 35 Wh are required for SILVER2 to stand without operating. The advantages of benthic systems compared to hovering ones in terms of energy consumption are intuitively clear, and our reported results suggest possible energy savings of up to one order of magnitude.

Using the legs and the gripper [Figure 7(a)], we recorded a momentary but significant reduction in the average pulling force (8 N) and a corresponding increase in the power demand (roughly 132 W) for less than 1 s (0.8 s). The increase in the power consumption is consistent with a quick activation of the 12 motors to raise the body. The reduction in the pulling force is related to the opening of

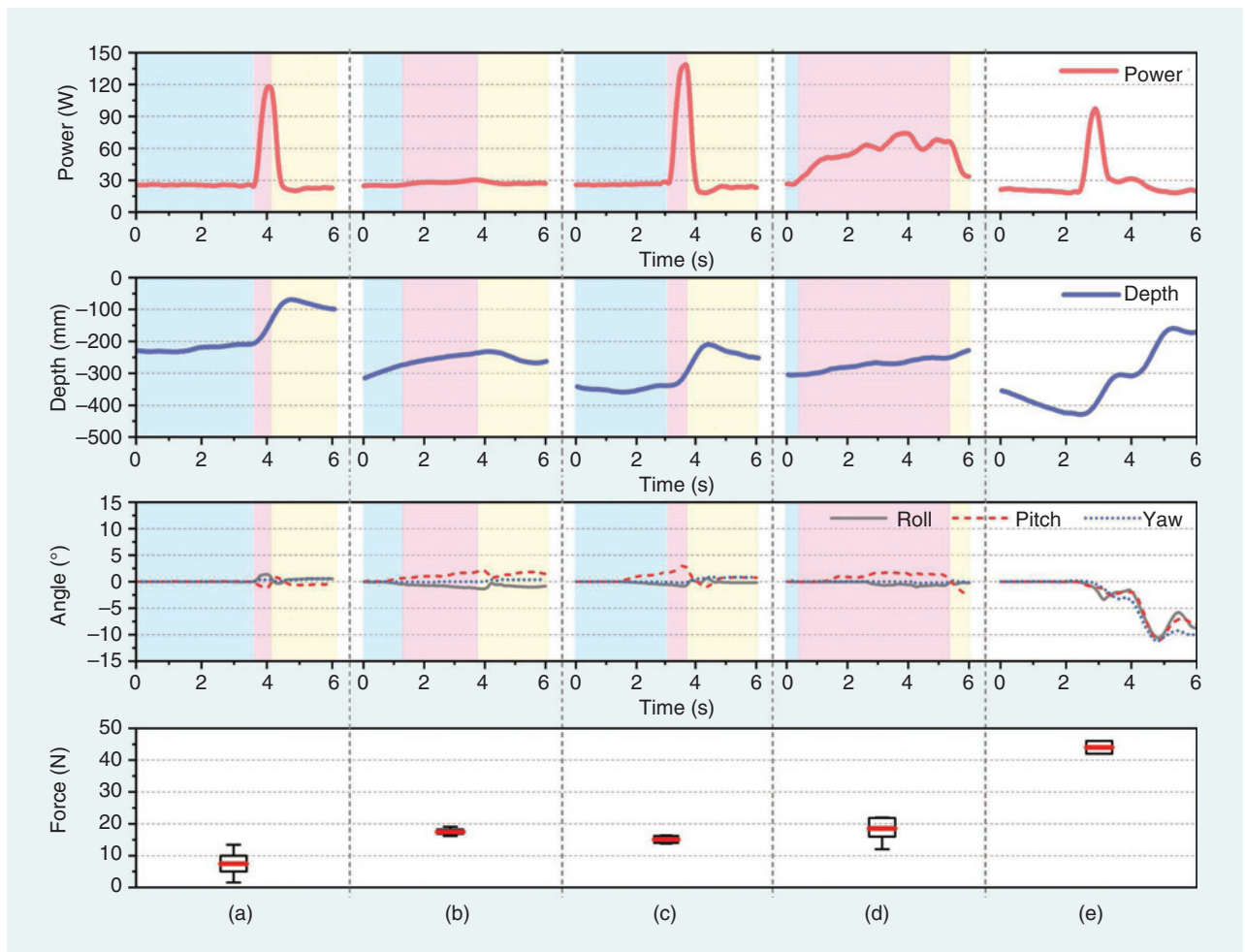


Figure 7. Typical results of the force protocol. The different experimental conditions are as follows: (a) the quick action of the legs and the gripper, (b) the arm movement alone, (c) the combined action of the legs and the arm, (d) the slow action of the legs and the gripper, and (e) the action of the legs alone (with a direct connection between the force sensor and the robot body). The power consumption, depth, tilt, and force of the robot are reported in the different rows of the figure. The force is given as a box plot of all collected data. The blue, pink, and yellow backgrounds represent the grasping, pulling, and releasing phases, respectively. Identical time windows are shown in the supplementary video, which can be found on IEEE *Xplore*.

the soft gripper, which, subject to high acceleration, is not capable of conforming to the handle and establishing a firm grip. By using the arm and the legs together, we recorded a pulling force of 15 N [Figure 7(c)], similar to that achieved by the arm alone. By activating the arm first, the robot positioned the gripper in a suitable grasping position, so the subsequent activation of the legs fully exploited the potential of the gripper. By activating the legs very slowly and allowing the soft gripper to conform well to the handle [Figure 7(d)], we recorded an average force of approximately 18 N, confirming that slow acceleration enables a greater pulling force. In this case, the power consumption was reduced to a maximum value of roughly 96 W, even though the motion was maintained for 6 s, with an average power draw of 70 W [Figure 7(c)–(d)].

We also measured the power consumption of the soft manipulator (while grasping a shell with a size similar to the one that had been gripped on the seafloor) in the laboratory water tank. The system's power was recorded every 5 s by a power meter device (Zhejiang Shixin Electric). We calculated the average power consumption of the soft manipulator by recording data for 40 s. We also repeated each experimental scenario five times to acquire the mean value. The pneumatic control system's average power consumption was 25 ± 1 W. This result highlights a less-studied aspect of using a soft gripper for underwater grasping. Most existing research examines novel actuation methodologies, modeling, sensing, and fabrication methods. Our results indicate that the arm's speed and acceleration greatly influence the maximum grasping force. In addition to underwater operations, this finding may be particularly relevant for factories, warehouses, and other industrial settings that require quick handling.

Finally, the pulling force of the legs was measured by directly connecting a cable between the force sensor and the robot's body, without the involvement of the soft arm. Theoretically, the stall torque of the motors ($3.8 \text{ N}\cdot\text{m}$) exerted on a tibia length of approximately 0.35 m should result in a force of roughly 65 N for all the legs together. Actual measurements from experiments reported an average force of 44 N [Figure 7(e)]. The ratio between the measured and nominal forces is roughly 0.68, consistent with the expected losses from a servo motor system. For underwater vehicles, even with optimized blade designs, the efficiency would be reduced by the propeller efficiency to approximately 0.8 [29]. For an optimized AUV, the overall power efficiency for 7-N navigation is reported as 0.49. It is a reasonable expectation that direct transmission would slightly increase the force management and possibly exert a higher force on the environment. However, an ROV of comparable size to SILVER2 (the BlueROV2) demonstrates a nominal bollard vertical thrust of between 69 and 88 N. Without the necessary data for comparison, we can assume that the force and power consumption of SILVER2's legs alone fall between those of a small ROV and an I-AUV.

Workspace Protocol

An intrinsic advantage of mobile manipulation is that locomotion enables the manipulator workspace to be extended. Our protocol investigated vertical extensions first, as shown in Figure 8. In this case, the robot moved into a starting position and initiated a test. Compared with the soft manipulator working alone, we found that the vertical workspace of the soft manipulator increased 85% (from 20 to 37 cm) when it was integrated on SILVER2. With an average release error of 6.1 cm, the arm was capable of placing a portion of the shell in the red target area. Such an error is comparable to remotely controlled tests performed in the swimming pool [6], where a yellow tube was grasped during a collection task. In that example, precise positioning was not required if the mission was satisfactorily completed.

In previous work [5], simulations were performed for button-pushing and valve-turning tasks. The reported alignment error and the gripper and button modeling were slightly better than our present results. However, our results suggest that the button-pushing task could be accomplished, even with our average placement offset. In [30], the authors report good results for the end effector positioning within an experimental tank and under a monodirectional simulated current. In that experiment, six cameras and Qualisys Track Manager (QTM) software were employed to evaluate the system's underwater pose. With an error of approximately 5.8 ± 3 cm, the experimental results demonstrate very accurate mobility and positioning. It is worth noting that the testing conditions presented in our experiments are poorly represented in the existing literature. All related work either accomplishes the target task through simulation or in controlled environments, such as a swimming pool or a tank. It is correctly reported in [30] that the position error via the QTM is difficult to obtain in field conditions, so the reported performance could vary significantly among different underwater environments.

Mobile Pick and Place

Compared to the results of the workspace protocol, the performance decreased in the horizontal workspace extension during an evaluation known as the *pick-and-place test*. In all attempts, the robot succeeded in bringing the target within the manipulator workspace (i.e., between the legs). During the release, we observed an average error of roughly 15.7 cm [Figure 9(d)]. This result enabled us to place the object in the desired area but not always within the red, circular target. We observed a primary reason for this decrease in the performance: disturbances on the benthic platform and the soft manipulator. SILVER2 does not have closed-loop station-keeping control, and we did not modify the position of the robot when unexpected currents significantly shifted it from the desired final location. With respect to the arm, although we never observed significant displacements, small vibrations may have impaired the release speed and increased the error.

It is worth mentioning that, in one trial, the shell was accidentally released during the walking phase from the starting

point to the target area. This happened when we tested a faster walking speed (20 cm/s) and induced additional shaking in the arm. All the remaining trials were performed at an approximate walking speed of 5 cm/s. It is also worth remarking that all tests were conducted in conditions with relatively poor visibility that limited the details the underwater cameras could provide.

Litter and Fragile Object Collection

The results of this protocol are presented by object type. We qualitatively report (Figure 10) the binary success/failure of approaching, grasping, releasing, and collecting each object. The whole set of tested objects was successfully approached and grasped. The legs did not induce disturbances on the objects themselves, and the arm was capable of gripping and lifting the articles. Objects with a defined and solid shape (the plastic bottle, eggshell, and silicone seashell) were also positively released and collected. Objects that significantly deformed, namely, the plastic bag and the fishing net (protocols C and D), posed significant challenges for the gripper. Even though the objects were successfully released in some

situations, in most trials, they got tangled in the gripper's fingers. The prevention of a proper release also impaired the collection into the onboard basket. In addition, we tested the system's disentangling force by placing the net below a large rock [Figure 10(f)]. In this case, the gripper was able to grasp the net, the legs helped disentangle the net by increasing the vertical workspace, and the motion eventually freed the net from the robot. In this case, the net was easily released by using a clear pinching grasp.

Collecting Objects in a Confined Space

This final protocol showcased the soft arm's ability to navigate and grasp in confined spaces. Given the rigid part of the manipulator's nominal size of 12 cm, we tested how well we were able to collect objects in a confined space. The minimum height of the overhang [Figure 11(a)] under which the robot succeeded in retrieving an object was 17 cm. The arm alone was sufficient for this task. During the box test [Figure 11(b)], the arm successfully negotiated a minimum 14-cm aperture. In this case, the legs controlled the vertical workspace to enable the arm to reach the most distant part of the

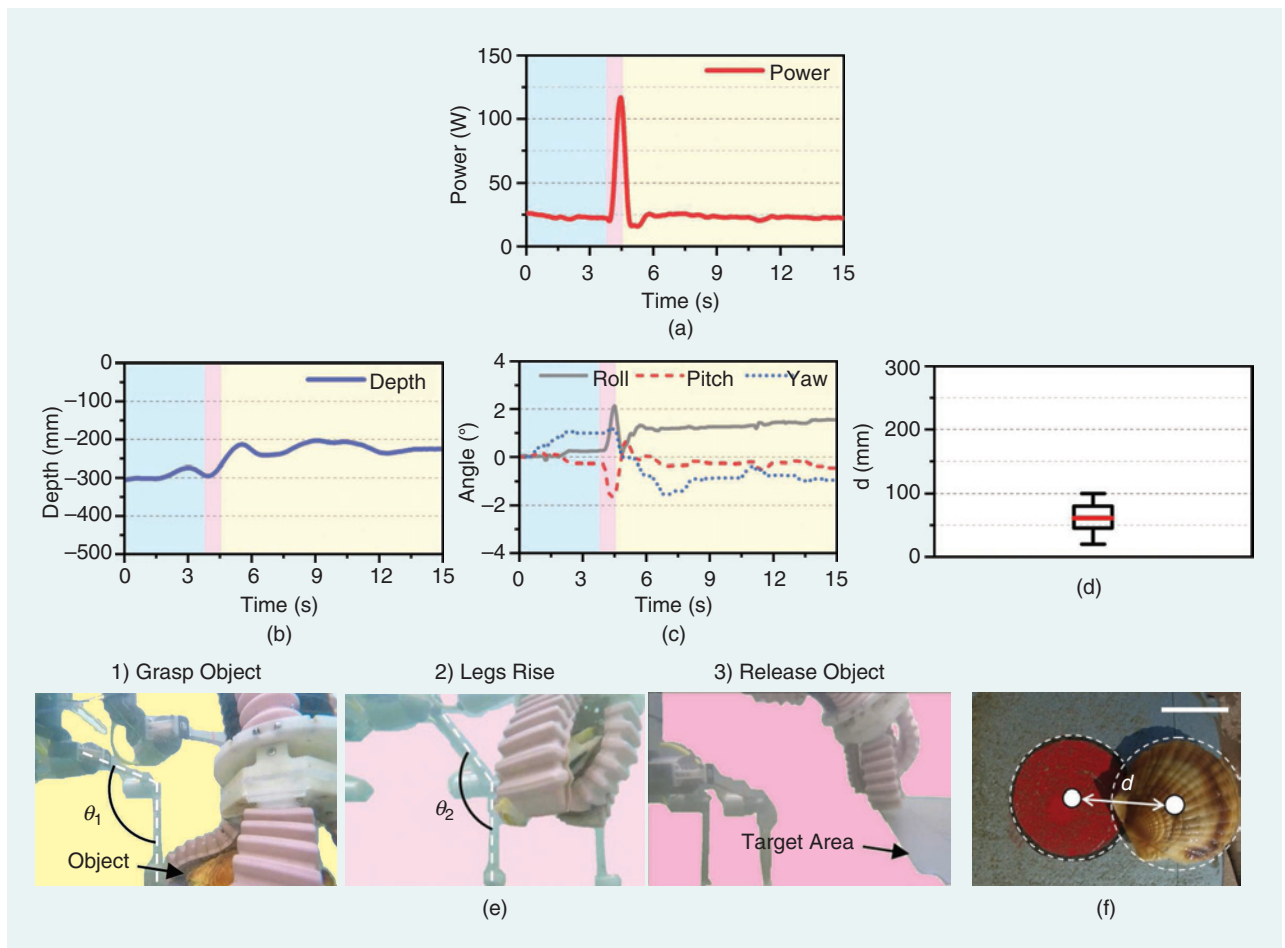


Figure 8. The results of the workspace protocol. The (a) power consumption, (b) SILVER2 depth, (c) body orientation and (d) placement error distances, representing all data collected during the experiments. (e) The yellow, pink, and purple backgrounds represent the grasping, standing, and releasing phases, respectively. (f) The object placement results. Scale bar: 5 cm.

box and helped move the object outside the box once the item was grasped. Without assistance from the legs, the arm released the shell after trying to force its way out of the confined environment.

Discussion

Our study investigated the interaction between a completely soft arm and a legged robot in a real-world underwater environment. In this section, we discuss the experimental results of the underwater manipulation, including both force and precision, and the application of those features for more complicated mission-like underwater experiments.

Simplifying the Soft Manipulator's Inverse Kinematics Problem

Solving higher-order nonlinear equations and training a practical kinematics model in oceanic environments remain challenging [28]. In this article, we proposed a simple and inverse kinematics solution for a soft manipulator—the opposite-bending S shape. The structure design offers advantages for the kinematic modeling of the manipulator since the attitudes

of the two bending segments are directly related. As a result, solving the inverse kinematics of the soft manipulator with opposing curvature requires computing only geometric functions when modeling the whole manipulator. Compared with the previous opposite-bending-and-stretching structure modeling method [28] (with a computational time of 8.2 ms), the computational time (11 μ s) of the current modeling method is notably shortened.

Meanwhile, with the addition of the bending of the third soft segment, the workspace of the current soft manipulator (500 mm in length, 520 mm in width, and 304 mm in height) is greatly enhanced compared with the previous version (260 mm in length, 240 mm in width, and 220 mm in height). Therefore, this method enhances the practical use of the manipulator for underwater grasping in the natural environment. Note that there is a tradeoff between the reduced deformation configuration space and the computational complexity. This tradeoff depends on the application backgrounds. We expect that this method will have a broader range of applications in the future: it may shed light on the modeling of other soft continuum robots that use actuation approaches other

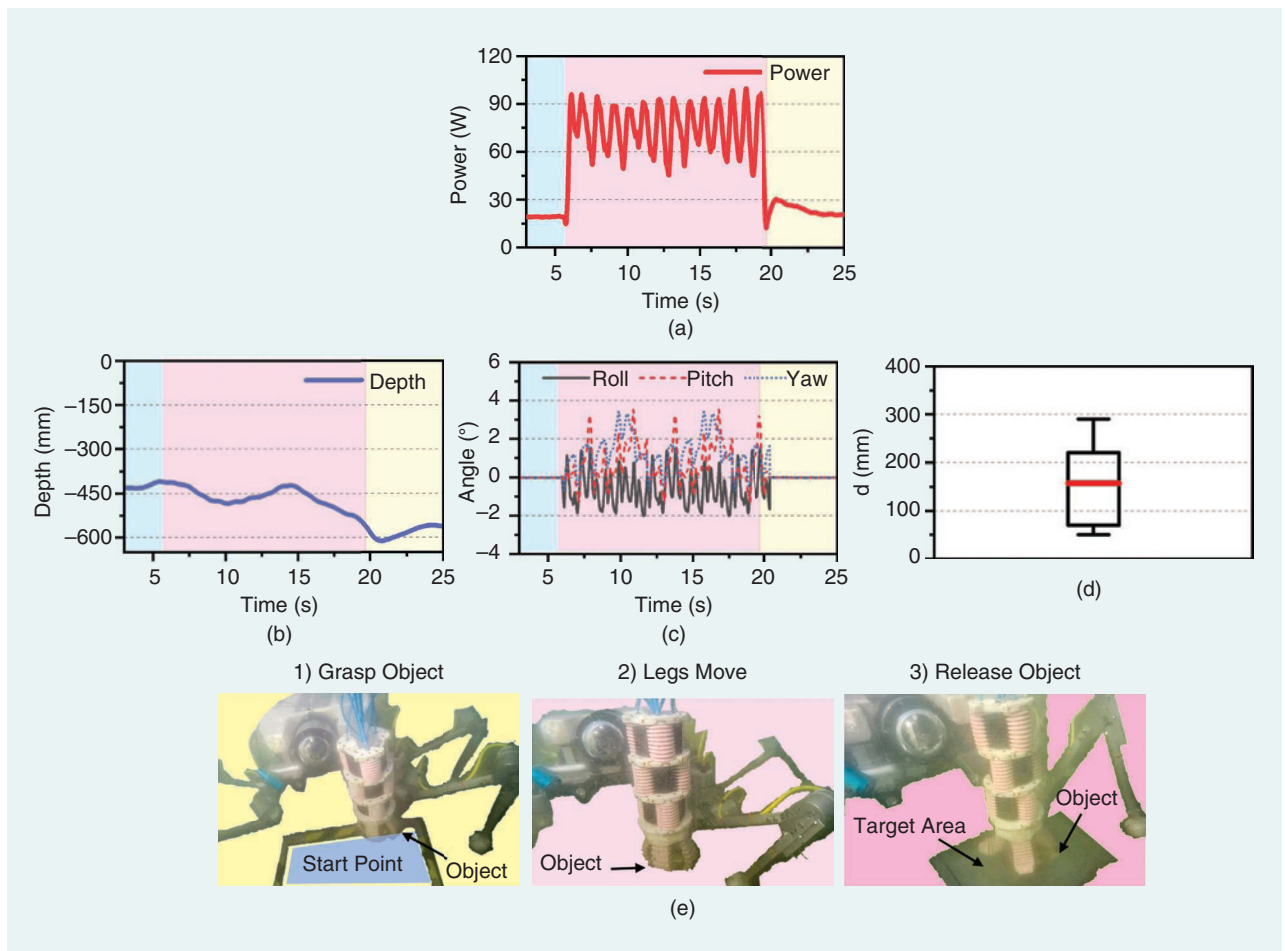


Figure 9. The results of the mobile pick and place. The (a) power consumption, (b) gripper depth, (c) body orientation, and (d) object placement offset distances, representing all the data collected during the experiments. (e) The yellow, pink, and purple backgrounds represent the grasping, standing, and releasing phases, respectively.

than pneumatic, such as tendon-driving manipulators, origami-structure-based manipulators, and so forth [31].

Protocols A–C

In all three scenarios, data were collected in uncontrolled sea conditions, with waves ranging from 5 to 15 cm. The experiments were conducted at an average depth of roughly 80 cm. Drag forces, depending on the wave motion and the water speed, were constantly influencing the performance of the system. Furthermore, the tests were performed only a few meters from shore, which increased the hydrodynamic

disturbance. Although the pitch, roll, and yaw of the robot were somewhat affected by these disturbances, the compliance of the arm and the gripper compensated for this to some extent. Eventually, the experiments assessed the system performance in real-world conditions, which demonstrated the effectiveness of the presented solution.

The results of these protocols highlight how the robotic system was capable of exerting significant forces comparable to those obtained with an I-AUV or a small ROV but with significantly decreased power requirements. However, our benthic approach exhibits limitations related to long-range

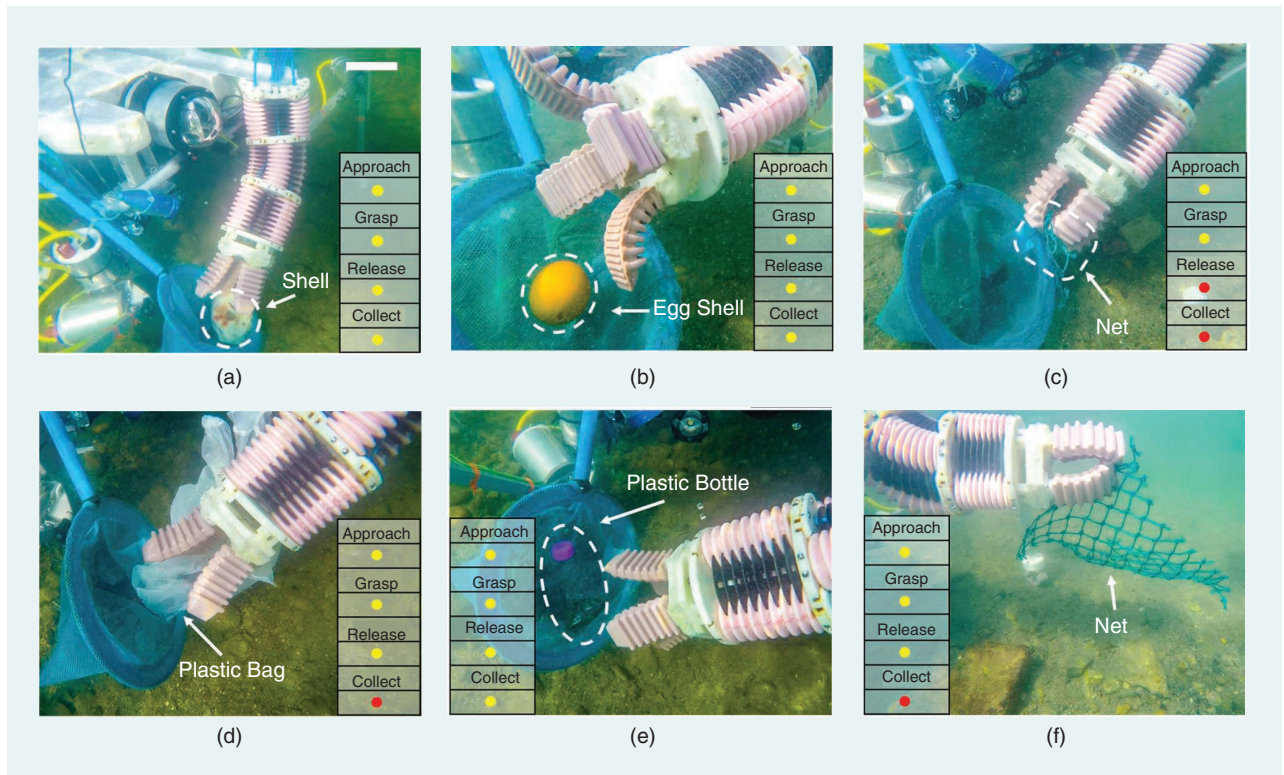


Figure 10. The results of the litter and fragile object collection protocol. The color of the marker in the table denotes a successful (yellow) or failed (red) step of each test. Different objects, such as (a) a seashell, (b) an eggshell, (c) and (f) a net, (d) a plastic bag, and (e) a plastic bottle, were used during the experiments. Scale bar: 5 cm.

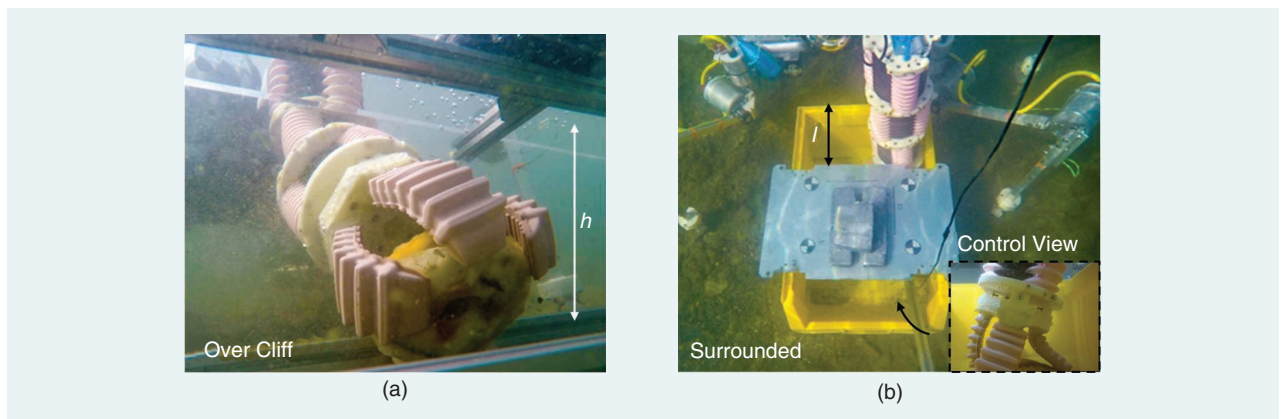


Figure 11. The results of undersea grasping in confined spaces. (a) The simulated overhang environment, where h is the height of the overhang. (b) The simulated enclosed environment, where l is the length of the opening. Scale bar: 5 cm.

(kilometer-range) mobility. We expect benthic vehicles to complement AUV operations in small, defined areas where more accurate exploration and intervention tasks are required, while AUVs will remain the preferred choice for wide-area screening. Additionally, the soft arm benefited from operating from a stable base, and, even with real sea disturbances, effectively manipulated objects within a target area. A benthic mobile robot from which active controls can be executed seems to be a practical enhancement for UVMs. The soft arm alone is able to exert significant force, with the qualitative advantages of grasping adaptation and high dexterity. The gripper design [32] could be improved to exploit the full potential of a pneumatic arm: a stiffness-changing solution, as presented in [33], could possibly improve both the strength and the compliance.

Protocols D–E

Tasks such as collecting objects from the sea bed require precise locomotion, arm dexterity to collect and place items, enough force to lift and free entangled objects, and a delicate touch from the gripper. The objects selected for protocol D represented a small variety of heterogeneous yet relevant categories: fragile objects, plastic litter, and solid articles. The confined spaces prepared for protocol E also represent possible man-made environments where similar tasks have to be performed. Results from these two protocols highlight the positive interaction between the legged system and the soft arm. The thruster dynamics of other systems may displace low-density target objects and damage fragile ones. With the current approach, we were able to select a slow operating speed that barely affected the environment and enabled the robot to precisely approach a target object.

In protocol D, the uncontrolled lowering motion of the legs at the end of the walking phase influenced the arm's final position, which suggests the adoption of other stopping strategies, but, in all experiments, the robot was capable of placing the object within the arm's workspace and retrieving objects from the seabed. There were some unexpected problems during the object release. We recognize that quasi-floating, low-density objects, such as plastic bags and fishing nets, are unique articles and poorly investigated. The dexterity required to free the gripper from ensnaring objects (i.e., those that wrap around the gripper fingers) is not present in our current solution and in other grippers. We believe that, as robotic hands and grippers face increasingly complex tasks, the release problem may be the subject of further research.

Eventually, costly and dangerous tasks that human divers currently perform, such as turning valves, replacing components, and pushing buttons in confined spaces and cluttered environments, will become common applications for underwater robotic systems. However, even these apparently simple tasks are complex for underwater robots, and, to our knowledge, no attempts have been made to analyze underwater manipulation in confined environments.

Our tests, although straightforward, conceptually highlight the benefit of a continuum soft arm for underwater environments. Contact with side walls did not impair the task completion, and the dexterity of the arm and gripper mostly compensated for disturbances and inaccurate positioning of the robot.

Furthermore, with the contribution of a mobile base, it was possible to retrieve objects from even very deep and narrow apertures. In constrained environments, where the arm alone was unable to exit, the robot's legs could effectively retract the arm from the aperture. Unexpected contact was damped by the passive elastic components of the arm, which helped maintain the stability of the system as a whole. A rigid solution would require computation and sensing capabilities that are often not available for underwater systems.

Conclusions

To our knowledge, this article is the first to document a synergistic robotic system composed of a benthic legged platform and soft continuum manipulator performing real-world underwater mission-like experiments. We examined the workspace extensibility, force, energy consumption, and grasping ability of the robot under different experimental scenarios. We found that the soft manipulator's workspace could be significantly extended by adding a benthic legged robot as a mobile base. The robot precisely approached and collected objects without disturbing the undersea environment, which is a common challenge for traditional screw propeller-driven ROV systems. The robot could also retrieve objects from deep apertures in overhang environments. One current limitation is that the soft manipulator and legged robot are controlled by separate systems. In the future, we aim to develop a robot with a fully integrated control system for both the soft continuum manipulation and the benthic legged locomotion.

Acknowledgments

This research was supported by the Blue Resolution Project, which is funded by Arbi Dario spa; the Chinese National Science Foundation (grants 61822303, 91848105, 61633004, and 91848206); and the National Key R&D Program of China (grants 2019YFB1309600 and 18YFB1304600).

References

- [1] J. Yuh, G. Marani, and D. R. Blidberg, "Applications of marine robotic vehicles," *Intell. Serv. Robot.*, vol. 4, no. 4, pp. 221–231, 2011. doi: 10.1007/s11370-011-0096-5.
- [2] "The 2018 annual report on EU blue economy," Center for Coastal & Marine Studies, Brussels, Belgium, 2018. [Online]. Available: <https://op.europa.eu/en/publication-detail/-/publication/79299d10-8a35-11e8-ac6a-01aa75ed71a1>
- [3] G. Antonelli, *Underwater Robots, Motion and Force Control of Vehicle-Manipulator Systems* (Springer Tracts in Advanced Robotics). New York: Springer-Verlag, 2006.
- [4] B. Siciliano and O. Khatib, *Springer Handbook of Robotics*. Berlin: Springer-Verlag, 2008.


- [5] E. Cataldi and G. Antonelli, "Basic interaction operations for an underwater vehicle-manipulator system," in *Proc. 2015 Int. Conf. Adv. Robot.*, pp. 524–529. doi: 10.1109/ICAR.2015.7251506.
- [6] E. Simetti et al., "Autonomous underwater intervention: Experimental results of the MARIS project," *IEEE J. Ocean. Eng.*, vol. 43, no. 3, pp. 620–639, 2018. doi: 10.1109/JOE.2017.2733878.
- [7] R. D. Christ and R. L. Wernli, *The ROV Manual: A User's Guide to Remotely Operated Vehicles*. Amsterdam, The Netherlands: Elsevier, 2013.
- [8] T. Inoue, T. Shiosawa, and K. Takagi, "Dynamic analysis of motion of crawler-type remotely operated vehicles," *Ocean. Eng. IEEE J.*, vol. 38, no. 2, pp. 375–382, 2013. doi: 10.1109/JOE.2012.2225292.
- [9] Y. Kojio et al., "Walking control in water considering reaction forces from water for humanoid robots with a waterproof suit," in *Proc. IEEE Int. Conf. Intell. Robot. Syst.*, 2016, pp. 658–665. doi: 10.1109/IROS.2016.7759123.
- [10] M. Ishida, D. Drotman, B. Shih, M. Hermes, M. Luhar, and M. T. Tolley, "Morphing structure for changing hydrodynamic characteristics of a soft underwater walking robot," *IEEE Robot. Autom. Lett.*, vol. 4, no. 4, pp. 4163–4169, 2019. doi: 10.1109/LRA.2019.2931263.
- [11] G. Picardi, C. Laschi, and M. Calisti, "Model-based open loop control of a multigait legged underwater robot," *Mechatronics*, vol. 55, pp. 162–170, 2018. doi: 10.1016/j.mechatronics.2018.09.006.
- [12] G. Picardi, S. Iacoponi, M. Chellapurath, C. Laschi, and M. Calisti, "Surveying and cleaning plastic pollution in the sediment: SILVER+ approach," in *Proc. Oceans 2019*, pp. 1–8. doi: 10.1109/OCEANSE.2019.8867331.
- [13] I. Vasilescu et al., "AMOUR V: A hovering energy efficient underwater robot capable of dynamic payloads," *Int. J. Robot. Res.*, vol. 29, no. 5, pp. 547–570, 2010.
- [14] C. Laschi, B. Mazzolai, M. Cianchetti, L. Margheri, M. Follador, and P. Dario, "Soft robot arm inspired by the octopus," *Adv. Robot.*, vol. 26, no. 7, pp. 709–727, 2012. doi: 10.1163/156855312X626343.
- [15] D. M. Lane et al., "AMADEUS: Advanced manipulation for deep underwater sampling," *IEEE Robot. Autom. Mag.*, vol. 4, no. 4, pp. 34–45, 1997. doi: 10.1109/100.637804.
- [16] F. Renda, M. Cianchetti, M. Giorelli, A. Arienti, and C. Laschi, "A 3D steady-state model of a tendon-driven continuum soft manipulator inspired by the octopus arm," *Bioinspir. Biomime.*, vol. 7, no. 2, p. 025006, 2012. doi: 10.1088/1748-3182/7/2/025006.
- [17] M. Calisti et al., "Design and development of a soft robot with crawling and grasping capabilities," in *Proc. IEEE Int. Conf. Robot. Autom.*, 2012, pp. 4950–4955. doi: 10.1109/ICRA.2012.6224671.
- [18] K. C. Galloway et al., "Soft robotic grippers for biological sampling on deep reefs," *Soft Robot.*, vol. 3, no. 1, pp. 23–33, 2016. doi: 10.1089/soro.2015.0019.
- [19] S. Kurumaya et al., "A modular soft robotic wrist for underwater manipulation," *Soft Robot.*, vol. 5, no. 4, pp. 399–409, 2018. doi: 10.1089/soro.2017.0097.
- [20] B. T. Phillips et al., "A dexterous, glove-based teleoperable low-power soft robotic arm for delicate deep-sea biological exploration," *Sci. Rep.*, vol. 8, p. 14,779, Oct. 2018. doi: 10.1038/s41598-018-33138-y.
- [21] S. Licht, E. Collins, M. L. Mendes, and C. Baxter, "Stronger at depth: Jamming grippers as deep sea sampling tools," *Soft Robot.*, vol. 4, no. 4, pp. 305–316, 2017. doi: 10.1089/soro.2017.0028.
- [22] G. Picardi, M. Chellapurath, S. Iacoponi, S. Stefanni, C. Laschi, and M. Calisti, "Bioinspired underwater legged robot for seabed exploration with low environmental disturbance," *Sci. Robot.*, vol. 5, no. 42, 2020. [Online]. Available: <https://robotics.sciencemag.org/content/5/42/eaaz1012.full.pdf>, doi: 10.1126/scirobotics.aaz1012.
- [23] A. Parmiggiani, G. Metta, and N. Tsagarakis, "The mechatronic design of the new legs of the iCub robot," in *Proc. IEEE-RAS Int. Conf. Human. Robots*, 2012, pp. 481–486. doi: 10.1109/HUMANOIDS.2012.6651563.
- [24] M. Calisti and C. Laschi, "Underwater running on uneven terrain," in *Proc. OCEANS 2015-Genova*, pp. 1–5. doi: 10.1109/OCEANS-Genova.2015.7271366.
- [25] J. Burgner-Kahrs, H. B. Gilbert, J. Granna, P. J. Swaney, and R. J. Webster, "Workspace characterization for concentric tube continuum robots," in *Proc. IEEE Int. Conf. Intell. Robots Syst.*, 2014, pp. 1269–1275. doi: 10.1109/IROS.2014.6942720.
- [26] B. A. Jones, W. McMahan, and I. D. Walker, "Practical kinematics for real-time implementation of continuum robots," in *Proc. IEEE Int. Conf. Robot. Autom.*, 2006, pp. 1840–1847. doi: 10.1109/ROBOT.2006.1641974.
- [27] T. George Thuruthel, Y. Ansari, E. Falotico, and C. Laschi, "Control strategies for soft robotic manipulators: A survey," *Soft Robot.*, vol. 5, no. 2, pp. 149–163, 2018. doi: 10.1089/soro.2017.0007.
- [28] Z. Gong et al., "A soft manipulator for efficient delicate grasping in shallow water: Modeling, control, and real-world experiments," *Int. J. Robot. Res.*, 2020. [Online]. Available: <https://doi.org/10.1177/0278364920917203>, doi: 10.1177/0278364920917203.
- [29] J. G. Bellingham et al., "Efficient propulsion for the tethys long-range autonomous underwater vehicle," in *Proc. 2010 IEEE/OES Auton. Underwater Veh.*, pp. 1–7. doi: 10.1109/AUV.2010.5779645.
- [30] B. O. A. Haugaløkken, E. K. Jørgensen, and I. Schjølberg, "Experimental validation of end-effector stabilization for underwater vehicle-manipulator systems in subsea operations," *Robot. Autom. Syst.*, vol. 109, pp. 1–12, Nov. 2018. doi: 10.1016/j.robot.2018.08.007.
- [31] L. Wen, F. Pan, and X. Ding, "Tensegrity metamaterials for soft robotics," *Sci. Robot.*, vol. 5, no. 45, p. eabd9158, Aug. 2020. doi: 10.1126/scirobotics.abd9158.
- [32] Y. Hao et al., "Modeling and experiments of a soft robotic gripper in amphibious environments," *Int. J. Adv. Robot. Syst.*, vol. 14, no. 3, 2017. doi: 10.1177/1729881417707148.
- [33] H. Stuart, S. Wang, O. Khatib, and M. R. Cutkosky, "The Ocean One hands: An adaptive design for robust marine manipulation," *Int. J. Robot. Res.*, vol. 36, no. 2, pp. 150–166, 2017. doi: 10.1177/0278364917694723.

Jiaqi Liu, School of Mechanical Engineering and Automation, Beihang University, Beijing. Email: jiaqiliu@buaa.edu.cn.

Saverio Iacoponi, BioRobotics Institute and Department of Excellence in Robotics and AI, Scuola Superiore Sant'Anna, Pisa, Italy. Email: saverio.iacoponi@santannapisa.it.

Cecilia Laschi, BioRobotics Institute and Department of Excellence in Robotics and AI, Scuola Superiore Sant'Anna, Pisa, Italy. Email: cecilia.laschi@santannapisa.it.

Li Wen, School of Mechanical Engineering and Automation, Beihang University, Beijing. Email: liwen@buaa.edu.cn.

Marcello Calisti, BioRobotics Institute and Department of Excellence in Robotics and AI, Scuola Superiore Sant'Anna, Pisa, Italy. Email: marcello.calisti@santannapisa.it. 



©SHUTTERSTOCK/SIMON BRAAT

Design Optimization of Soft Robots

A Review of the State of the Art

By Feifei Chen and Michael Yu Wang

Robotics has undergone a profound revolution in the past 50 years, moving from the laboratory and research institute to the factory and home. Kinematics and dynamics theories have been developed as the foundation for robot design and control, based on the conventional definition of robots: a kinematic chain of rigid links.

Currently, the boundaries among materials, structures, biology, intelligence, and robotics are blurring. We have a much wider interpretation of what a robot is. The past decade has seen the increasing use of soft materials (Young's modulus on the order of kilopascals

to megapascals) to build robots, which are generally referred to as soft robots. This new generation of robots, originally inspired by natural lives, has grown rapidly and is enabling new robot abilities for applications ranging from wearable devices and biomedical engineering to search and rescue in unstructured environments [1]–[3].

Instead of relying on sliding or rolling motions as in conventional rigid robots, soft robots produce mobility based on the inherent compliance of soft materials. This fundamental change enables the integration of multiple functions into simple topologies by embedding actuators and sensors to build fully functional machines that can perform complex tasks. Here, the physical presence of soft robots plays a central role in generating adaptable behaviors. The body design

Digital Object Identifier 10.1109/MRA.2020.3024280

Date of current version: 22 October 2020

in free form is expected to imbue soft robots with programmable mechanical properties and desired responses to external stimuli, which unlocks new functionalities in the paradigm of so-called morphological computation and embodied intelligence [4], [5].

The transformative involvement of soft materials in robots also poses unprecedented challenges. The increased complexities of soft robotic systems, which may come from geometry, material, actuation, and their intricate coupling, are making conventional theories of robot design poorly applicable. The difficulties come not only from the lack of simulation and analysis tools to effectively and efficiently predict complex mechanical behaviors of soft robots but also from the lack of powerful optimization algorithms to automate the design process. One must often rely on intuitions, experiences, or bioinspiration for soft robot design, which can provide only limited scope. Research efforts have increasingly been made toward a comprehensive design paradigm to bridge the gap from theoretical and algorithmic perspectives.

In this article, instead of limiting the discussion to specific applications, we articulate the fundamental concepts of design optimization for soft robots. We exclude chemical- or material-level modifications but focus on mathematical design

approaches to soft robots based on widely available materials. State-of-the-art progress is highlighted, with particular emphasis on the methods to approach design problems and their mathematical representation. The term *optimization* is not necessarily limited to algorithms to solve a formulated problem but more generally refers to innovations in any design aspect leading to better performance of soft robots. We conclude this review with a prospective look at future trends for design optimization in soft robotics.

Design Architecture

The entire framework of design optimization for soft robots is generally hierarchical and iterative, as presented in Figure 1. A high-level task, such as locomotion and grasping, can be decomposed into a sequence of motion behaviors, including stretching, bending, twisting, or their combination. For example, bending motions typically dominate a grasping process, while alternating elongations and compressions may dominate locomotion. Once the desired mechanical behavior is determined, one may formulate it as an inverse design problem to be addressed by mathematical programming.

The translation of the physical problem as a mathematical optimization problem requires identifying and quantifying

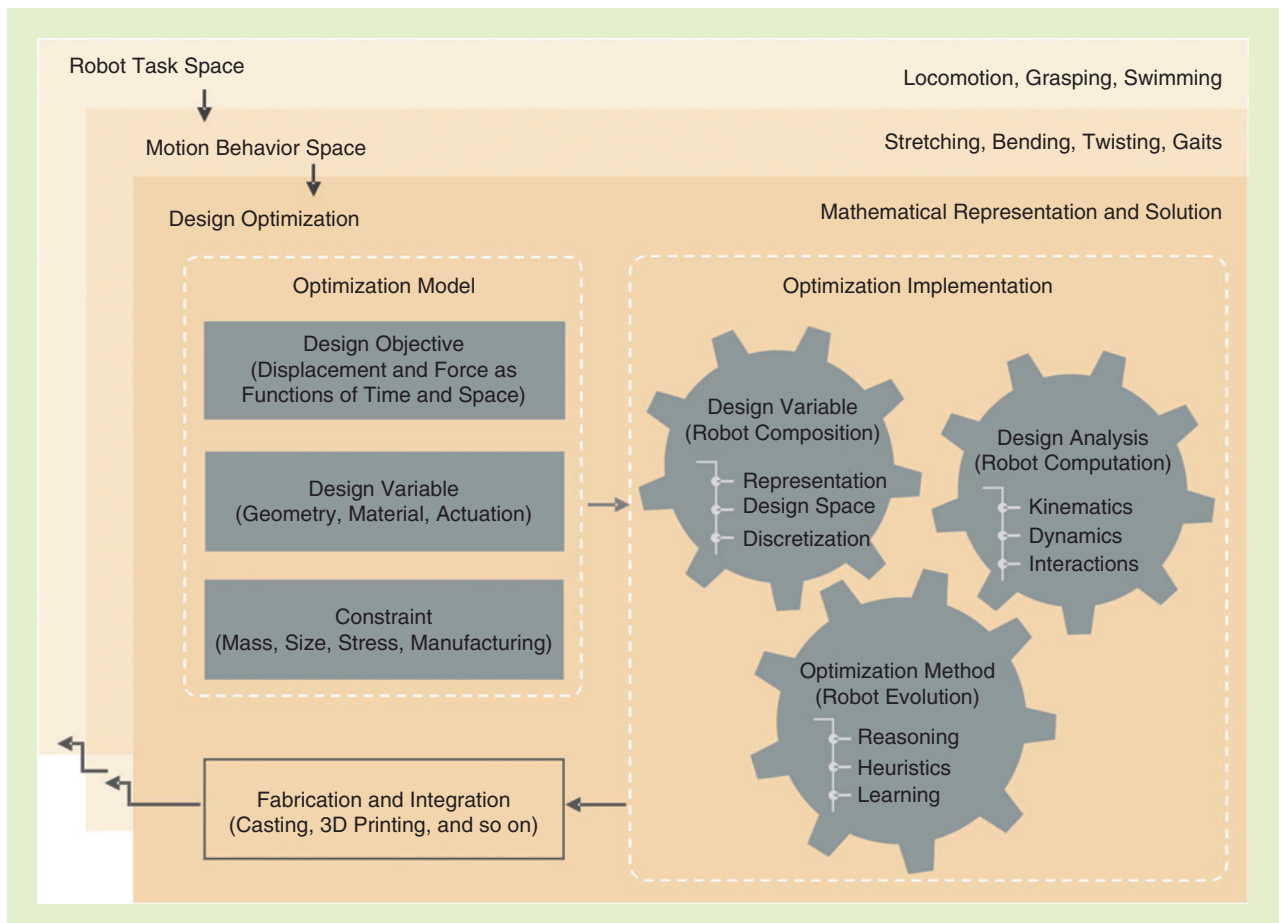


Figure 1. The architecture for design optimization of soft robots.

the objective, variables, and constraints. This process is also referred to as *modeling*. The appropriate model plays an essential role in the optimization process by bridging the robotic tasks and optimization algorithms. The optimization implementation necessitates an integration of the optimization model, analysis, and search algorithms. Here, we clarify several important concepts that will be mentioned throughout this review.

Design Objective (Robotic Behavior)

The design objective of a soft robot is the mathematical abstraction of desired mechanical behaviors. In general, the behaviors can be described by a function of deformation and force of interest that may vary with time and space. For example, a soft actuator may be expected to replicate the motion of human fingers upon activation. The pursued robotic behaviors sometimes cannot readily be formulated in a mathematical sense. For example, one may expect a soft gripper to conform and adapt to unknown objects of different sizes and shapes. In this case, the challenge is to capture the “adaptability” in a rigorous mathematical language.

Design Variable (Robotic Composition)

Design variables are concerned with how designers can approach the design problem and refer to the variables tunable to improve the design. The design variables of a soft robot translate into its composition, including the geometry, its material (and metamaterial), and the applied actuation field. These tunable variables shape the physical presence of soft robots and determine the mechanical behavior of robots in the environment under external stimuli. The mathematical representation of design variables has an important impact on the posedness and convexity of the optimization problem. All feasible design candidates create the design space to be explored.

Design Analysis (Robotic Computation)

Simulation and analysis tools are required to evaluate the fitness of a design candidate. This prerequisite applies to all optimization algorithms. To shed light on practical robot design, it is necessary to involve physical properties and working conditions at the evaluation stage, which has been very challenging for soft robots. Due to the huge complexities of soft robotic systems, the evaluation is generally computationally difficult and expensive and usually takes the most time during an optimization process.

Optimization Method (Robotic Evolution)

Optimization methods are required to guide designers to search for the optimal design candidate in the vast design space. In addition to knowledge of the fitness of design candidates, the optimization algorithm may call for further information, such as gradients and Hessians (usually not readily attainable), to accelerate convergence. Designers must always address the ubiquitous speed–accuracy tradeoff: more

accurate information promises a better search direction, but it comes at a higher computational cost.

Design optimization is an iterative process. For a design candidate described by a set of design variables, one needs to evaluate its mechanical behavior by computation. If the design objective is not fulfilled in the numerical process, optimization algorithms are implemented for the robot evolution. The evolution process translates into changes in design variables, i.e., a new design is generated. Finally, the optimized design is prototyped, e.g., with advanced manufacturing technologies, and tested to see whether the design achieves the desired performance. If not, a redesign process is required. Observations based on optimization solutions, the manufacturing process, and experimental results may inspire further refinement of the optimization model in terms of its objective or constraints.

The optimization model can be characterized by its design variables, i.e., the designable ingredients of robots.

Optimization Model

The optimization model can be characterized by its design variables, i.e., the designable ingredients of robots. Virtually all combinations of design variables are possible implementations for the design optimization of soft robots, but only some design candidates have been investigated. In this section, we review how researchers have approached design optimization problems from the perspectives of geometry, material, metamaterial, and actuation.

Design Variable: Geometry

The geometry of a robot concerns how the robot should be shaped, which generally includes its lengths, areas, and volumes, and undoubtedly plays an essential role in defining the robotic behavior. In terms of the complexity and generality of the geometric representation, researchers have conducted geometry optimization of soft robots on the level of size, shape, and topology.

Size optimization represents the initial step and typically addresses regular shapes that can be explicitly described by parameters such as length, width, height, and angle. The exploration of soft pneumatic actuators has offered notable examples. The design objective is generally concerned with elongation, contraction, bending, and twisting motions, and the geometric parameters are related to the shape and arrangement of inner chambers. Dämmer et al. [6] described the cross section of a linear bellows-type pneumatic actuator with a set of parameters [Figure 2(a)] and implemented a gradient-based optimization to decrease the induced maximal principal strain for the given output deflections and forces.

The chamber cross section has also been optimized at the size level for the 1D bending actuator by Elsayed et al. [11], where they aimed to minimize the ballooning effect.

To incorporate the twisting motion in addition to bending, Wang et al. [13] tailored the widely adopted pneumatic networks (often referred to as PneuNets [12]) by shifting the chamber arrangement from vertical to oblique and investigated how the oblique angle programmed the combined bending and twisting motion. PneuNets were also modified in terms of chamber size to handle deformable objects using hybrid optimization algorithms, where the design objective was to match the deformed shape of objects such as a Dixie cup [14].

Shape optimization makes a further step toward design space exploration. The space of allowable shapes within which designers search does not admit a vector space structure, which causes an infinite-dimensional problem. Shape optimization problems are usually iteratively solved. In other words, one starts with an initial guess about a shape and

gradually evolves it until convergence. This is the case reported in [7], where researchers developed a computational model for the inverse design of custom-shaped rubber balloons [Figure 2(b)]. They aimed to find the optimal balloon that approximates the target shape as closely as possible upon inflation. This inverse design problem was recast as a constrained optimization problem and solved by augmented Lagrangian methods. The same group further incorporated seams into the computational model to reproduce complex shapes with sharp creases [15].

Another excellent example of shape-matching design is provided by Siéfert et al. in [8], where, instead of iteratively solving the optimization problem, the authors developed a direct geometric solution based on an analytical model to program arbitrary 3D shapes. The key idea is to precisely control the spatially varying expansions of soft materials by a well-designed airway network embedded inside the matrix [Figure 2(c)]. This work offers a powerful tool to transform soft rubbery plates into desired 3D structures.

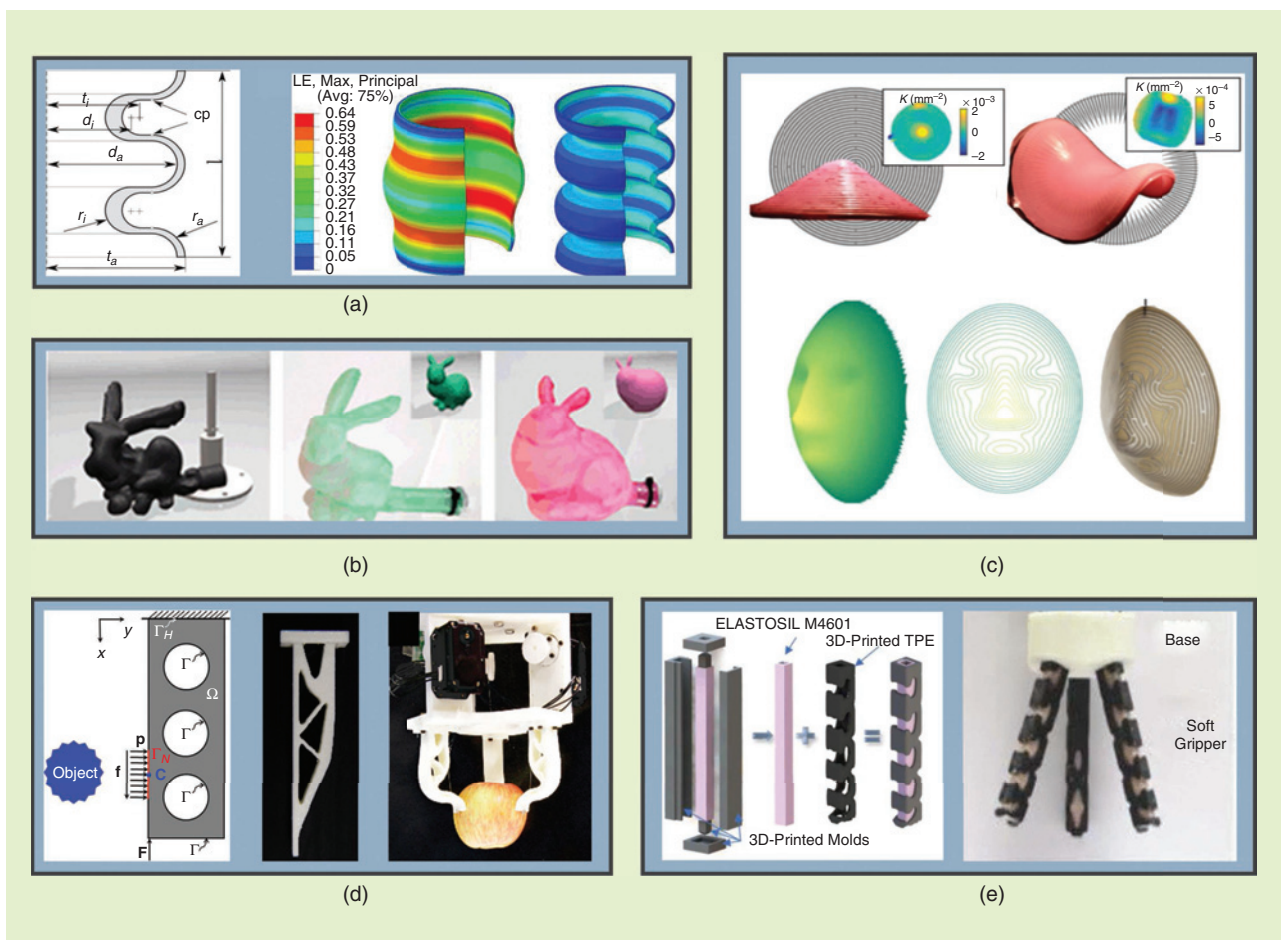


Figure 2. The geometry optimization. (a) A linear bellows-type pneumatic actuator described with a set of parameters (left) is optimized to minimize the induced maximal (Max.) principal strain (right) [6]. (b) The inverse design of the rubber balloons enables them to expand to the desired shapes upon pressurization [7]. (c) By precisely controlling the spatially varying expansions of soft materials with a well-designed airway network embedded inside the materials, one can program arbitrary 3D shapes [8]. (d) A cable-driven soft finger is modeled as a beam, subject to topology optimization (left), and the optimized fingers (middle) are assembled to make a soft gripper (right) [9]. (e) A pneumatic soft gripper is composed of an inner chamber made of rubber and an outer layer made of Tango (left), and the outer layer is topologically optimized to deliver maximum bending motion for conformal grasping (right) [10]. LE: logarithmic strain; TPE: thermoplastic elastomer.

To enable generally free-form evolution of shapes, e.g., changes in the connectivity of inner cavities of a deformable body, insight at the topology level is required. In comparison with size or shape optimization, topology optimization depends less on the initial design and works well when intuitive designs fail. Although topology optimization has been widely used in traditional computer-aided design as a versatile tool, few attempts have been made toward the automatic design of soft robots. The main challenge lies in integrating complicated soft material properties and actuation fields into the optimization framework, which causes difficulties in both theory and computation.

As initial attempts, researchers have applied topology optimization methods to design soft bending actuators for use in grippers driven by cables [9] [Figure 2(d)], [16], [17] or pneumatic actuators [10] [Figure 2(e)], [18], [19]. In these works, the gripper design problems were simply translated into the design of fingers modeled by cantilever beams, and their topological shapes were optimized by gradient-based algorithms. The optimization results typically have irregular structural forms and, thus, usually are difficult to manufacture using traditional methods such as molding and casting. Instead, they can be directly prototyped using additive manufacturing technologies [9], [10], [17], [18].

These initial attempts at topology optimization for soft robots did not fully capture the physics in their optimization models, such as the material nonlinearity, interactions, and frictions. In this sense, these works in principle still fall into the framework of traditional compliant mechanism design with topology optimization approaches by Sigmund [20] and Wang et al. [21], [22]. The incorporation of nonlinearities of soft materials may further unlock the potential of topology optimization for the generative design of soft robots [23].

Design Variable: Material

Material represents another dimension in the design space to be explored and plays another key role in determining the behaviors of soft robots. A straightforward example is that, in addition to the geometry-based design, the directionality of motion can be programmed by combining different materials. From a mechanics perspective, multiple materials may imbue a structure with complex deformation modes under a given load, which enables novel functionalities that are hard, if not impossible, to access using a single material. Compared to the geometry approach, the material optimization approach may result in functional soft robots with geometrically simple and compact-sized bodies.

An intuitive case is that one may use fibers to passively constrain the deformation of flexible, fluid actuators along the user-defined directions to generate differential motions. This design concept is akin to the actuation principle of muscular hydrostats. Elastomers to fabricate fluid actuators are typically isotropic, while the fibers can be treated as an anisotropic

material. Thus, the fibers can tailor the deformation of the actuator through their layout, leading to various motions, including extension, contraction, bending, and twisting. In [24], Connolly et al. presented a design strategy to track a pre-defined kinematic trajectory and developed an analytical model to identify the optimal fiber layout [Figure 3(a)]. In fact, this inherent mechanism has been well explored since the preliminary prototypes of McKibben artificial muscles [25], [26] and is still being employed in recent soft actuators and robots [27]–[31]. The focus of these examples is on the fiber layouts, while the fluid channels remain unchanged as the nondesign domain.

Among the feasible multimaterial approaches to design optimization of soft robots, functionally graded materials (FGMs) are opening up new possibilities. Despite being well investigated in material science, FGMs recently attracted the interest of roboticists because they can combine soft and rigid materials empowered by multimaterial printing technologies. One of the first efforts to exploit FGMs to design soft robots can be found in [32], where Bartlett et al. developed a robot powered by combustion and the bodies consisted of nine types of materials with gradient Young's modulus spanning three orders of magnitude. The smooth stiffness gradient avoids the stress concentration that typically occurs on the interface of two significantly different materials [Figure 3(b)]. However, the material gradient in the FGMs has yet to be optimized with fewer human interventions to fully unlock their potential to produce spatially varying stiffness and motions upon actuation.

To leverage the full design space spanned by multimaterials, free-form distributions of multimaterials and associated optimization algorithms are in high demand. Hiller and Lipson [33] demonstrated cantilever beams that deflected in pre-defined profiles by virtue of spatially varying soft and rigid materials, and the optimization was implemented with evolutionary search algorithms [Figure 3(c)]. Ma et al. [34] presented a systematic design and fabrication framework for soft pneumatic machines, with the desired motions of a heart beating upon pressurization, by first optimizing the chamber arrangement and subsequently optimizing the multimaterial distributions [Figure 3(d)].

The incorporation of active materials may further equip soft robots with new functions, although design optimization is in its earliest infancy. For example, inspired by bones and joints in human fingers, Yang et al. [35] incorporated shape memory polymers (SMPs) into the finger design as stiffness-tunable joints. The rational design of active materials such as SMPs in soft robots has not been explored much and represents a research direction to enrich the functionalities of soft robots.

Design Variable: Metamaterial

A metamaterial is generally defined as a material encoded at microscopic or mesoscopic scales to exhibit physical properties, rarely found in natural materials, with various engineering applications. Metamaterials derive their properties not

only from the base material but, more importantly, also from the featured structures at the microscopic scale in terms of shape, orientation, and arrangement.

Recently, metamaterials have been receiving increasing attention in soft robotics. The involvement of metamaterials may lead to paradigm shifts in the design of soft robots by directly encoding the desired complex motion within the material architectures, leading to conformable monolithic systems [42]. Currently, the rational design optimization of metamaterials remains in its early infancy, and we focus here on how various metamaterials provide new insight into the design of soft robots.

As mentioned, fibers have features of anisotropy and can be exploited to program motions of soft robots. By

assembling fibers with user-defined patterns, general anisotropies that span more directions can be achieved. Textile fabrics are such examples whose anisotropies are directly encoded by the weaving or knitting paths at the stage of fabrication [Figure 4(a)]; they have been widely used in wearable robotic devices for hand, ankle, and foot rehabilitation [36], [43], [44]. Inspired by layered human muscles, such as the transverse abdominis, Zhu et al. [45] recently presented a new family of fluidic fabric muscle sheets based on composite fabric structures that admitted design options at multiple scales, adaptability to curved structures, and large work densities. They also investigated how combinations of the fabric type and stitch design modulate the patterns of stretchability.

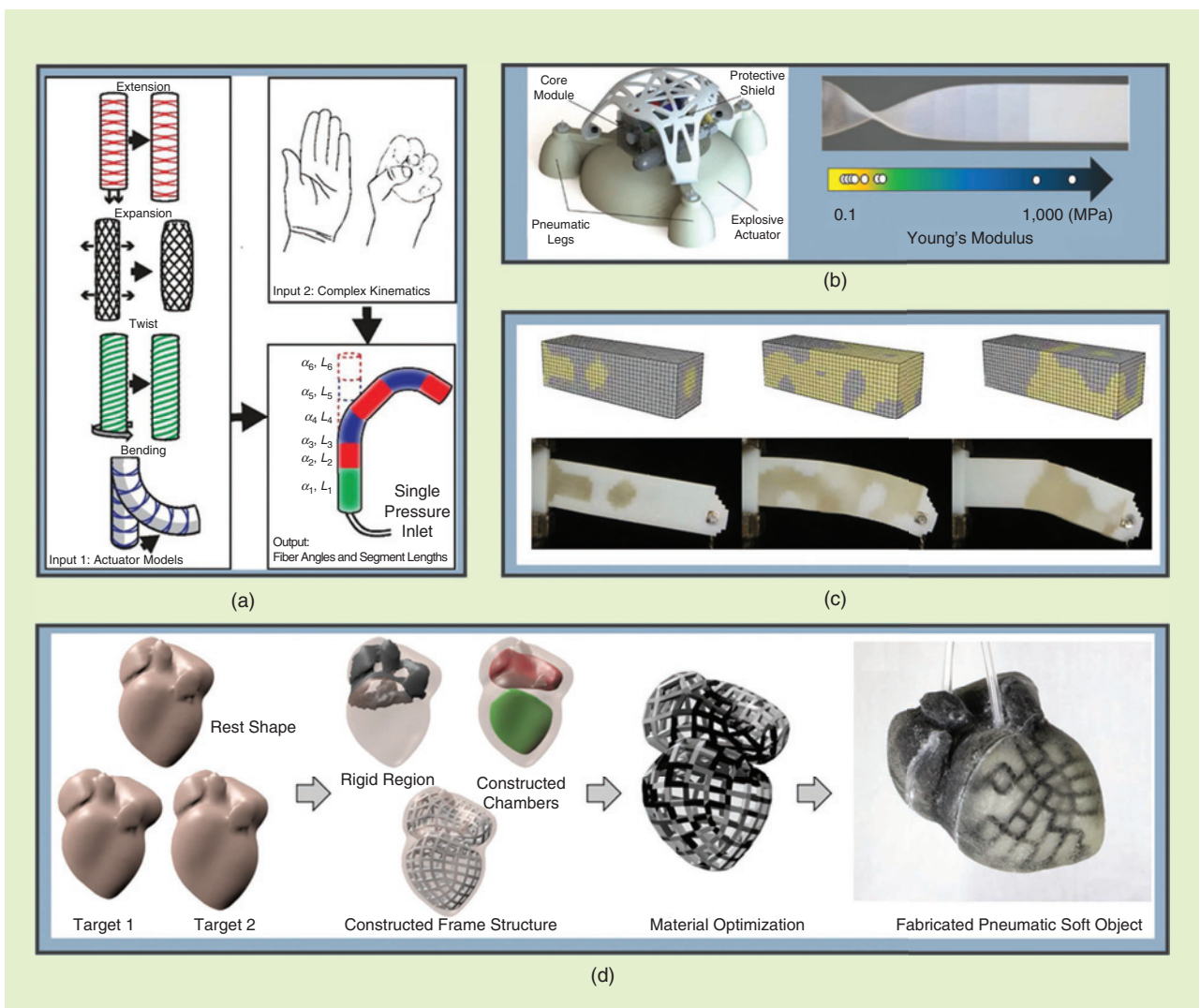


Figure 3. The material optimization. (a) The fibers can passively constrain the deformation of pneumatic tubes along user-defined directions to program the output motions (left); one may take a prescribed motion (top right) as the input and optimize the design parameters for actuators to replicate the desired motion upon pressurization (bottom right) [24]. (b) A combustion-powered robot made of nine different materials in terms of modulus attains a smooth stiffness gradient [32]. (c) Soft and hard materials in a cantilever beam are automatically designed using evolutionary algorithms to enable the beam to deflect in a user-defined profile [33]. (d) A systematic design and fabrication framework for soft pneumatic matters with desired shapes upon pressurization. Taking a rest shape and target shapes of a heart model as the input (left), the method first optimizes the chamber arrangement and frame structures (middle left) and subsequently optimizes the material distribution (middle right) of the frames to reproduce the motion behavior of a beating heart (right) [34].

Origami and kirigami represent a special category of metamaterials that lend themselves to programmable morphing of robots. Origami-based metamaterials are usually made by folding thin-walled sheets along predesigned creases to form ridges and valleys [46]. Driving rigid origami by vacuuming, artificial muscles were developed in [47] for use in soft grippers with excellent load capability. Jeong and Lee employed an origami twisted tower to fabricate the fingers of a robotic manipulator [Figure 4(b)], which potentially can be used to manipulate fragile objects [37]. Rafsanjani et al. [38] harnessed kirigami principles to remarkably improve the crawling speed of a soft actuator [Figure 4(c)]. The deformable kirigami surfaces buckle and induce remarkable directional frictional properties. Readers may refer to [48] for a comprehensive review of soft origami robots.

Slender beams are widely used as basic units in flexible metamaterials. The designable arrangements of elastic beam elements may lead to desired mechanical behaviors that are otherwise difficult to achieve, such as negative Poisson's ratio

(auxetics). Mark et al. [39] provided an excellent example using auxetic and nonauxetic clutches to simplify the locomotion of a soft robot with only one actuator instead of three [Figure 4(d)]. More generally, auxetic metamaterials may endow a soft robot with the capability of shape matching upon actuation using cellular structures, which consist of auxetic and nonauxetic units [49].

Elastic beam elements may buckle when subjected to axial compressions. This simple phenomenon opens up a new avenue for reversible pattern transformations in metamaterials that consist of networks of elastic beams. This mechanism was exploited by Yang et al. [40] in soft grippers to produce several classical motions driven by a single negative pressure [Figure 4(e)]. To improve structural stiffness and enhance grasping force, the design was further improved in [50], where the output work was taken as the objective function.

More generally, a metamaterial derives its properties by encoding its constituent microstructures [5]. Schumacher et al.

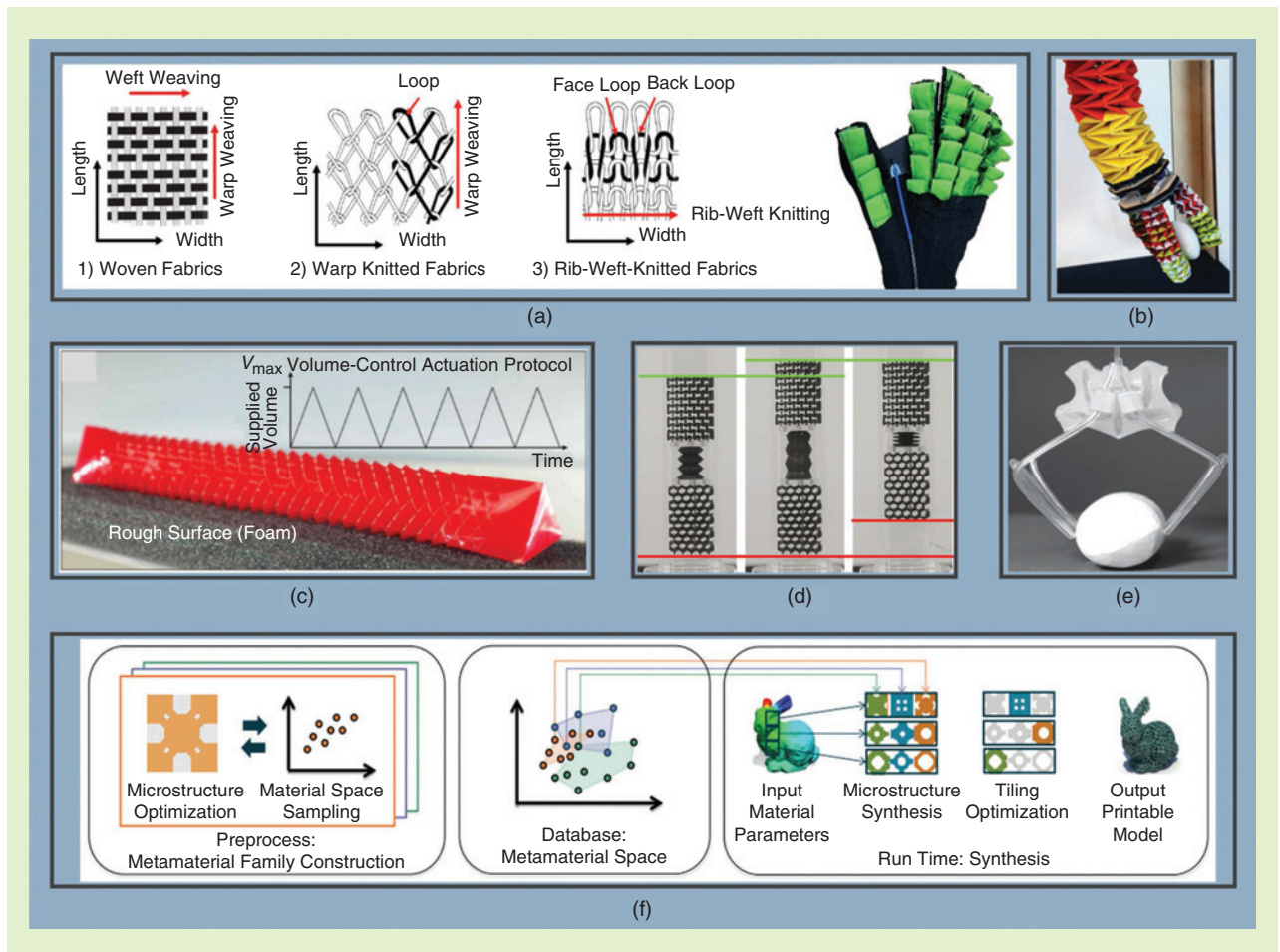


Figure 4. The metamaterial optimization. (a) Textile fabrics produced by weaving and knitting methods (left) are used to simultaneously program the motions and increase the load capabilities of a soft wearable assistive glove (right) [36]. (b) An origami twisted tower to fabricate the fingers of a robotic manipulator [37]. (c) An efficient crawling robot benefits from kirigami surfaces wrapped around an extending soft actuator [38]. (d) Auxetic and nonauxetic clutches simplify the locomotion of a soft robot with only one actuator [39]. (e) Elastic beams buckle under negative pressure and enable a soft gripper [40]. (f) An automatic design strategy of microstructures for physical prototypes with desired mechanical properties. Taking specified material parameters as the input, the method automatically optimizes the local microstructures that generate the target deformation behavior [41].

[41] proposed a method to design deformable objects with spatially varying microstructures using 3D printing. Optimization was conducted to design tiled microstructures by interpolating families of related structures to smoothly vary the material properties over a wide range [Figure 4(f)]. However, the microstructure configurations were limited by the prescribed family. The microstructure design may further benefit from unconstrained topology optimization with natural interconnections [51] and consideration of large deformation [52] and buckling phenomena [53].

Design Variable: Actuation

Actuation plays an equally important role in design approaches for soft robots by directly determining the external stimuli. From the perspective of mechanics, actuators

Soft robots provide excellent examples of design-dependent problems, where the actuation is typically coupled with soft bodies.

define the form, magnitude, and direction of the input loads applied to a soft robot. Various actuation technologies in soft robotics introduce new opportunities and challenges. Unlike rigid robots, where the input force and torques are applied only at the joints, soft robots can be driven by mechanical loads and more often by active materials that are responsive to multiple physical fields,

which offers designers more freedom to modulate the actuation fields.

Cable tension and pneumatics represent the traditional actuation technologies in soft robots. Skouras et al. [54] developed a method to automate the design of cable-driven deformable characters that exhibit the desired deformation behaviors. The locations of cables on the character and material distribution were simultaneously optimized, which made the character deform to the target shape [Figure 5(a)]. Hiller and Lipson [33] proposed the concept of volumetric actuation materials for a pneumatic locomotive soft robot. Evolutionary algorithms were used, the fitness function taken to be the moving distance of the center of mass.

Dielectric elastomer actuators (DEAs), which form a classic category of electric active polymers, can generate large deformation when subjected to external high voltages [59]. Due to their advantages of large deformability and rapid response, DEAs have been widely used in soft robotic systems [60], [61]. However, current DEA design paradigms are mostly based on people's intuition or experiences, and a systematic mathematical modeling and optimization methodology is still lacking to exploit their actuation potentials for the desired motion tasks.

Hajiesmaili and Clarke [55] made a first attempt by applying gradient electric fields to DEAs along the thickness direction through a layer-by-layer fabrication, and voltage-tunable negative and positive Gaussian curvatures were produced [Figure 5(b)].

More generally, Chen et al. [56] recently developed an automatic design methodology to maximize the displacements of interest of DEAs by topology optimization of the spatially varying electric fields. The optimized design remarkably improved the output displacements by up to 75% compared to their intuitive counterparts, with applications in triggering planar sheets to shape-morph into the desired 3D configurations [Figure 5(c)]. A density-based topology optimization method was applied to the automatic design of DEAs by Wang et al. [62]. In addition, metastructures encoded with designable anisotropies can be combined with DEAs to produce programmable deformations, as demonstrated by a unidirectional actuator in [63].

Magnetic fields are also widely used to drive soft robots by providing a far-field actuation controlled in an untethered manner, and their advantages are long-range, dexterous, precise, fast, and robust characteristics. The magnetically responsive materials are expected to largely deform, navigate in complex workspaces, and perform specific tasks. To program their deformations, a popular avenue is to embed magnetic particles into a soft matrix to create spatially varying magnetic actuations and lead to the desired motions. Kim et al. [64] offered a delicate fabrication solution by directly encoding the layout of ferromagnetic particles in the printing process. Lum et al. [57] developed a design methodology to automatically generate the required magnetization profile and actuating fields, so that a soft cantilever deformed to the desired shapes [Figure 5(d)]. Recently, Tian et al. [58] employed a topology optimization approach to automate the layout design of the ferromagnetic domain. The objective function consists of subobjective functions for kinematics and stiffness requirements. The optimization method was verified on a gripper [Figure 5(e)].

Integrated Design

Although we have classified the optimization model of soft robots in terms of design variables, including geometry, material, metamaterial, and actuation, the boundaries among these variables are not clear. A metamaterial deals with both geometry and material at a small scale. A spatially varying actuation field is usually embodied within the geometry or material. This is the case for pneumatic actuation, where the pressurization is closely associated with the chamber geometry, and magnetic actuation, where the external magnetic field is distributed on the 3D distributed ferromagnetic domain. Thus, an integrated strategy for design optimization is

necessary, and consideration of a single design variable generally does not suffice.

In the context of topology optimization, the applied loads may depend on the specific design candidates, which are generally referred to as *design-dependent problems*. The load dependency has been difficult to address, even in cases of linear elasticity [65]. In general, all structures involving solid and fluid interactions carry such design-dependent loads.

Soft robots provide excellent examples of design-dependent problems, where the actuation is typically coupled with soft bodies. Thus, designers must cooptimize the actuation fields with the structural features, and powerful algorithms are in high demand.

Furthermore, the morphology of a soft robot can be codesigned with the control strategies, since its performance is concurrently determined by the soft bodies,

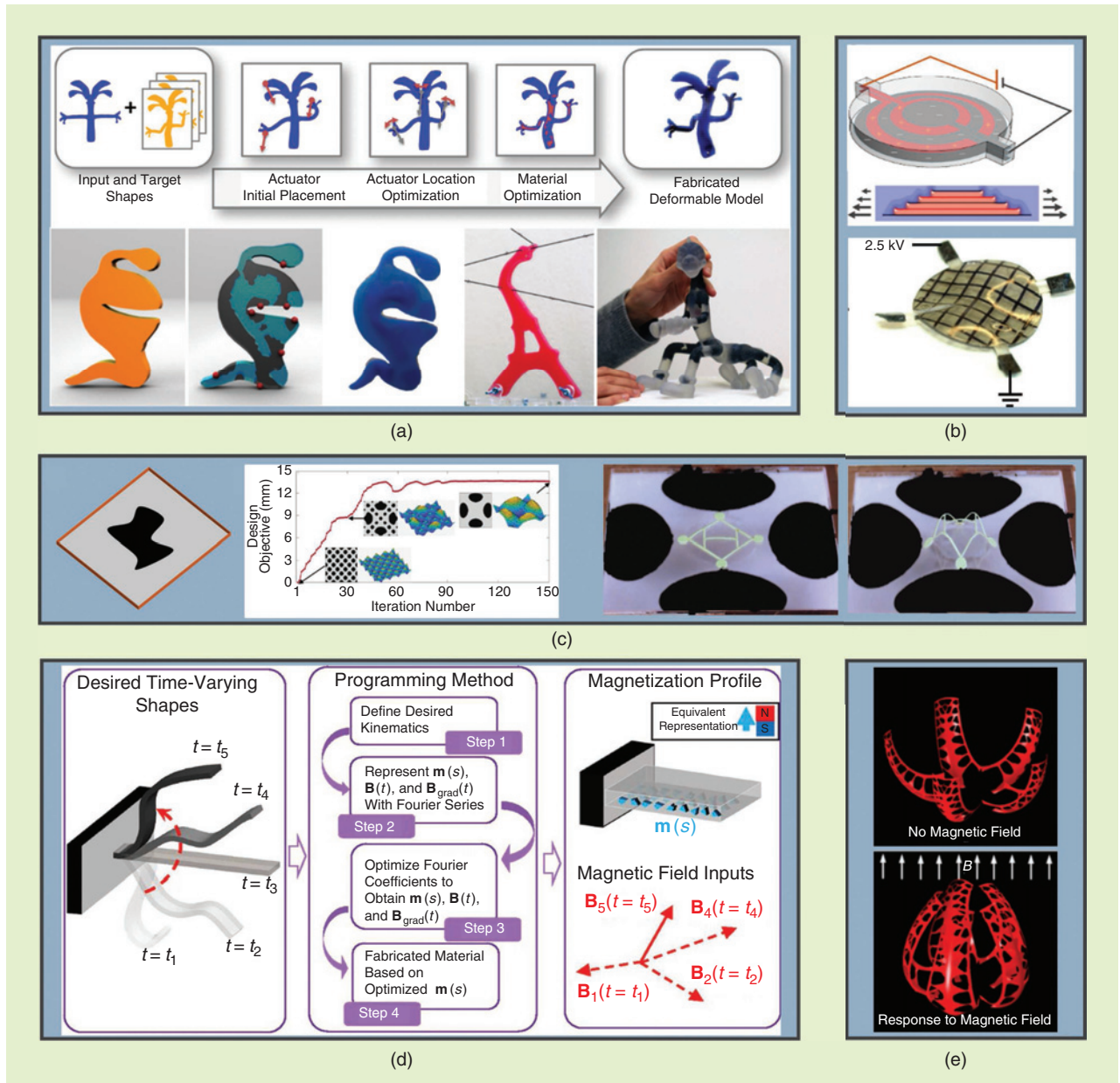


Figure 5. The actuation optimization. (a) The automatic design of cable-driven objects to produce physical replicas of the designed characters [54]. (b) Shape-morphing with dielectric elastomers is achieved by gradient electric fields along the thickness direction (top), which results in tunable Gaussian curvatures (bottom) [55]. (c) An automatic design methodology to maximize the displacements of interest of DEAs is enabled by topology optimization of the external spatially varying electric fields (left). The optimization process (middle) creates a design that triggers a planar sheet to buckle into 3D shapes upon electric activation (right) [56]. (d) A programming methodology automatically generates the required magnetization profile and actuating fields, so that soft magnetic materials deform to the time-varying shapes [57]. (e) A soft gripper made of ferromagnetic soft elastomers performs the desired motions from the reference state (top) to a deformed state (bottom) by optimizing the ferromagnetic domain using a topology optimization approach [58].

interactions, and control signals. Deimel et al. [66] investigated the feasibility of codesigning the morphology of soft hands and their control strategies for grasping and found that the codesign always outperformed the counterpart optimization limited to only one design domain. Spielberg et al. [67] proposed a “learning-in-the-loop optimization” design method that allows for the cooptimization of the controller and material parameters, using differentiable simulation techniques. These works represent initial attempts to create an end-to-end design paradigm for soft robots and should be further generalized to more complicated scenarios and validated through physical experiments.

Design Space Representation

To incorporate the physical design variables into an optimization model, a first prerequisite is the mathematical representation of the design space, which is spanned by the aforementioned design variables. The representation should, in general, be able to describe all candidates in the full design space in a unified mathematical framework.

In the framework of topology optimization, to describe an arbitrary topological shape, two classes of representation methods have been widely used.

In the framework of topology optimization, to describe an arbitrary topological shape, two classes of representation methods have been widely used. The first category is density-based methods, where the design

variables are represented by the continuous “artificial density” of 0–1 [68], [69]. Depending on the physical problem, the spatially varying density may describe the existence or removal of a material or an actuation field, and its distribution is typically discretized by finite elements and interpolated using shape functions. The other representation approach uses an implicit description of boundaries to parameterize the geometry, i.e., level-set-based methods that implicitly define the interfaces among material phases or actuation fields by iso-contours of a level-set function [70]–[72]. This implicit function enables a crisp description of the free-form boundaries. In comparison with explicit boundary descriptions, level-set functions enable the much more convenient tracking of topological changes.

When dealing with structural shape and topology optimization on free-form surfaces, the conformal mapping theory originating from differential geometry on the Riemannian manifold can be combined with topology optimization theories to recast the manifold embedded in the 3D space as a 2D topology optimization problem in the Euclidean space.

Ye et al. [73] provided a unified level-set-based computational framework for the generative design of free-form structures by conformally mapping the manifolds onto a 2D rectangle domain where the level-set function is defined, which allows for the convenient use of conventional computational schemes for level set methods.

Optimization Implementation

To explore the vast design space spanned by the geometry, material, and actuation fields, optimization tools that can automatically search for the optimal design candidates are essential. Powerful optimization algorithms are expected to refine the existing designs and, more importantly, create novel free-form designs that are otherwise hardly attainable by human intuitions or experiences. As summarized in Table 1, we organize the referred works in the “Optimization Model” section in terms of the design variable, report the employed optimization methods, and briefly comment on their generality and applications.

Simulation and Analysis

An important prerequisite to the implementation of optimization algorithms is the simulation and analysis tool that enables designers to evaluate the performance of the current robot design. This prerequisite has been very challenging for soft robots, mainly due to the nonlinearity, multiphysical coupling, and complex interplay between multiple bodies and the environments. In general, one can hardly derive analytical (or semianalytical) solutions for the kinematics of a soft robot but must resort to numerical computation. The analytical solutions listed in Table 1 are case specific or simplified by assumptions such as linearity. Nonlinear finite element analysis has dominated because it can accurately capture complex mechanical behaviors. However, nonlinear solvers tend to suffer convergence issues and are usually limited to relatively small deformations. In addition, the computational cost is very high, which hinders efficient evaluations of designs.

Many attempts have been made to perform fast and robust simulation. Instead of computing the continuous deformation fields, Hiller and Lipson [77] applied nonlinear relaxation where the structure was represented as a network of basic elements, including springs, beams, and masses. However, the parameter identification of the elements is a great challenge, and various actuation technologies can hardly be incorporated into the framework.

Based on the finite element method (FEM), Duriez and colleagues [78] have developed a well-known physics-based simulation engine, SOFA, which simulates the deformation of soft robots by progressively solving a quasi-static equilibrium function for each sample time. The method was recently further improved to achieve real-time computation with a reduced model [74] and has been verified on real soft robots [Figure 6(a)]. The computation efficiency requires further improvement, and

the complicated interactions of soft robots with the environment need to be captured.

An alternative approach is to transform the actuation of soft robots into a geometric change. Recently, Fang et al. [75] attempted to solve the kinematics of soft robots from a

geometry approach, and their framework incorporated cables, DEAs, and pneumatic actuations using varying line, area, and volume elements, respectively [Figure 6(b)]. The properties of multiple materials are geometrically modeled by calibration, and the kinematics solving is recast as a

Table 1. A summary of some representative works on soft robot design optimization.

Design variable					Design Space	Analysis	Optimization Method	Generality	Application	References	
□	■	★	↑	Objective							
□				Stress	Pneumatic	Size	N-FEM	Gradient	+	Linear actuator	[6]
□				Bending	Pneumatic	Size	N-FEM	Enumerative	+	Bending actuator	[11]
□				Twisting	Pneumatic	Size	N-FEM	Enumerative	+	Combined bending and twisting	[13]
□	■			Bending	Pneumatic	Size	N-FEM	Hybrid	+	Gripper	[14]
□				Shape matching	Pneumatic	Shape	N-FEM	Gradient	++	Inverse shape design	[7]
□			↑	Shape matching	Pneumatic	Shape	Analytical	N/A	+++	Inverse shape design	[8]
□				Bending	Cable	Topology	L-FEM	Gradient	+++	Gripper	[9], [16], [17]
□				Bending	Pneumatic	Topology	L-FEM	Gradient	+++	Gripper	[10], [18], [19]
	■			Extension, bending, twisting	Pneumatic	Size	Analytical	Nonlinear least square	+++	Finger	[24]
	■			Gradient stiffness	Combustion	Size	N-FEM	N/A	+	Conceptual	[32]
	■		↑	Bending, extension	Cable, pneumatic	Topology	N-FEM	Heuristics	++	Actuator	[33]
	■			Shape matching	Pneumatic	Topology	N-FEM	Gradient	+++	Artificial heart	[34]
		★		Shape matching	Compression	Size	N-FEM	N/A	++	Not specific	[49]
		★		Output work	Pneumatic	Size	N-FEM	Gradient	+	Gripper	[50]
		★		Shape and force	Pneumatic	Size	Analytical	Inspiration	++	Artificial muscle	[45]
		★		Microstructure material property	N/A	Topology	L-FEM	Gradient	+++	General	[41]
	■		↑	Desired motion	Cable	Topology	L-FEM	Gradient	+++	General	[54]
			↑	Gaussian curvature	DEA	Size	N-FEM	N/A	++	General	[55]
			↑	Point displacement	DEA	Topology	N-FEM	Gradient	+++	Not specific	[56], [62]
			↑	Shape matching	Magnetic	Shape	N-FEM	Gradient	++	General	[57]
□			↑	Bending	Magnetic	Topology	L-FEM	Gradient	+++	Gripper	[58]

□: geometry; ■: material; ★: metamaterial; ↑: actuation; L-FEM: linear FEM; N-FEM: nonlinear FEM; N/A: not applicable. Generality is described by the qualitative evaluation scale, +++, ++, +, from highest to lowest values.

constrained optimization problem. This geometry approach suffers from the limitation that it is based on a linear blending method; thus, it cannot well capture deformation with large strains.

To predict the dynamic behaviors of multiple bodies, Macklin et al. [76] further developed a simulation framework for hybrid rigid and soft bodies, in consideration of contacts and frictions, using a nonsmooth Newton method to address the underlying nonlinear complementarity problems. The nonlinear dynamics models of different bodies were coupled through a smooth isotropic friction model, and a complementarity preconditioner was applied to improve the convergence. To model the pressure loading, the authors adopted an activation function that applies a uniform internal volumetric stress to the domain of interest [Figure 6(c)]. However, more physical experiments need to be conducted to validate the computation framework.

Despite these attempts, there is no fast and effective simulation tool for the computation of soft robots, and this has been a major barrier to their design optimization. Some portable solutions have been developed, but they do not represent a universal solution. The ideal simulation tool is expected to have high efficiency and acceptable accuracy, robustness in a wide variety of problems, numerical stability, and the capability of addressing

various actuation fields, multiphysics, nonlinearities, and interactions with the environment.

Optimization Method

The vast design space of soft robots is extremely difficult for designers to manage. To explore the space and identify the (locally) optimal design, one usually starts from an initial guess and updates the existing design with a better one until the algorithm converges to a feasible solution or the prescribed objective is fulfilled. The search direction is crucial, and designers typically must conduct a sensitivity analysis. In the strategy of line search or trust region, one may define the direction of search based on the information of the objective function and its gradients or Hessians, which require that the problem is differentiable and twice differentiable, respectively. The gradient-based methods include the steepest descent and conjugate gradient as employed in the works [9], [10], [16], [17], [56], while Newton's method requires information of the Hessian matrix.

Although gradient-based optimization algorithms tend to get stuck in local optima, they have better scalability to the number of variables, which is particularly advantageous for handling large-scale problems. This is generally the case for topology optimization of soft robots with an extremely large number of design variables. There are numerous methods to

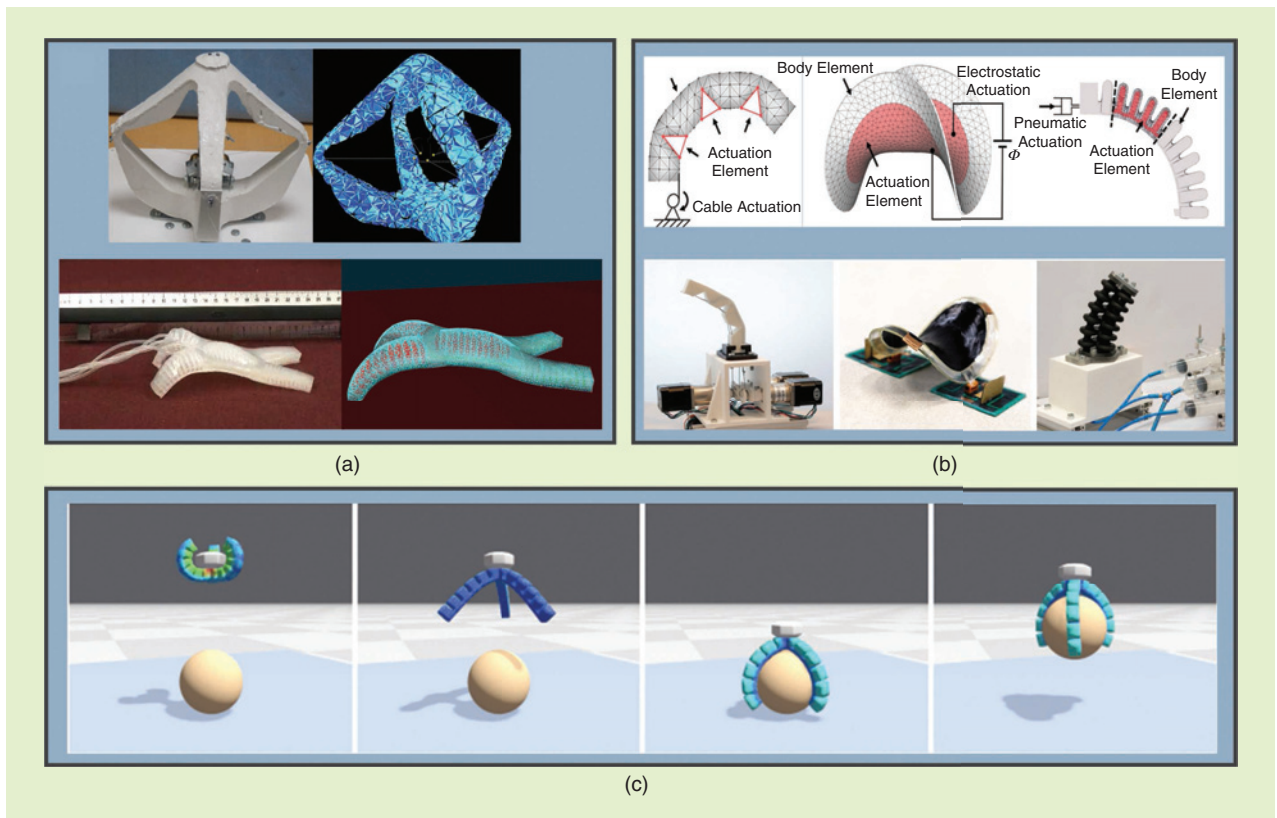


Figure 6. The simulation of kinematics and dynamics of soft robots. (a) A physics-based simulation engine, SOFA, realizes real-time simulation with a reduced model [74]. (b) A geometry approach to transforming the kinematics of soft robots into geometric change, which incorporates cables, DEAs, and pneumatic actuations using varying line, area, and volume elements respectively [75]. (c) The dynamics simulation of a soft gripper with robust contact coupling between the gripper and the object [76].

obtain the gradient information, including the simplest finite difference method in a numerical manner and the direct method and adjoint method in an analytical manner. Readers may refer to [79] and [80] for a comprehensive review on methods of sensitivity analysis of computational models in a unified mathematical framework.

Since soft robots have high nonlinearities in terms of geometry, material, and multiphysical fields, the gradients and Hessians of structural responses with respect to the associated design variables sometimes can be elusive to derive (if they exist). In addition, for discrete systems in which the derivative of the objective with respect to the design variables does not exist, gradient-based methods do not apply, e.g., for jamming-driven soft robots, where the behavior of jamming particles can hardly be captured by continuum mechanics.

There may be constraints imposed on the design optimization problems of soft robots, related to stress, mass, volume, and manufacturing. In the optimization model, one may combine the constraints as penalty functions with the objective function to translate the problem into an unconstrained one and solve it using the Lagrangian method. The augmented Lagrangian method is more widely used, especially in the field of topology optimization, since it helps suppress the ill conditioning by incorporating explicit Lagrange multipliers into the objective function.

Recently, evolutionary algorithms, e.g., genetic algorithms, have become a popular alternative approach in the design optimization of soft robots. This approach is essentially heuristic and does not require knowledge of gradients. Researchers have provided examples of evolutionary algorithms employed to design soft manipulators [81], joints [82], locomotion robots [33], [83], [84], and DEAs [85], [86] by stochastically exploring the design space [87]. With a representation, e.g., the Gaussian mixtures, genetic algorithms typically produce new designs by mutating or combining existing ones. The key step is the selection of existing designs to combine, e.g., the deterministic crowding selection method in [33].

The use of evolutionary algorithms does not exclude the computation of soft robots. In other words, when evaluating the fitness of each new design, one still must perform nonlinear simulation and analysis of the physical model to guide the search process. Without knowledge of the gradients, evolutionary algorithms usually suffer from poor scalability, premature convergence, and slow convergence speed, which may result in extremely high computational costs for large-scale design variables of soft robots.

Learning from nature is another alternative approach when rational design optimization is difficult, i.e., the so-called bio-inspired design. Natural intelligence is the delicate result of the long-term evolution of a body and a brain together. Many examples of bioinspired soft robots have been offered based on learning from octopuses [88], [89] and elephant trunks [90], [91], but many of them are limited to a copy of natural organisms instead of engineering replicates created based on the

inherent physical principles [92]. This phenomenon is mainly caused by the lack of powerful and reliable actuators and multifunctional materials on par with natural counterparts. Nevertheless, designers can greatly benefit from bioinspiration by identifying key principles and transforming them into the design of soft robots.

Discussion and Future Outlook

Despite progress on the design optimization of soft robots, significant research gaps need to be filled to create new robots that can perform complex tasks in practical applications. Here, we list some main limitations.

- 1) The optimization model is usually simple and restrictive, based on either the geometry space, material properties, or simplified robotic behaviors. The soft robot design involves strong interplay among geometry, material, structural conditions, and actuation paths to achieve motion and power performance customized for a particular class of tasks the robots are expected to perform. Current optimization models can provide only limited insights into the design problems.
- 2) There is no effective, efficient, and robust simulation tool to rapidly evaluate the performance of a design candidate. The large deformation in the material of soft robots typically induces nonlinearities, multiphysical coupling, and stability issues. Their full kinematics and dynamics are complex mechanics problems that are difficult to tackle.
- 3) Reliable and robust optimization algorithms have not been developed. The conventional optimization methods based on gradients require a great deal of mathematical reasoning. Heuristic algorithms promise a feasible solution, but their poor scalability cannot handle large-scale optimization problems. The potential of optimization to create new designs for soft robots remains to be explored.

These limitations also point to potential future research efforts and prospects, as these problems may be addressed from the following perspectives.

Modeling of Soft Active Materials

Soft active materials in response to external stimuli are increasingly used in the construction of soft robots, as summarized in recent articles [93]–[95]. Structural engineering of these materials is enabling novel controllable mechanical responses and extending the functionalities of soft robots. However, many material systems have no mechanical models to mathematically describe their properties. To be readily encoded in optimization, the mechanical model is expected to be simple and sufficient to capture the key material properties.

Modeling of Robotic Behaviors

Performing a given task generally requires a sequence of movements. An analog can be found in the rigid robot design. Rodriguez and Mason translated the desired mechanical function of an end effector for manipulation

into a sequence of contact constraints in a geometry sense, and they subsequently derived the shape of the effector by synthesizing these constraints in a field vector [96]. The key insight was to create an extended space spanned by the Cartesian product of the configuration space of the mechanism and its workspace. In the future, the workspace of a soft robot when performing a given task, instead of only one working state as in most existing studies, may be incorporated into the optimization model.

In some scenarios, the physical model of soft robots may not be fully specified, e.g., when it depends on interactions that are unknown at the stage of formulation. Instead of guessing about the uncertain quantities, designers may expect more robust solutions by introducing extra knowledge of the quantities into the model. For example, the interactions between a soft gripper and objects may be characterized by a number of possible scenarios with different contact conditions [9], and the probabilities of each scenario can be estimated through experimental tests. Therefore, one may employ stochastic optimization algorithms to quantify these uncertainties so that the model can be optimized to generate the desired performance.

Efficient Simulation Tools

The major concerns for the simulation of soft robots are computational cost, convergence, and stability. In addition to large-scale computation, simulation may suffer from convergence issues. Since soft robots typically experience large deformation, extensive distortions may occur locally, thin members may easily buckle, and there may be multiple stable solutions. These phenomena usually need to be addressed case by case, which hinders the automatic evaluation in an optimization loop.

In the field of computer graphics, people usually need to produce physically plausible solutions. In particular, simulation tools developed to animate deformable bodies are promising to lend themselves to simulations of soft robots [97], [98]. In their simulation framework, analysis problems are commonly modeled as constrained optimization problems, refined by preconditioning treatments, decomposed into a set of subproblems, and iteratively solved by various algorithms, such as sequential quadratic programming. Recently, Hu et al. [99] developed ChainQueen, a real-time differentiable physical simulator for soft robots based on the moving least-squares material point method. The differentiable simulator can be naturally incorporated into gradient-based optimization algorithms to allow for the codesign of soft robots. However, these promising simulation frameworks have not been well verified in physical scenarios. In addition, commonly used computational tricks in the context of computer graphics for numerical convergence and speed must be carefully addressed according to physical laws, and more actuation technologies should be encoded into the simulation framework.

Powerful Optimization Algorithms

Mathematical formulations of design optimization for soft robots can be addressed in the framework of current optimization theory [100], except they are generally complicated and characterized by large scale, nonlinearity, nonconvexity, and possibly discontinuity and uncertainty. The optimization model may be ill conditioned, and the sensitivity of the objective to the design variables can be elusive to obtain. The theory of topology optimization from a structure or mechanism perspective can help lay a foundation for design optimization of soft robots by further incorporating the nonlinearities and various actuation technologies into the framework.

Selection and development of optimization algorithms largely depend on the optimization model. There is no universal solution; instead, people need to employ appropriate algorithms for the formulated problem. For continuous and smooth design objective and variables, gradient- and Hessian-based algorithms are preferred to find (locally) optimal solutions. For discrete problems, the design space is not continuous, and heuristic algorithms may apply. When the optimization problem is not deterministic, stochastic optimization techniques should be developed. Tradeoffs between convergence and storage and between robustness and speed are always important numerical issues in the optimization implementation.

Conclusions

Soft robot design rests on the twin pillars of material–structure and properties–performance relations, in an analogy to the well-known Olson’s linear concept of “materials by design.” The process of relating materials to structure is essentially a modeling simulation task, while the process of relating properties to performance is effectively a synthesis optimization exercise. Establishing optimization-based design methods is an important step toward enabling the rapid and concurrent design for both materials and machines with the potential for significant advancement.

The performance of soft robots can be enhanced by exploring the ample design space offered by geometry, material, metamaterial, and actuation. With the support of high-performance computing, robust and efficient simulation tools and optimization algorithms are essential. Once promising designs are identified, their practical implementation may require advanced technologies for fabrication and manufacturing. Advances in multimaterial 3D printing are promising to address the fabrication challenges.

In the long term, an end-to-end design framework will incorporate robot morphologies, interactions with the environment, and control signals. Optimization-based design methods will encompass a unified mathematical representation of the state variables and physical laws of soft materials, powerful simulators, and optimization algorithms, which open up new possibilities of encoding complex behaviors of a soft robot within its physical body. We have proposed possible research prospects with an expectation that design optimization tools will empower soft robots with currently unforeseen functionalities.

Acknowledgment

Feifei Chen would like to acknowledge support from the National Natural Science Foundation of China under Grant No. 51905340 and from the Shanghai Sailing Program under Project 19YF1422900.

References

- [1] C. Majidi, "Soft robotics: A perspective-current trends and prospects for the future," *Soft Robot.*, vol. 1, no. 1, pp. 5–11, 2014. doi: 10.1089/soro.2013.0001.
- [2] D. Rus and M. T. Tolley, "Design, fabrication and control of soft robots," *Nature*, vol. 521, no. 7553, pp. 467–475, 2015. doi: 10.1038/nature14543.
- [3] C. Laschi, B. Mazzolai, and M. Cianchetti, "Soft robotics: Technologies and systems pushing the boundaries of robot abilities," *Sci. Robot.*, vol. 1, no. 1, p. eaah3690, 2016. doi: 10.1126/scirobotics.aah3690.
- [4] C. Laschi and B. Mazzolai, "Lessons from animals and plants: The symbiosis of morphological computation and soft robotics," *IEEE Robot. Autom. Mag.*, vol. 23, no. 3, pp. 107–114, 2016. doi: 10.1109/MRA.2016.2582726.
- [5] D. Howard, A. E. Eiben, D. F. Kennedy, J.-B. Mouret, P. Valencia, and D. Winkler, "Evolving embodied intelligence from materials to machines," *Nature Mach. Intell.*, vol. 1, no. 1, pp. 12–19, 2019. doi: 10.1038/s42256-018-0009-9.
- [6] G. Dämmer, S. Gablenz, A. Hildebrandt, and Z. Major, "Design and shape optimization of PolyJet bellows actuators," in *Proc. 2018 IEEE Int. Conf. Soft Robot. (RoboSoft)*, pp. 282–287. doi: 10.1109/ROBO-SOFT.2018.8404933.
- [7] M. Skouras, B. Thomaszewski, B. Bickel, and M. Gross, "Computational design of rubber balloons," *Comput. Graph. Forum*, vol. 31, no. 2, pp. 835–844, 2012. doi: 10.1111/j.1467-8659.2012.03064.x.
- [8] E. Siéfert, E. Reyssat, J. Bico, and B. Roman, "Bio-inspired pneumatic shape-morphing elastomers," *Nature Mater.*, vol. 18, no. 1, pp. 24–28, 2019. doi: 10.1038/s41563-018-0219-x.
- [9] F. Chen et al., "Topology optimized design, fabrication, and characterization of a soft cable-driven gripper," *IEEE Robot. Autom. Lett.*, vol. 3, no. 3, pp. 2463–2470, 2018. doi: 10.1109/LRA.2018.2800115.
- [10] H. Zhang, A. S. Kumar, F. Chen, J. Y. Fuh, and M. Y. Wang, "Topology optimized multimaterial soft fingers for applications on grippers, rehabilitation, and artificial hands," *IEEE/ASME Trans. Mechatronics*, vol. 24, no. 1, pp. 120–131, 2019. doi: 10.1109/TMECH.2018.2874067.
- [11] Y. Elsayed et al., "Finite element analysis and design optimization of a pneumatically actuating silicone module for robotic surgery applications," *Soft Robot.*, vol. 1, no. 4, pp. 255–262, 2014. doi: 10.1089/soro.2014.0016.
- [12] B. Mosadegh et al., "Pneumatic networks for soft robotics that actuate rapidly," *Adv. Functional Mater.*, vol. 24, no. 15, pp. 2163–2170, 2014. doi: 10.1002/adfm.201303288.
- [13] T. Wang, L. Ge, and G. Gu, "Programmable design of soft pneu-net actuators with oblique chambers can generate coupled bending and twisting motions," *Sensors Actuators A, Phys.*, vol. 271, pp. 131–138, Mar. 2018. doi: 10.1016/j.sna.2018.01.018.
- [14] Z. Wang and S. Hirai, "Geometry and material optimization of a soft pneumatic gripper for handling deformable object," in *Proc. 2018 IEEE Int. Conf. Robot. Biomimetics (ROBIO)*, pp. 612–617. doi: 10.1109/ROBIO.2018.8665234.
- [15] M. Skouras et al., "Designing inflatable structures," *ACM Trans. Graph.*, vol. 33, no. 4, pp. 1–10, 2014. doi: 10.1145/2601097.2601166.
- [16] Y. Liu and M. Y. Wang, "Topology design of a conforming gripper with distributed compliance via a level set method," in *Proc. 2014 IEEE Int. Conf. Robot. Biomimetics (ROBIO 2014)*, pp. 2191–2196. doi: 10.1109/ROBIO.2014.7090662.
- [17] C.-H. Liu et al., "Optimal design of a soft robotic gripper for grasping unknown objects," *Soft Robot.*, vol. 5, no. 4, pp. 452–465, 2018. doi: 10.1089/soro.2017.0121.
- [18] H. Zhang, M. Y. Wang, F. Chen, Y. Wang, A. S. Kumar, and J. Y. Fuh, "Design and development of a soft gripper with topology optimization," in *Proc. 2017 IEEE/RSJ Int. Conf. Intell. Robot. Syst. (IROS)*, pp. 6239–6244. doi: 10.1109/IROS.2017.8206527.
- [19] Y. Chen, Z. Xia, and Q. Zhao, "Optimal design of soft pneumatic bending actuators subjected to design-dependent pressure loads," *IEEE/ASME Trans. Mechatronics*, vol. 24, no. 6, pp. 2873–2884, 2019. doi: 10.1109/TMECH.2019.2943418.
- [20] O. Sigmund, "On the design of compliant mechanisms using topology optimization," *J. Struct. Mech.*, vol. 25, no. 4, pp. 493–524, 1997. doi: 10.1080/08905459708945415.
- [21] M. Y. Wang, S. Chen, X. Wang, and Y. Mei, "Design of multimaterial compliant mechanisms using level-set methods," *J. Mech. Design*, vol. 127, no. 5, pp. 941–956, 2005. doi: 10.1115/1.1909206.
- [22] M. Y. Wang, "A kinetoelastic formulation of compliant mechanism optimization," *J. Mechanisms Robot.*, vol. 1, no. 2, p. 021011, 2009. doi: 10.1115/1.3056476.
- [23] F. Chen, Y. Wang, M. Y. Wang, and Y. Zhang, "Topology optimization of hyperelastic structures using a level set method," *J. Comput. Phys.*, vol. 351, pp. 437–454, Dec. 2017. doi: 10.1016/j.jcp.2017.09.040.
- [24] F. Connolly, C. J. Walsh, and K. Bertoldi, "Automatic design of fiber-reinforced soft actuators for trajectory matching," *Proc. Nat. Acad. Sci.*, vol. 114, no. 1, pp. 51–56, 2017. doi: 10.1073/pnas.1615140114.
- [25] M. Gavrilović and M. Marić, "Positional servo-mechanism activated by artificial muscles," *Med. Biol. Eng.*, vol. 7, no. 1, pp. 77–82, 1969. doi: 10.1007/BF02474672.
- [26] C.-P. Chou and B. Hannaford, "Measurement and modeling of McKibben pneumatic artificial muscles," *IEEE Trans. Robot. Autom.*, vol. 12, no. 1, pp. 90–102, 1996. doi: 10.1109/70.481753.
- [27] G. Singh and G. Krishnan, "An isoperimetric formulation to predict deformation behavior of pneumatic fiber reinforced elastomeric actuators," in *Proc. 2015 IEEE/RSJ Int. Conf. Intell. Robot. Syst. (IROS)*, pp. 1738–1743. doi: 10.1109/IROS.2015.7353602.
- [28] J. Bishop-Moser and S. Kota, "Design and modeling of generalized fiber-reinforced pneumatic soft actuators," *IEEE Trans. Robot.*, vol. 31, no. 3, pp. 536–545, 2015. doi: 10.1109/TRO.2015.2409452.
- [29] P. Polygerinos et al., "Modeling of soft fiber-reinforced bending actuators," *IEEE Trans. Robot.*, vol. 31, no. 3, pp. 778–789, 2015. doi: 10.1109/TRO.2015.2428504.
- [30] S. Y. Kim, R. Baines, J. Booth, N. Vasios, K. Bertoldi, and R. Kramer-Bottiglio, "Reconfigurable soft body trajectories using unidirectionally stretchable composite laminae," *Nature Commun.*, vol. 10, no. 1, p. 3464, 2019. doi: 10.1038/s41467-019-11294-7.
- [31] J. Zhang et al., "Geometric confined pneumatic soft-rigid hybrid actuators," *Soft Robot.*, early access, Feb. 21, 2020. doi: 10.1089/soro.2018.0157.
- [32] N. W. Bartlett et al., "A 3D-printed, functionally graded soft robot powered by combustion," *Science*, vol. 349, no. 6244, pp. 161–165, 2015. doi: 10.1126/science.aab0129.
- [33] J. Hiller and H. Lipson, "Automatic design and manufacture of soft robots," *IEEE Trans. Robot.*, vol. 28, no. 2, pp. 457–466, 2012. doi: 10.1109/TRO.2011.2172702.

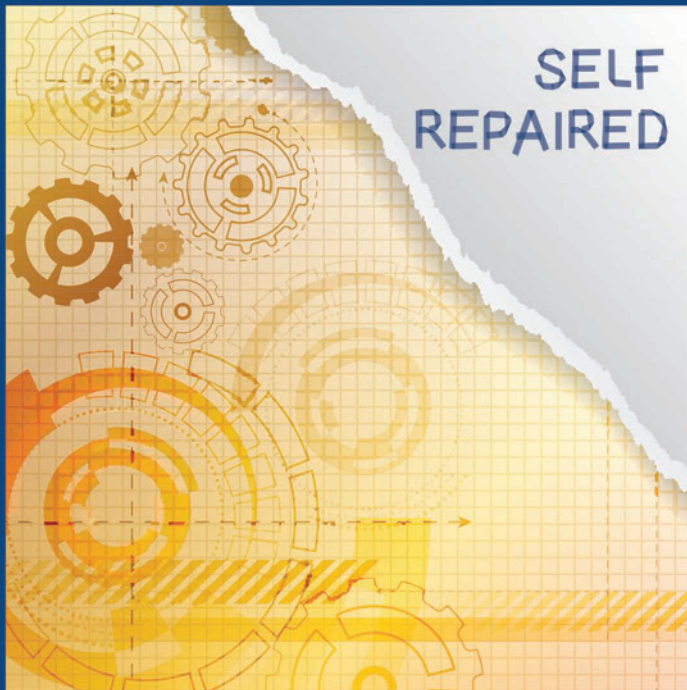
- [34] L.-K. Ma, Y. Zhang, Y. Liu, K. Zhou, and X. Tong, "Computational design and fabrication of soft pneumatic objects with desired deformations," *ACM Trans. Graph.*, vol. 36, no. 6, pp. 1–12, 2017. doi: 10.1145/3130800.3130850.
- [35] Y. Yang, Y. Chen, Y. Li, M. Z. Chen, and Y. Wei, "Bioinspired robotic fingers based on pneumatic actuator and 3d printing of smart material," *Soft Robot.*, vol. 4, no. 2, pp. 147–162, 2017. doi: 10.1089/soro.2016.0034.
- [36] L. Ge et al., "Design, modeling, and evaluation of fabric-based pneumatic actuators for soft wearable assistive gloves," *Soft Robot.*, early access, Jan. 29, 2020. doi: 10.1089/soro.2019.0105.
- [37] D. Jeong and K. Lee, "Design and analysis of an origami-based three-finger manipulator," *Robotica*, vol. 36, no. 2, pp. 261–274, 2018. doi: 10.1017/S0263574717000340.
- [38] A. Rafsanjani, Y. Zhang, B. Liu, S. M. Rubinstein, and K. Bertoldi, "Kirigami skins make a simple soft actuator crawl," *Sci. Robot.*, vol. 3, no. 15, p. eaar7555, 2018. doi: 10.1126/scirobotics.aar7555.
- [39] A. G. Mark, S. Palagi, T. Qiu, and P. Fischer, "Auxetic metamaterial simplifies soft robot design," in *Proc. 2016 IEEE Int. Conf. Robot. Automation (ICRA)*, pp. 4951–4956. doi: 10.1109/ICRA.2016.7487701.
- [40] D. Yang et al., "Buckling of elastomeric beams enables actuation of soft machines," *Adv. Mater.*, vol. 27, no. 41, pp. 6323–6327, 2015. doi: 10.1002/adma.201503188.
- [41] C. Schumacher, B. Bickel, J. Rys, S. Marschner, C. Daraio, and M. Gross, "Microstructures to control elasticity in 3D printing," *ACM Trans. Graph.*, vol. 34, no. 4, pp. 1–13, 2015. doi: 10.1145/2766926.
- [42] A. Rafsanjani, K. Bertoldi, and A. R. Studart, "Programming soft robots with flexible mechanical metamaterials," *Sci. Robot.*, vol. 4, no. 29, p. eaav7874, 2019. doi: 10.1126/scirobotics.aav7874.
- [43] P. Polygerinos, Z. Wang, K. C. Galloway, R. J. Wood, and C. J. Walsh, "Soft robotic glove for combined assistance and at-home rehabilitation," *Robot. Auton. Syst.*, vol. 73, pp. 135–143, Nov. 2015. doi: 10.1016/j.robot.2014.08.014.
- [44] M. Cianchetti, C. Laschi, A. Menciassi, and P. Dario, "Biomedical applications of soft robotics," *Nature Rev. Mater.*, vol. 3, no. 6, pp. 143–153, 2018. doi: 10.1038/s41578-018-0022-y.
- [45] M. Zhu, T. N. Do, E. Hawkes, and Y. Visell, "Fluidic fabric muscle sheets for wearable and soft robotics," *Soft Robot.*, vol. 7, no. 2, pp. 179–197, 2020. doi: 10.1089/soro.2019.0033.
- [46] Z. Zhakypov and J. Paik, "Design methodology for constructing multimaterial origami robots and machines," *IEEE Trans. Robot.*, vol. 34, no. 1, pp. 151–165, 2018. doi: 10.1109/TRO.2017.2775655.
- [47] S. Li, D. M. Vogt, D. Rus, and R. J. Wood, "Fluid-driven origami-inspired artificial muscles," *Proc. Nat. Acad. Sci.*, vol. 114, no. 50, pp. 13,132–13,137, 2017. doi: 10.1073/pnas.1713450114.
- [48] D. Rus and M. T. Tolley, "Design, fabrication and control of origami robots," *Nature Rev. Mater.*, vol. 3, no. 6, pp. 101–112, 2018. doi: 10.1038/s41578-018-0009-8.
- [49] M. Mirzaali, S. Janbaz, M. Strano, L. Vergani, and A. A. Zadpoor, "Shape-matching soft mechanical metamaterials," *Sci. Rep.*, vol. 8, no. 1, p. 965, 2018. doi: 10.1038/s41598-018-19381-3.
- [50] D. Guo and Z. Kang, "Chamber layout design optimization of soft pneumatic robots," *Smart Mater. Struct.*, vol. 29, no. 2, p. 025017, 2020.
- [51] Y. Wang, F. Chen, and M. Y. Wang, "Concurrent design with connectable graded microstructures," *Comput. Method Appl. Mech. Eng.*, vol. 317, pp. 84–101, Apr. 2017. doi: 10.1016/j.cma.2016.12.007.
- [52] A. Clausen, F. Wang, J. S. Jensen, O. Sigmund, and J. A. Lewis, "Topology optimized architectures with programmable Poisson's ratio over large deformations," *Adv. Mater.*, vol. 27, no. 37, pp. 5523–5527, 2015. doi: 10.1002/adma.201502485.
- [53] G. L. Bluhm, O. Sigmund, F. Wang, and K. Poulios, "Nonlinear compressive stability of hyperelastic 2d lattices at finite volume fractions," *J. Mech. Phys. Solid*, vol. 137, p. 103,851, Apr. 2020. doi: 10.1016/j.jmps.2019.103851.
- [54] M. Skouras, B. Thomaszewski, S. Coros, B. Bickel, and M. Gross, "Computational design of actuated deformable characters," *ACM Trans. Graph.*, vol. 32, no. 4, pp. 1–10, 2013. doi: 10.1145/2461912.2461979.
- [55] E. Hajiesmaili and D. R. Clarke, "Reconfigurable shape-morphing dielectric elastomers using spatially varying electric fields," *Nature Commun.*, vol. 10, no. 1, p. 183, 2019. doi: 10.1038/s41467-018-08094-w.
- [56] F. Chen, K. Liu, Y. Wang, J. Zou, G. Gu, and X. Zhu, "Automatic design of soft dielectric elastomer actuators with optimal spatial electric fields," *IEEE Trans. Robot.*, vol. 35, no. 5, pp. 1150–1165, 2019. doi: 10.1109/TRO.2019.2920108.
- [57] G. Z. Lum et al., "Shape-programmable magnetic soft matter," *Proc. Nat. Acad. Sci.*, vol. 113, no. 41, pp. E6007–E6015, 2016. doi: 10.1073/pnas.1608193113.
- [58] J. Tian, X. Zhao, X. Gu, and S. Chen, "Designing ferromagnetic soft robots (FerroSoRo) with level-set-based multiphysics topology optimization," in *Proc. 2020 Int. Conf. Robot. Automation (ICRA)*, pp. 10,067–10,074. doi: 10.1109/ICRA40945.2020.9197457.
- [59] R. Pelrine, R. Kornbluh, Q. Pei, and J. Joseph, "High-speed electrically actuated elastomers with strain greater than 100%," *Science*, vol. 287, no. 5454, pp. 836–839, 2000. doi: 10.1126/science.287.5454.836.
- [60] G.-Y. Gu, J. Zhu, L.-M. Zhu, and X. Zhu, "A survey on dielectric elastomer actuators for soft robots," *Bioinspiration Biomimetics*, vol. 12, no. 1, p. 011003, 2017. doi: 10.1088/1748-3190/12/1/011003.
- [61] U. Gupta, L. Qin, Y. Wang, H. Godaba, and J. Zhu, "Soft robots based on dielectric elastomer actuators: A review," *Smart Mater. Struct.*, vol. 28, no. 10, p. 103,002, 2019.
- [62] B. Chen, N. Wang, X. Zhang, and Y. Kuang, "Design of dielectric elastomer actuators using topology optimization on electrodes," *Smart Mater. Struct.*, vol. 29, no. 7, p. 075029, 2020. doi: 10.1088/1361-665X/ab8b2d.
- [63] K. Liu, S. Chen, F. Chen, and X. Zhu, "A unidirectional soft dielectric elastomer actuator enabled by built-in honeycomb meta-structures," *Polymers*, vol. 12, no. 3, p. 619, 2020. doi: 10.3390/polym12030619.
- [64] Y. Kim, H. Yuk, R. Zhao, S. A. Chester, and X. Zhao, "Printing ferromagnetic domains for untethered fast-transforming soft materials," *Nature*, vol. 558, no. 7709, pp. 274–279, 2018. doi: 10.1038/s41586-018-0185-0.
- [65] B.-C. Chen and N. Kikuchi, "Topology optimization with design-dependent loads," *Finite Element Anal. Design*, vol. 37, no. 1, pp. 57–70, 2001. doi: 10.1016/S0168-874X(00)00021-4.
- [66] R. Deimel, P. Irmisch, V. Wall, and O. Brock, "Automated co-design of soft hand morphology and control strategy for grasping," in *Proc. 2017 IEEE/RSS Int. Conf. Intell. Robot. Syst. (IROS)*, pp. 1213–1218. doi: 10.1109/IROS.2017.8202294.
- [67] A. Spielberg, A. Zhao, Y. Hu, T. Du, W. Matusik, and D. Rus, "Learning-in-the-loop optimization: End-to-end control and co-design of soft robots through learned deep latent representations," in *Proc. Adv. Neural Inf. Process. Syst.*, 2019, pp. 8284–8294.
- [68] M. P. Bendsoe and N. Kikuchi, "Generating optimal topologies in structural design using a homogenization method," *Comput. Methods Appl. Mech. Eng.*, vol. 71, no. 2, pp. 197–224, 1988. doi: 10.1016/0045-7825(88)90086-2.

- [69] O. Sigmund, "A 99 line topology optimization code written in Matlab," *Struct. Multidisciplinary Optim.*, vol. 21, no. 2, pp. 120–127, 2001. doi: 10.1007/s001580050176.
- [70] J. A. Sethian, *Level Set Methods and Fast Marching Methods: Evolving Interfaces in Computational Geometry, Fluid Mechanics, Computer Vision, and Materials Science*, vol. 3. Cambridge, U.K.: Cambridge Univ. Press, 1999.
- [71] M. Y. Wang, X. Wang, and D. Guo, "A level set method for structural topology optimization," *Comput. Methods Appl. Mech. Eng.*, vol. 192, nos. 1–2, pp. 227–246, 2003. doi: 10.1016/S0045-7825(02)00559-5.
- [72] G. Allaire, F. Jouve, and A.-M. Toader, "Structural optimization using sensitivity analysis and a level-set method," *J. Comput. Phys.*, vol. 194, no. 1, pp. 363–393, 2004. doi: 10.1016/j.jcp.2003.09.032.
- [73] Q. Ye, Y. Guo, S. Chen, N. Lei, and X. D. Gu, "Topology optimization of conformal structures on manifolds using extended level set methods (X-LSM) and conformal geometry theory," *Comput. Method Appl. Mech. Eng.*, vol. 344, pp. 164–185, Feb. 2019. doi: 10.1016/j.cma.2018.08.045.
- [74] O. Goury and C. Duriez, "Fast, generic, and reliable control and simulation of soft robots using model order reduction," *IEEE Trans. Robot.*, vol. 34, no. 6, pp. 1565–1576, 2018. doi: 10.1109/TRO.2018.2861900.
- [75] G. Fang, C.-D. Matte, R. B. Scharff, T.-H. Kwok, and C. C. Wang, "Kinematics of soft robots by geometric computing," *IEEE Trans. Robot.*, vol. 36, no. 4, pp. 1272–1286, 2020. doi: 10.1109/TRO.2020.2985583.
- [76] M. Macklin, K. Erleben, M. Müller, N. Chentanez, S. Jeschke, and V. Makoviychuk, "Non-smooth newton methods for deformable multi-body dynamics," *ACM Trans. Graph.*, vol. 38, no. 5, pp. 1–20, 2019. doi: 10.1145/3338695.
- [77] J. Hiller and H. Lipson, "Dynamic simulation of soft multimaterial 3d-printed objects," *Soft Robot.*, vol. 1, no. 1, pp. 88–101, 2014. doi: 10.1089/soro.2013.0010.
- [78] C. Duriez et al., "Framework for online simulation of soft robots with optimization-based inverse model," in *Proc. 2016 IEEE Int. Conf. Simul., Model., Program. Auton. Robot. (SIMPAN)*, pp. 111–118. doi: 10.1109/SIMPAN.2016.7862384.
- [79] K. K. Choi and N.-H. Kim, *Structural Sensitivity Analysis and Optimization 1: Linear Systems*. New York: Springer-Verlag, 2006.
- [80] J. R. Martins and J. T. Hwang, "Review and unification of methods for computing derivatives of multidisciplinary computational models," *AIAA J.*, vol. 51, no. 11, pp. 2582–2599, 2013. doi: 10.2514/1.J052184.
- [81] D. M. Bodily, T. F. Allen, and M. D. Killpack, "Multi-objective design optimization of a soft, pneumatic robot," in *Proc. 2017 IEEE Int. Conf. Robot. Autom. (ICRA)*, pp. 1864–1871. doi: 10.1109/ICRA.2017.7989218.
- [82] X. Li, K. Sun, C. Guo, T. Liu, and H. Liu, "Design, modeling and characterization of a joint for inflatable robotic arms," *Mechatronics*, vol. 65, p. 102,311, Feb. 2020. doi: 10.1016/j.mechatronics.2019.102311.
- [83] J. Rieffel, D. Knox, S. Smith, and B. Trimmer, "Growing and evolving soft robots," *Artif. Life*, vol. 20, no. 1, pp. 143–162, 2014. doi: 10.1162/ARTL_a_00101.
- [84] H. Lipson, "Challenges and opportunities for design, simulation, and fabrication of soft robots," *Soft Robot.*, vol. 1, no. 1, pp. 21–27, 2014. doi: 10.1089/soro.2013.0007.
- [85] Y. Wang, L. Zhang, S. Daynes, H. Zhang, S. Feih, and M. Y. Wang, "Design of graded lattice structure with optimized mesostructures for additive manufacturing," *Mater. Design*, vol. 142, pp. 114–123, Mar. 2018. doi: 10.1016/j.matdes.2018.01.011.
- [86] E. Bortot, O. Amir, and G. Shmuel, "Topology optimization of dielectric elastomers for wide tunable band gaps," *Int. J. Solid Struct.*, vol. 143, pp. 262–273, June 2018. doi: 10.1016/j.ijsolstr.2018.03.014.
- [87] G. Zames et al., "Genetic algorithms in search, optimization and machine learning," *Inform. Technol. J.*, vol. 3, no. 1, pp. 301–302, 1981.
- [88] C. Laschi, M. Cianchetti, B. Mazzolai, L. Margheri, M. Follador, and P. Dario, "Soft robot arm inspired by the octopus," *Adv. Robot.*, vol. 26, no. 7, pp. 709–727, 2012. doi: 10.1163/156855312X626343.
- [89] M. Wehner et al., "An integrated design and fabrication strategy for entirely soft, autonomous robots," *Nature*, vol. 536, no. 7617, pp. 451–455, 2016. doi: 10.1038/nature19100.
- [90] X. Wang, H. Faraji, and Y. Mengüç, "Incorporate oblique muscle contractions to strengthen soft robots," in *Proc. 2018 IEEE Int. Conf. Robot. Autom. (ICRA)*, pp. 4200–4205. doi: 10.1109/ICRA.2018.8461139.
- [91] M. Schaffner, J. A. Faber, L. Pianegonda, P. A. Rühls, F. Coulter, and A. R. Studart, "3' printing of robotic soft actuators with programmable bioinspired architectures," *Nature Commun.*, vol. 9, no. 1, pp. 1–9, 2018. doi: 10.1038/s41467-018-03216-w.
- [92] B. Mazzolai and C. Laschi, "A vision for future bioinspired and bio-hybrid robots," *Sci. Robot.*, vol. 5, no. 38, p. eaba6893, 2020. doi: 10.1126/scirobotics.aba6893.
- [93] J. M. McCracken, B. R. Donovan, and T. J. White, "Materials as machines," *Adv. Mater.*, vol. 32, no. 20, p. 1,906,564, 2020. doi: 10.1002/adma.201906564.
- [94] J. Zhang et al., "Robotic artificial muscles: Current progress and future perspectives," *IEEE Trans. Robot.*, vol. 35, no. 3, pp. 761–781, 2019. doi: 10.1109/TRO.2019.2894371.
- [95] Z. Shen, F. Chen, X. Zhu, K.-T. Yong, and G. Gu, "Stimuli-responsive functional materials for soft robotics," *J. Mater. Chem. B*, early access, Aug. 18, 2020. doi: 10.1039/D0TB01585G.
- [96] A. Rodriguez and M. T. Mason, "Effector form design for 1DOF planar actuation," in *Proc. 2013 IEEE Int. Conf. Robot. Autom.*, pp. 349–356. doi: 10.1109/ICRA.2013.6630599.
- [97] J. Kim and N. S. Pollard, "Fast simulation of skeleton-driven deformable body characters," *ACM Trans. Graph.*, vol. 30, no. 5, pp. 1–19, 2011. doi: 10.1145/2019627.2019640.
- [98] J. Tan, G. Turk, and C. K. Liu, "Soft body locomotion," *ACM Trans. Graph.*, vol. 31, no. 4, pp. 1–11, 2012. doi: 10.1145/2185520.2185522.
- [99] Y. Hu et al., "Chainqueen: A real-time differentiable physical simulator for soft robotics," in *Proc. 2019 Int. Conf. Robot. Autom. (ICRA)*, pp. 6265–6271. doi: 10.1109/ICRA.2019.8794333.
- [100] J. Nocedal and S. Wright, *Numerical Optimization*. New York: Springer-Verlag, 2006.

Feifei Chen, State Key Laboratory of Mechanical System and Vibration, Shanghai Jiao Tong University, and Robotics Institute, School of Mechanical Engineering, Shanghai Jiao Tong University. Email: ffchen@sjtu.edu.cn.

Michael Yu Wang, Robotics Institute, Department of Mechanical and Aerospace Engineering, and Department of Electronic and Computer Engineering of Hong Kong University of Science and Technology, Clear Water Bay, Kowloon. Email: mywang@ust.hk.





By Seppe Terryn, Joost Brancart, Ellen Roels, Guy Van Assche, and Bram Vanderborcht

Room Temperature Self-Healing in Soft Pneumatic Robotics

Autonomous Self-Healing in a Diels-Alder Polymer Network

Healable soft robotic systems have been developed by constructing flexible membranes out of Diels–Alder (DA) polymer networks. In these components, relatively large amounts of damage, on the centimeter scale, can be healed, provided that the temperature is increased to 80–90 °C. This article presents a new DA polymer network that can heal at room temperature through a smart design of the network that increases the molecular mobility in the material. This new material is used to develop the first healable soft robotic prototype that can autonomously recover from severe, realistic damage. The soft pneumatic hand can recover from various types of injuries, including being cut completely in half, without the need for a temperature increase. After

healing, the performance of the soft robotic prototype is recovered.

Introduction

Soft robots can resist strong mechanical impacts [1], [2]. However, throughout their lifetime, they are susceptible to other damaging conditions. They are prone to fatigue, which is the formation of microscopic cracks that propagate into macroscopic defects. In addition, their membranes can be perforated and cut by sharp objects, such as broken glass, corners, nails, and splinters. Soft grippers [3], [4] are being designed to manipulate delicate fruits and vegetables in agriculture and food packaging. Jagged twigs, thorns, sharp plastics, and glass can end up on the sorting lines and harm these grippers. Damage can influence the performance of the soft component. If the membrane of a pneumatic soft actuator is perforated, fluid escapes, and the actuator performance decreases. In many cases, the actuator can be used in this

Digital Object Identifier 10.1109/MRA.2020.3024275

Date of current version: 9 December 2020

low-efficiency, damaged state for a limited time, as the cut or perforation will tear further, leading to complete failure.

Many soft actuators are constructed out of silicone-based elastomeric networks, such as the Ecoflex series from Smooth-On [5], [6]. These elastomers are not expensive, and therefore it is relatively cheap to produce soft actuators. One way to solve the problem of a failed soft actuator is by replacing it completely with a new one. Although the production is cheap, the replacement of a soft actuator can be costly since it is usually done through human intervention. Most soft actuators are manufactured through casting silicone monomers in a (3D-printed) mold, followed by a curing step. During curing, the silicone-based network is formed by irreversible crosslinking. The permanently formed crosslinks do not enable the material to be reprocessed. Consequently, like most elastomeric polymers, these silicone-based networks are not recyclable. Hence, replacing failed soft actuators with new, cheaply produced parts is not the most ecological solution. Alternatively, the vulnerability of soft robots can be addressed by overdimensioning the components through substantial safety factors, avoiding the possibility of damage in dangerous situations. However, this leads to larger designs and less-energy-efficient systems, while potentially compromising the soft and safe characteristic.

Recently, by using smart materials, soft robotic designs have been improved, and new actuation principles are being generated [7]. This includes the use of shape memory, piezoelectric and self-healing (SH) materials, and integrating embodied intelligence [8]. In previous work [9]–[12], soft robotic actuators were developed out of SH polymers—more specifically, out of reversible elastomeric networks. The crosslinks in these elastomers are reversible DA bonds and provide the material with a healing ability [13]. Macroscopic damages, such as perforations and cuts, as well as microscopic fatigue cracks can be healed by heating these flexible materials. Out of these, SH soft grippers and hands were constructed [9], [14]. All of them could entirely recover from realistic damages.

Incorporating a healing function is an eco-friendlier solution to the vulnerability of soft robotics. In addition, a healing ability facilitates reducing the overdimensioning of systems and supports optimizing a design based on the function to be performed instead on potential damaging conditions. If these healable actuators are damaged very badly, they can still be recycled because the reversible characteristic of the crosslinks in the network enables reprocessing [9]. This can further decrease the ecological footprint. For successful healing, typically, a temperature increase to 80 °C is required. This can be done by heating the entire soft robotic part (the soft gripper [9]) in a healing station (e.g., an oven) or by integrating a heating device in the actuator design [15]. The need for a heat stimulus provides a certain control over the healing process. However, additional controlled heating systems are required, making the overall robotic system larger and more complex.

This research focuses on lowering the healing temperature of DA polymers toward room temperature, avoiding the need for an additional heating system. Such polymers that do not need an external stimulus to heal, other than the mechanical force of the formation of the damage itself, are called *autonomous SH polymers*. This article first introduces different mechanisms for autonomous healing that hold potential for soft robotics. Next, it gives a detailed explanation of how an autonomous SH DA polymer was synthesized. Healing at 25 °C is experimentally validated through extensive tensile testing. The applicability of this DA network for soft robotics is proven through the development of a soft hand prototype that is able to heal autonomously from centimeter-scale damage. Last, we address the recovery of the component's properties after healing.

Autonomous SH Polymers

There exist in the literature many autonomous SH polymers that rely on divergent healing mechanisms. Extrinsic autonomous SH polymers depend on healing agents embedded in micro/nanocapsules [16]. The downside of these extrinsic mechanisms is that the healing action can take place only a limited number of times at the same location. In addition, the healing mechanism usually allows recovery from only relatively small injuries. For the capsules to crack open, their shell must have a brittle characteristic, and the material of the matrix must be stiffer than that of the shell [16]. Consequently, extrinsic healing mechanisms work well for thermoset matrices, but they are not adequate for elastomers. Although they have potential for hard polymer components in robotics, extrinsic SH polymers are not interesting for constructing flexible soft robotic components.

There are intrinsic autonomous SH polymers having a healing mechanism that works at room temperature. These rely on reversible bonds and complexes that have fast dynamics at room temperature. A particularly impressive example is the hydrogel presented by Leibler et al. [17], a supramolecular network formed through physical hydrogen bonds. When slicing these materials, the hydrogen bonds are locally mechanically broken, producing many nonassociated groups near the fracture surface that are “eager” to link again. When pressing the fracture surfaces back together immediately after damage, these nonassociated groups will re-form hydrogen bonds, and the cut can be healed at room temperature. Using tensile tests, Leibler et al. proved that, after three hours of mending, up to 90% of the original strength was regained.

More recently, SupraPolix reported another autonomous SH elastomer, SupraB [18], with great potential for soft robotics. This supramolecular material is formed by hydrogen bond complexes that act as physical crosslinks. Again, when cut, the hydrogen complexes are de-bonded, and free groups created at the fracture surface can reconnect when its fractured areas are pressed back together. Using hydrogen bond complexes as crosslinks not only enhances the strength of polymer but also allows faster healing. This is explained by

the fact that a firm physical crosslink can be established when only a fraction of the hydrogen bonds of the complex have been formed. This is the case for SupraB, which instantaneously recovers part of its strength after the fracture surfaces are placed together [18], [19]. Longer healing times further increase the strength since a growing fraction of the hydrogen bonds is formed in the crosslink complex.

It is important to mention that, aside from the DA polymer used in this article, other autonomous, intrinsic SH polymers that rely on various mechanisms have mechanical and healing properties suitable to introduce healability with high

efficiency in soft robotics. Other intrinsic SH polymers with interesting properties (Young's modulus E , fracture stress σ , fracture strain ϵ , and healing efficiency η at 25 °C) are listed in Table 1, and others are discussed in [20].

Healing in DA Networks

DA polymers are networks containing reversible covalent crosslinks formed by a DA bond between a furan and a maleimide [Figure 1(a)]. The networks are formed using two monomers; bismaleimide (DPBM) and a furan-functionalized Jeffamine (FTx), obtained by irreversibly binding FGE on a Jeffamine (JT_x) using an epoxy-amine reaction (further details appear in the "Reagents" section). The DA reaction between a furan and a maleimide is an equilibrium reaction; consequently, the crosslink bonds are dynamic. This means that, for a specific temperature (in equilibrium conditions), a crosslink density can be defined. Although the crosslink density remains constant if the temperature continues unchanged, bonds are constantly broken and reformed in the dynamic network.

DA networks, in general, require heat to heal macroscopic damage [Figure 1(a)]. When damage occurs,

Table 1. Autonomous SH networks suitable for soft robotics.

Reversible Reaction	Institution	E (MPa)	σ (Maximum) (MPa)	ϵ (Maximum) (%)	η at 25 °C (%)
Hydrogen	SupraPolix [18]	0.8	0.35	250	90 (24 h)
	ESPCI Paris [17]	0.25	3	550	90 (3 h)
	UC [21]	17	1.94	780	90 (24 h)
Metal ligand	SU [22]	0.5	0.25	4,500	90 (48 h)
Exchange	Cidetec [23]	0.05	0.5	3,000	97 (24 h)
DA	VUB	0.12	0.1	245	80–97 (Seven to 14 days)

UC: University of California; VUB: Vrije Universiteit Brussel; SU: Stanford University.

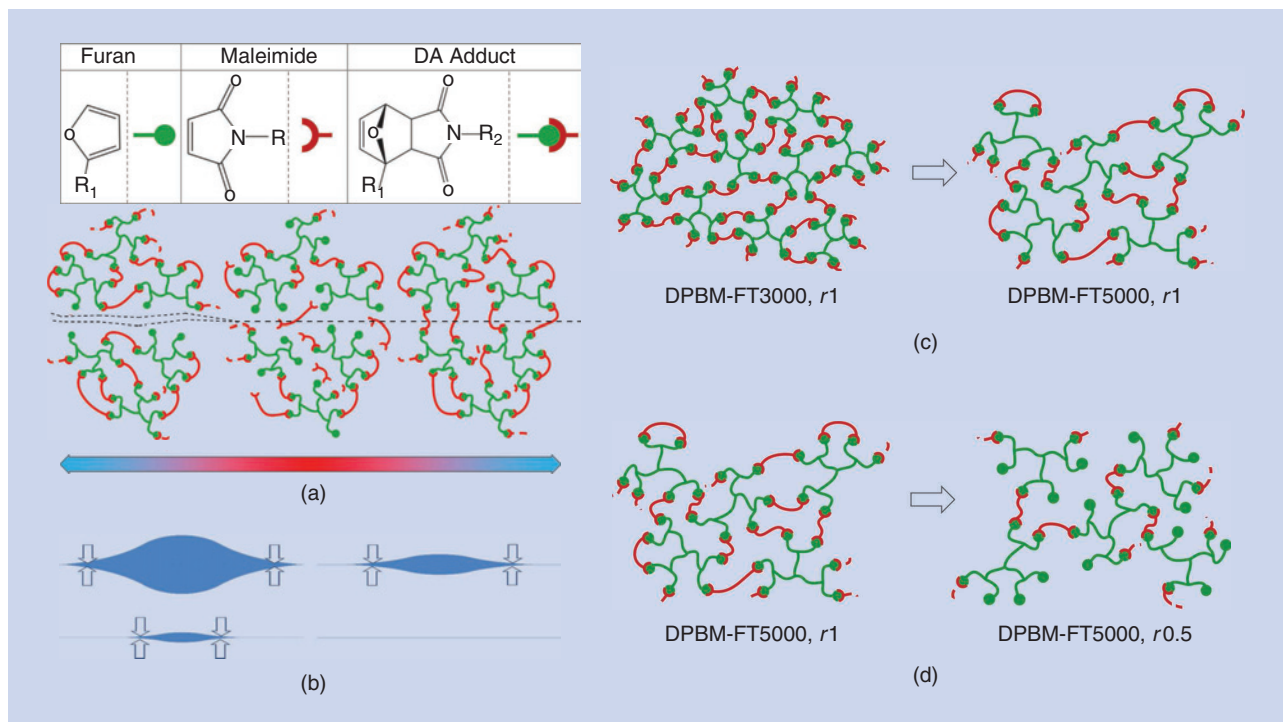


Figure 1. (a) Separated DA parts can be healed using a mild heating treatment. The result is a strong interface due to covalent DA bonds formed between a reactive furan and a maleimide. (b) The self-sealing zipping effect in DA networks with sufficient microscopic mobility enables cavities to slowly seal. (c) The molecular mobility in the network can be increased by decreasing the crosslink density, by raising the molecular weight of the monomer units, in this case, the molecular weight of the furan-functionalized compound (green). (d) Alternatively, the crosslink density can be decreased by lessening the maleimide-to-furan (r) ratio and by employing a deficit of reactive maleimide components (red) in the synthesis.

locally the DA bonds, which are the weakest links in the network [24], are mechanically broken, and the fracture surfaces are pulled apart. Healing starts by bringing the fracture surfaces back into contact. Upon reconnecting, microscopic misalignment is unavoidable, and cavities are created. To fill these microscopic voids, mobility in the network is essential so that the material can slowly close the openings through a “self-sealing zipping effect” [Figure 1(b)]. At the edges of the cavities, the exothermal formation of DA bonds and cohesive forces pull the fracture surfaces together, and the resulting self-sealing zipping effect gradually fills the entire cavity.

Mobility can be created by heating the network. Upon heating, the equilibrium of the DA reaction shifts toward the unbonded state, and the crosslink density decreases, increasing mobility (additional details are in [9]). As a result of the increased mobility, the cavities are slowly sealed. In this heated state, the number of reactive components as well as the furan and the maleimide increase. When the cavities are completely sealed, the network is cooled, after which the reactive components that were either mechanically formed (by the damage) or thermally created (by heating) react with one another and re-form the DA crosslinks. The result is that the damage is completely healed and the initial properties are entirely recovered. In other words, healing relies on two aspects: polymer chain mobility and the available reactive groups.

Reagents

Furfuryl glycidyl ether (96%) and 1,1'-(methylenedi-1,4-phenylene) DPBM (95%) were obtained from Aurora Chemicals. Jeffamine JT5000 and JT3000 (polypropylene glycol) bis(2-aminopropyl ether) with an average molecular weight of 5,649 g.mol⁻¹ and 2,916 g.mol⁻¹ were also obtained from Aurora Chemicals.

Lowering the Healing Temperature

To lower the healing temperature toward room temperature, the network mobility and available reactive groups at 25 °C must be increased. The network mobility can be augmented by decreasing the DA crosslink density. This crosslink density is affected by the molar weight of the monomer units, a furan-functionalized compound (Figure 1, in green), and a maleimide compound (Figure 1, in red). Increasing the molar weight (e.g., from FT3000 to FT5000; additional details are given in the “Reagents” section) decreases the crosslink density, which results in a higher molecular mobility [Figure 1(c)] and greater flexibility, which is expressed in lower mechanical moduli (Table 2).

A second parameter that influences the crosslink density is the ratio between the maleimide and the furan, denoted r :

$$r = [M]_0 / [F]_0, \quad (1)$$

in which $[M]_0$ and $[F]_0$ are the initial concentration of maleimide and furan used at the start of the synthesis of the network, respectively. Decreasing the r ratio leads to a deficit of maleimide and a decrease in the crosslink density, which again increases the molecular mobility [Figure 1(d) and Table 2]. On the other hand, a decrease in the crosslink density means that, when fractures occur, fewer DA bonds will be broken in a specific area, which results in fewer “free” available reactive groups at the fracture surfaces.

It is clear that the two motives for healing in DA networks—concentration of reactive components at the fracture surfaces and network mobility—are complementary. A higher crosslink density provides more reactive groups at the fracture surface, enhancing the interfacial bonding. On the other hand, a higher crosslink density greatly decreases network mobility, limiting the self-sealing zipping effect. In practice, network mobility is the determining factor for healing macroscopic damage that creates relatively large cavities between fracture surfaces.

For networks with a higher crosslink density (DPBM-FT5000, with $r = 4/6$ or $r = 6/6$), to heal macroscopic damage, the mobility must be increased by heating the polymer (to 80–90 °C) [12], [14], [25]. The decrease in the DA crosslink density at these elevated temperatures not only provides more network mobility but also increases the number of reactive maleimide and furan groups at the fracture surface. Because of the required higher molecular network mobility, only very soft DA networks are able to heal macroscopic damages at 25 °C with high efficiency. In previous work, the room temperature healing of DA networks was established by increasing only the number of reactive groups through the judicious choice of monomers that had a lower molecular weight [24]. This resulted in an increase in crosslink density and hence a tougher elastomer. Because of the limited molecular mobility, healing efficiencies of up to 40% could be reached at 30 °C (based on the fracture stress). To increase the healing efficiency, both the molecular mobility and the number of reactive components are increased in this article.

Table 2. The properties of DA polymers at 25 °C, including results for the DMA (1 Hz, 0.2%) and stress-strain (1%.s⁻¹).

	r	E (MPa)	E' (MPa)	E'' (MPa)	δ
DPBM-FT3000-r1	1	139	202.4	23.4	6.6
DPBM-FT5000-r1	1	8.21	16.7	2.15	8.3
DPBM-FT5000-r5/6	0.833	2.4	3.98	0.58	8.2
DPBM-FT5000-r4/6	0.667	0.72	1.67	0.26	8.7
DPBM-FT5000-r3/6	0.5	0.12	0.46	0.08	9.9

DMA: dynamic mechanic analysis.

In what follows, it will be experimentally demonstrated that the DPBM-FT5000 network with an off-stoichiometric maleimide-to-furan ratio of $r = 3/6 = r0.5$ has enough network mobility and reactive components to heal macroscopic damage at room temperature with high efficiency. A high network mobility is translated into a very flexible character, as indicated by the mechanical properties in Table 1 and 2. Because of the low crosslink density, the available reactive components on the fracture surfaces are limited, resulting in slow healing that takes several days to fully recover initial properties. When an increase in network mobility is required to perform healing, it is recommended to decrease the crosslink density by lessening the maleimide-to-furan (r) ratio (as done with the r0.5 material), rather than reducing both the maleimide and the furan concentration in a stoichiometric network by using larger FTxs. The excess furan present in the off-stoichiometric network provides more reactive furan components on the fracture surface, which enhances healing.

Instantaneous Room Temperature Healing

To check the healing properties at room temperature, DPBM-FT5000-r0.5 samples with a width of 5.5 mm and a thickness of 2–2.5 mm were synthesized. A first test was performed by cutting a sample in two with a knife and immediately putting the fracture surfaces back together manually [Figure 2(a)]. After firmly pressing the two halves together for 3 s, the pieces were already merged, and the sample could be strained by a few percentage points without fracturing. This first nonquantitative experiment illustrates that a small amount of the healing is instantaneous. When fractures occur, DA bonds are broken at the surface, and reactive maleimide and furan components are generated. Upon bringing the fracture surfaces back into contact only a few seconds later, the available reactive components start to interact with one another. The first interfacial covalent bonds as well as physical interaction, such as van der Waals forces, and the interdiffusion of pendant chains lead to the instantaneous healing of the parts. Since only a few covalent bonds are immediately formed due to slow reaction kinetics, the interface still has very limited strength. It mainly relies on adhesion rather than covalent bonding, and the sample can resist only very limited stresses.

For all autonomous SH networks (Table 1), this instantaneous healing works only if the fracture surfaces are brought back into contact soon after damage takes place. Otherwise, the available reactive groups (in this case, maleimide and furan) will react with one another in the separate parts. As a result, the healing efficiency decreases significantly if the waiting time between the damage and the contact of the fracture surfaces is too long [24]. Under the hypothesis that all bonds are broken at the fracture surfaces, the availability of the reactive maleimide and furan as a function of time can be modeled using the kinetics/thermodynamics simulation [Figure 2(b)]. Details on the simulation can be found in [26]. In Figure 2(b), the conversions are calculated using following equation:

$$x_M = \frac{[M]}{[M_0]} \wedge x_F = \frac{[F]}{[F_0]} \wedge x_{DA} = \frac{[DA]}{[M_0]}. \quad (2)$$

Looking at the maleimide content (x_M), after 1 h, only 84% of the reactive maleimide groups that were immediately available after damage occurred are expected to remain present on the fracture surfaces. After 12 and 24 h, this amount is reduced to only 23 and 10%, respectively. This emphasizes the importance of bringing the fracture surfaces back into contact as soon as possible. Although the duration between the fracture happening and the mending might not influence the eventual healing efficiency, it most certainly strongly influences the speed of the healing.

Healing Efficiency as a Function of the Healing Time

Because of the limited number of available reactive components at the fracture surface in low-crosslink-density DA networks and given the slow reaction kinetics at 25 °C,

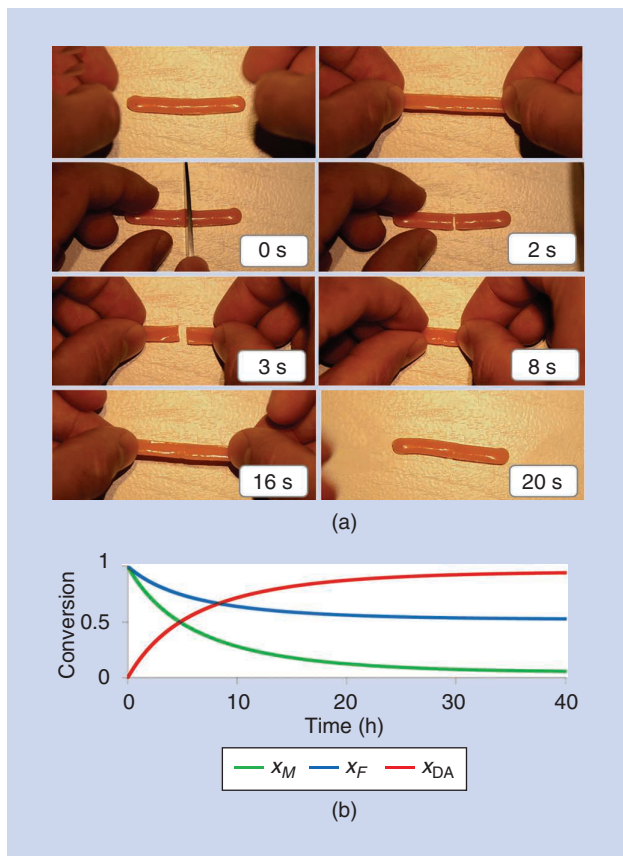


Figure 2. (a) The DPBM-FT5000-r0.5 sample with a width of 5.5 mm and a thickness of 2.5 mm is completely cut in two using a knife. Immediately after cutting, the two halves are manually put back together at room temperature. After pressing the two parts together for 3 s, the fracture surfaces merge, and the sample can already be strained by a few percentage points without fracturing (a video is available at <https://youtu.be/2A7eKtRixOU>). (b) A simulation of the relative maleimide content (x_M), the relative furan content (x_F), and the DA conversion (x_{DA}) as a function of time at 25 °C.

the healing of macroscopic damage takes time. In a second experiment, the healing efficiency, based on the recovery of the fracture strain and the fracture stress, is experimentally measured as a function the healing time. Samples with a width of 5.5 mm and a thickness of 2–2.5 mm were subjected to stress–strain tensile tests until they fractured [Figure 3(a)]. As a reference, six (undamaged) samples were fractured in a stress–strain test [Figure 4(a)]. These samples failed, on average, at an approximate strain of 245% and a stress of 0.1 MPa. The Young’s modulus of this material (the slope of the tangent line in the origin of the stress–strain curve) is 0.12 MPa.

Next, 24 samples were sliced in two with a clean scalpel blade [Figure 3(b)]. Immediately after the cut, the two ends were manually brought back into contact. When macroscopic misalignments are avoided while fitting the fracture surfaces back together, the instant healing ability of the DPBM-FT5000-r0.5 network facilitates the precise merging of the parts so that the cut is no longer visible when investigated through optimal microscopy [Figure 3(e)–(g)]. These samples were left to heal at room temperature for one, three, seven, and 14 days. For each healing time, six samples were fractured in a stress–strain test [Figure 4(a), $1\% \cdot s^{-1}$]. The mean fracture stresses and strains are presented in the block diagrams in Figure 4(b). In Figure 4(c), the mean healing efficiencies for the different healing times (Ht) were calculated by comparing the fracture strains and stresses with those measured in the reference experiment:

$$\eta_{\epsilon}(Ht) = \epsilon_{\text{fract}(Ht)} / \epsilon_{\text{fract}(\text{not damaged})} \quad (3)$$

$$\eta_{\sigma}(Ht) = \sigma_{\text{fract}(Ht)} / \sigma_{\text{fract}(\text{not damaged})} \quad (4)$$

Figure 4(a) illustrates that, after healing occurs at room temperature, very similar stress–strain characteristics are measured, but failure results at much lower stresses. Due to slow reaction kinetics, creating interfacial DA bonds clearly takes time. After healing for one day at 25 °C, only 50% of the fracture stress (η_{σ}) was recovered [Figure 4(c)]. Visual inspection showed that the fracture took place at the same location where the cut was made. The formed fracture surfaces again looked clean and identical to the picture in Figure 3(b). The healing efficiencies (η_{ϵ} and η_{σ}) can be increased by prolonging the healing time. Indeed, after three, seven, and 14 days, the fracture stress recovered by, respectively, 62, 91, and 97%. Although DA reactions are generally considered to be too slow for room temperature autonomous healing, the increasing failure strength

through time clearly proves the contribution of the re-formation of these reversible links to the healing process at room temperature.

After 14 days of healing at room temperature, the fracture no longer took place at the location where the cut was made but, rather, at a location where an imperfection caused stress concentrations [e.g., a cavity caused by a solvent bubble or a dust particle; Figure 3(d)]. Taking into account the standard error of the mean presented in the block diagrams in Figure 4(c) and the fact that the fracture did not happen at the location of the “scar” of the cut, it can be concluded that, after 14 days, the cuts are completely healed and that the initial strength of the samples has been completely recovered. The presented results were all obtained at 25 °C. At lower application temperatures, healing takes slightly longer, while at higher temperatures, the duration of healing is shortened.

Healing Efficiency as Function of Healing Cycles

The samples that were healed for one, three, and seven days were fractured in the stress–strain tensile test to evaluate the restoration efficiency, and the generated pieces [Figure 3(b)] were immediately brought back into contact [Figure 3(c)]. After again healing for the same duration—one, three, and seven days—the samples were again fractured in the tensile tests. For all healing times, the fracture strain and the fracture stress of the second

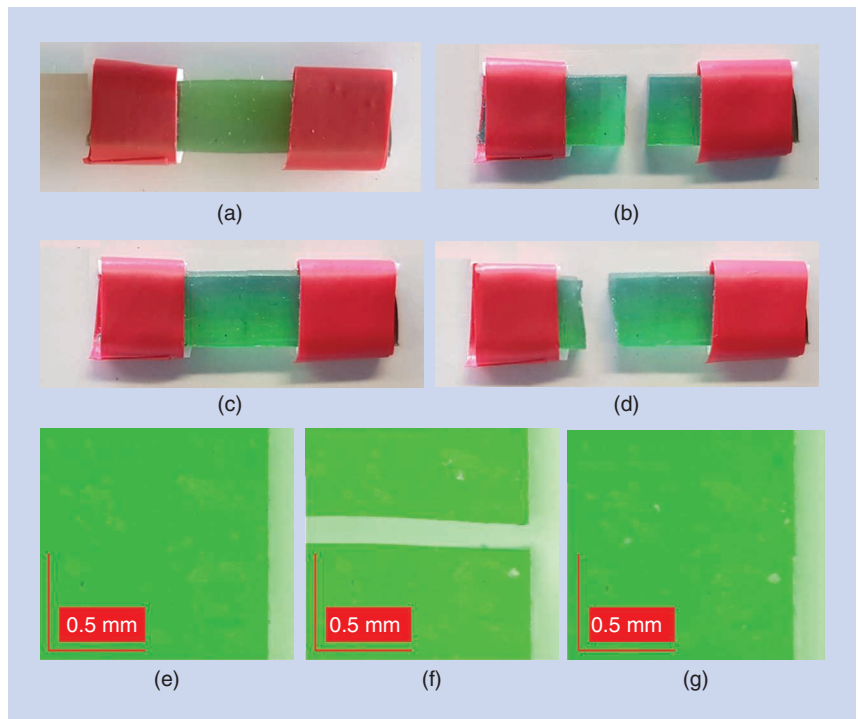


Figure 3. Testing autonomous healing at room temperature. (a) Samples with a width of 5.5 mm, a thickness of 2–2.5 mm, and a length of 8–10 mm. (b) The samples are sliced in two using a scalpel blade. (c) The samples are pressed back together seconds after the damage was inflicted and placed at room temperature for one, three, seven, or 14 days before being subjected to a stress–strain tensile test until they fracture. (d) The samples that were cured for 14 days do not fracture at the location of the initial damage but at a new location. Microscopic images of (e) the sample prior to damage, (f) the sample after it is damaged, and (g) the sample when it is reconnected.

healing cycle was slightly lower [Figure 4(b)]. A possible explanation is that, at the surface of cavities generated in the merger zone, the number of available reactive maleimide and furan groups decreases slowly as function of time [Figure 2(b)]. After intermediate healing times of one, three, and seven days, not all cavities are completely sealed. Consequently, when broken in the stress–strain tensile test, the resulting fracture surfaces have fewer reactive components on their surface compared to the fracture surfaces generated by cutting a fresh sample. As a result, the recovery of the fracture strain and stress will take longer in the second healing cycle.

In addition, the cavities that remain after incomplete healing can be enlarged in the first tensile test before a rupture

occurs. When the two parts are placed back together for the second healing cycle, the surfaces probably match less well, and the cavities are slightly bigger than in the first cycle. As a result, more extensive “zipping” is required, increasing the necessary duration of the process. For the same reasons, the recovery of the initial properties in the third healing cycle is even poorer than for the second. Although not yet experimentally validated because of time limitations, we believe that, even when fracturing a sample before all cavities are healed (e.g., after one day), a complete recovery of that sample can still be achieved in another, longer healing cycle (e.g., >14 days).

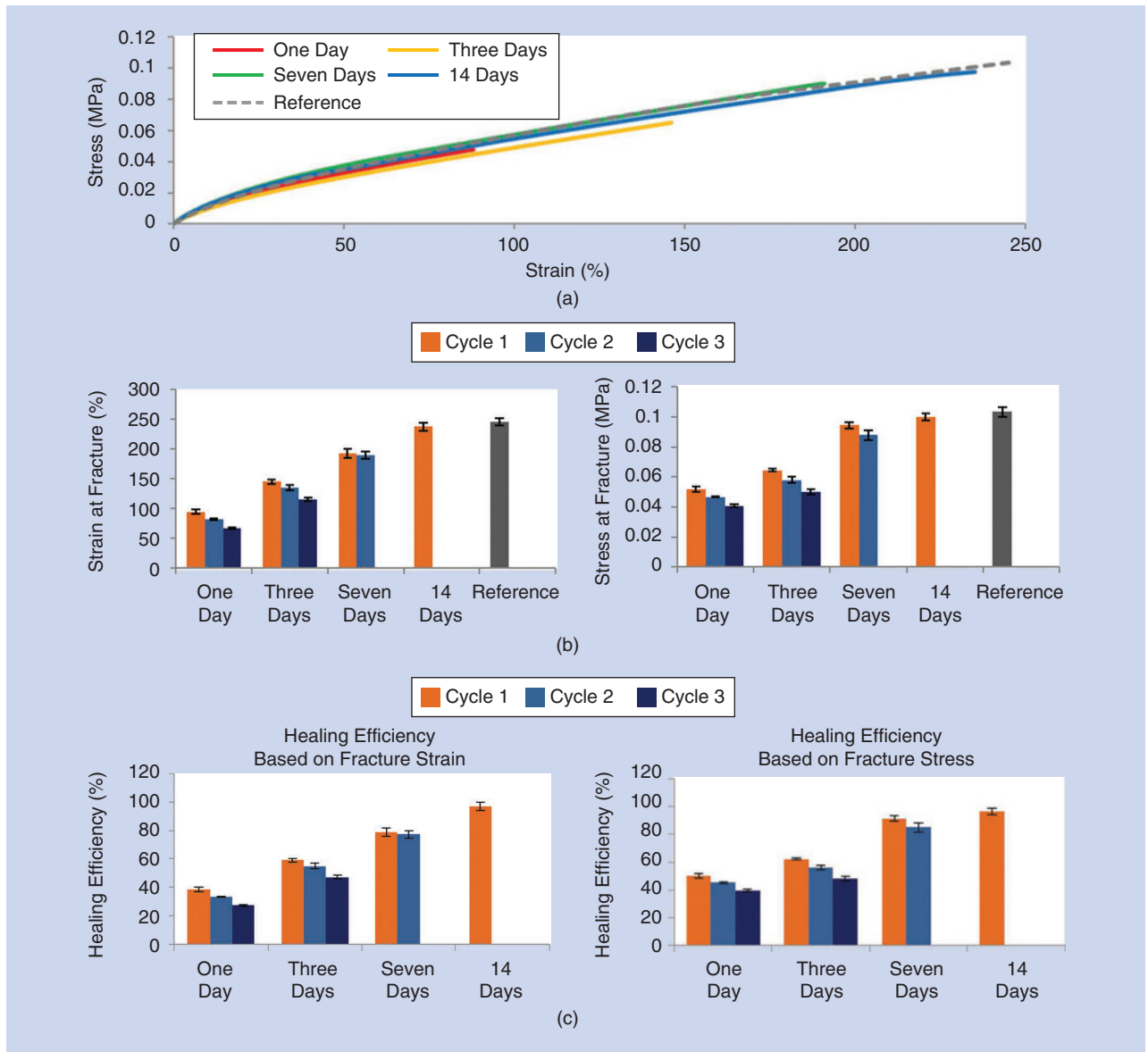


Figure 4. (a) A comparison of the stress–strain curves of reference (undamaged) samples and samples that were cut all the way through and subsequently healed at room temperature for one, three, seven, and 14 days. Stress–strain tests are performed with a strain ramp of $1\%s^{-1}$. (b) The mean values (of six samples) of the strain and stress at the fracture, derived through tensile testing, are presented for the reference sample and samples healed for one, three, seven, and 14 days at 25 °C. (c) The healing efficiencies based on the fracture strain and fracture stresses of the healed samples relative to the fracture parameters of the reference samples. The error bars represent the standard error of the mean.

Design of Soft Actuators That Heal at Room Temperature

To illustrate that the DPBM-FT5000-r0.5 network is suitable to develop soft robotic components that can heal at room temperature, bending soft pneumatic actuators (BSPAs) were constructed using this material. The design is based on previously published BSPAs (details of the design and the working principle can be found in [9] and [14]). The new BSPA is entirely made out of the DPBM-FT5000-r0.5. Because of the hyperelasticity of this network [the Young's modulus is 0.12 MPa, derived from the stress-strain curve in Figure 4(a)], the bottom sheet is now thicker, at 3.5 mm (Figure 5), compared to the design in [9]. If that were not the case, the actuator would be too flexible, as Abaqus simulations indicate that it would deform under its own weight. By designing the bottom layer to be thicker, the strains are limited, and, consequently, the actuator has an anisotropic bending response to overpressure in the air chambers (Figure 6). The manufacturing of this actuator is not addressed in this article, as it is identical to the shaping technique used for the BSPA, which is described in [9] and [14].

Validation of the Mechanical Properties

The constructed actuator was evaluated on a dedicated test bench containing a digital camera to measure deformations and a closed-loop pressure controller to regulate the overpressure in the air chambers (details of the controller are in [9]). The bending characteristics, including the tip trajectory

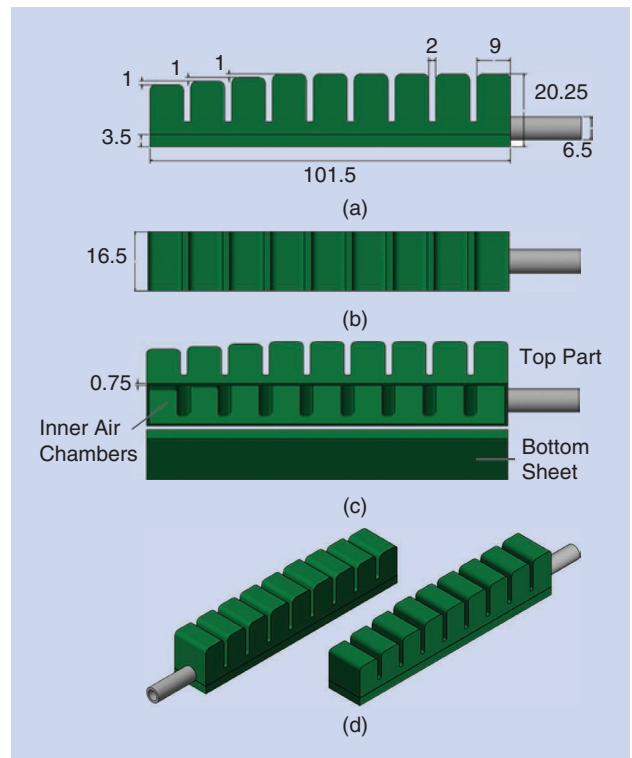


Figure 5. The design of the SH BSPA, which is completely constructed out of a DPBM-FT5000-r0.5 polymer: the (a) side, (b) top, (c) exploded, and (d) 3D isometric views. The dimensions are in millimeters.

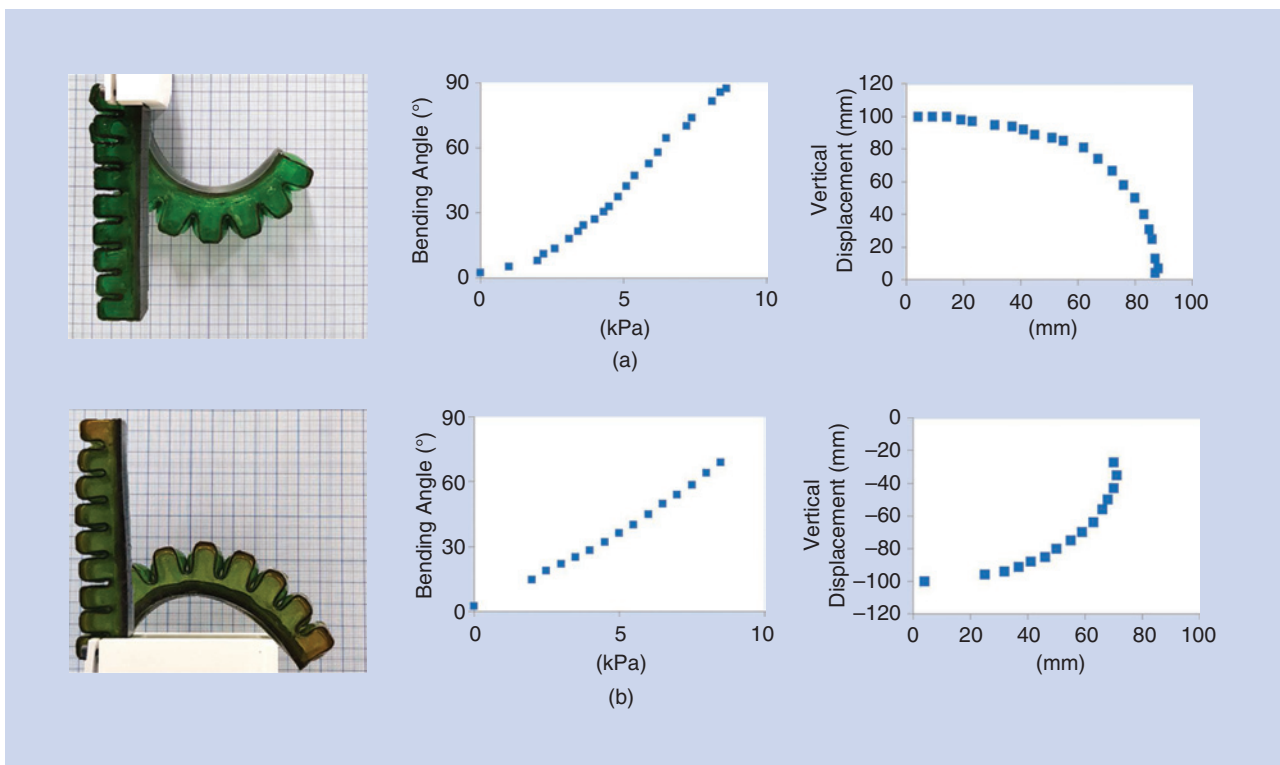


Figure 6. The bending characteristic of the BSPA is measured using a digital camera. To check the influence of gravity, the bending characteristic is derived for downward and upward movement. The deformation trajectory and the bending angle are measured as a function of the overpressure of the air chambers when the actuator is mounted with (a) the tip facing down and with (b) the tip facing up.

and the relation between the bending angle and the overpressure in the air chambers for downward and upward bending, can be found in Figure 6. Because of the hyperflexibility, the direction of the gravity field has an influence on the bending characteristic. This highlights the importance of adding feedback to the controller of these soft actuators. The model-free feedforward controller used in this article is insufficient when these finger actuators are used in industrial and commercial applications because the response characteristic of the actuators changes when orientated differently.

Feedback control requires the integration of one or more sensors in the actuator. To avoid losing the desired flexible characteristic of the soft actuator, the integrated sensor will have to be soft, as well. In general, in many soft robots, feedback control is required, hence the recent development of a new field in robotics: “soft sensors.” In future work, soft sensors and feedback controllers will be added to the SH soft actuators. Five identical actuators were manufactured out of DPBM-FT5000-r0.5. By placing them in one soft hand assembly, we demonstrated the BSPAs’ usability for social soft robotics applications (Figure 7). The five fingers can be separately controlled, which enables the hand to perform simple gestures that can be employed in social soft robots to express emotions.

Validation of the Healing Ability in the Soft Hand

The healing ability of the BSPAs was demonstrated by applying macroscopic cuts all the way through the soft

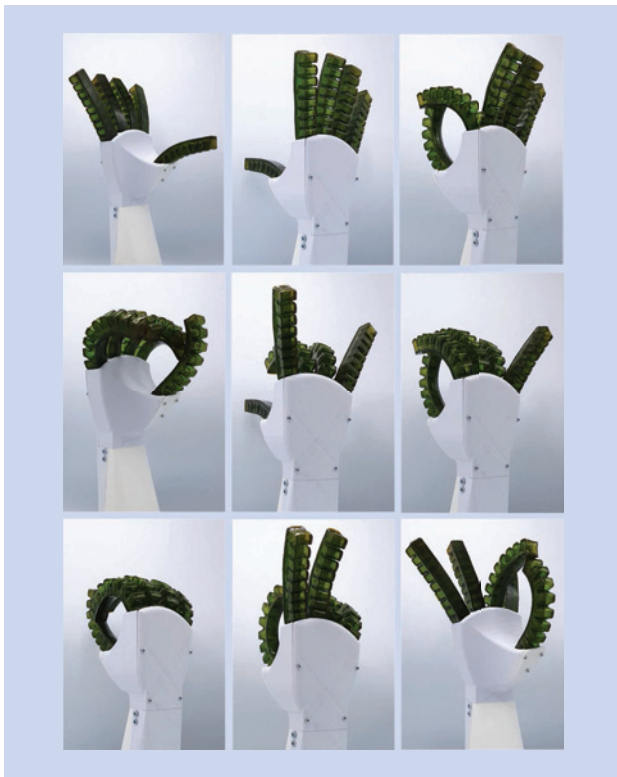


Figure 7. The five BSPAs can function together in a soft hand, illustrating the potential of autonomously healable DA materials for social soft robotic applications. The fingers can be controlled separately, which enables the hand to make simple gestures (a video is available at <https://youtu.be/ejblcpHqplU>).

membranes at different locations on the actuator (Figure 8). For these tests, a clean blade was used. The first cut (with a length of 12 mm, extending all the way through the material) was made in the thick bottom sheet, perpendicular to the longitudinal axis of the noninflated actuator [Figure 8(a)]. When the blade was taken out, the elastic response of the DA material pushed the cut surfaces back together. The actuator was left untouched for only 30 s, after which it was inflated. After 30 s of healing at room temperature, the actuator was airtight and could resume its activities. The airtightness was confirmed when the actuator was submerged in water. No air bubbles escaped through the membrane during actuation across the full bending range. From the previous material tests [Figure 4(a)], it is known that the cut is far from fully healed after only 30 s. However, during actuation, the freshly healed cut perpendicular to the longitudinal axis is compressed, increasing contact. Thus, the instantaneous adhesion that relies on secondary interactions and the very low number of covalent DA bonds is sufficient to keep the actuator airtight.

The actuator is fully recovered when the cut is healed and remains completely airtight in the actuation range of the actuator, while the actuator performance is recovered. As a result, for this particular damage, the actuator is fully healed after only 30 s. This illustrates very well the dependence of the required duration of the healing process on the size of the damage and, even more, on the location of the injury. After only 30 s, in this case, the actuator can be reused. During further operation, the interfacial strength of the “scar” increases progressively because the number of interfacial DA bonds will gradually grow. Eventually, all microscopic cavities at the scar will be completely sealed, and the strength at the location of the scar will be recovered.

In a second test [Figure 8(b)], a cut with the same size was made in the thick bottom sheet but along the longitudinal axis of the actuator. During inflation, the stresses on this cut are larger, and 30 s of healing time was not sufficient to make the actuator airtight again. For this cut, which had the same dimensions but another orientation, a healing time of 2 h at room temperature was required. In the first test, after 30 s, we can say only that there is enough adhesion to keep the cut closed, as we do not know whether DA bonds already play an important role. In the case of the cut along the longitudinal axis of the actuator, the stresses on the scar during actuation are higher, and it is clear that covalent bonds are needed to keep the actuator airtight (physical adhesion is not enough). After 2 h, enough interfacial DA bonds were formed to keep the part airtight.

A third cut [Figure 8(c)] was made in the thinner top membrane of one of the rectangular cells. In this membrane, the stresses during actuation are higher than the ones in the bottom layer. This translates to a longer healing time of 16 h because many more DA bonds must be formed across the cut surfaces to ensure sufficient interfacial strength to keep the actuator airtight. However, even this damage could be healed without the need of a heat stimulus and in a relatively short time of 16 h.

To push the healing ability to its limits, one of the finger actuators was completely severed [Figure 8(d)]. Immediately after the damage was inflicted, the two halves were precisely, though manually, fit together. Next, the actuator was left to heal for seven days at room temperature. After this longer healing time, sufficient DA bonds should have formed across the cut to enable the actuator to be reused. To validate the recovery of the initial actuator performance, the bending characteristic of the healed device was measured and compared to that of the undamaged one (Figure 9). The results were the same, indicating that the actuator properties were fully recovered.

Autonomous Versus Nonautonomous SH in Soft Robots

When using autonomous intrinsic SH elastomers for soft robots, there is no need for an add-on system that provides a (heat) stimulus. However, there is another advantage of autonomous materials. When heat is applied, the DA networks' crosslink density decreases, which affects the mechanical properties of the material. In [9] and [12], damage in the soft robotic components was healed by heating the entire actuator to 80–90 °C. When the damage was completely sealed, the parts could be cooled to 25 °C. At that temperature, the kinetics of the DA reaction are relatively slow, and therefore it takes the material up to 24 h to reach a near-equilibrium crosslink density and recover the initial actuator properties.

During autonomous healing, except for the damaged location, the crosslink density across the entire actuator

remains constant. The DA concentration will change only at the location of the damage. As a result, the actuator recovers at the moment that the interfacial strength of the healed cut is high enough to withstand the local stresses that come from pressurizing the air chambers. Thus, the actuator properties will not be affected by the healing, providing more consistency [Figure 9(b)].

A downside of using autonomous healable polymers is the loss in control over the healing process compared with nonautonomous healable materials. When heat is required, the robotic system can decide when to start the process by increasing the temperature. In the case of autonomous healing, the process will start from the moment the fracture surfaces touch. In addition, the healing should be performed right away because leaving the fracture surfaces without contact leads the reactive groups to bond with one another in the separate parts. It should be noted that the lost autonomous healing potential of the aged surfaces can be replenished by a heat treatment [24]. In summary, for actuators made out of nonautonomous SH DA material, healing can be performed at any desired time, while the healing in actuators made out of autonomous SH DA material should be instantaneously done after damage.

Self-contact in an actuator for very long period of time can lead to undesired merging when using autonomous SH DA materials. If, for example, the membranes of different cells of the actuator are in contact for several weeks or months, they will be merged, as well, and this can lead to a change in performance and even failure. This also applies to two different actuators that are in contact for a very long period. This

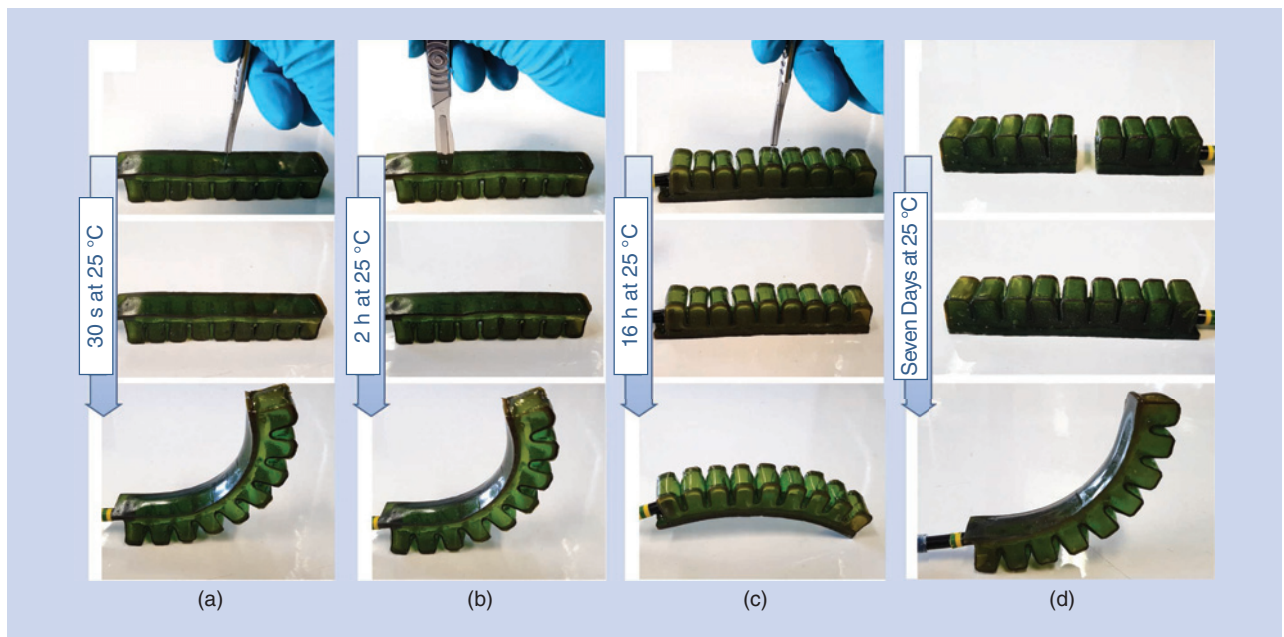


Figure 8. The BSPAs are damaged using a scalpel blade. Macroscopic damage of different sizes and shapes is inflicted at different locations. The duration of the healing procedure depends on the size of the damage and the stresses that take place during actuation at the location of the “scar.” (a) A 12-mm cut all the way through the bottom layer of the actuator, perpendicular to the longitudinal axis. (b) The same cut is made but along the longitudinal axis. (c) A 10-mm cut all the way through the top membrane of one of the cells of the actuator. (d) The actuator is completely cut in half. All damage could be completely healed at room temperature (roughly 25 °C). Depending on the location of the damage, the healing takes only 30 s or up to seven days (a video can be viewed at <https://youtu.be/dZEocbiwiS4>).

merging takes longer than the healing between two freshly made fracture surfaces because few reactive maleimide and furan components are available on the surface of the actuator, in comparison with newly formed fracture surfaces. On fracture surfaces, upon damage, a large additional number of maleimide and furan components is created by mechanically breaking the DA bonds.

In the future, the formation of bonds between two surfaces with equilibrium conversion and in contact should be experimentally validated. Luckily, soft robots, like soft grippers and hands, are generally used in dynamic applications, where self-contact occurs for short durations. If the healing time at application temperatures in next-generation SH polymers in soft robotics can be further reduced, the undesired merging of planes will be able to take place faster, a condition that will definitely have to be considered.

In this research, the macroscopic damages were applied in a clean lab environment and with clean blades. Of course, when evolving toward industrial and commercial applications, the influence of contamination on the fracture surfaces on the healing performance has to be investigated. In future

applications, to enhance the cleanliness of the fracture surfaces prior to healing, dirt and dust can be blown off using compressed air, which is available in pneumatic systems, or cleaned away by submerging a part in water, which can be done because the DA materials are insoluble.

Tradeoff Between Mechanical Properties and Healing at Room Temperature

According to our knowledge, for all intrinsic SH polymer technologies (excluding healing agent-based materials), a general tradeoff between mechanical properties (the Young's modulus and the tensile strength) of the SH polymer network and its healing temperature has to be considered. As a result, all autonomous intrinsic SH polymers have a limited mechanical strength and a high flexibility, as illustrated in the examples in Table 1. For the DA network described in this article, the same tradeoff applies. Autonomously healable DA networks must have a lot of molecular network mobility to heal damage at room temperatures. Consequently, they need to be very soft. The high flexibility of these networks limits the force output of the actuators that are built from them.

Soft robotic applications where higher force outputs are needed can be developed from DA material with a higher Young's modulus and greater strength, such as the DPBM-FT5000-r1 material [12], [14]. However, these networks have less molecular mobility. The temperature must be substantially increased (to nearly 90 °C) before sufficient molecular mobility enables the closing and healing of relevant macroscopic damages. Currently, a DA network with high mechanical properties and a healing mechanism that performs at room temperature cannot be synthesized.

Conclusion

For the first time, soft robotic actuators have been developed that are able to recover their performance at room temperature after severe damage, without the need for an externally applied stimulus. These were constructed from a newly created autonomous SH polymer network that obviates the need for additional heating devices that would increase the complexity of the overall robotic system. The SH polymer network based on the reversible DA reaction was designed to increase the molecular mobility by means of working at a low maleimide-to-furan ratio. This reduces the crosslink density and results in an excess of furan groups, compensating for the lower maleimide concentration. A DA network was synthesized that can autonomously heal catastrophic macroscopic damage at room temperature. The healing efficiency of a fractured part, evaluated through the recovery of the stress at fracture, is 62, 91, and 97% after three, seven, and 14 days, respectively.

This material was used to develop a healable soft pneumatic hand. Relevant large cuts could be entirely healed without the need of a heat stimulus. Depending on the size of the damage and, even more, on the location of the damage, the healing takes only seconds or up to one week. For this evaluation, the actuator was considered to be healed whenever it

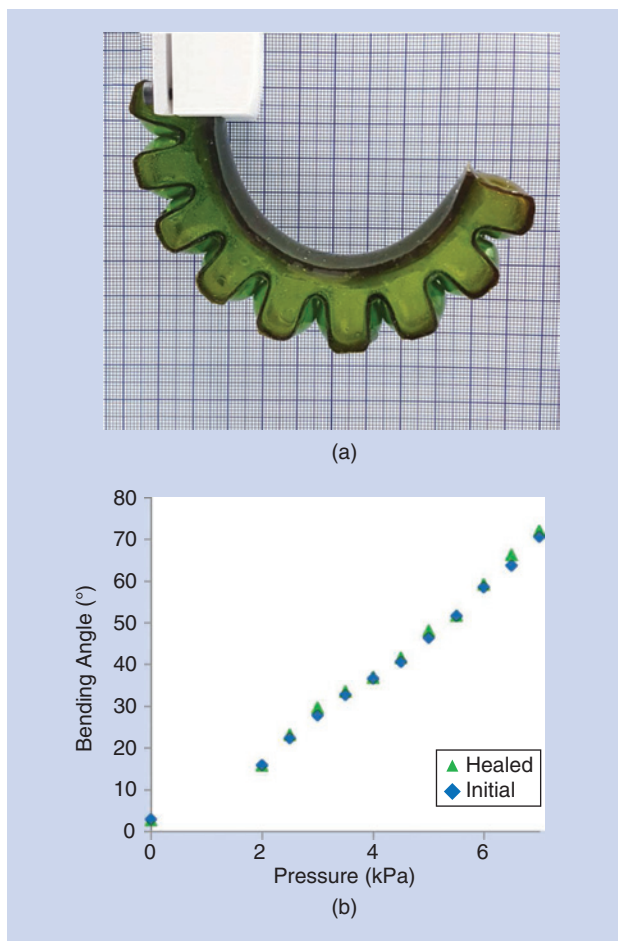


Figure 9. (a) After being cut through completely [Figure 8(d)] and healed, the actuator is again completely airtight and can be pressurized without leaking. (b) The bending characteristic of the healed actuator is compared to the initial characterization prior to the damage.

was completely airtight and the scar did not tear open during actuation. Damage on locations on the actuator that were subjected to very small stresses was instantaneously healed. Although only a limited number of DA bonds formed in seconds across the merged fracture surfaces, the process provided sufficient interfacial strength to keep the actuator airtight during actuation. Severe damage, such as cutting the actuator in two, took seven days to heal without the need of any external heat stimulus and resulted in a full recovery of the actuator performance.

Acknowledgments

This work was supported by Fonds Wetenschappelijk Onderzoek, under grants FWOTM784 (Terryyn), 12W4719N (Brancart), and 1S84120N (Roels), and by European Union Future and Emerging Technologies Self-Healing for Soft Robotics grant 828818.

References

- [1] M. T. Tolley et al., "A resilient, untethered soft robot," *Soft Robot.*, vol. 1, no. 3, pp. 213–223, 2014. doi: 10.1089/soro.2014.0008.
- [2] R. V. Martinez, A. C. Glavan, C. Keplinger, A. I. Oyetibo, and G. M. Whitesides, "Soft actuators and robots that are resistant to mechanical damage," *Adv. Funct. Mat.*, vol. 24, no. 20, pp. 3003–3010, 2014. doi: 10.1002/adfm.201303676.
- [3] J. Hughes, U. Culha, F. Giardina, F. Guenther, A. Rosendo, and F. Iida, "Soft manipulators and grippers: A review," *Front. Robot. AI*, vol. 3, pp. 69, 2016. doi: 10.3389/frobt.2016.00069.
- [4] J. Shintake, V. Cacucciolo, D. Floreano, and H. Shea, "Soft robotic grippers," *Adv. Mat.*, vol. 30, no. 29, p. 1707035, 2018. doi: 10.1002/adma.201707035.
- [5] A. D. Marchese, R. K. Katzschmann, and D. Rus, "A recipe for soft fluidic elastomer robots," *Soft Robotics*, vol. 2, no. 1, pp. 7–25, 2015. doi: 10.1089/soro.2014.0022.
- [6] D. Rus and M. T. Tolley, "Design, fabrication and control of soft robots," *Nature*, vol. 521, no. 7553, pp. 467–475, 2015. doi: 10.1038/nature14543.
- [7] C. Laschi, B. Mazzolai, and M. Cianchetti, "Soft robotics: Technologies and systems pushing the boundaries of robot abilities," *Sci. Robot.*, vol. 1, no. 1, p. eaah3690, 2016. doi: 10.1126/scirobotics.aah3690.
- [8] R. Pfeifer, H. G. Marques, and F. Iida, "Soft robotics: The next generation of intelligent machines," in *Proc. IJCAI Int. Joint Conf. Artif. Intell.*, 2013, pp. 5–11. doi: 10.5555/2540128.2540131.
- [9] S. Terryyn, J. Brancart, D. Lefeber, G. Van Assche, and B. Vanderborght, "Self-healing soft pneumatic robots," *Sci. Robot.*, vol. 2, no. 9, 2017. doi: 10.1126/scirobotics.aan4268.
- [10] S. Terryyn, G. Mathijssen, J. Brancart, D. Lefeber, G. Van Assche, and B. Vanderborght, "Development of a self-healing soft pneumatic actuator: A first concept," *Bioinspir. Biomim.*, vol. 10, no. 4, p. 046007, 2015. doi: 10.1088/1748-3190/10/4/046007.
- [11] S. Terryyn, J. Brancart, D. Lefeber, G. Van Assche, and B. Vanderborght, "A pneumatic artificial muscle manufactured out of self-healing polymers that can repair macroscopic damages," *IEEE Robot. Autom. Lett.*, vol. 3, no. 1, pp. 16–21, 2017. doi: 10.1109/LRA.2017.2724140.
- [12] E. Roels, S. Terryyn, J. Brancart, G. Van Assche, and B. Vanderborght, "A multi-material self-healing soft gripper," in *Proc. IEEE Int. Conf. Soft Robot. (RoboSoft)*, 2019, pp. 316–321. doi: 10.1109/ROBOSOFT.2019.8722781.
- [13] J. Brancart, G. Scheltjens, T. Muselle, B. Van Mele, H. Terryyn, and G. Van Assche, "Atomic force microscopy based study of self-healing coatings based on reversible polymer network systems," *J. Intell. Mat. Syst. Struct.*, vol. 25, no. 1, pp. 40–46, 2014. doi: 10.1177/1045389X12457100.
- [14] S. Terryyn, E. Roels, G. Van Assche, and B. Vanderborght, "Self-healing and high interfacial strength in multi-material soft pneumatic robots via reversible Diels-Alder bonds," *Actuators*, vol. 9, no. 2, pp. 1–17, 2020. doi: 10.3390/act9020034.
- [15] B. Willocq, R. K. Bose, F. Khelifa, S. J. Garcia, P. Dubous, and J. M. Raques, "Healing by Joule effect of electrically-conductive poly (esterurethane) carbon nanotubes nanocomposites," *J. Mat. Chem. B*, vol. 4, no. 11, pp. 4089–4097, 2016. doi: 10.1039/C5TA09793B.
- [16] S. R. White et al., "Autonomic healing of polymer composites," *Nature*, vol. 409, no. 6822, pp. 794–797, 2001. doi: 10.1038/35057232.
- [17] L. Leibler, P. Cordier, and C. Soulie, "Self-healing and thermoreversible rubber from supramolecular assembly," *Nature*, vol. 451, no. 7181, pp. 977–980, 2008. doi: 10.1038/nature06669.
- [18] G. M. L. Van Gemert, J. W. Peeters, S. H. M. Söntjens, H. M. Janssen, and A. W. Bosman, "Self-healing supramolecular polymers in action," *Macromol. Chem. Phys.*, vol. 213, no. 2, pp. 234–242, 2012. doi: 10.1002/macp.201100559.
- [19] Suprapolix. www.suprapolix.com (accessed Oct. 9, 2020).
- [20] R. Adam Bilodeau and R. K. Kramer, "Self-healing and damage resilience for soft robotics: A review," *Front. Robot. AI*, vol. 4, p. 48, Oct. 2017. doi: 10.3389/frobt.2017.00048.
- [21] Y. Chen, A. M. Kushner, G. A. Williams, and Z. Guan, "Multiphase design of autonomic self-healing thermoplastic elastomers," *Nat. Chem.*, vol. 4, no. 6, p. 467, 2012. doi: 10.1038/nchem.1314.
- [22] C. Li, et al. "A highly stretchable autonomous self-healing elastomer," *Nat. Chem.*, vol. 8, no. 6, pp. 618–624, 2016. doi: 10.1038/nchem.2492.
- [23] A. Rekondo, R. Martin, and A. R. De Luzuriaga, "Catalyst-free room-temperature self-healing elastomers based on aromatic disulfide metathesis," *Mat. Horiz.*, vol. 20, pp. 3–6, Sept. 2013. doi: 10.1039/C3MH00061C.
- [24] M. M. Diaz, J. Brancart, G. Van Assche, and B. Van Mele, "Room-temperature versus heating-mediated healing of a Diels-Alder cross-linked polymer network," *Polymer*, vol. 153, pp. 453–463, Sept. 2018. doi: 10.1016/j.polymer.2018.08.026.
- [25] E. Roels, S. Terryyn, J. Brancart, R. Verhelle, G. Van Assche, and B. Vanderborght, "Additive manufacturing for self-healing soft robots," *Soft Robot.*, early access, Mar. 10, 2020. doi: 10.1089/soro.2019.0081.
- [26] A. Cuvellier, R. Verhelle, J. Brancart, B. Vanderborght, G. Van Assche, and H. Rahier, "Polymer Chemistry The influence of stereochemistry on the reactivity of the Diels-Alder cycloaddition," *Polym. Chem.*, vol. 10, no. 4, pp. 473–485, 2019. doi: 10.1039/C8PY01216D.

Seppie Terryyn, Vrije Universiteit Brussel and Flanders Make, Brussels, Belgium. Email: seterryyn@vub.be.

Joost Brancart, Vrije Universiteit Brussel, Belgium. Email: joost.brancart@vub.ac.be.

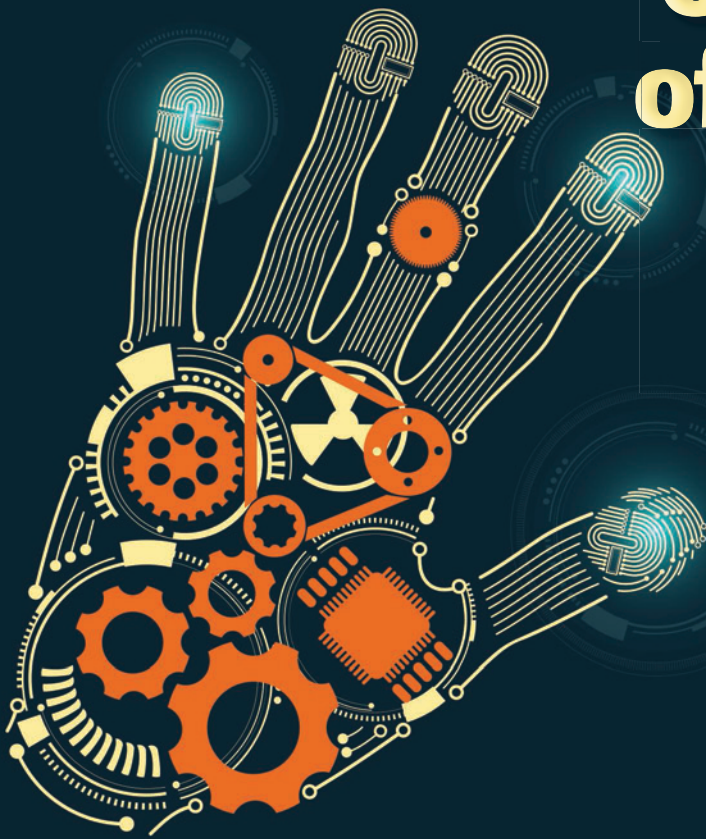
Ellen Roels, Vrije Universiteit Brussel and Flanders Make, Brussels, Belgium. Email: ellen.roels@vub.be.

Guy Van Assche, Vrije Universiteit Brussel, Belgium. Email: gvassche@vub.ac.be.

Bram Vanderborght, Vrije Universiteit Brussel, Belgium. Email: bram.vanderborght@vub.ac.be.

Design and Optimization of a Dexterous Robotic Finger

Incorporating a Sliding, Rotating, and Soft-Bending Mechanism While Maximizing Dexterity and Minimizing Dimensions



©SHUTTERSTOCK/JACKIE NIAM

By Amir Pagoli, Frédéric Chapelle, Juan-Antonio Corrales-Ramon, Youcef Mezouar, and Yuri Lapusta

In this article, we introduce a new soft finger with a pneumatic-actuated movable joint that is optimized and characterized in terms of the degrees of freedom (DoF), workspace, and fingertip force. The finger consists of one soft link as the body and the bending pneumatic joint as the actuator. Due to the additional translation and rotation movement capabilities of the joint, carried out by two stepper motors, the finger can bend in any direction while having different lengths, thanks to a configurable bending point. This results in more dexterity for the finger when dealing with a target inside its 3D workspace by increasing the number of configurations it can use to reach the target and exert force. The finite element method (FEM) and the Nondominated Sorting Genetic Algorithm II (NSGA-II) algorithm are applied to optimize the joint

geometry and so maximize the bending angle and minimize the joint dimensions. Furthermore, the variations of each design parameter and consequent effects on the optimization objectives are analyzed. The optimal geometrical parameters are used to fabricate a prototype with silicone rubber. Tests on the bending angle and tip force variability are conducted on the prototype to validate the numerical modeling. The experimental results show that the finger exerts force up to 650 mN with a response time of fewer than 3 s. The stiffness of the finger can be changed by applying pneumatic pressure in the hollow space inside the link. This consequently varies the amount of applied force at the tipping point of the finger up to two times.

Fluidic Elastomer Actuation Actuators

Introduced as a novel technology in recent years, soft robotics broadens new horizons in the field of robotics, thanks to

Digital Object Identifier 10.1109/MRA.2020.3024283

Date of current version: 8 October 2020

promising characteristics such as adaptability, light weight, less required assembly, and low cost [1]. The intrinsic deformable structure of soft robots encourages scientists to engage different technologies for their dynamization. One of the most widely used actuating technologies for soft robotics is the fluidic elastomer actuator (FEA), powered by a pressurized fluid (gas or liquid) [2]. Due to their many advantages including easy fabrication, production high forces and large strokes, and low-cost elastomer materials [3], FEAs have been used in numerous configurations for various purposes, such as locomotion [4], manipulation [5], medical applications [6], and wearable devices [7]. These actuators can generate distributed forces that are proportional to the operating pressure of the fluid and the surface area on which the pressure is applied [8]. Even though there is a large diversity of applications for FEAs, many challenges remain in this field, including stiffness control and shape configuration. Researchers have increased the performance of these kinds of actuators by integrating them with other types of methods that help FEAs in terms of shape control and variable stiffness. These lateral technologies are mainly based on using variable-stiffness materials, including shape memory polymers (SMPs) [9], combinations of SMPs with thermoplastic polyurethane [10], and low melting point alloys (LMPAs) [11]. The main drawbacks of SMPs are a high hysteresis and a low actuation speed that differs from 5 to 60 s, regarding the size of the actuator [3]. Using LMPAs is another suggested method for changing the bending point and shape configuration in FEAs. Applying an electric current to the alloy and heating, the structure phase-changes locally from rigid to soft, and, thus, variable stiffness can be achieved [12]. Like SMPs, the transition time is the main issue in LMPAs. Depending on size and geometry, the melting time for LMPAs differs from 1 to 30 s, while cooling takes more than 60 s [13].

In this article, we introduce a novel type of soft finger based on bending point control and variable stiffness. The proposed finger achieved is more flexible than previous solutions in terms of the attainable 3D space and applicable contact forces at the fingertip, by changing the position of its joint and, thus, the bending point. The design consists of one elastomer tube as the soft link and one movable soft joint as the actuator. Applying air pressure to the joint, it and the link will bend concurrently. Two stepper motors are responsible for moving the joint longitudinally along the link as well as rotating it around its axis. The joint can thus change the effective length of the finger and the bending direction. Unlike previously proposed integrating methods with FEAs based on SMPs or LMPAs, the position of the bending point is movable along the length of the link, which makes the finger more dexterous and reconfigurable.

Due to the nonlinear behavior of FEAs, their performance strongly depends on the geometry and dimensions of the actuator. Elsayed et al. [14] showed the effects of the position and shape configuration of the chamber on the bending direction and angle value; they deployed an FEM to study and optimize these design parameters. Decroly et al. [15]

conducted an optimization study using a numerical model to miniaturize FEAs to be applicable in minimally invasive surgery. In our work, developing an optimization procedure is also essential to achieve our operating objectives: reconfigurability and variable stiffness. The NSGA-II algorithm is chosen as the optimization method due to its fast, nondominated sorting approach; fast crowded distance-estimation procedure; and simple crowded-comparison operator [16]. We use these capabilities for maximizing the bending angle up to 90° and simultaneously minimizing the length and diameter of the joint while dealing with a variety of design parameters. Moreover, we investigate the sensitivity of each parameter to reduce the computational cost and, thus, increase the convergence speed of the design procedure.

Operating Principles and Design

The schematic of the proposed soft finger is illustrated in Figure 1. The finger is composed of a pneumatically actuated joint (the blue cylinder) and a soft link (the gray cylinder). A longitudinal channel, embedded inside the joint, inflates by supplying the air pressure (P_1) and leads to the bending of the joint and, consequently, the link [Figure 1(a)]. The bending location can be longitudinally changed by sliding the joint along the link [Figure 1(b)]. The joint can also rotate around its main axis while the link remains steady due to its fixed connection to the base. This causes the finger to bend in any direction in 3D space [Figure 1(c)].

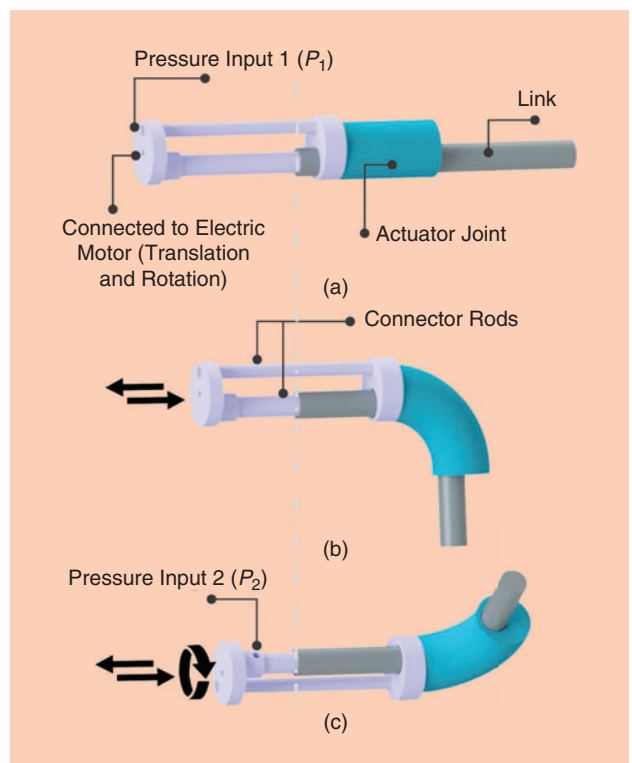


Figure 1. (a) A schematic view of the proposed finger. (b) The sliding of the joint along the link changes the bending point and effective length of the finger. (c) The rotation of the joint along its axis results in changing the bending direction in 3D space.

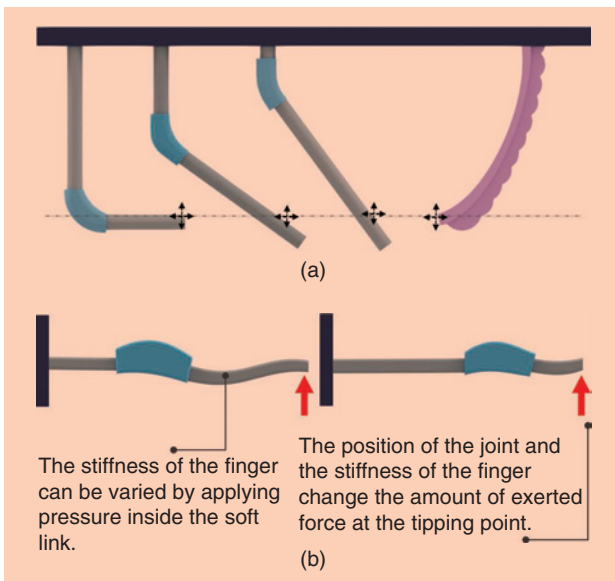


Figure 2. A comparison between the configurations of the proposed finger (left) and a conventional FEA-based finger (right) when (a) reaching a particular point and (b) exerting a different amount of force to a tipping point.

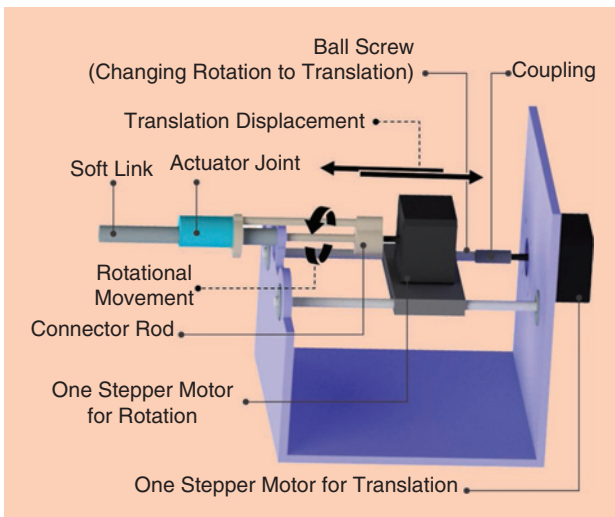


Figure 3. The assembly structure of the proposed finger and motors.

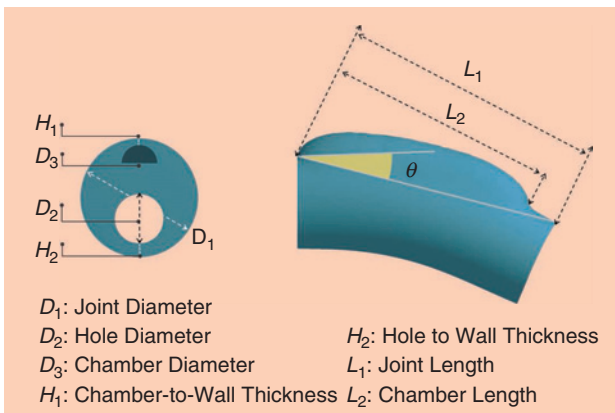


Figure 4. The geometrical optimization parameters.

In Figure 2(a), a conventional FEA finger (on the right) and the proposed finger (on the left) are compared in terms of dexterity and the strategies used to reach a particular point in the workspace. Due to the uniform structure of conventional FEA fingers and their limited DoF, it is not possible for them to attain each point in their workspace with various configurations. On the contrary, the design of the proposed finger suggests an array of possible configurations in which the finger can reach each point. This not only results in more flexibility of the finger in dealing with obstacles that limit the workspace but also enhances the possible configurations in which it can exert a different amount of force to a particular point [Figure 2(b)]. The workspaces of these two fingers are compared in the “Results and Discussion” section.

The mechanism used for changing the bending point of the finger consists mainly of two stepper motors connected to the joint (Figure 3). The first is linked directly to the joint and is responsible for its rotational displacement. The connection includes two rigid rods: one for transmitting the rotational movement of the motor to the joint and the other, with a tubular shape passing through the center of the link, for enhancing the stiffness of its region between the vertical support and the joint, which facilitates deformation downstream and improves controllability. As for the linear longitudinal movement of the joint, its assembly and that of the first motor are entirely displaced by the second stepper motor using a ball screw mechanism. We chose to use a stepper motor solution for the movable joint due to its position accuracy and fast reactivity. Two air streams with different pressures are supplied to the finger: P_1 deforms the joint, and P_2 regulates the stiffness of the link. These two air streams are applied via the two rods between the joint and the stepper motor for rotation.

Design Optimization

Finite Element Modeling

In this section, we describe the optimization procedure for a finger with the approximate dimensions of a human finger (diameter = 10 mm and length = 150 mm). The goal of the optimization is to find the best values of the parameters to meet the design objectives—as in maximizing the bending angle of the finger (θ) and minimizing the joint dimensions (length and diameter) under an approximate value of applied pressure to the joint (P_1). This value is numerically determined based on the 80% of pressure that causes the joint to burst with a 1-mm-thick chamber wall (H_1), which is equal to 14 kPa. Figure 4 summarizes the design parameters under investigation, including the main geometrical ones of the joint. The range of variation for each design parameter is tabulated in Table 1. The lower and upper bounds are specified based on fabrication considerations and also the dimensions of the finger, which is expected to be equivalent to the human finger. The pressure inside the link (P_2) is taken into account as another design parameter, and the range of variation is selected in a way such that a sensible

variation can be observed in the stiffness of the finger. An FEM is employed to numerically solve the relevant equations for flexible materials, with the aim of evaluating the candidates within the design search space. ANSYS Workbench, with the option of large nonlinear deformation for hyperelastic materials, is used as the framework for solving these numerical equations and performing optimizations. As for selecting the materials, two variations of platinum-catalyzed silicones are nominated to fabricate the actuator module: Ecoflex 00-30 and 00-50, the code numbers referring to the material's shore hardness. As studied by Elsayed et al. [17], both silicones exhibited the same bending behavior; however, lower pressure is required to deform the joint made of Ecoflex 00-30. Accordingly, here, this material is selected to fabricate the joint. As for the link, Dragonskin 00-30 is selected. This is due to the direct interaction of the link with objects and, consequently, the need for higher stiffness. Simulating the behaviors of these materials, silicone rubber is presumed as an isotropic and hyperplastic one. According to Steck et al. [18], for the Ecoflex 00-30, the third-order Ogden model ($N = 3$) for the strain energy potential is expressed with μ and α as the empirical parameters (1). The parameters' values $\mu_1 = 22$ kPa, $\alpha_1 = 1.3$, $\mu_2 = 0.4$ kPa, $\alpha_2 = 5$, $\mu_3 = -2$ kPa, and $\alpha_3 = -2$ show the best curve fit with the experimental stress-strain data of the mechanical tests:

$$U = \sum_{i=1}^N \frac{2\mu_i}{\alpha_i} (\lambda_1^{\alpha_i} + \lambda_2^{\alpha_i} + \lambda_3^{\alpha_i} - 3). \quad (1)$$

As for Dragon skin 00-30, the second order Yeoh model is chosen due to the promising fitting with the stress-strain data of the mechanical tests considering the parameter values of $N = 2$, $C_{10} = 1.190$ kPa, and $C_{20} = 23.028$ kPa [17]. This model can be presented for incompressible materials as in (2):

$$U = C_{10}(\bar{I}_1 - 3) + C_{20}(\bar{I}_1 - 3)^2. \quad (2)$$

Due to the large deformations in the joint structure, SOLID187 elements are used to mesh the model. These elements with quadratic-displacement behavior are defined by 10 nodes having 3 DoF at each node. This characteristic, along with capabilities such as plasticity, hyperelasticity, creep, stress stiffening, large deflection, and large strain, makes them well suited for irregular model meshes (such as those produced in this analysis). Fixed-support boundary conditions are applied to the beginning of both the link and the joint, while the tips are set free to move. As for simulating the pressures in the joint and the link chambers (P_1 and P_2), constant normal pressure boundary conditions are considered with relevant values. Figure 5(a) illustrates the results of the bending simulation of a sample up to 90° , under the actuation pressure of 14 kPa.

Sensitivity Analysis

Before optimization, local sensitivity analysis helps to find the positive or negative effect of each design parameter on

the objective output. This analysis is useful when a large number of variables exists and one needs to figure out the most critical design parameters to reduce the computational cost of the optimization [19]. The local sensitivity is calculated according to

$$\text{Local Sensitivity (\%)} = \pm \frac{(\text{output}_{\max} - \text{output}_{\min})_{\text{local}}}{(\text{output}_{\max} - \text{output}_{\min})_{\text{global}}} \times 100, \quad (3)$$

Table 1. The ranges for design optimization parameters.

Design Parameters	Lower Bound	Upper Bound
Joint length: L_1 (mm)	40	60
Chamber length: L_2 (mm)	30	50
Joint diameter: D_1 (mm)	20	40
Chamber diameter: D_3 (mm)	6	10
Chamber-to-wall thickness: H_1 (mm)	1	2
Hole-to-wall thickness: H_2 (mm)	1	5
Pressure inside the link: P_2 (kPa)	110	150

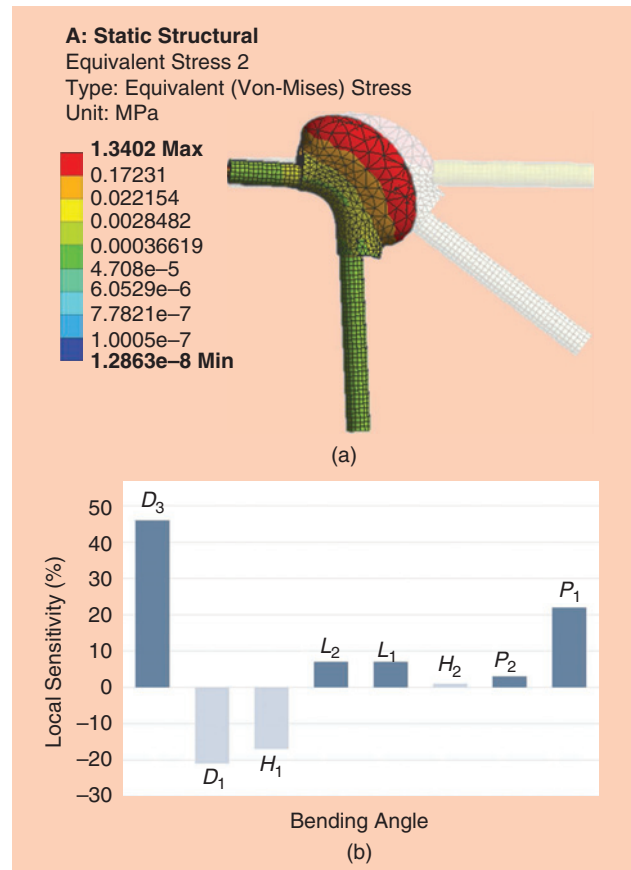


Figure 5. (a) The FEA simulation of a finger up to 90° under actuation pressure of 14 kPa. (b) The local sensitivity of the optimized result to each design parameter.

where $(\text{output}_{\max} - \text{output}_{\min})_{\text{local}}$ is calculated when one input value varies and others are assumed to be constant in particular geometry and $(\text{output}_{\max} - \text{output}_{\min})_{\text{global}}$ is quantified when all of the inputs vary. Figure 5(b) presents the local sensitivity analysis of each design parameter in percentages. As can be observed, the chamber diameter (D_3) and actuation pressure (P_1) are estimated to be the most important elements with direct relation to the bending angle; in other words, compared to other variables, increasing these two elements results in more intense positive changes in the final bending angle. The joint diameter (D_1) and chamber-to-wall distance (H_1) stand next in the ranks of the most influential parameters but in reverse relation to the main objective, which means that reducing the values of these parameters causes the final bending angle to increase. On the other hand, variations of the hole-to-wall distance (H_2) and the pressure inside the link (P_2) are estimated to be almost ineffective for the main objectives of the optimization and, hence, can be neglected. Nevertheless, it should be noted that P_2 is an important parameter for changing the finger stiffness and thus the applied fingertip force. The effect of this

parameter is discussed in the following section. As for H_2 , the value is determined according to manufacturing considerations and is set to 2 mm. The low value of this parameter would result in aligning the surfaces of the joint and the link in the bending direction. This would eventually lead to a uniform smooth surface in that area, which can be beneficial in future possible grasping applications.

Optimization Process

After identifying the influential design parameters with local sensitivity review, an optimization analysis must be conducted. The goal is to maximize the bending angle up to 90° and simultaneously minimize the length and diameter of the joint (miniaturizing the dimension of the finger to be more like a human's) under the applied pressure [(P_1) around 14 kPa]. The optimization process and prerequisites are shown in the flowchart in Figure 6. Due to the multiple numbers of the design parameters, objectives, and constraints, the adaptive multiple-objective optimization method is selected to find the global optimum parameters. This method is a variation of the NSGA-II based on controlled elitism concepts [16]. This average

value is selected through trial and error so that the finger with the specified ranges of geometrical dimensions can bend up to 90° and not burst. The calculation converged by generating 400 samples with 50 samples per iteration and finding the best candidate in eight iterations. Furthermore, during the process, if the FEM simulation of a sample failed (for example, bursting), it was eliminated and replaced by a new sample. In total, 146 new samples have been generated to replace the failed ones. The optimization charts are shown in Figure 7(a)–(e), where the empty circles show the samples and the blue lines illustrate the moving average, i.e., the best-fitted line that represents the convergence trend of the samples to the optimized values. Table 2 summarizes the eventual optimized values. These dimensions will be used to manufacture the prototype of the finger. The molds are printed with the Ultimaker3 3D printer. Thanks to recent advances in 3D printing technology, the fabrication process of soft components has been facilitated significantly, which leads to producing more complex parts with higher precision. For each silicone, two liquid parts should be mixed with the same ratio, followed by a 2–3-min vacuum degassing to eliminate any entrapped air bubbles. This is done by placing the molds in a vacuum chamber.

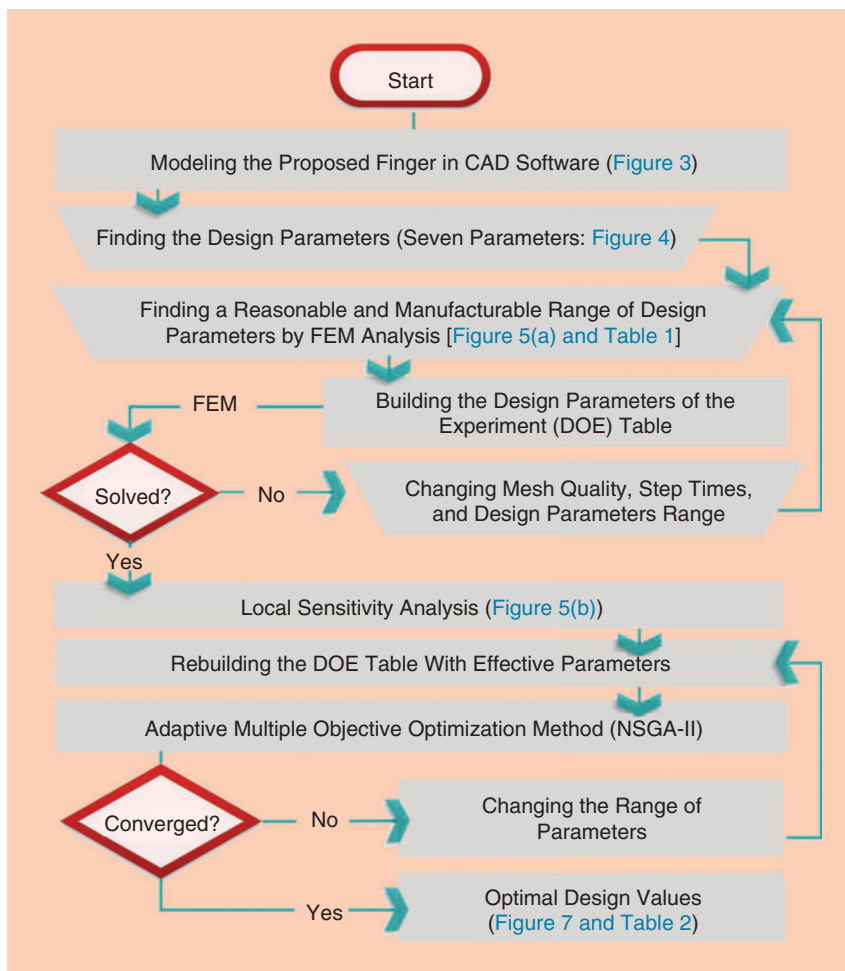


Figure 6. A flowchart of the proposed optimization methodology. The trapezoid shapes represent a manual operation, and the other rectangular shapes are the automated process. DOE: design of experiment.

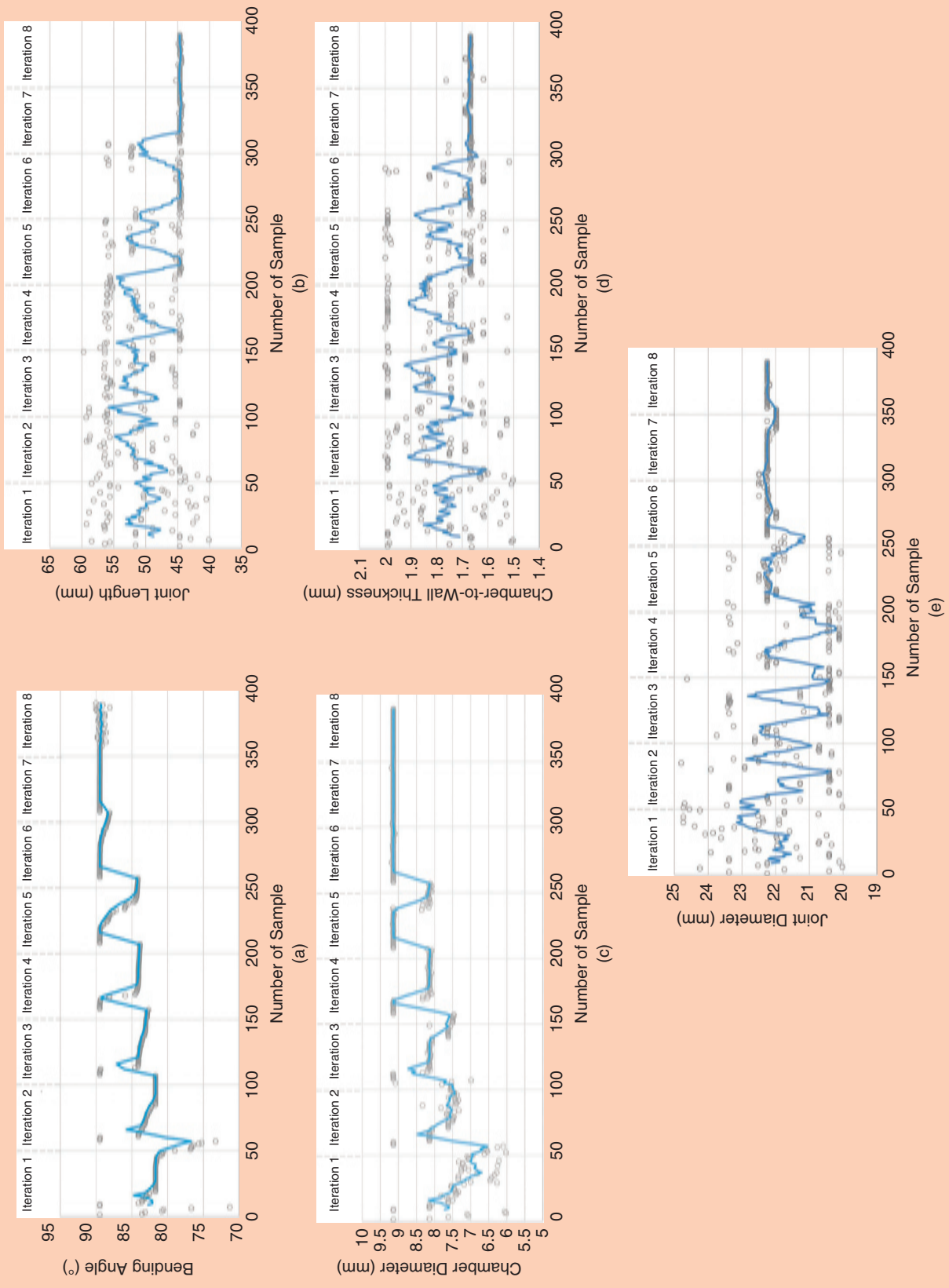


Figure 7. (a)–(e) Optimization of the proposed soft finger: convergence of the design parameters to the final optimized values (the blue lines show the moving average of each design parameter). The (a) bending angle, (b) joint length, (c) chamber diameter, (d) chamber-to-wall thickness, and (e) joint diameter.

Table 2. The FEM optimized parameters.

Design Parameters	Optimized Value
Joint length: L_1 (mm)	44.6
Chamber length: L_2 (mm)	42.5
Joint diameter: D_1 (mm)	22.3
Chamber diameter: D_3 (mm)	9.14
Chamber-to-wall thickness: H_1 (mm)	1.68

Results and Discussions

Workspace Analysis

For a better understanding of the finger mechanism, the workspace analysis is evaluated (Figure 8). The kinematic model of the finger is considered as one joint and two links. The first link (red) is fixed, and the second one (blue) can bend up to 90° in the xy -plane. The whole finger can rotate around the x -axis about 300° . By changing the position of the joint, the bending point and the length of the two links are changed. As noted in the “Design Optimization” section, the length of the finger and joint were presumed to be within the range of 4.46 and 15 cm. The bending point (center of joint) can be moved along the x -axis from 2.5 to 12.5 cm, and the resulting workspace of every point touched by a fingertip in 2D [Figure 8(a)] and 3D [Figure 8(b)] is calculated. The 2D workspace comparison between the proposed finger and a traditional design shows that changing the position of bending increases the number of accessible points, while the

tipping point workspace of previous traditional FEAs is assumed to be a constant arc [20].

Experimental Results

Validating the numerical model introduced in the previous sections, the fabricated finger undergoes two sets of experiments, as in bending and force tests. Figure 9(a) shows the prototype assembled to conduct the tests.

An Arduino Uno board controls the whole process, including reading sensors, switches, and electric motors, and it is connected to the computer via a USB wire. A 12-V, 350-kPa air pump is used for supplying the pressurized air for the system. Regulating the pressures P_1 and P_2 independently, one solenoid valve and one silicon piezoresistive pressure sensor are embedded in each air stream. The feedback signals that transfer from each pressure sensor to the Arduino are used to switch the air pump and the relevant solenoid valve on and off. Two test benches are developed to characterize the bending angle as well as the blocking force of the fingertip. The bending angle of the finger is checked using a printed protractor, placed at the joint's center of bending [Figure 9(b)]. As for measuring the force applied by the fingertip, a sensor is situated below the tipping point of the finger and directly transfers the force data to the computer [Figure 9(c)]. Due to the weight of the link, at the initial state, a deflection of 10° at the tipping point can be observed; this will be resolved by applying the pressure P_2 inside the link. Different pressures P_1 are applied to the joint, and the consequent bending angles are measured. These angles are compared with the numerical results in Figure 10(a). It can be noticed that there is an acceptable agreement between the experimental and numerical data, which can be taken as the validity of the model and thus the optimization results. As the second test with the assembled prototype, the force at the

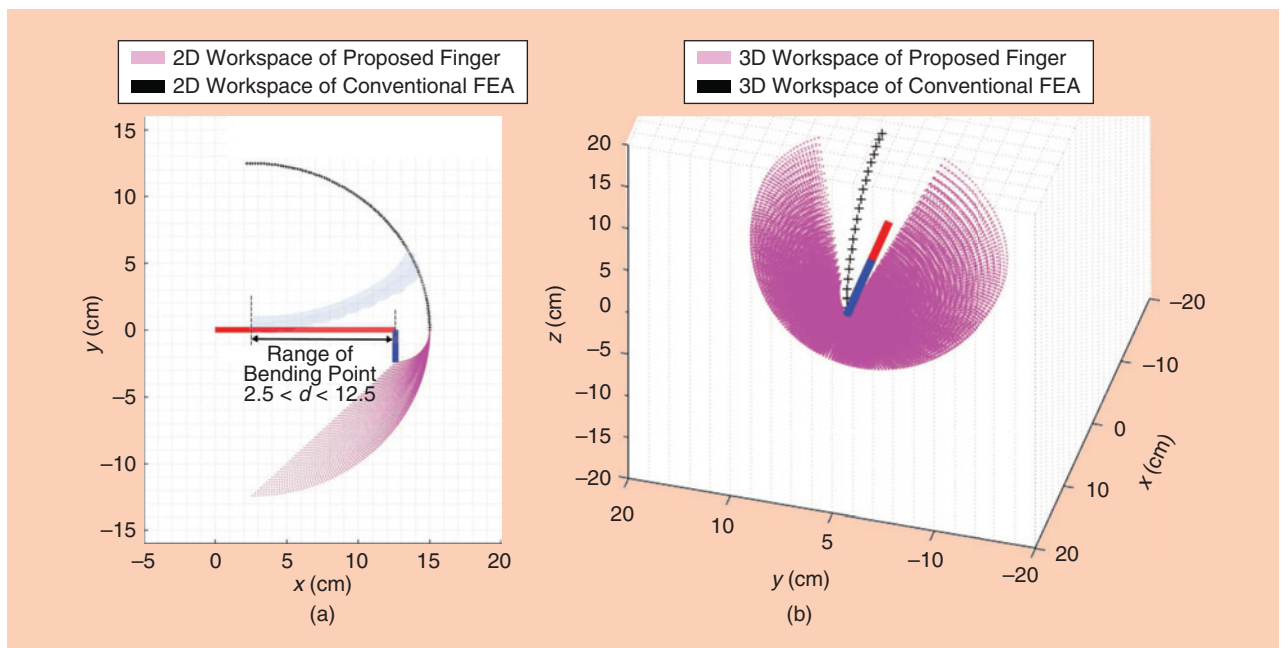


Figure 8. A workspace evaluation of the proposed finger compared to conventional FEAs with 12.5-cm length in (a) 2D space and (b) 3D space (the finger can rotate around its axis about 300°).

tipping point of the finger is measured as a function of different parameters, including the longitudinal position of the joint and the stiffening pressure (P_2). All of the tests are conducted under the actuation pressure of $P_1 = 14$ kPa. The results are presented in Figure 10(b). As illustrated, by changing the position of the joint toward the tip of the finger, the

applied force increases by almost three times. Furthermore, applying the pressurized air into the link results in higher stiffness and thus a higher amount of force, up to 650 mN, which is twice the initial value.

Conclusions

In this article, an innovative variable-stiffness soft finger with a fluid-actuated movable joint was introduced and optimized in terms of its primary characteristics. The finger consists mainly of one soft sliding and rotating joint as the bending actuator and a soft link as the body. Applying pressurized air into the joint's chamber, the joint and, consequently, the link both bend in a specific direction. The location and direction of the bending can be changed by sliding the joint longitudinally along the link and rotating it around its main axis using two electric motors. The variable length of the finger with the capability of bending in different directions results in a large diversity of configurations. The workspace analysis exhibited the advantage of this reconfigurability by extending the available workspace of the fingertip, in contrast to conventional FEAs. The local sensitivity of the design parameters involved in the problem was analyzed. Optimization over the important parameters was performed to minimize the joint dimensions and maximize the bending angle of the finger. The model included a large number of design parameters with nonlinear relations, which made prediction of the deformation difficult, i.e., small changes in each one could lead to large deviations in the final results. Hence, implementing the optimizing process is necessary to investigate the acceptable and manufacturable range of these parameters. The optimal geometrical parameters were used for fabricating a prototype that validates the numerical model. Another experiment was designed to study the amount of

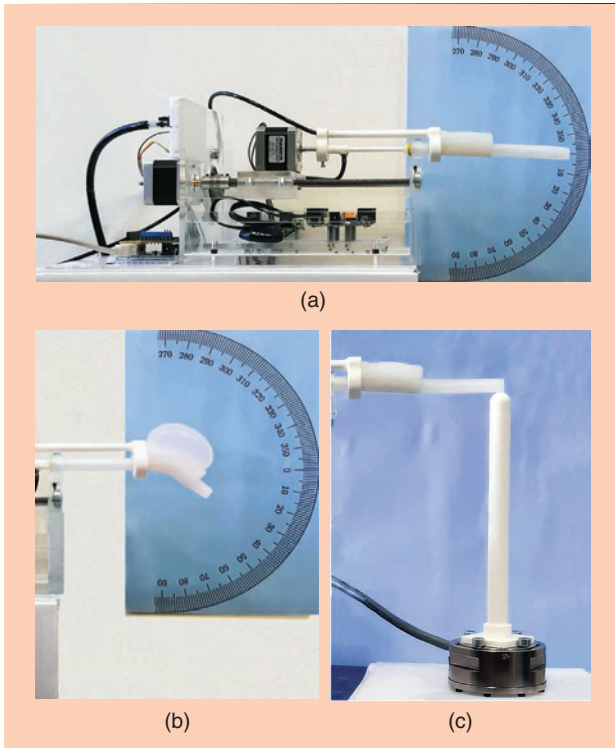


Figure 9. (a) The overall view of the assembled prototype. (b) The test bench for measuring the joint angle. (c) The test bench for measuring the fingertip force.

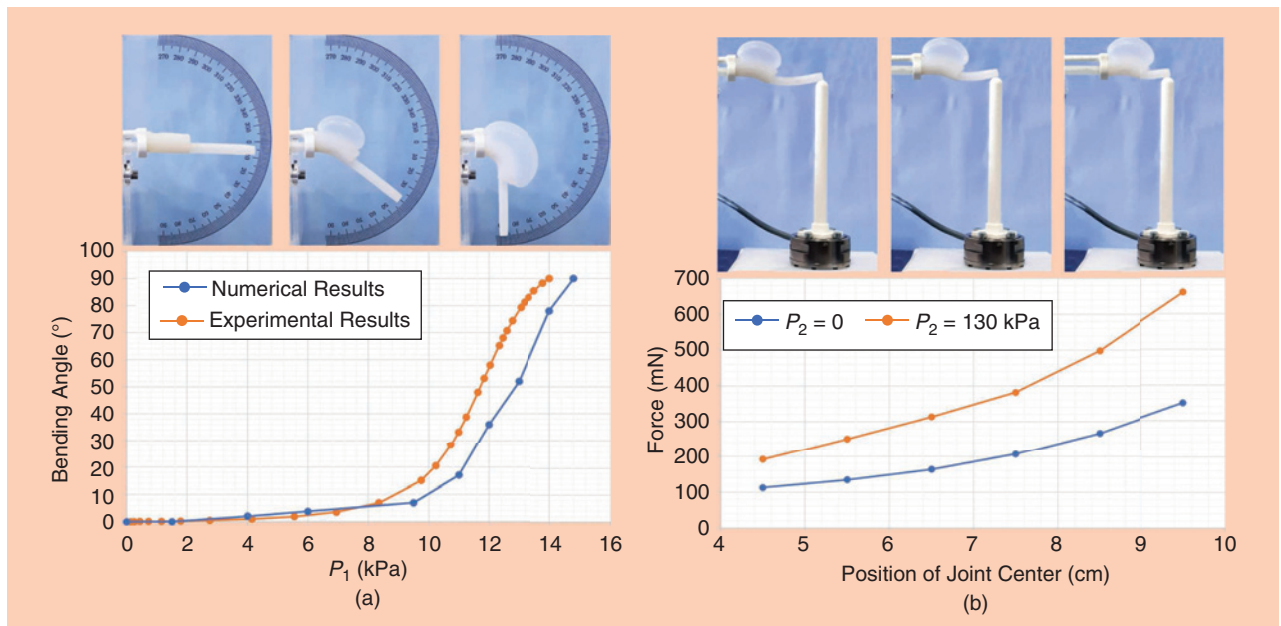


Figure 10. (a) The bending angles of the finger under different applied pressures: a comparison between the ANSYS FEM numerical simulation and the experimental results. (b) The fingertip force test results as a function of stiffening pressure (P_2) and joint longitudinal position.

force applied by the fingertip. It was shown that the longitudinal location of the joint and the pressure inside the link (P_2) were highly effective for this force. The wide range of force applied to the fingertip as well as the diversity of possible configurations to reach a given target leads to a variety of strategies to deal with situations such as the variable amount of force required or the presence of any obstacles in the workspace. Optimizing the dimension of the finger allowed us to reduce the volume of the required air and, consequently, the response time. The experiments showed that the joint can bend up to 90° in less than 3 s, in contrast with previous approaches (as in SMPs or LMPAs).

Future Works

As for future works, the idea of using these fingers in a dexterous gripper with miniaturized pumps and electric motors will be studied. Furthermore, combining sensitivity analysis and NSGA-II optimization provides a design basis for this future gripper, especially in considering an energy criterion.

Acknowledgment

This work has been sponsored by the French government research program “Investissements d’Avenir” through the IDEX-ISITE initiative 16-IDEX-0001 (CAP20-25).

References

[1] D. Trivedi, C. D. Rahn, W. M. Kier, and I. D. Walker, “Soft robotics: Biological inspiration, state of the art, and future research,” *Appl. Bionics Biomechanics*, vol. 5, no. 3, pp. 99–117, 2008. doi: 10.1155/2008/520417.

[2] A. D. Marchese and D. Rus, “Design, kinematics, and control of a soft spatial fluidic elastomer manipulator,” *Int. J. Robot. Res.*, vol. 35, no. 7, pp. 840–869, 2016. doi: 10.1177/0278364915587925.

[3] J. Shintake, V. Cacucciolo, D. Floreano, and H. Shea, “Soft robotic grippers,” *Adv. Mater.*, vol. 30, no. 29, p. 1,707,035, 2018. doi: 10.1002/adma.201707035.

[4] R. F. Shepherd et al., “Multigait soft robot,” *Proc. Nat. Acad. Sci.*, vol. 108, no. 51, pp. 20,400–20,403, 2011. doi: 10.1073/pnas.1116564108.

[5] W. McMahan et al., “Field trials and testing of the OctArm continuum manipulator,” in *Proc. 2006 IEEE Int. Conf. Robot. Automat. (ICRA 2006)*, pp. 2336–2341. doi: 10.1109/ROBOT.2006.1642051.

[6] M. Cianchetti, T. Ranzani, G. Gerboni, I. De Falco, C. Laschi, and A. Menciassi, “STIFF-FLOP surgical manipulator: Mechanical design and experimental characterization of the single module,” in *Proc. 2010 3rd IEEE RAS EMBS Int. Conf.*, pp. 461–466.

[7] P. Polygerinos, Z. Wang, K. C. Galloway, R. J. Wood, and C. J. Walsh, “Soft robotic glove for combined assistance and at-home rehabilitation,” *Robot. Auton. Syst.*, vol. 73, pp. 135–143, Nov. 2015. doi: 10.1016/j.robot.2014.08.014.

[8] H. K. Yap, H. Y. Ng, and C.-H. Yeow, “High-force soft printable pneumatics for soft robotic applications,” *Soft Robot.*, vol. 3, no. 3, pp. 144–158, 2016. doi: 10.1089/soro.2016.0030.

[9] Y. Yang, Y. Chen, Y. Li, M. Z. Chen, and Y. Wei, “Bioinspired robotic fingers based on pneumatic actuator and 3D printing of smart material,” *Soft Robot.*, vol. 4, no. 2, pp. 147–162, 2017. doi: 10.1089/soro.2016.0034.

[10] Y. Yang, Y. Chen, Y. Li, Z. Wang, and Y. Li, “Novel variable-stiffness robotic fingers with built-in position feedback,” *Soft Robot.*, vol. 4, no. 4, pp. 338–352, 2017. doi: 10.1089/soro.2016.0060.

[11] Y. Hao et al., “A eutectic-alloy-infused soft actuator with sensing, tunable degrees of freedom, and stiffness properties,” *J. Micromech. Microeng.*, vol. 28, no. 2, p. 024004, 2018. doi: 10.1088/1361-6439/aa9d0e.

[12] H. K. Yap, J. H. Lim, F. Nasrallah, J. C. Goh, and R. C. Yeow, “A soft exoskeleton for hand assistive and rehabilitation application using pneumatic actuators with variable stiffness,” in *Proc. 2015 IEEE Int. Conf. Robot. Automat. (ICRA)*, pp. 4967–4972. doi: 10.1109/ICRA.2015.7139889.

[13] B. E. Schubert and D. Floreano, “Variable stiffness material based on rigid low-melting-point-alloy microstructures embedded in soft poly (dimethylsiloxane) (PDMS),” *RSC Adv.*, vol. 3, no. 46, pp. 24,671–24,679, 2013. doi: 10.1039/c3ra44412k.

[14] Y. Elsayed, C. Lekakou, T. Geng, and C. M. Saaj, “Design optimisation of soft silicone pneumatic actuators using finite element analysis,” in *Proc. 2014 IEEE/ASME Int. Conf. Adv. Intell. Mechatronics*, pp. 44–49. doi: 10.1109/AIM.2014.6878044.

[15] G. Decroly, B. Mertens, P. Lambert, and A. Delchambre, “Design, characterization and optimization of a soft fluidic actuator for minimally invasive surgery,” *Int. J. Comput. Assisted Radiol. Surg.*, vol. 15, no. 2, pp. 333–340, 2020. doi: 10.1007/s11548-019-02081-2.

[16] K. Deb, A. Pratap, S. Agarwal, and T. Meyarivan, “A fast and elitist multiobjective genetic algorithm: NSGA-II,” *IEEE Trans. Evol. Comput.*, vol. 6, no. 2, pp. 182–197, 2002. doi: 10.1109/4235.996017.

[17] Y. Elsayed et al., “Finite element analysis and design optimization of a pneumatically actuating silicone module for robotic surgery applications,” *Soft Robot.*, vol. 1, no. 4, pp. 255–262, 2014. doi: 10.1089/soro.2014.0016.

[18] D. Steck, J. Qu, S. B. Kordmahale, D. Tscharnuter, A. Muliana, and J. Kameoka, “Mechanical responses of Ecoflex silicone rubber: Compressible and incompressible behaviors,” *J. Appl. Polym. Sci.*, vol. 136, no. 5, p. 47,025, 2019. doi: 10.1002/app.47025.

[19] K. L. Lawrence, “ANSYS workbench tutorial release 14.” SDC Publications, 2012.

[20] P. Polygerinos et al., “Modeling of soft fiber-reinforced bending actuators,” *IEEE Trans. Robot.*, vol. 31, no. 3, pp. 778–789, 2015. doi: 10.1109/TRO.2015.2428504.

Amir Pagoli, Université Clermont Auvergne, CNRS, SIGMA Clermont, Institut Pascal, Clermont-Ferrand, France, E-mail: amir.pagoli@sigma-clermont.fr.

Frédéric Chapelle, Université Clermont Auvergne, CNRS, SIGMA Clermont, Institut Pascal, Clermont-Ferrand, France, E-mail: frederic.chapelle@sigma-clermont.fr.

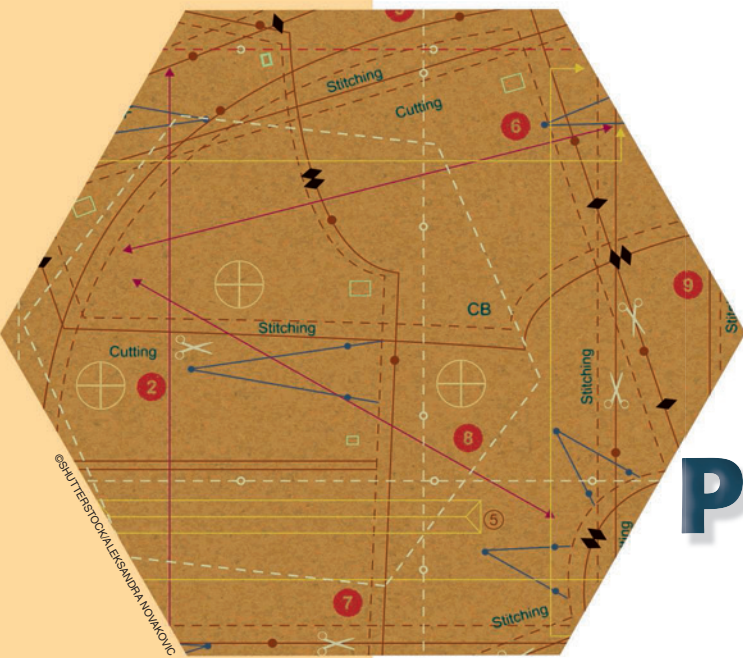
Juan-Antonio Corrales-Ramon, Université Clermont Auvergne, CNRS, SIGMA Clermont, Institut Pascal, Clermont-Ferrand, France, E-mail: juan-antonio.corrales-ramon@sigma-clermont.fr.

Youcef Mezouar, Université Clermont Auvergne, CNRS, SIGMA Clermont, Institut Pascal, Clermont-Ferrand, France, E-mail: youcef.mezouar@sigma-clermont.fr.

Yuri Lapusta, Université Clermont Auvergne, CNRS, SIGMA Clermont, Institut Pascal, Clermont-Ferrand, France, E-mail: yuri.lapusta@sigma-clermont.fr.



Expanding Pouch Motor Patterns for Programmable Soft Bending Actuation



By Haneol Lee, Namsoo Oh, and Hugo Rodrigue

Enabling Soft Robotic System Adaptations

The use of soft robots to interact with soft, fragile, and even living things has spurred interest in the development of soft robotic systems that can deform and adapt themselves to their environment through their inherent compliance. Current soft pneumatic actuator concepts require significant redesign to be repurposed from one function to another, and a complete soft robotic system may be composed of multiple types of actuators with varying materials, designs, and manufacturing methods. This complicates the process of designing and manufacturing soft robots that can tackle new tasks and environments. This work introduces a repeatable pattern of pouch motors with geometric constraints allowing the actuator to produce a programmable bending deformation. By varying the dimensions of the pattern, it is possible to produce different motions that can be used to build diverse robotic components, such as a soft robotic arm or a large soft robotic gripper.

Background

Pneumatic artificial muscles (PAMs) that use the lateral expansion of a chamber to produce a linear contraction have been used in a wide range of robotic applications but require high pressures [1], [2]. Polymeric chambers with asymmetric properties have been used to transfer the volumetric expansion of the structure into a bending deformation employing

either different material thicknesses or anisotropic material properties [3], [4]. Tentacle-like, continuum-based soft robotic members have also been developed using these mechanisms [5], [6]. However, these bending actuators rely on the deformation and stretching of a thick polymeric matrix and produce a bending force that does not scale well at larger sizes due to the weight and stretchability of the polymer. This means that they require significant redesign for new applications.

Soft pneumatic actuators making use of thin films rather than thicker polymeric structures have been introduced as lighter and easier to manufacture alternatives to polymer-based soft actuators. Film-based soft linear actuators, such as pouch motors, series PAMs, and fabric PAMs, have been developed based on principles similar to those of PAMs [7]–[10]. The bending deformation of film-based soft pneumatic actuators has been realized through anisotropic expansion using materials with different extensibilities [11], employing folds to produce anisotropic expansion of the structure [12], and applying different knitted elements with diverse patterns and stretchability properties [13]. Another approach has been to use the lateral expansion of parallel pouches under pressurization to produce a bending deformation [14]. Although these designs offer interesting new capabilities, they are not versatile for different applications due to their specialization.

Bellows textile muscles are made from thin films like pouch motors but are connected in parallel on the flat portion of their bodies and can be used to produce extensions or contractions, depending on whether they are pressurized or vacuumed [15]. Bellows textile muscles can be used to

Digital Object Identifier 10.1109/MRA.2020.3023969
Date of current version: 5 October 2020

produce joint-like motions by connecting the ends of the stack of actuators to a rigid joint [16]. A 2-degree of freedom (2-DoF) pneumatic soft/rigid hybrid robot using a bellows textile muscles design has been presented, but its capability was not assessed [17]. An arm with a similar concept was capable of precise planar positioning using potentiometers located in each joint [18]. Folding a series of pouch motors, rather than connecting them individually through their center, could also simplify the assembly process while still using the expansion of the volume to produce jointed motions [19]. However, these actuators require a large number of actuator units to make higher forces at higher displacements as the pouches separate throughout the motion. These designs are also focused on joint-like motion with a smaller radius of curvature and cannot be used to produce simple bending actuators with a larger radius of curvature.

A universal design that is easy to repurpose for different functions, simple to manufacture, and controllable and that has good actuation properties could find use in a wide range of robotic applications. This article presents a new

design for an inflatable soft bending actuator that uses repeated patterns of pouch motors with constraints that interact with each other, through their multidirectional expansion, to produce large forces and large bending deformations. The shape of the deformation of the actuator can be easily modified by changing the dimensions of the pouches and constraints. The behavior of different actuator configurations is measured using a testing jig, and the concept of the actuator is adapted into both a soft robotic finger and a controllable robotic joint. Multiple joints and fingers are then assembled to form a 3-DoF robotic arm with a three-fingered gripper based entirely on the expansion of pouch motors as well as a large soft robotic gripper capable of grasping large objects, such as basketballs or watermelons.

Design and Manufacturing

The proposed soft bending actuator functions through the expansion of a pattern of pouch motors consisting of an outer and inner layer of motors with geometric constraints [Figure 1(a)]. The expansion of these motors throughout the

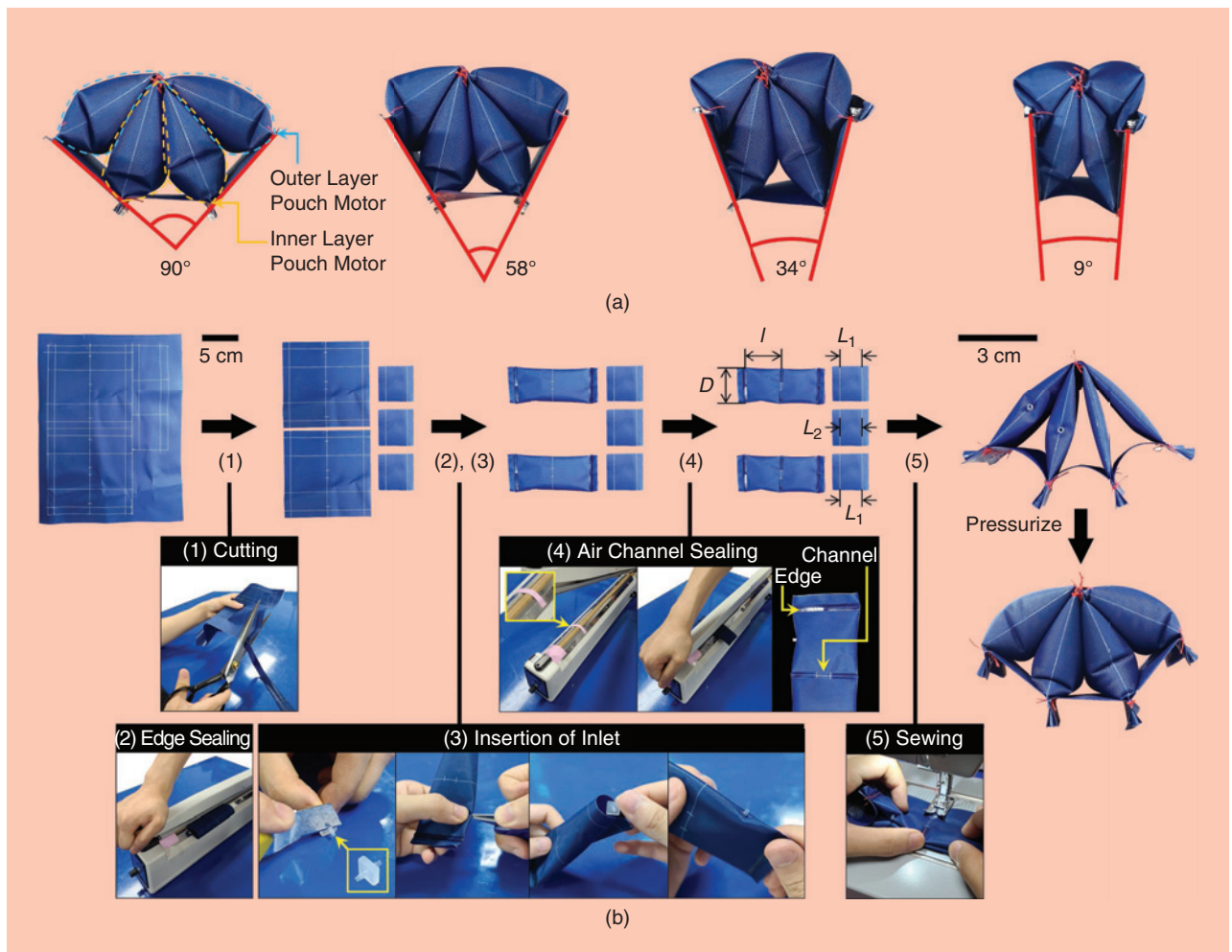


Figure 1. (a) The bending motion of a single pouch motor pattern. (b) Its manufacturing method by cutting the material, sealing the edge, inserting the inlet, sealing the air channels, and sewing the pouch motors and constraint together.

actuator's motion is responsible for the force produced by the actuator throughout its bending motion, while the geometric constraints force the motors to produce a bending deformation at each end of the pattern. Changing the dimensions of the pouches and geometric constraints has a significant effect on the properties of the actuator and can be used as the main tool to change its intended motion.

It is possible to repeat the pattern of pouch motors in a series to increase the actuator's range of motion and the pattern width to increase its force. Examples of these will be shown later in this article. The most basic pattern consists of the case with four pouch motors, where each of the inner and outer layers contains two pouches each. It is also possible to make minor variations to the pattern by adding or removing pouches; one such variation demonstrated later in this article is to remove one from the outer layer to reduce the bending angle while maintaining actuator stiffness.

Manufacture of the actuator begins by cutting the film used for the bottom and lateral constraints as well as for the two series of pouch motors [Figure 1(b)]. The series of pouch motors is then sealed to form a tubular structure of width D , using an impulse sealer or another heat-bonding device; the inlet is inserted into the structure, and then the structure is sealed at the ends and partially bonded at the required intervals to form the individual pouch motors of length l . Approximately one-third of the pouch is bonded on each side, allowing air to flow between pouches through the middle gap. The series of pouch motors is then attached to the constraints through sewing or other methods.

The actuator can be made from most thermoplastic films: air bladders inserted into other materials or technical textiles consisting of a fabric coated with an impermeable layer. The actuators described in this article are made from nylon fabric coated with thermoplastic polyurethane (TPU), which can be bonded together on the side coated with TPU. Air inlets (5116K193, Mc-Master-Carr) should be added for each series of pouch motors as air does not flow between them. As described in this article, the air inlets were added either on the side or middle of the pouches closest to their attachment points.

There are three main advantages of this design compared to previous bellows textile muscles and folded tube joint actuators [16]–[19]: 1) the radius of the curvature of the actuator can be adjusted by varying the dimensions of the pouches and constraints to produce either joint-like or finger-like motions as well as by varying the actuation properties throughout the actuator, which is not possible with previous designs; 2) the use of an outer layer of pouches produces more force versus using only one layer of pouches, while also providing a resistance to out-of-plane deformations; and 3) the fabrication method of the actuator is simplified by bonding and sewing only constant-width tubular elements versus requiring precise positioning and bonding of inner and outer seams, as in bellows textile muscles.

Results

Pouch Pattern Performance Evaluation

A testing jig was developed to measure the bending force produced by pouch motor patterns of different dimensions at different bending angles [Figure 2(a)]. The bending angle was controlled using pins that fixed it, but the distance between its inner points was free to move laterally to reflect the natural motion of the actuator while measuring the bending force [Figure 2(b)]. The bending force was measured using a force-torque sensor (RFT60, Robotous), and the pressure was supplied using an air compressor (MD 75/250, Bambi), regulated using an electro-pneumatic regulator (ITV1030, SMC). Throughout this article, the same pressure was applied uniformly to all pouch motors of the actuators.

A base actuator was manufactured with a single pouch motor pattern with four pouch motors, all having a length l and a width D , both equal to 50 mm, and a lateral constraint length L_1 and bottom constraint length L_2 , both equal to 30 mm [Figure 2(c)]. The actuator was then tested, using the jig described previously, for pressures ranging from 5 to 60 kPa in increments of 5 kPa [Figure 2(d)]. The bending force produced by the actuator decreased linearly with an increase in the bending angle and reached equilibrium at an angle of 90°, where the actuator produced no bending force. This equilibrium angle could be adjusted by changing the dimensions of the pouch motors and constraints.

A second actuator, with a width of 10 cm, was then manufactured, tested, and compared to the base actuator, which had a width of 5 cm for pressures ranging from 10 to 60 kPa in increments of 10 kPa [Figure 2(e)]. The actuator with a width of 10 cm contained two air channels between the pouch motors, rather than a single channel for increased airflow [Figure 2(f)]. In this case, the behavior of the actuator changed slightly with the bending force at zero—the bending angle more than doubling and the bending force being very small at bending angles close to 90°. It would have been expected that the force doubled uniformly at all bending angles. This is because the segment of the actuator toward the edges had different actuation properties than the middle due to the difference in inflation shape [8]. The wider actuator's behavior corresponded more closely to the behavior of the section at the middle.

The base actuator was then compared to one consisting of two base actuators in a series, where one of the lateral constraints was shared by the two pouch motor patterns [Figure 2(g)]. The addition of a second pouch motor pattern increased the equilibrium angle to 180° and caused a slight

In this case, the behavior of the actuator changed slightly with the bending force at zero.

decrease in the bending force, which could be due to some unintended motions often present in longer soft bending actuators. Then, the actuator with two series of pouch motors was compared to a variation of the base actuator [Figure 2(h)]. In this variation, the lateral constraint between two serially connected pouch motor patterns was removed as well as one of the pouch motors connected to it [Figure 2(i)]. The goal of this variation was to maintain the bending force of the actuator while significantly decreasing the bending angle created between successive patterns of pouch motors, as it could be noticed that the bottom constraints remained nearly flat.

Implementation as a Robotic Finger

One of the interesting aspects of the design is that the dimensions of a single pattern of pouch motors will

determine the properties of this specific set of motors without affecting the following one. Thus, it is possible to change the deformed shape of the actuator by changing the dimensions of the pouch motors and constraints throughout its length. Two actuators were built from a series of four pouch patterns, where one had constant pattern dimensions throughout and the other had varying ones [Figure 3(a) and (b)]. The two central pouch motor patterns contained four pouch motors each, while the base and tip patterns contained only three motors, to make it easier to fix the finger, and did not affect the bending angle or force in this implementation. The two actuators were built such that the total length of the pouch motors and constraints was equal between both. However, the dimensions of all elements in the second actuator were varied throughout the length, while proportionally scaling all

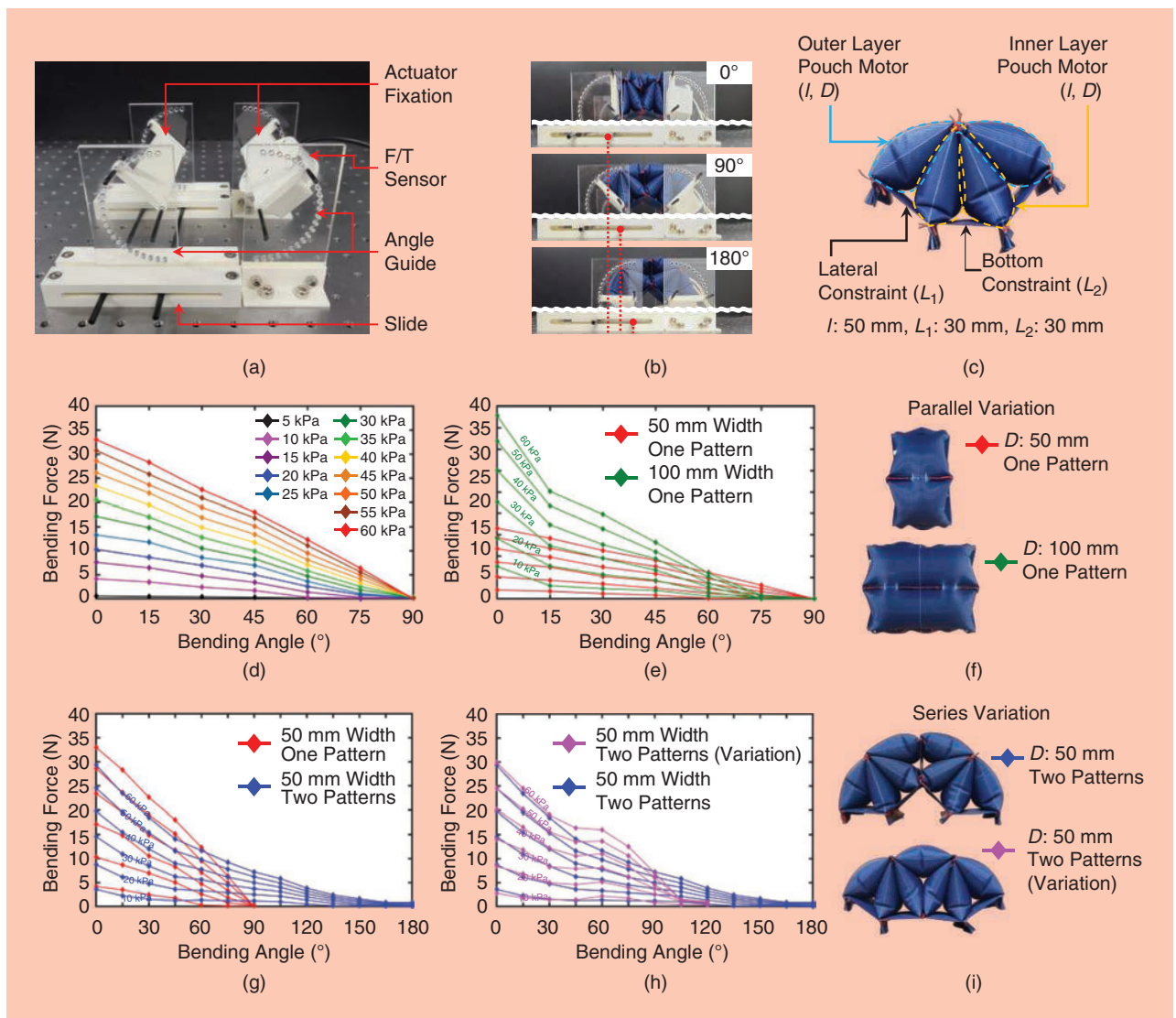


Figure 2. (a) The jig for testing the bending force. (b) The motion of the testing jig for different bending angles. (c) The dimensions. (d) The actuation properties of the base actuator. (e) The actuation properties of the base actuator and an actuator with double the width. (f) The top-view of the two actuators. (g) The actuation properties of the base actuator compared to an actuator with two units in a series. (h) A comparison of the actuator with two units in a series to an actuator with a modified pattern. (i) The side-view of the two actuators.

dimensions of the patterns. It can be seen that the uninflated and inflated shape of the first actuator is constant throughout the length, and that the shape of the second actuator varies throughout its length. This freedom can help in designing actuators with specific deformation shapes or in adjusting the torque produced at specific regions of the actuator.

As the equilibrium angle of the actuator does not depend on pressure, the actuator does not return to its original state when depressurized. This is because it does not rely on the stretching of a polymeric matrix, which would produce an elastic force to bring it back to its unstretched shape. This issue can be easily remedied by adding a separate mechanism to return the actuator to its original position. In this case, a second actuator was implemented into it by replacing the bottom constraint with a straight tube, made from the same material as the pouch motors, that pushed the actuator back to the straight position upon inflation. Thus, the actuator can be inflated to produce a bending deformation, and then it can be deflated, while the bottom constraint is inflated, to return to the straight position [Figure 3(c)]. To be used as a robotic finger, the inner portion of this actuator was also coated with polymer (Eco-Flex 00–30, Smooth-On) to increase its coefficient of friction. The last pattern at the tip of the finger contains only one pouch motor in the outer layer, to reduce its bending angle while maintaining the stiffness throughout. Using this design, a single finger was easily capable of holding

a load of 1 kg at a pressure of 30 kPa while maintaining its intended shape [Figure 3(d)].

Implementation as a Robotic Joint

The dimensions of the pouch motors and constraints determine the characteristics of the actuator, including its radius of curvature. Significantly shortening its radius of curvature by reducing the length of the bottom constraint makes the actuator behave as a rotary around a central axis. Two of these can then be installed antagonistically to control the output angle of a robotic joint. A robotic joint with two antagonistic, pouch-based rotary actuators was built using a 3D printed polylactic acid frame [Figure 4(a)]. Each of the rotary actuators contained three patterns of four pouch motors with dimensions $L_1 = 0.03$ m, $L_2 = 0.015$ m, $l = 0.05$ m, and $D = 0.1$ m. A rotary encoder (AMT103, CUI Inc.) was installed onto the central shaft of the robotic joint to read its position. Based on the design of the frame, the range of motion of the joint is 180° , and the maximum angle of the actuator itself is 270° . This allows the joint to produce a sustained force throughout the motion as the actuator produces more force at lower rotation angles.

In the vertical plane, the joint can operate with a payload at the tip, using only the rotary actuator located below the joint. A weight of 800 g was attached at the end of an inflatable element, connected to the joint such that the moment arm length of the weight was 35 cm. At a pressure of 20 kPa, the joint

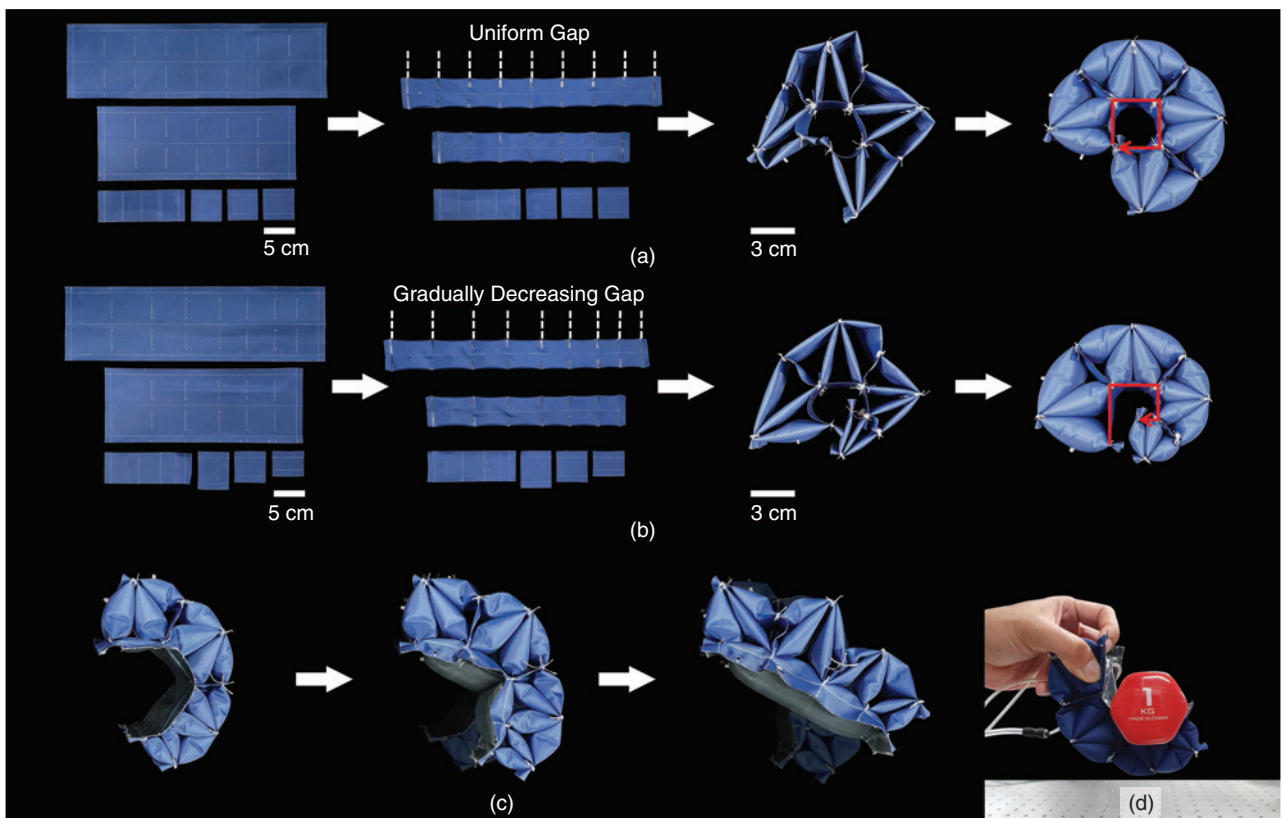


Figure 3. (a) The assembly of the finger with constant pattern dimensions. (b) The assembly of the finger with variable pattern dimensions. (c) The finger with a chamber to return to the straight position. (d) A single finger grasping a 1 kg load.

reached an angle of 58.1° , and at 60 kPa, it reached 115.4° , as measured by the encoder [Figure 4(b)]. Some hysteresis of the motion was observable by the joint actuator not reducing in angle with a slight reduction in pressure, such that the actuator remained at an angle of 115.4° , even after lowering its pressure

to 40 kPa. This could be due to the force required for bending the unfolded fabrics or other nonlinearities of the structure. The joint angle as a function of pressure during pressurization and depressurization was measured using the encoder, and it could be seen that the joint actuator produced significantly

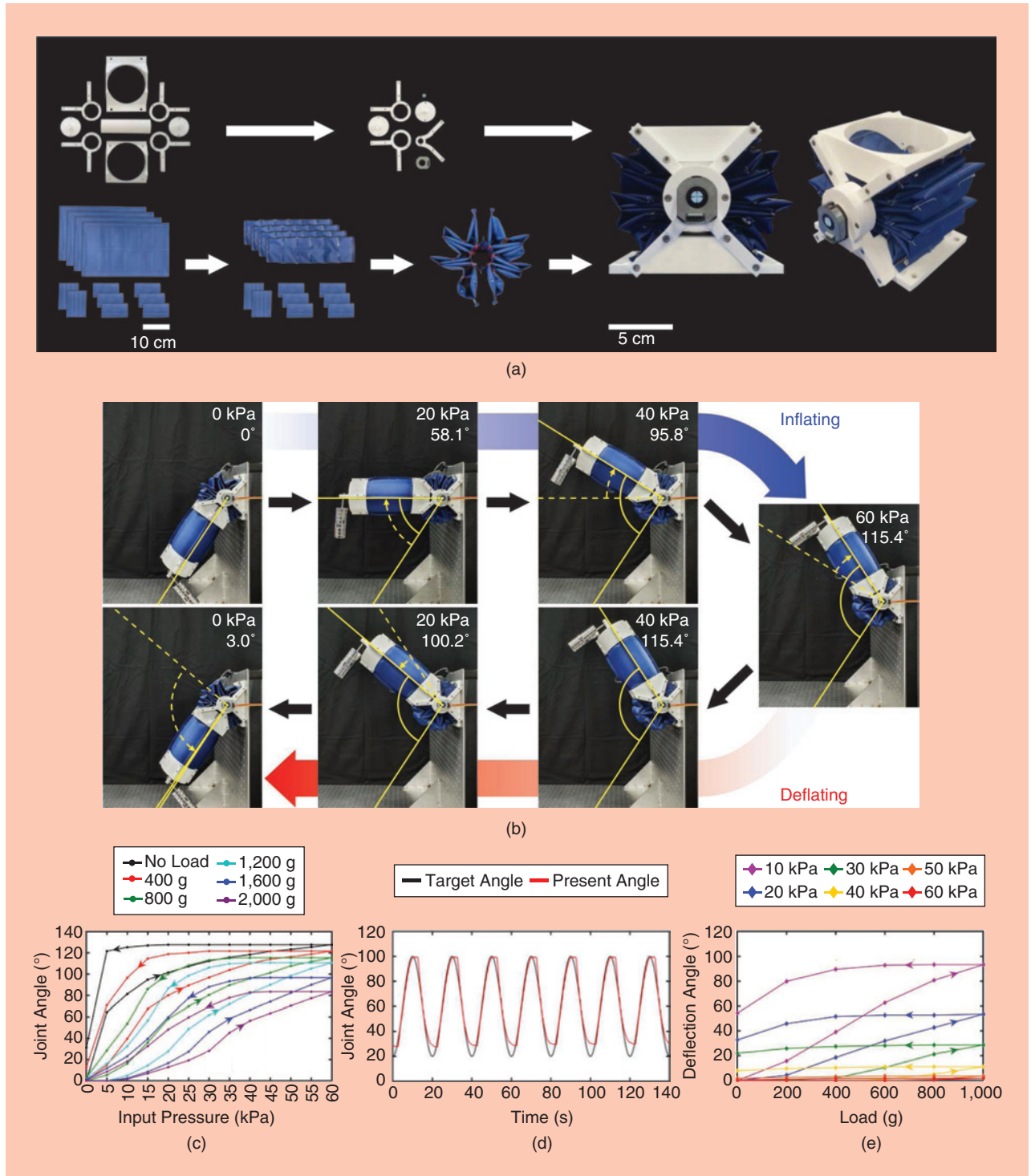


Figure 4. (a) The assembly of the pouches with the 3D printed parts to form a robotic joint. (b) The angle of the joint at different pressures of the bottom chamber with a load of 800 g. (c) The joint angle versus input pressure for different tip loads. (d) The proportional-integral-derivative control of the joint with a sinusoidal input with a load of 800 g. (e) The deflection of the joint versus load for different pressures.

larger forces during depressurization, as observed in the previous experiment [Figure 4(c)]. This effect was observable at all loads but might cause significant issues for control at lower payloads, as the actuator then requires very low pressures to lower its joint angle.

The encoder was then used to realize proportional-integral-derivative (PID) control of the joint (P: 1.200, I: 0.010, D: 0.001) and made to follow a sinusoidal wave with an amplitude of 80°, from 20 to 100°, with a period of 20 s and a load of 800 g [Figure 4(d)]. Although the joint can follow the input reasonably well for most of the motion, the inflation speed is too slow to follow the desired input at high pressures, and the deflation speed is too slow at low pressures. This could be due to the pneumatic hardware but appears to be mainly due to reduced airflow between pouch motors as the channel between them gets compressed. The hysteresis of the joint also causes the actuator to stay at 100°, while the pressure is reduced sufficiently to overcome the hysteresis. These experiments show that the joint is controllable but that its inflation and deflation speed could be an issue if high speeds are required and that position sensing with feedback control is necessary for precise control. Higher airflow, during both inflation and deflation, could also help overcome the hysteresis. Such a soft robotic joint, coupled with a precise sensor, could be used to realize precise motions with safe human–robot interaction due to its innate compliance and low inertia.

The stiffness of the joint at different pressures was tested by setting the pressure in both antagonistic chambers to equal values while the arm was unloaded and by adding a payload at the tip. The payload was then increased in increments of 200 g until 1,000 g and then decreased back to 0 g in decrements of 200 g while measuring the bending angle of the joint [Figure 4(e)]. The results show that an increase in pressure of the actuators of the joint significantly increases its stiffness and that adjusting the antagonistic actuator can be used to modify the behavior of the joint for different applications. The hysteresis of the joint can be seen in this experiment by the joint not returning to its original angle after unloading.

Applications

Soft Robotic Arm

A 3-DoF soft robotic arm with a three-fingered gripper was built by assembling three joints with designs identical to the previously presented joint using rigid elements [Figure 5(a)]. The first joint is connected directly to the second, an inflatable member is used to distance the second and third, and a second inflatable member is used to distance the third and the gripper. The total length of the arm from its base to the tip of the gripper is 80 cm [Figure 5(b)]. The first joint is used to produce a horizontal rotary motion at the base of the arm and produces a range of motion of 140°, while the second joint is used to

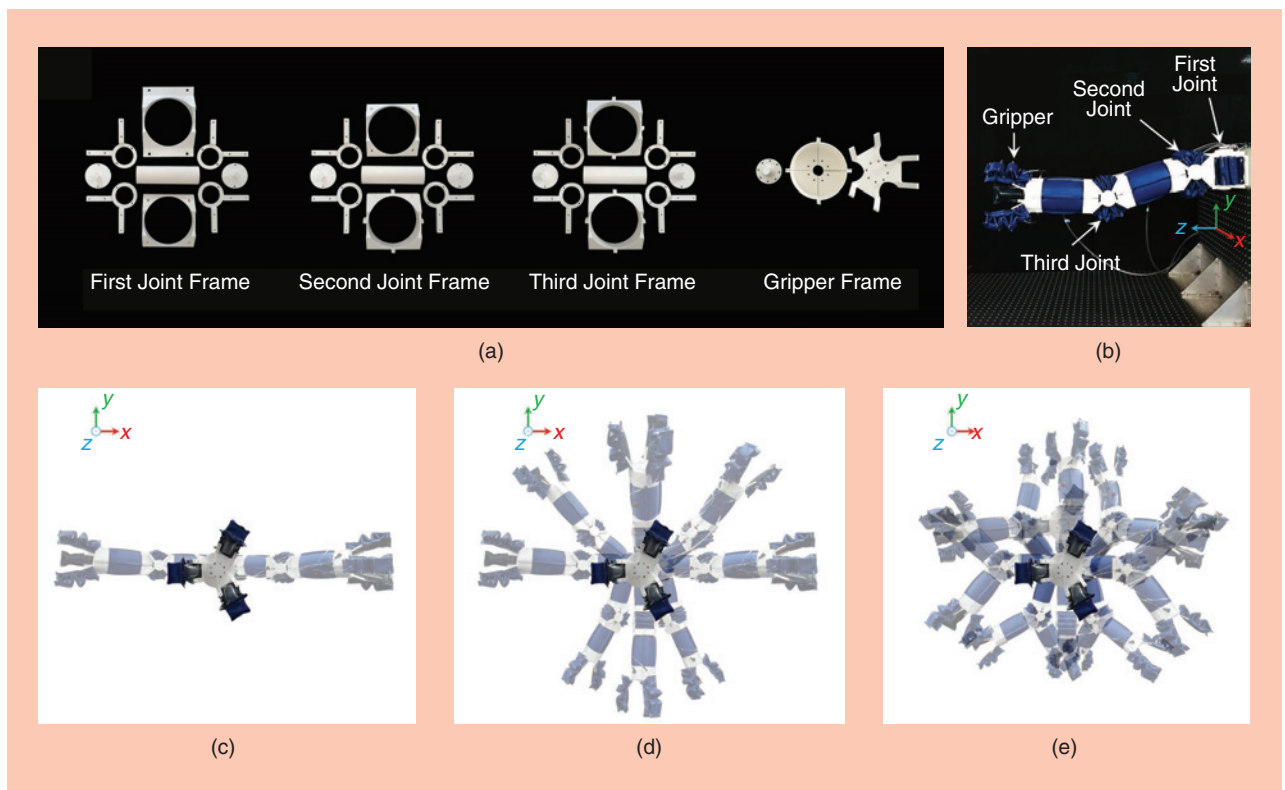


Figure 5. (a) The rigid parts for assembly of the robotic arm. (b) The assembled robotic arm with three joints and three fingers. (c) The horizontal motion of the first joint. (d) The combined motion of the first and second joint. (e) The combined range of motion of all three joints.

produce a vertical rotary motion directly after the first joint, such as to have 2 DoF at the base of the robotic arm [Figure 5(c) and (d)]. The third joint serves as the elbow of the arm and helps achieve a wide range of arm positions [Figure 5(e)].

The arm was made to pick up an orange, with a weight of 420 g, off a surface and then to stack it on top of others, to show the capability of the arm to be used for pick-and-place operations [Figure 6(a)]. This operation was done using open-loop control for both the arm and fingers, and pressure ratios between the chambers were set manually to adjust the joint stiffness for the different operations. This operation shows the ability of the gripper to grab objects without needing perfect knowledge of their shape or weight. It is also possible to vary the stiffness of the joints by changing the ratio of pressures within the antagonistic

chambers. The robotic arm is easily deflected by an external stimulus when the joints have low pressures. For example, a knife was attached at the tip of the arm, and the pressure of the first joint was set at 5 kPa in both chambers. The arm was then easily displaced by using a piece of paper to push on the tip of knife [Figure 6(b)]. This allowed the robotic arm to achieve inherent safety, where no sensor was required to ensure minimal impact on objects in the vicinity of the robot, and made the arm useful around humans where safety is paramount. Increasing the pressure in the same inflatable joint increases its stiffness, and the knife easily pierces the sheet of paper when pushed against it [Figure 6(c)]. This means that the stiffness of the joints within the robotic arm can easily be adjusted based on its current objective. Certain tasks, such as lifting objects,

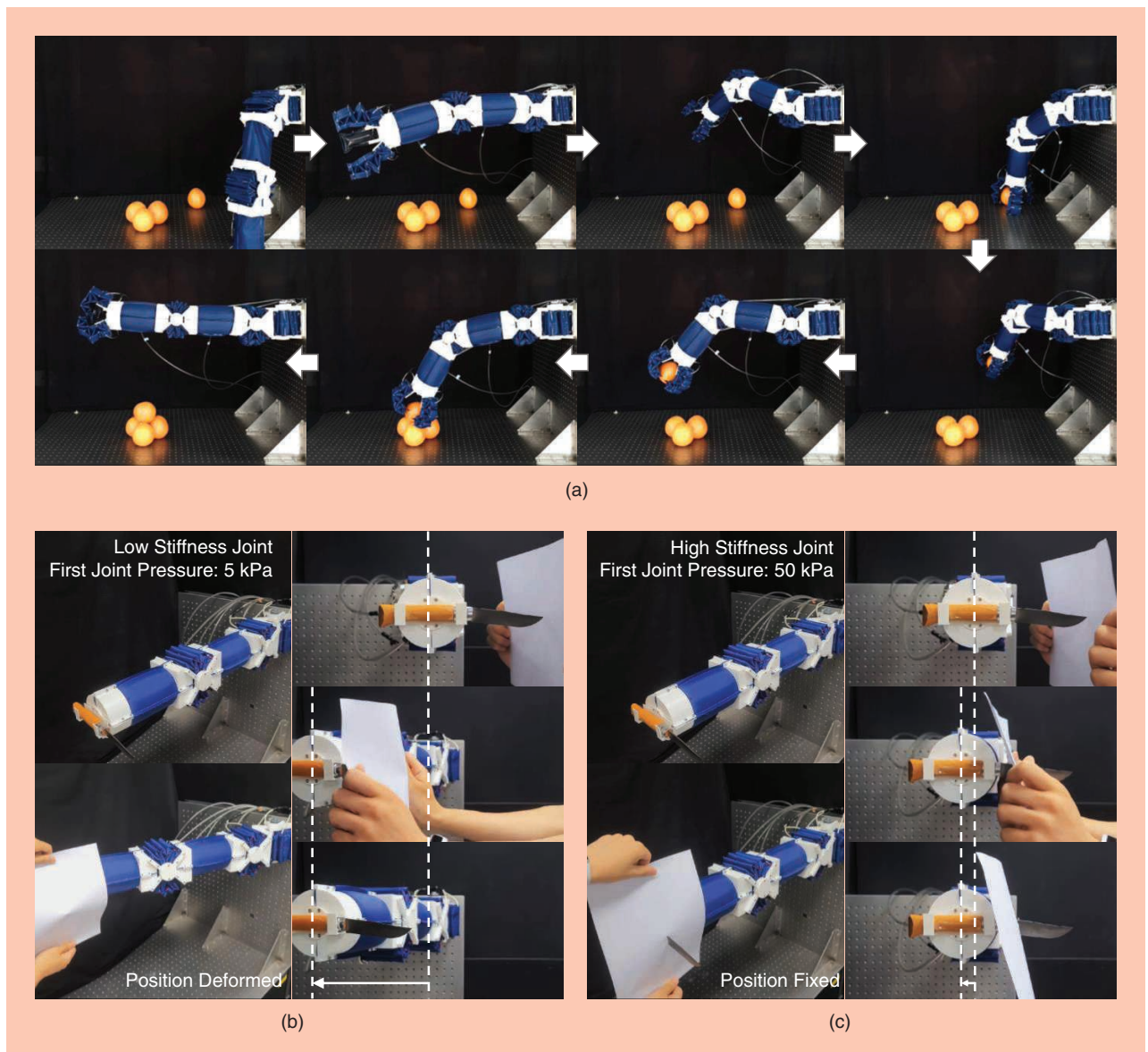


Figure 6. (a) The pick-and-place operation of the robotic arm. (b) The arm with low stiffness members can be used to ensure safety when encountering an obstacle. (c) The motion of the arm with high stiffness can be used to push and move objects.

cannot be executed without some degree of stiffness, but it would be possible to find a pressure point where both performance and safety can be guaranteed. Three supplementary videos illustrate the functioning of this soft robotic arm during motion and pick-and-place operation and its behavior at different joint pressures.

Large Soft Robotic Gripper

Many existing soft pneumatic actuator concepts do not scale very well at larger sizes due to either the weight of the polymers or to the many additional structures required to scale, which has often prevented the development of bigger grippers capable of grasping large objects. Film-based actuators generally scale better with size, due to the low weight of their materials, while having good physical properties. The proposed design can also help with developing larger grippers since the motion can be defined by the dimensions of the geometric constraints and pouch motors, and the use of the second pouch layer in the proposed design helps with the stability of the gripper when moving and when grasping large objects.

Increasing the width of the pouch pattern will help increase the contact area and the grasping force, while an increase in length will help the gripper produce a power grasp, even on large objects. The soft robotic finger proposed

earlier was widened to 150 mm and lengthened to 180 mm, with four patterns of pouch motors and using straight tubes for the bottom surface to enable bidirectional actuation. The dimensions of the pouch patterns were adjusted to produce more deformation at the base of the actuator as this section needed to have a large deformation to go from flat to nearly straight. The final pattern of pouch motor contained a single outer layer pouch motor to decrease the bending angle at the tip, as done previously. The bottom surface was then coated with polymer (Eco-Flex 00-30, Smooth-On) to increase surface friction.

Two such fingers were positioned antagonistically to produce a handheld soft gripper that could singlehandedly grab objects which would generally require two hands [Figure 7(a)]. Since the chambers have a large volume, the fingers can produce large forces even at lower pressures. The lower pressure allows the fingers to deform on contact and wrap around objects, such that a large contact area can be achieved. This gripper can grab large and/or heavy objects, such as basketballs, white radishes, watermelons, and bags of rice [Figure 7(b)–(d)]. Three supplementary videos illustrate the behavior of the large soft robotic gripper and its performance for grabbing different types of objects, such as a watermelon, a piece of meat, and a piece of acorn jelly, which is very fragile.

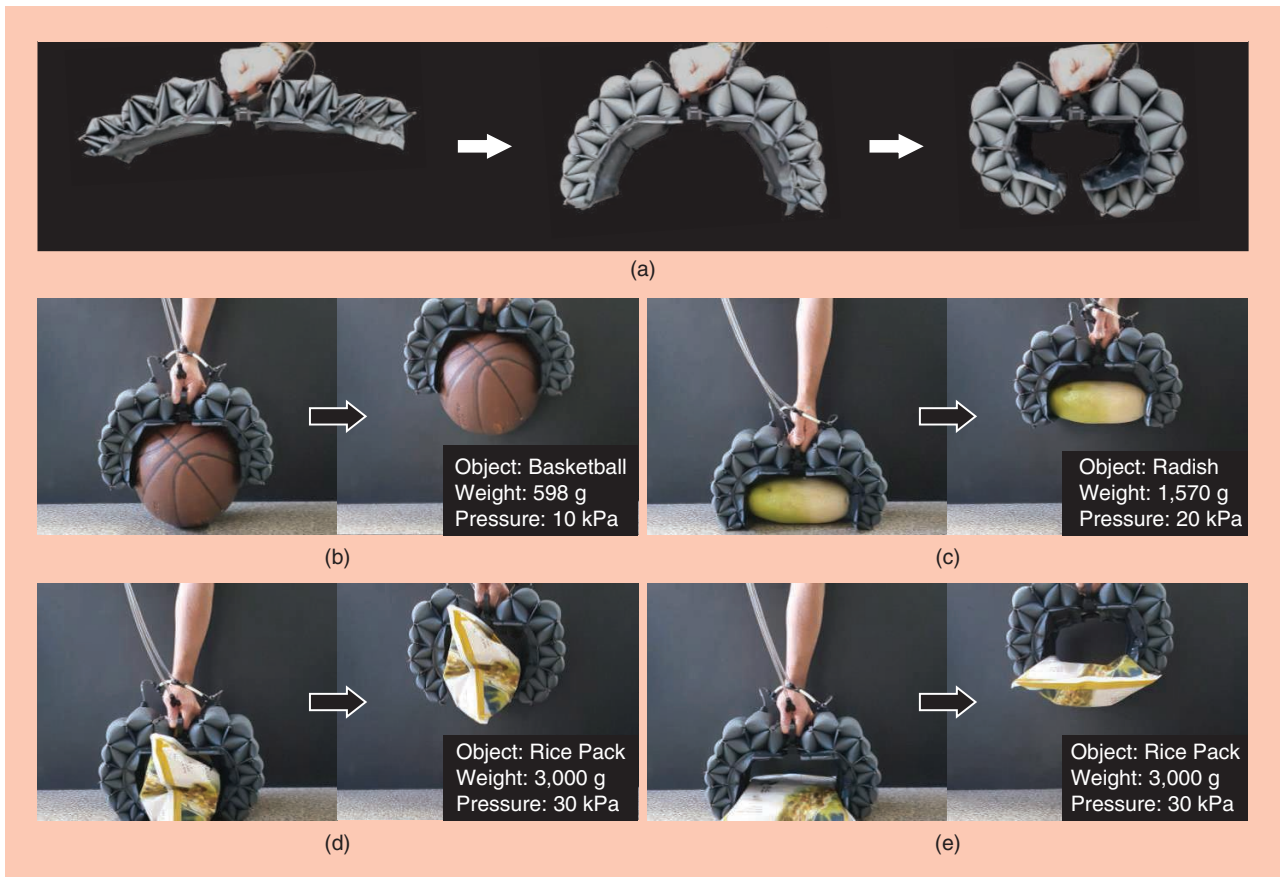


Figure 7. (a) A large soft robotic gripper for grasping large and heavy objects. The large soft robotic gripper grasping (b) a basketball, (c) a white radish, (d) a bag of rice laying on its side, and (e) a bag of rice lying flat.

Conclusions

A pattern of pouch motors combining two layers with geometric constraints was proposed as a versatile and repeatable pattern for producing large bending deformations with a controllable force. The pattern of deformation of the actuator can be easily modified to produce actuators that behave like bending ones or rotary joints. These can then be used to fabricate either robotic fingers or joints with only small adjustments in dimensions, using the proposed pattern of pouch motors. A robotic arm with 3 DoF and a large soft robotic gripper was built using this actuation concept to demonstrate its versatility and potential applicability for low-cost and large-scale soft robots.

This kind of simple soft robotic actuation concept could be further adjusted to a wider range of robotic concepts and its construction further improved to allow for higher pressures and forces. A pouch-based actuator like this could find use in a wide range of robots, including patient care and service robots, due to their good actuation capabilities, low weight, versatility, and low cost. Future work will focus on improvements in design, manufacturing, and materials, to increase the capability of the robotic arm; finding ways to improve airflow between pouch motors; and the integration of complete position feedback for control of the entire robotic arm.

Acknowledgments

This work was supported by the National Research Foundation of Korea grant funded by the Korea government (Ministry of Science, ICT and Future Planning) 2018R1C1B6003990 and 2020R1A4A1018227).

References

- [1] C. Laschi, B. Mazzolai, and M. Cianchetti, "Soft robotics: Technologies and systems pushing the boundaries of robot abilities," *Sci. Robot.*, vol. 1, no. 1, p. eaah3690, 2016. doi: 10.1126/scirobotics.aah3690.
- [2] P. Ohta et al., "Design of a lightweight soft robotic arm using pneumatic artificial muscles and inflatable sleeves," *Soft Robot.*, vol. 5, no. 2, pp. 204–215, Apr. 2018. doi: 10.1089/soro.2017.0044.
- [3] R. V. Martinez, C. R. Fish, X. Chen, and G. M. Whitesides, "Elastomeric origami: Programmable paper-elastomer composites as pneumatic actuators," *Adv. Funct. Mater.*, vol. 22, no. 7, pp. 1376–1384, 2012. doi: 10.1002/adfm.201102978.
- [4] B. Mosadegh et al., "Pneumatic networks for soft robotics that actuate rapidly," *Adv. Funct. Mater.*, vol. 24, no. 15, pp. 2163–2170, 2013. doi: 10.1002/adfm.201303288.
- [5] M. Manti, A. Pratesi, E. Falotico, M. Cianchetti, and C. Laschi, "Soft assistive robot for personal care of elderly people," in *Proc. 6th IEEE RAS/EMBS Int. Conf. Biomedical Robotics Biomechatronics (BioRob)*, Singapore, 2016, pp. 833–838. doi: 10.1109/BIOROB.2016.7523731.
- [6] W. McMahan et al., "Field trials and testing of the octarm continuum manipulator," in *Proc. IEEE Int. Conf. Robot. Automat., Orlando, FL*, 2006, pp. 2336–2441. doi: 10.1109/ROBOT.2006.1642051.
- [7] R. Niiyama, X. Sun, C. Sung, B. An, D. Rus, and S. Kim, "Pouch motors: Printable soft actuators integrated with computational design," *Soft Robot.*, vol. 2, no. 2, pp. 59–70, 2015. doi: 10.1089/soro.2014.0023.
- [8] J. D. Greer, T. K. Morimoto, A. M. Okamura, and E. W. Hawkes, "Series pneumatic artificial muscles (sPAMs) and application to a soft continuum robot," in *Proc. IEEE Int. Conf. Robot. Automat. (ICRA)*, Singapore, 2017, pp. 5503–5510. doi: 10.1109/ICRA.2017.7989648.
- [9] N. Oh, Y. J. Park, S. Lee, H. Lee, and H. Rodrigue, "Design of paired pouch motors for robotic applications," *Adv. Mater. Technol.*, vol. 4, no. 1, 2019, Art. no. 1800414. doi: 10.1002/admt.201800414.
- [10] N. D. Naclerio and E. W. Hawkes, "Simple, low-hysteresis, foldable, fabric pneumatic artificial muscle," *IEEE Robot. Automat. Lett.*, vol. 5, no. 2, pp. 3406–3413, 2020. doi: 10.1109/LRA.2020.2976309.
- [11] A. A. Amiri Moghadam et al., "Laser cutting as a rapid method for fabricating thin soft pneumatic actuators and robots," *Soft Robot.*, vol. 5, no. 4, pp. 443–451, Aug. 2018. doi: 10.1089/soro.2017.0069.
- [12] H. Sareen et al., "Printflatables: Printing human-scale, functional and dynamic inflatable objects," in *Proc. CHI Conf. Human Factors Comput. Syst.*, Denver, CO, 2017, pp. 3669–3680. doi: 10.1145/3025453.3025898.
- [13] L. Cappello et al., "Exploiting textile mechanical anisotropy for fabric-based pneumatic actuators," *Soft Robot.*, vol. 5, no. 5, pp. 662–674, July 19, 2018. doi: 10.1089/soro.2017.0076.
- [14] R. Natividad, M. Del Rosario, P. C. Y. Chen, and C.-H. Yeow, "A reconfigurable pneumatic bending actuator with replaceable inflation modules," *Soft Robot.*, vol. 5, no. 3, pp. 304–317, 2018. doi: 10.1089/soro.2017.0064.
- [15] G. Belforte, G. Eula, A. Ivanov, and A. L. Visan, "Bellows textile muscle," *J. Textile Inst.*, vol. 105, no. 3, pp. 356–364, 2014. doi: 10.1080/00405000.2013.840414.
- [16] M. Hofer, L. Spannagl, and R. D'Andrea, "Iterative learning control for fast and accurate position tracking," in *Proc. IEEE/RSJ Int. Conf. Intell. Robots Syst. (IROS)*, Macau, China, 2019, pp. 6602–6607. doi: 10.1109/IROS40897.2019.8967636.
- [17] H. D. Yang and A. T. Asbeck, "A new manufacturing process for soft robots and soft/rigid hybrid robots," in *Proc. IEEE/RSJ Int. Conf. Intell. Robots Syst. (IROS)*, Madrid, Spain, 2018, pp. 8039–8046. doi: 10.1109/IROS.2018.8593688.
- [18] H.-J. Kim, A. Kawamura, Y. Nishioka, and S. Kawamura, "Mechanical design and control of inflatable robotic arms for high positioning accuracy," *Adv. Robot.*, vol. 32, no. 2, pp. 89–104, 2017. doi: 10.1080/01691864.2017.1405845.
- [19] W. Felt, "Folded-tube soft pneumatic actuators for bending," *Soft Robot.*, vol. 6, no. 2, pp. 174–183, Apr. 2019. doi: 10.1089/soro.2018.0075.

Haneol Lee, School of Mechanical Engineering, Sungkyunkwan University, Suwon, South Korea. E-mail: bigspirit@skku.edu.

Namsoo Oh, School of Mechanical Engineering, Sungkyunkwan University, Suwon, South Korea. E-mail: dhnamsoo@skku.edu.

Hugo Rodrigue, School of Mechanical Engineering, Sungkyunkwan University, Suwon, South Korea. E-mail: rodrigue@skku.edu.



Soft Robotics: The Journey Thus Far and the Challenges Ahead

By Surya G. Nurzaman, S.M.Hadi Sadati, Marwa Eldiwiny, and Fumiya Iida

In the past decade, the use of soft, deformable materials has gained widespread interest due to their potential to carry out tasks in unstructured environments, such as grasping or manipulating objects with a wide variety of shapes and sizes, locomotion in irregular terrains, and enabling safe and flexible interactions between humans and robots. This emerging research field, generally known as *soft robotics*, also pushes the boundaries of visionary research topics, such as self-growing and self-healing robotic systems.

In comparison with classical robots made of rigid materials, soft robots can be characterized by several distinctive aspects, such as their elastic and deformable bodies, the possible use of unconventional materials to compose the robot's body, a large number of degrees of freedom, and the involvement of intrinsic passive mechanical dynamics in explaining the robot's behaviors. To deal with these aspects, soft robotics also heralds the emergence of a modern view of intelligence, known as *embodied intelligence* or *morphological computation*, which emphasizes the importance of task distribution among the robot's brain, its morphology including the shape and materials composing the robot, and its physical interaction with the environment.

To bring together scientists with different backgrounds and disciplines who

will advance the emerging research field of soft robotics, the IEEE Robotics and Automation Society (RAS) Technical Committee (TC) on Soft Robotics was established in October 2012. The TC also aims to provide opportunities to share the latest publications, experiences, cutting-edge technologies, and other pertinent information among those with a similar interest in soft robotic systems. This article summarizes the journey thus far in achieving the stated goals along with the remaining challenges ahead.

The Organizational Structure and Priority Areas

The main organizational structure of the TC consists of four co-chairs, several founding members, a newsletter and podcast editor-in-chief, and editorial members as well as its Student Chapter.

When it was formed, several priority areas were determined for the TC, including scientific problems related to soft robots; the use of soft material for robots, soft actuators, and sensors; modeling and simulation techniques for soft bodies; the fabrication and control of soft bodies; interdisciplinary interaction with biological and medical sciences, material sciences, chemistry, and other related disciplines; and soft robotics applications.

Activities Organized by or Related to the TC

Since the official formation of the TC, a significant number of activities related to soft robotics have been supported and organized effectively. The

first major event was the International Workshop on Soft Robotics and Morphological Computation in Monte Verita, Ascona, Switzerland, 14–19 July 2013, which, for the first time, gathered leading researchers in this field. Afterward, several relevant activities were arranged, such as the Robosoft Grand Challenge, Robosoft Spring School, and Soft Robotics Week in 2016.

Numerous workshops attached to major IEEE robotics conferences were also organized, including “Soft Technologies for Wearable Robots” at the 2013 IEEE/RSJ International Conference on Intelligent Robots and Systems; “Soft and Stiffness-Controllable Robots for Minimally Invasive Surgery” at the 2014 IEEE International Conference on Robotics and Automation (ICRA); “Soft Robots” at ICRA 2014; “Soft Robotics: Actuation, Integration, and Applications—Blending Research Perspectives” at ICRA 2015; “Innovative Haptic Interfaces Emerging from Soft Robotics” at ICRA 2017; “Advanced Fabrication and Morphological Computation for Soft Robotics” at ICRA 2017; “Soft Robotics Across Length Scales” at ICRA 2019; “Soft Haptic Interaction” at ICRA 2019; and “Beyond Soft Robotics: Pioneer Perspectives and Interdisciplinary Collaboration” at ICRA 2020.

The TC has formed and regularly uses several channels to organize its efforts to address challenges.



Figure 1. Attendees of IEEE Robosoft 2019, an international conference dedicated to soft robotics, in Seoul.

After organizing many workshops on a wide range of topics, one of the major advances in the field was probably the initiation of the first international conference for soft robotics: IEEE Robosoft. The first IEEE Robosoft was held in 2018 Livorno, Italy, the second in 2019 in Seoul, South Korea (Figure 1), and the third as a virtual event in 2020 due to the COVID-19 pandemic. The next IEEE Robosoft is to be held as a hybrid event in 2021 in Connecticut, United States.

In addition to organizing other activities, the TC has since May 2013 consistently published bimonthly newsletters on its official website (softrobotics.org), with the 44th edition

published in July 2020. Thus far, the newsletter has featured 871 scientific journal articles and 349 popular articles related to soft robotics. In 2013, the newsletter featured 64 journal and six popular articles, while in 2020 it has so far featured 126 journal and 31 popular articles, showing a significant increase of community size and the popularity of the field. The newsletter covers topics such as soft grasping and manipulation, soft locomotion, soft sensing, soft actuators, soft robots fabrication, embodied intelligence, and stretchable electronics.

Since 2019, the TC has also promoted a series of podcasts that have attracted considerable attention. For

example, by the end of 2019, just a few months after this new program began, it had drawn approximately 5,000 listeners from more than 50 countries, ranging in age from 18 to over 60 years old. With more than 184 clips at present, the podcasts attract guests from academia and industry as well as high-profile podcasters including George Whitesides, Allison Okamura, Carmel Majidi, and Jonathan Rossiter from Harvard, Stanford, Carnegie Mellon, and Bristol University, respectively, and Kelly Kay, vice president of the Toyota Research Institute. As shown in Figure 2, the audience also thinks the podcasts are an educational tool that can be used to learn about their favorite researchers, with 90% expressing as much, while 80% believe the podcasts can enhance the level of understanding of the subject being discussed. Full episodes of the podcasts can also be found on the TC's official website.

In 2020, the first soft robotics debate was presented: "Morphological Contribution Versus Traditional Methods for Control and Planning in Soft Robotics." The debate's five panelists were divided into three categories: one supporting each side of the debate and another representing a gray zone. A

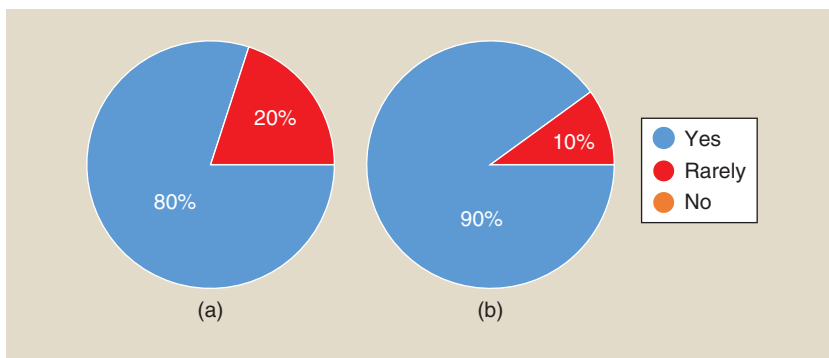


Figure 2. Soft robotics podcasts statistics. (a) The percentage of people who consider the podcasts to be a widely used educational tool and (b) the percentage of people who believe that they enhance the level of understanding of the subject being discussed.

poll carried out before and after the debate drew 25 audience members out of the 71 participants. The post-debate poll results showed that the audience favored morphological computation, with 60% support, compared to only 12% in favor of traditional control methods and 28% undecided on the issue. The second debate, “Bridging the Gap Between Soft Robots and Soft Materials: Discovering New Material Functionalities Versus Creating Architected Compliance,” was held on 15 October 2020 with eight panelists. Past debate recordings are available on the TC’s official website, and we aim to publish the debate summary as short articles in the near future.


To promote and set the direction for this field, two special issues of *IEEE Robotics and Automation Magazine (RAM)* have been published since the formation of the TC. The first was “Soft Robotics and Morphological Computation” in 2016, while the second is this issue (“Design Optimization of Soft Robots”).

Last but not least, it’s also worth mentioning that the TC won the RAS Most Active Technical Committee Award in 2019 due to the breadth and quality of its activities.

Future Challenges

Since its formation, the TC has continually supported the community to address a variety of scientific and technological challenges. The first was the development of functional and intelligent materials with controllable mechanical properties. Such materials should ideally be equipped with adaptive functions for sensing and actuating; be easily fabricated, assembled, and mass produced; and also be safe. Second, it is also significantly important to have a thorough grounding in biology and other related disciplines to understand how soft bodies are used pertinently by animals. Third, the simulation and modeling techniques of soft body behavior have been addressed, encouraging collaboration among scientists from various disciplines. Finally,

the integration aspects that would make soft robots ready for practical uses, ranging from underwater exploration to biomedical applications, have also been faced. Nevertheless, these issues are still far from completely solved, and efforts are continuously being made to further the field of soft robotics.

The TC has formed and regularly uses several channels to organize its efforts to address challenges. The main channel is the public home page (cited previously) where bimonthly newsletters, podcast episodes, debates, selected lecture notes, and other information used to promote the latest achievements of members are published. The TC has an associated mailing list of members that has grown significantly from approximately 50 members in 2012 to 913 members as of September 2020. The TC always encourages new members to join by subscribing to mailing lists at <https://lists.cam.ac.uk/mailman/listinfo/eng-softrobotics-tc>. 

STUDENT’S CORNER *(continued from page 9)*

value and a real need to have modeling tools that can converge. They can run very rapidly and have been the focus of his lab, which has collaborated with groups including Khalid Jawed’s at the University of California, Los Angeles, to build a soft robot physics engine that can run faster than real time.

Prof. Maijdi stresses there is still room for deterministic modeling because, as anybody who has worked with finite element analysis knows, these computational tools, governing equations, and theories are pretty accurate at capturing the actual physics of the system being modeled. There is not necessarily a need to run some learning algorithm and treat your system as a black box. It’s not a mystery that the system is going to be governed by prin-

ciples of mechanics, electrodynamics, and hydraulics, for example. Why don’t we leverage that knowledge for accurate modeling?

There is another important aspect: How does the controller complete a task without destroying the natural dynamics? Should we look for new control approaches? What are the most important morphological parameters for enhancing controller design? To answer these questions, we have to take a deeper look at designing descriptive models, taking into account the morphology of the dynamic shape. Nonlinearities can bring opportunities. You can ask yourself what kind of nonlinearities could be beneficial or detrimental to your soft robots. The solution isn’t always to linearize your model.

Coming back to simulation, the most important question—how to match the gap between replication and reality—can yield insights. You have to ask what the right properties are and what behavior you expect from the material. I want to bring your attention to the material point method (MPM), which is not well explored in the field. The MPM has key advantages; e.g., it can simulate multimaterials, and it can handle large topological changes as well as anisotropic materials, which are challenging to simulate using the FEM. As some final thoughts, never take anything for granted, always be skeptical, and seek a profound understanding of the physics behind materials, even if doing so takes time.



Best Practices: Becoming a Leader Through Conference Organization

By Lydia Tapia and Elena Delgado

The IEEE Robotics and Automation Society (RAS) organizes or co-organizes roughly 78 conferences and workshops each year, including 11 fully sponsored conferences, 19 financially cosponsored conferences, and 48 technically cosponsored conferences. Additionally, several positions within the RAS help with conference content and activities, including committees such as the Conference Activities Board (CAB), Member Activities Board, and Technical Activities Board. There are many opportunities for individuals to volunteer and become the next leaders by contributing to the organization of these multiday events. In 2019, four such individuals were interviewed by the Women in Engineering Committee at the IEEE/RSJ International Conference on Intelligent Robots and Systems (IROS). This article shares their perspectives of, and experiences with, becoming involved with RAS-sponsored conferences and earning their high-level leadership roles.

Yi Guo, a professor at Stevens Institute of Technology, served as finance chair for the 2015 IEEE International Conference on Robotics and Automation (ICRA) as well as for IROS 2019 and 2020. She has been a CAB Member At Large since 2019, and she is the 2021 incoming editor-in-chief of *IEEE Robotics and Automation Magazine*. Prof. Yi has found every service role within the RAS rewarding, saying, “You learn how



Yi Guo



Karinne Ramirez-Amaro



Marcia O'Malley



Jing Xiao

to serve the community, interact with smart people, and every conference you go to is a different experience.”

Marcia O'Malley is the Thomas Michael Panos Family Professor in

Mechanical Engineering at Rice University. She served as cochair of the 2012 and 2014 IEEE Haptics Symposium and of the IEEE World Haptics Conference editorial board; program chair of IROS

Digital Object Identifier 10.1109/MRA.2020.3029232
Date of current version: 9 December 2020

2020; associate editor of *IEEE Transactions on Robotics*, *IEEE Transactions on Haptics*, and *IEEE/ASME Transactions on Mechatronics*; senior editor of *IEEE/ASME Transactions on Mechatronics*; associate editor-in-chief of *IEEE Transactions on Haptics*; and chair of the IEEE Technical Committee on Haptics. Prof. O'Malley found being a conference cochair rewarding. When she led the transition of the Haptics Symposium to a fully independent conference, she found the role "scary." However, she said her work greatly enhanced the conference experience for the research community by providing autonomy in determining the conference location and activities.

Karinne Ramirez-Amaro, an assistant professor at Chalmers University of Technology, has served as associate vice president (VP) for CAB operations and as a member of the organizing committees for ICRA 2023 and 2024. Prof. Ramirez-Amaro finds serving as a CAB VP to be most rewarding, as she has constant communication with more than 50 conference organizers. Currently, she and her team are collecting data about all conferences sponsored by the RAS to determine participation levels during past years. Robotics conferences, such as ICRA and IROS, have shown rapid growth, and Prof. Ramirez-Amaro is using these data to identify "ways to adapt" in coordination with conference organizers.

Jing Xiao is a Dean's Excellence Professor and William B. Smith Distinguished Fellow in Robotics Engineering at Worcester Polytechnic Institute. She served as a member of the RAS Administrative Committee, RAS Executive Committee, and RAS Awards Committee and as the RAS VP for member activities. In addition, she has held many leadership positions on ICRA and IROS conference committees. One of Prof. Jing's most rewarding accomplishments is serving as VP for RAS member activities. In this role, she helped "increase the funding for student travel awards and for attendees from developing countries." She saw the positive impact of her work through increased student participation and paper author-

ship at conferences, including ICRA and IROS.

These women took very different paths to their current service roles, but they all suggested starting out by performing well at small tasks. After starting as a reviewer for several ICRA conferences, Prof. Jing helped the Society as a Program Committee member for ICRA 1994. She found it was "a very frightening and rewarding experience." Through this, she learned how to be a good reviewer by working with more seasoned researchers, back when they sat around a table together and assessed papers.

Similarly, Prof. Ramirez-Amaro started out as a paper reviewer for conferences. She acquired the role by becoming known in the community through conference attendance and by talking with people and convincing them that she knew her research. She gave business cards to professors and thought, "Oh! The business cards worked!" when she was contacted to be a reviewer. Later, she realized the recognition was more about the quality of her own work and the visibility she earned by getting to know other researchers. After successfully reviewing papers for several years, she was nominated to become an associate editor, a position that required her to enhance her network to find suitable reviewers for submissions.

Prof. O'Malley recommended submitting articles, which helps get new authors into the database that associate editors use to find reviewers. She got started as an associate editor by proposing a journal special issue. To do this, she had to convince the editor that there would be enough submissions. After her pitch was accepted, she distributed a call for submissions, found reviewers, and suggested articles for publication.

All four of these professionals experienced times when they felt unprepared for certain leadership opportunities they had been offered. However, they emphasized that it is important to take some risks. Prof. Ramirez-Amaro recommends "trusting your gut." For example, when she was

offered her current role as a CAB VP, she didn't even know what the CAB was. But she quickly saw the advantages of helping with ICRA and IROS organization. Prof. O'Malley noted that "it can be intimidating" when you get offered a new role. However, she remarked that, in robotics, it is very easy "to call up someone who was in that role previously and find out about their prior experience." This helps identify the true workload, time requirement, and necessary skills. Prof. Yi found there is a "learning curve" for every role but that adaptation enables the discovery of better and more efficient ways to solve many different problems. "Tasks come in, and you have to address them within a time frame" she said, emphasizing how people become more efficient each time they serve in a role.

Each of the professors has performed service activities as an extra part of her workload. Prof. Jing noted that it is hard to balance work, family, and leadership roles, but "you find ways to become more efficient." She added that it is important to have a team and to hand off tasks to volunteers. Prof. O'Malley said she makes sure she "understands what is being asked of me" when she takes on a position and keeps in mind two things: finding out about the workload for the specific role and knowing the time commitment. For example, the role of associate editor can vary among journals and may mean "three papers at a time for one journal or 30 papers at a time for another." Additionally, when organizing a conference, it is important to note that "different roles are busy at different times—the registration chair can sit back until a couple months before the conference and then is really busy,

Begin with networking at conferences, organizing workshops, reviewing papers, and putting together special journal issues.

Finally, they each suggested some concrete ways to get started on a path toward leadership.

whereas the finance chair is busy way before the conference with the budget and then is busy long after the conference resolving all the finances.”

Since much of their service was beyond what was required for career enhancement, the leaders talked

about the benefits they gained from helping the robotics community. Prof. Jing said that it helped her realize a “sense of community.” Prof. Ramirez-Amaro thought of it as a “service” she performed to enhance the community. Prof. O’Malley also thought it was important to help the research community, but she notes the career benefit from service. “If you’re on an academic track, at some point, you’re going to be up for tenure and promotion, and you need external reviewers. And, if you have been involved in the community,

then they’re going to know you.” Prof. Yi felt the true reward was “interacting with the leaders in the community.” Finally, they each suggested some concrete ways to get started on a path toward leadership. Begin with networking at conferences, organizing workshops, reviewing papers, and putting together special journal issues. Doing well at these tasks will lead toward new opportunities and the chance to work with others to shape the direction of robotics research.



THE IEEE APP:

Let's stay connected...



Create a personalized experience



Get geo and interest-based recommendations



Schedule, manage, or join meetings virtually



Read and download your IEEE magazines



Stay up-to-date with the latest news



Locate IEEE members by location, interests, and affiliations



Download Today!



How ICRA 2020 Went From Paris to the Cloud

By Sinan Haliyo

2020 is the year of tremendous disruption, and it has reached our community like a tidal wave, sweeping across all continents. Our flagship conference, the IEEE International Conference on Robotics and Automation (ICRA), was not safe either. Originally scheduled to be held in Paris, France, from 31 May to June 5, we had to transform our esteemed annual meeting to a virtual event.

It came as quite a blow to the ICRA Organizing Committee, who had been working extremely hard for the past two years to make it a maximally memorable experience. ICRA had never been held in France despite its thriving robotics community, and its growing popularity warranted a huge mobilization to host the event with proverbial French hospitality. In recent years, ICRA's attendance has risen significantly from a few hundred to 3,500 at ICRA 2019 in Montreal, and we were expecting an even greater number of attendees in Paris. The largest conference venue in Paris, Palais des Congrès, was reserved with its freshly renovated 3,700-seat amphitheater, 30 pristine conference and meeting rooms, and a 4,000-m² exhibition area. The industrial exhibition would have been the largest ever, as Paris has attracted an unprecedented number of professionals. Tapping into the liveliness of the Parisian arts scene, an exhibition regarding the impact of robotics and technology on modern interactions was curated in collaboration with the prestigious École des Arts

Décoratifs, thanks to a considerable budget. Additionally, the Palais de Congrès' amphitheater is the largest performing arts venue in Paris, and we had planned to share with you two pieces from its rich portfolio of entertainment: Aurélien Bory's live robotics performance "Sans Objet" as well as a live orchestra screening of the cult-classic *The Terminator*. With considerable string-pulling, the Louvre Museum agreed to host the gala evening, with a private visit of its collections—an honor generally reserved only to official state affairs. Naturally, the complete conference schedule, with numerous keynotes, 1,500 presentations on 12 tracks, 80 workshops, and various meetings, was carefully laid out.

When Europe started the lockdowns for quarantine measures in March, the Organizing Committee realized that all their efforts would go to ashes. Although we tried to keep our hopes high to believe that the event could still be held in person, by April it was quite clear that attendees from Asia wouldn't be able to travel and that more restrictions were on the way. Finally, when the French administration forbade all meetings of more than 1,000 people (later to be banned completely), we realized that we needed to go back to the drawing board.

It was out of question to simply drop Paris 2020 from the ICRA schedule or to push every event to next year. At that time, not knowing how the pandemic would evolve, we focused on two options: to postpone the event for a few months, maybe until the end of 2020, or to go completely virtual and keep the original dates. The poll taken at that point showed that the lat-

ter choice was the preference of the community. However, even today it seems that this option would still not be possible. Together with its scientific glamour, ICRA is undoubtedly the largest social event of our community, and we obviously did not want to let it go. But, even at that time, postponing it was not so straightforward either, as lots of other events were being cancelled and rescheduled. By the end of April, a little more than a month before the originally scheduled launching of the event, the Organizing Committee, after thorough consideration, decided to keep the dates and to go virtual, setting sail into uncharted waters. Naturally, nobody on the team had had a similar experience before, and few conferences around us had taken this new route. For example, the 2020 IEEE Conference on Virtual Reality and 3D User Interfaces was successfully held virtually some weeks previously, but attendance for that event is usually much lower, and that community is naturally more familiar with everything virtual.

In the absence of role models and a trustworthy supplier with a turnkey solution, we started to design the conference from scratch by recycling our usual conference tools. An unexpected drawback came from China, where a significant portion of our attendees would be accessing our conference. Many of the well-known video-hosting solutions such as YouTube or Dailymotion used on network platforms were blocked by the Great Firewall.

The first hard decision was how to handle the technical presentations. We had to keep all 1,500 live on the original schedule. This seemed quite hard both

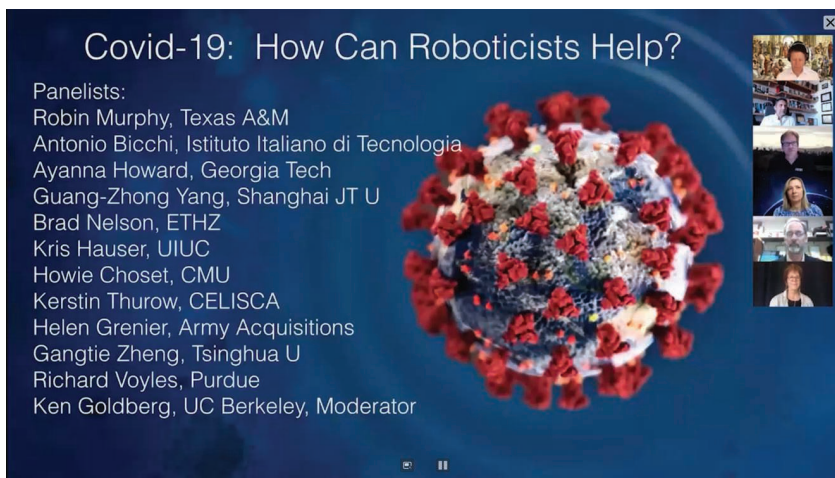


Figure 1. The 1 June plenary panel.

technically and with respect to the time zone differences, as our audience spanned from Japan to California and even farther. Holding these talks asynchronously while retaining the possibility to make changes efficiently pushed us to look for a well-developed corporate communication framework. Hence, we settled on Slack. Although not designed for this purpose, Slack offers a very interesting set of tools, such as multichannel chat threads, integration with major video conferencing tools, member administration, and so on. During the lockdown, its usage rose considerably in a few months, and, as a growing number of institutions and labs adopted it, many participants were already familiar with the platform.

The IEEE Robotics and Automation Society (RAS) also has a couple of digital tools previously used for conferences; these were upgraded for the purpose. PaperCept, which has been used extensively for paper submissions and proceedings at RAS conferences, and InfoVaya, the platform used as a companion app and personal scheduler, all went through major developments to provide a backbone for the online conference. The Organizing Committee is very grateful to both teams for their support and the countless hours they spent on these developments on such short notice.

To implement this asynchronous approach, we then asked our speakers to record a video of their presentation to be distributed to all attendees at the

launch of the conference. We set up a chat channel for each paper on Slack, where all interested parties could ask questions and discuss them with the presenters. Fortunately, Slack has an accessible application programming interface, which allowed for the creation of these 1,500 channels, linking each to the paper's PDF and presentation. An additional advantage stemming from the use of Slack is the ease with which one can chat and reach out to others. Additionally, the upcoming generation of young roboticists is apparently quite comfortable with this mode of communication. More than 6,000 messages were exchanged on the first day of the conference. Moreover, the community quickly played along and spontaneously came up with novel propositions, such as focused topic discussion channels, online happy hour meetings, sessions of



Figure 2. Plenary Speaker and IEEE Fellow Lydia E. Kavraki presented "Planning in Robotics and Beyond" on 2 June 2020.

binge-watching presentation videos, and so forth. It was a true joy to see the young generation getting involved so readily and starting to animate the online space.

Another advantage of adopting this asynchronous communication was that it enabled us to extend the originally planned five-day period to three months. Hoping that little maintenance would be required once things were on the rails technically, an extension until the end of August became possible. However, an important piece of the puzzle was how to maintain the original conference feel. We focused on plenary and keynote talks, which attract a large audience and are always the high points of ICRA. We turned to IEEE.tv for a real-time video-streaming solution. As matter of fact, IEEE.tv has been quietly growing for the past several years and has progressed from hosting prerecorded talks to providing real-time discussions and Q&A tools. ICRA 2020 took advantage of this real-time opportunity, as we scheduled a plenary or keynote talk for each day of the conference over two weeks during midday hours in Europe, the only time period roughly convenient for everyone from Japan to California. In total, an opening plenary panel on COVID-19 (see Figure 1) and 12 talks were broadcast (see Figures 2 and 3), which incited lively responses. Because these live events did not require registration to participate, they attracted an audience of approximately 1,500 for some presentations, each was followed by intense Q&A sessions, and recordings of the proceedings have surpassed 20,000 viewings as of today.

The RAS staff and the Student Activities Committee organized online events to enliven the social activities. Thanks to our community's members' willingness to participate in the games, the traditional Lunch with Leaders was moved online. The Robot Trivia, SAC Logo Contest Video Challenges, and Women in Engineering events were all moved online and were a great success. The first-ever virtual RAS Town Hall Meeting was also held.

On the workshops' front, most remained with ICRA and adapted their

sessions to virtual versions. Organizers were free to choose the when and the how of their workshops, and the participation of the attendees was registration free. Most organizers used a combination of real-time video conference presentations with discussions on Slack, and a few experimented with different approaches, such as weekly seminars. Their feedback was quite positive, and their attendance was much higher compared to previous years. All had the feeling that their purpose was fulfilled.

Regarding registrations, fees were revised and lowered to €100 in general and to €25 for students. As a result, this ICRA was the most accessible ever, with nearly 5,500 participants from 82 different countries.

In conclusion, ICRA 2020 was a huge experiment for creating large-scale virtual meetings among our rather tech-savvy community. Lowering the material barrier to join, the conference attracted a larger crowd of enthusiastic



Figure 3. Keynote Speaker Jaeheung Park delivered his talk “Compliant Whole-Body Control for Real-World Interactions” on 11 June 2020.

students and professionals, with an unprecedented number from developing countries. During the Q&A sessions, the questions and comments coming from all over the world all at the

same time provided a very impressive, unusual, and memorable sight!

Looking back a month later, there is certainly a lot of pride in our hearts to have pulled this off under these unfavorable circumstances. We can now say that it was worth all the blood, sweat, and tears the team put in. It was a first try for our community; obviously, we didn’t get everything right, and there is still plenty of room for improvement. However, facing these times of deep worldwide concerns regarding growing climate changes, the uncertain future of health issues, and travel bans, we feel that virtual conferences are likely here to stay.

Still, our disappointment is real that we couldn’t welcome you in Paris—one of the most wonderful cities in the world—for ICRA this year. We hope that, in the near future, our robotics community will have the chance to experience France and its capital.

Au revoir!

Welcome to Seven New IEEE Robotics and Automation Society Chapters

Congratulations and welcome to the following newly organized IEEE Robotics and Automation Society (RAS) Chapters.

Region 8

- Egypt
 - Pharos University in Alexandria RAS Student Branch Chapter

- Menoufia University RAS Student Branch Chapter.

Region 10

- India
 - College of Engineering Perumon RAS Student Branch Chapter
 - GSSS Institute of Engineering and Technology for Women RAS Student Branch Chapter
 - Sreyas Institute of Engineering and Technology RAS Student Branch Chapter

- Sri Jayachamarajendra College of Engineering RAS Student Branch Chapter
- J.C. Bose University of Science and Technology, YMCA, RAS Student Branch Chapter.

2020 IEEE Robotics and Automation Society Publications Best Paper Award Recipients Announced

IEEE Transactions on Haptics Best Paper Award

Congratulations to the following winners of the 2020 IEEE Transactions on Haptics Best Paper Award. This award honors the best paper published in *IEEE Transactions on Haptics* in the previous year.

- “A Phonemic-Based Tactile Display for Speech Communication,” by Charlotte M. Reed, Hong Z. Tan, Zachary D. Perez, E. Courtenay Wilson, Frederico M. Severgnini, Jaehong Jung, Juan S. Martinez, Yang Jiao, Ali Israr, Frances Lau, Keith Klumb, Robert Turcott, and Freddy Abnoui (*IEEE Transactions on Haptics*, vol. 12, no.1, pp. 2–17, 2019).

IEEE Transactions on Haptics Best Application Paper Award

Congratulations to the following winners of the 2020 IEEE Transactions on Haptics Best Application Paper Award. This award honors the best paper published in *IEEE Transactions on Haptics* in the previous year.

- “Soft Wearable Skin-Stretch Device for Haptic Feedback Using Twisted and Coiled Polymer Actuators,” by Jean-Baptiste Chossat, Daniel K.Y. Chen, Yong-Lae Park, and Peter B. Shull (*IEEE Transactions on Haptics*, vol. 12, no. 4, pp. 521–532, 2019).

IEEE Transactions on Robotics King-Sun Fu Memorial Best Paper Award

Congratulations to the following winners of the 2020 King-Sun Fu Memorial Best Paper Award. This award honors the best paper published in

IEEE Transactions on Robotics in the previous year.

- “Active Learning of Dynamics for Data-Driven Control Using Koopman Operators,” by Ian Abraham and Todd D. Murphey (*IEEE Transactions on Robotics*, vol. 35, no. 5, pp. 1071–1083, Oct. 2019).

IEEE Robotics and Automation Letters Best Paper Award

Five Recipients This Year!

Congratulations to the following winners of the 2020 IEEE Robotics and Automation Letters Best Paper Award. This award honors the best papers published in *IEEE Robotics and Automation Letters* in the previous year.

- “Self-Supervised Correspondence in Visuomotor Policy Learning,” by Peter Florence, Lucas Manuelli, and Russ Tedrake (*IEEE Robotics and Automation Letters*, vol. 5, no. 2, pp. 492–499, Apr. 2020; published online Nov. 2019).
- “Fluid Lubricated Dexterous Finger Mechanism for Human-Like Impact Absorbing Capability,” by Yong-Jae Kim, Junsuk Yoon, and Young-Woo Sim (*IEEE Robotics and Automation Letters*, vol. 4, no. 4, pp. 3971–3978, Oct. 2019; published online July 2019).
- “A Minimally Actuated Reconfigurable Continuous Track Robot,” by Tal Kislasi and David Zarrouk (*IEEE Robotics and Automation Letters*, vol. 5, no. 2, pp. 652–659, Apr. 2020; published online Dec. 2019).
- “Fast Model-Based Contact Patch and Pose Estimation for Highly Deformable Dense-Geometry Tactile Sensors,” by Naveen Kupp-

swamy, Alejandro Castro, Calder Phillips-Grafflin, Alex Alspach, and Russ Tedrake (*IEEE Robotics and Automation Letters*, vol. 5, no. 2, pp. 1811–1818, Apr. 2020; published online Dec. 2019).

- “MapLite: Autonomous Intersection Navigation Without a Detailed Prior Map,” by Teddy Ort, Krishna Murthy, Rohan Banerjee, Sai Krishna Gottipati, Dhaivat Bhatt, Igor Gilitschenski, Liam Paull, and Daniela Rus (*IEEE Robotics and Automation Letters*, vol. 5, no. 2, pp. 556–563, Apr. 2020; published online Dec. 2019).

IEEE Robotics and Automation Magazine Best Paper Award

Congratulations to the following winners of the 2020 IEEE Robotics and Automation Magazine Best Paper Award. This award honors the best paper published in *IEEE Robotics and Automation Magazine* in the previous year.

- “Humanoid Robots in Aircraft Manufacturing: The Airbus Use Cases,” by Abderrahmane Kheddar, Stéphane Caron, Pierre Gergondet, Andrew Comport, Arnaud Tanguy, Christian Ott, Bernd Henze, George Mesesan, Johannes Engelsberger, Máximo A. Roa, Pierre-Brice Wieber, François Chaumette, Fabien Spindler, Giuseppe Oriolo, Leonardo Lanari, Adrien Escande, Kevin Chappellet, Fumio Kanehiro, and Patrice Rabaté (*IEEE Robotics and Automation Magazine*, vol. 26, no. 4, pp. 30–45, Dec. 2019).

IEEE Transactions on Automation Science and Engineering Best Paper Award

Congratulations to the following winners of the 2020 IEEE Transactions

on Automation Science and Engineering Best Paper Award. This award honors the best paper published in *IEEE Transactions on Automation Science and Engineering* in the previous year.

- “Dynamic Recommendation of Physician Assortment With Patient Preference Learning,” by Xin Pan, Jie Song, and Fan Zhang (*IEEE Transactions on Automation Science and Engineering*, vol. 16, no. 1, pp. 115–126, 2019).

IEEE Transactions on Automation Science and Engineering Best New Application Paper Award

Two Recipients This Year!

Congratulations to the following winners of the 2020 IEEE Transactions on Automation Science and Engineering Best New Application Paper Award. This award honors the best paper published in *IEEE Transactions on Automation Science and Engineering* in the previous year.

- “Optimal ICU Admission Control With Premature Discharge,” by Xuanjing Li, Dacheng Liu, Na Geng, and Xiaolei Xie (*IEEE Transactions on Automation Science and Engineering*, vol.16, no. 1, pp. 148–164, 2019).
- “Integration of Robotic Vision and Tactile Sensing for Wire-Terminal Insertion Tasks,” by Daniele De Gregorio, Riccardo Zanella, Gianluca Palli, Salvatore Pirozzi, and Claudio Melchiorri (*IEEE Transactions on Automation Science and Engineering*, vol. 16, no. 2, pp. 585–598, 2019).

IEEE Robotics and Automation Society Congratulates Recently Elevated Senior Members

Congratulations to the IEEE Robotics and Automation Society members recently elevated to Senior Member status by the IEEE Admission and Advancement Senior Member Review Panel.

To be eligible for application or nomination, candidates must

- be engineers, scientists, educators, technical executives, or originators in IEEE-designated fields
- have experience reflecting professional maturity
- have been in professional practice for at least 10 years (with some credit for certain degrees).

In addition, candidates for Senior Member grade must supply three references from current IEEE Members holding the grade of Fellow, Senior

Member, or Honorary Member. For more information, visit <https://www.ieee.org/membership/senior/> or email senior-member@ieee.org.

The names and affiliations of the new Senior Members are as follows:

- *Pradeep Kumara Abeygunawardhana*
Sri Lanka Institute of Information Technology
Sri Lanka Section
- *Maxwell Addison*
Ghana Section
- *Andi Adriansyah*
Universitas Mercu Buana
Indonesia Section
- *Kasim Al-Aubidy*
Philadelphia University
Jordan Section
- *Javier Alonso-Mora*
Delft University of Technology
Benelux Section
- *Rosario Aragues*
Universidad de Zaragoza
Spain Section
- *Jeffrey Arcand*
Ciena
Ottawa Section
- *Ashwin Ashok*
Georgia State University
Atlanta Section
- *Mohamed Awadallah*
University of Technology Sydney
New South Wales Section
- *M. Balaji*
Frontline Electronics Pvt Ltd
Madras Section
- *Giovanni Beltrame*
École Polytechnique de Montréal
Montreal Section
- *Patrick Benavidez*
University of Texas at San Antonio
Lone Star Section
- *Srijan Bhattacharya*
RCC Institute of Information Technology
Kolkata Section
- *Antonio Bo*
University of Queensland
Queensland Section

- *Pascual Campoy*
Universidad Politécnica de Madrid
Spain Section
- *Zheng Chen*
University of Houston
Houston Section
- *Anthony Choi*
Mercer University
Central Georgia Section
- *Richard Coogle*
Georgia Tech Research Institute
Atlanta Section
- *Eddy Deeb*
Alfa
Lebanon Section
- *Prakash Duraisamy*
University of South Alabama
Mobile Section
- *Floris Ernst*
University of Lübeck
Germany Section
- *Mariam Faied*
University of Detroit Mercy
Southeastern Michigan Section
- *Glenn Friedman*
GXTec Consulting
Santa Clara Valley Section
- *Chandra Gajula*
Worthington Industries
Columbus Section
- *Kishore Gajula*
Fusion Alliance
Columbus (OH) Section
- *Liang Gao*
Huazhong University of Science
and Technology
Wuhan Section
- *Ryan Gariepy*
Clearpath Robotics Inc.
Kitchener-Waterloo Section
- *Hammad Gilani*
Institute of Space Technology
Islamabad Section
- *Amit Gupta*
Avaya
Denver Section
- *KR Guruprasad*
National Institute of Technology
Karnataka
Bangalore Section
- *Md. Ahsan Habib*
Mawlana Bhashani Science and
Technology
Bangladesh Section
- *Sami Haddadin*
Technical University of Munich
Germany Section
- *Kensuke Harada*
Osaka University
Kansai Section
- *Aseef Iqbal*
Chittagong Independent
University
Bangladesh Section
- *Md. Zahidul Islam*
Islamic University
Bangladesh Section
- *Rodrigo Jamisola*
Botswana International University
of Science and Technology
Region 8-Subsections of Africa
Council
- *Li Jiangang*
Harbin Institute of Technology
Guangzhou Section
- *Maolin Jin*
Korea Institute of Robot and
Technology Convergence
Daejeon Section
- *Sungho Jo*
Korea Advanced Institute of Science
and Technology
Daejeon Section
- *Mvv. Prasad Kantipudi*
Visvesvaraya Technological
University
Hyderabad Section
- *Afthab Khan*
UCSI University
Malaysia Section
- *Joo Kim*
New York University
New York Section
- *Polychronis Kondaxakis*
ABB
Sweden Section
- *Emre Koyuncu*
Istanbul Technical University
Turkey Section
- *Makoto Kumon*
Kumamoto University
Fukuoka Section
- *Jaerock Kwon*
University of Michigan
Southeastern Michigan Section
- *Sandhya L*
Sree Chitra Thirunal College of
Engineering
Kerala (India) Section
- *Darwin Lau*
Chinese University of Hong Kong
Hong Kong Section
- *Nuno Lau*
Universidade de Aveiro
Portugal Section
- *Mi Li*
Shenyang Institute of Automation
Harbin Section
- *Zheng Li*
Chinese University of Hong Kong
Hong Kong Section
- *Gijs M Krijnen*
University of Twente
Benelux Section
- *Douglas Mackenzie*
Hyundai Mobis North America
Southeastern Michigan Section
- *Sagar Mahajan*
Prince Sultan University
Bombay Section
- *Ebrahim Mattar*
University of Bahrain
Bahrain Section
- *Harish Mekali*
B.M.S. College of Engineering
Bangalore Section
- *Ziyang Meng*
Tsinghua University
Beijing Section
- *Andres Mora Vargas*
NASA Ames Research Center
Santa Clara Valley Section
- *Mario Munich*
Embodied, Inc.
Metropolitan Los Angeles Section
- *Francisco Mur*
Universidad Nacional de Educación
a Distancia
Spain Section
- *H. Keith Nishihara*
Lu and Nishihara Associates
Santa Clara Valley Section
- *Emmanuel Nuno*
University of Guadalajara
Guadalajara Section
- *Calogero Oddo*
Scuola Superiore Sant'Anna
Italy Section
- *Robert Opalsky*
Qualcomm
San Diego Section
- *Huimin Ouyang*
Nanjing Tech University
Nanjing Section
- *Suresh P*
Muthayammal Engineering
College
Madras Section

- *Sujit P*
Indian Institute of Science Education and Research Bhopal
Bombay Section
- *Haseena P Y*
College of Engineering
Karunagappally
Kerala (India) Section
- *Claudio Pacchierotti*
Center National de la Recherche Scientifique
France Section
- *Theodore Pachidis*
International Hellenic University
Greece Section
- *Gianluca Palli*
University of Bologna
Italy Section
- *Jia Pan Hong*
University of Hong Kong
Hong Kong Section
- *Yongping Pan*
National University of Singapore
Guangzhou Section
- *Gaurav Pandey*
Ford Motor Company 5
Houston Section
- *Kyung-Joon Park*
Daegu Gyeongbuk Institute of Science and Technology
Seoul Section
- *Mukesh Patil*
Ramrao Adik Institute of Technology
Bombay Section
- *James Patton*
University of Illinois at Chicago
Chicago Section
- *Jeffrey Piasecki*
General Motors
Southeastern Michigan Section
- *Kishore Pinninti*
Vallurupalli Nageswara Rao Vignana Jyothi Institute of Engineering and Technology
Hyderabad Section
- *Sakthinathan Pitchaiah*
Philadelphia Section
- *Panagiotis Polygerinos*
BIC
Greece Section
- *Kuppan Chetty Ramanathan*
Hindustan University
Madras Section
- *Ludovic Righetti*
New York University
New York Section
- *Jee-Hwan Ryu*
Korea Advanced Institute of Science and Technology
Daejeon Section
- *Tanveer Saleh*
International Islamic University
Malaysia
Malaysia Section
- *Thomas Savarino*
Willow Glen Research
Santa Clara Valley Section
- *Russell Schwoerer*
Seattle Section
- *Dan Selisteanu*
University of Craiova
Romania Section
- *Tae Won Seo*
Hanyang University
Seoul Section
- *Adam Spring*
Atlanta Section
- *Danail Stoyanov*
University College London
United Kingdom and Ireland Section
- *Zhenglong Sun*
Chinese University of Hong Kong, Shenzhen
Guangzhou Section
- *Ning Tan*
Sun Yat-sen University
Guangzhou Section
- *Bhupinder Verma*
Lovely Professional University
Delhi Section
- *Atsushi Yamashita*
University of Tokyo
Tokyo Section
- *Zhi Yan*
University of Technology of Belfort-Montbéliard
France Section
- *Dana Yoerger*
Woods Hole Oceanographic Institution
Providence Section
- *Dongwon Yun*
Daegu Gyeongbuk Institute of Science and Technology
Seoul Section
- *Jing Zhao*
Medtronic
Denver Section

EA

We want to hear from you!

Do you like what you're reading?
Your feedback is important.
Let us know—send the editor-in-chief an e-mail!

IMAGE LICENSED BY GRAPHIC STOCK

2020

18–21 December

ICARM 2020: International Conference on Advanced Robotics and Mechatronics. Shenzhen, China. <http://www.ieee-arm.org/>

26–29 December

ICCR 2020: International Conference on Control and Robots. Tokyo, Japan. <http://www.iccr.net/>

2021

8–10 January

ICCCR 2021: The International Conference on Computer, Control, and Robotics. Shanghai, China. <http://www.iccr.org/>

11–14 January

SII 2021: IEEE/SICE International Symposium on System Integration. <https://sice-si.org/conf/SII2021/>

9–11 March

HRI 2021: ACM/IEEE International Conference on Human–Robot Interaction. Boulder, Colorado, United States. Hybrid Event. <https://humanrobotinteraction.org/2021/>

12–16 April

Robosoft 2021. Virtual Event. <http://softroboticsconference.org/>

30 May–5 June

ICRA 2021: International Conference on Robotics and Automation. Xi’an, China. <http://103.120.82.66/index.aspx>

22–25 June

MED 2021: Mediterranean Conference on Control and Automation. Puglia, Italy. <http://med2021.poliba.it/wordpress/>

6–9 July

WHC 2021: World Haptics Conference. Montreal, Canada. <https://2021.worldhaptics.org/>

19–23 July

MARSS 2021: International Conference on Manipulation, Automation and Robotics at Small Scales. Toronto, Canada. <https://marss-conference.org/>

Digital Object Identifier 10.1109/MRA.2020.3029240
Date of current version: 9 December 2020



Call for IEEE Fellow Nominations—Class of 2022

Deadline 1 March 2021

Nominations for the IEEE Fellows Class of 2022 are now being accepted. Nominate a colleague, coworker, or friend whose career and body of work you consider eligible for elevation to the IEEE Fellow grade. IEEE Fellow is a distinction reserved for select IEEE Members whose extraordinary accomplishments in any of the IEEE fields of interest are deemed fitting of this prestigious grade elevation.

APPLY ONLINE

All forms (nominations, references, and endorsements) must be submitted no later than 1 March 2021 at 11:59PM ET.

Eligibility

To be nominated as a Fellow, a recipient must

- have accomplishments that have contributed importantly to the advancement or application of engineering, science, and technology, bringing the realization of significant value to society
- hold Senior Member or Life Senior Member grade at the time the nomination is submitted
- have been a Member in good standing in any grade for a period of five years or more preceding 1 January of the year of elevation.

Find out more about the IEEE Fellows program and evaluation process here: http://www.ieee.org/membership_services/membership/fellows/steps.html

Digital Object Identifier 10.1109/MRA.2020.3029241



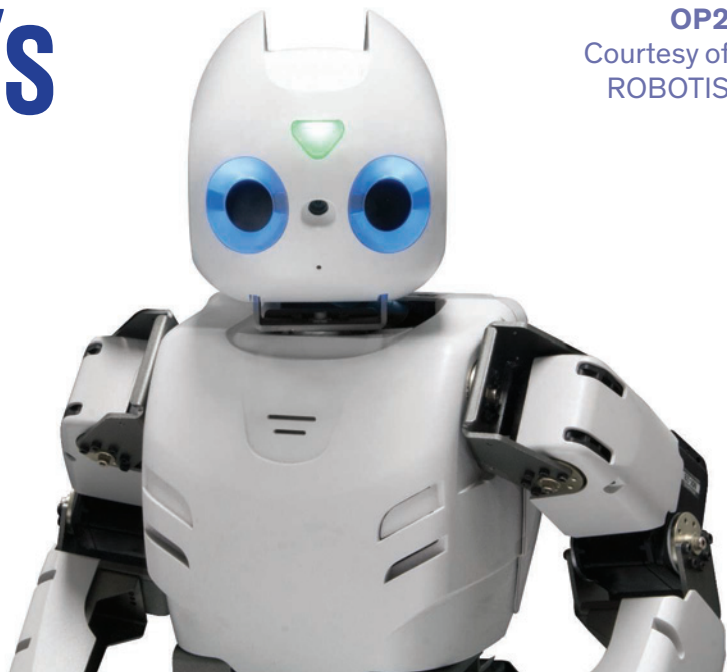
**The IEEE Robotics and Automation Award
For contributions in the field of robotics and automation
Nomination deadline: 15 January**

More about the IEEE Robotics and Automation Award and evaluation process found here:
<https://www.ieee.org/about/awards/tfas/robotauto.html>

Digital Object Identifier 10.1109/MRA.2020.3029242

The World's Best ROBOTIS GUIDE Is Here!

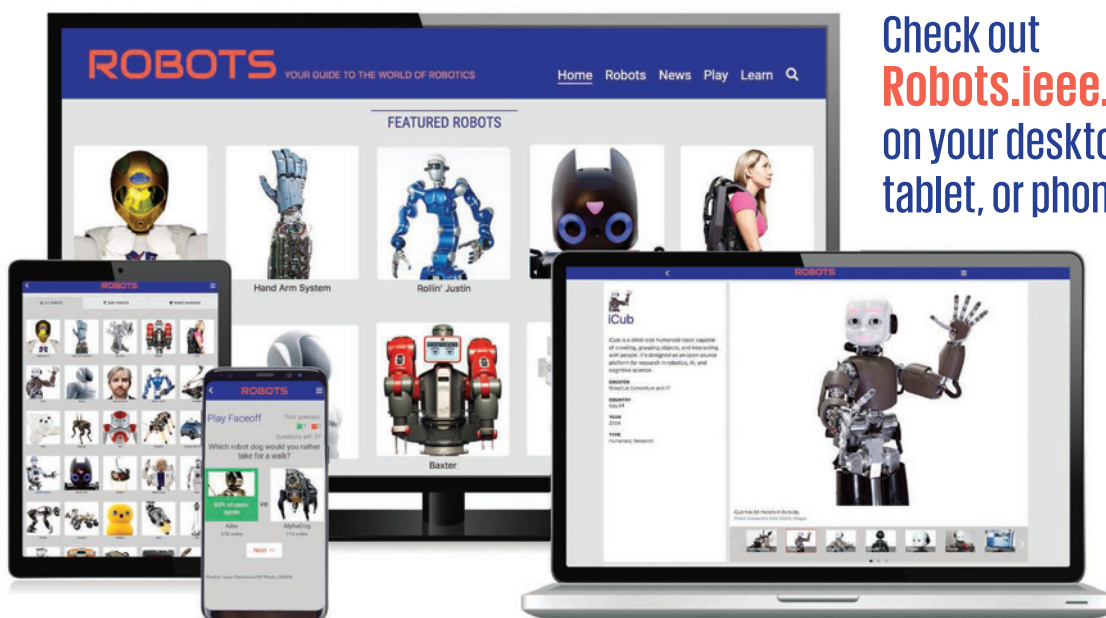
OP2
Courtesy of
ROBOTIS



ROBOTIS.IEEE.ORG

IEEE Spectrum's new **ROBOTIS** site features more than **200 robots** from around the world.

- Spin, swipe and tap to make robots move.
- Rate robots and check their ranking.
- Play *Faceoff*, an interactive question game.
- Read up-to-date robotics news.
- View photography, videos and technical specs.

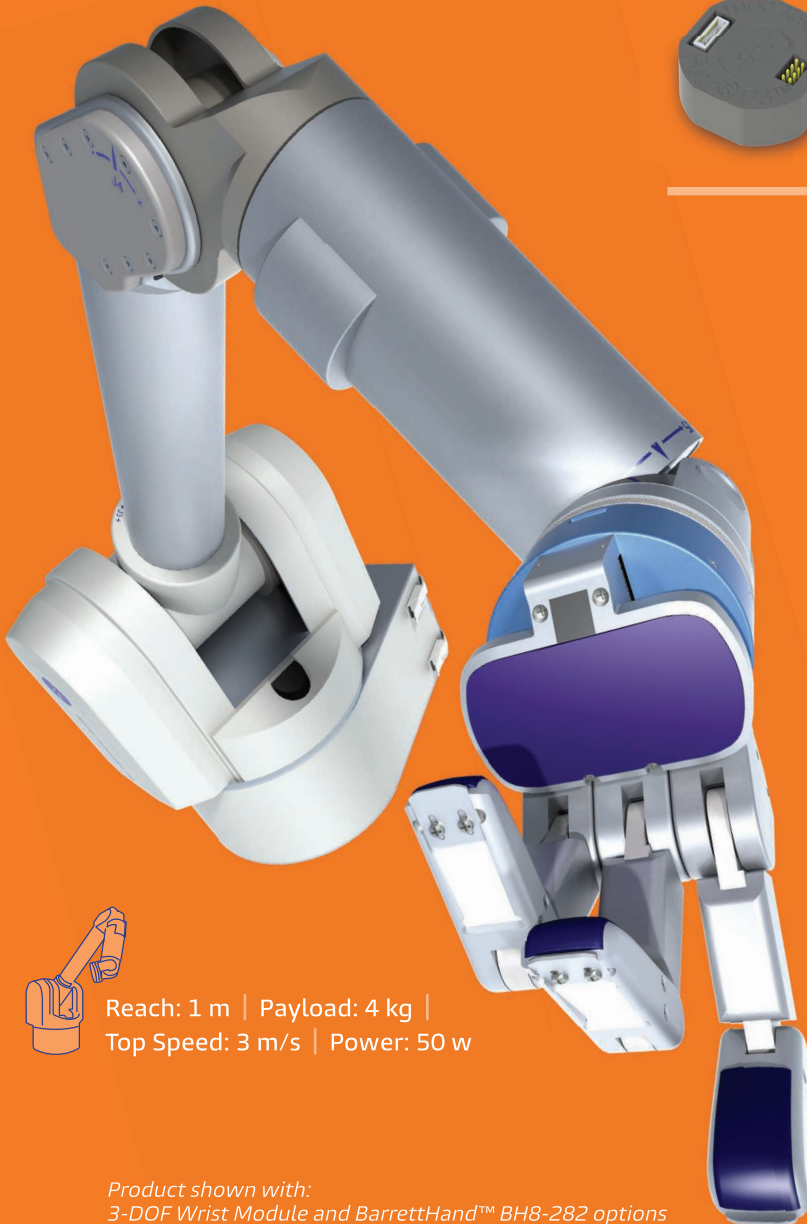


Check out
Robots.ieee.org
on your desktop,
tablet, or phone now!



POWER YOUR ADVANCED APPLICATIONS

WAM 3.0 starts at just \$69,500



Puck® Motor Control

Achieve high-fidelity torque control enabled by 3rd-generation Puck® motor controllers.



TRUE HAPTICS



BACKDRIVABLE



SAFETY LAYERED



UNIVERSAL



MOBILE READY



FEATHER TOUCH



Reach: 1 m | Payload: 4 kg |
Top Speed: 3 m/s | Power: 50 w

Product shown with:
3-DOF Wrist Module and BarrettHand™ BH8-282 options

Available upgrades

- High-speed (5 m/s)
- High-payload (8 kg)
- Force/Torque Sensor
- BarrettHand BH8-282

Flexible software

- Easy-to-use ROS interface
- High-performance, open-source C++ control library

Barrett has a large global customer base of leading research organizations utilizing the proven technology of the WAM®, BarrettHand™, and now Burt® for applications in vision, AI, mobile systems, medical, haptics, advanced manipulation, and automation. Visit us at advanced.barrett.com send email to sales@barrett.com, or phone us at **US+1.617.252.9000**.

US Patents 10,148,155, 10,130,546, 9,020,644, 8,858,374, 8,052,857, 7,893,644, 7,854,631, 7,511,443, 7,168,748. Similar patents issued internationally and additional patents pending. The BURT®, Puck®, and WAM® trademarks are registered internationally.